NATURAL ZEOLITE REMOVAL CAPACITY OF HEAVY METALLIC IONS

by

Amanda Lidia Alaica-Ciosek

B.Eng. (Hons.) (2010), M.A.Sc. (2012)

Ryerson University

A Dissertation

presented to Ryerson University

in partial fulfillment of the

requirements for the degree of

Doctor of Philosophy

in the Program of

Civil Engineering

Toronto, Ontario, Canada, 2018

AUTHOR'S DECLARATION
FOR ELECTRONIC SUBMISSION OF A DISSERTATION

I hereby declare that I am the sole author of this Dissertation. This is a true copy of the Dissertation, including any required final revisions, as accepted by my examiners.

I authorize Ryerson University to lend this Dissertation to other institutions or individuals for the purpose of scholarly research.

I further authorize Ryerson University to reproduce this Dissertation by photocopying or by other means, in total or in part, at the request of other institutions or individuals for the purpose of scholarly research.

I understand that my Dissertation may be made electronically available to the public.

NATURAL ZEOLITE REMOVAL CAPACITY
OF HEAVY METALLIC IONS

Amanda Lidia Alaica-Ciosek
Doctor of Philosophy
Civil Engineering, Ryerson University, 2018

ABSTRACT

Our ecosystem is at risk by many anthropogenic activities, which include the release of industrial wastewater effluents laden with toxic heavy metals. There is a long history and a continued demand for proper evaluation and predication of water quality and management, in order to protect surrounding water resources and all living species. Undeniably, these pollutants (heavy metallic ions; HMIs) are a detrimental threat, and must be removed by advanced treatment technology prior to discharge. One such strategy would be by the process of sorption (adsorption/ion-exchange), which has advanced among researchers. Zeolites in particular have attracted researchers' interests, being a naturally abundant, cost-effective mineral, with high cation exchange capacity and selectivity of certain metals. They are considered as a strong candidate for the removal of HMIs, and hold the potential for regeneration, recovery and reuse in pertinent industrial applications.

This study investigates the sorption process by natural zeolite (clinoptilolite) of HMIs that are commonly found in industrial wastewater effluent, namely lead (Pb^{2+}), copper (Cu^{2+}), iron (Fe^{3+}), nickel (Ni^{2+}) and zinc (Zn^{2+}). The HMIs are combined in acidic, synthetic simple-solute solutions of various (single-, dual-, triple-, multi-) component systems, in a controlled environment for improved quantification and identification of the important trends; in order to address existing limitations in multi-component system research. The analytical methodology of ICP-AES was employed for all quantitative detection and analyses.

The project consists of four phases in the analysis of: (1) the effects of preliminary parameters and operative conditions (particle size, sorbent-to-sorbate dosage, influent concentration, contact time, set-temperature, and heat pre-treatment), (2) HMIs component system combinations and selectivity order, (3) kinetic modelling trends, and (4) the design of a packed, fixed-bed, dual-column sorption treatment system prototype.

Under the testing conditions, this study demonstrates a strong correlation with the pseudo-second-order kinetic model in batch-mode analysis, as well as a relationship among the empty bed contact time, breakthrough capacity, and usage rate in continuous-mode investigations. A key sorption trend among the HMIs selected is well-established in all four phases as $Pb^{2+} \gg Fe^{3+} > Cu^{2+} > Zn^{2+} \gg Ni^{2+}$; providing significant validation of this experimental design. The system prototype is a platform for the advancement of intelligent process controls. It is envisaged that this research will provide essential information to the industrial wastewater treatment industry for the design and implementation of innovative zeolite-based sorption technology.

ACKNOWLEDGEMENTS

First and foremost, I would like to express my deepest gratitude to my direct supervisor Dr. Grace K. Luk. I sincerely appreciate all of her care and guidance throughout my academic career; it was an honour to be her student.

I would like to thank my supervisory committee members of the Department of Civil Engineering at Ryerson University; to Dr. James Li, my co-supervisor who provided significant support to the completion of my degree, for which I am truly grateful; to Dr. Ahmed Shaker and Dr. Darko Joksimovic for their thoughtful insight. Thank you to Dr. Lynda H. McCarthy of the Department of Chemistry and Biology at Ryerson University for her expertise and significant assessment of my research. Finally, thank you to Dr. Ronald L. Droste of the Department of Civil Engineering at the University of Ottawa, for his time and consideration, expertise and critical review of my research as the external examiner. I would also like to extend my gratitude to the numerous anonymous reviewers who provided helpful suggestions to improve the manuscripts presented in the Dissertation document.

Thank you to Ms. Valerie Phelan (Radiation/Chemical/Biosafety Officer) and Mr. Eric Ambroise (Lab Safety Officer) of the Ryerson Integrated Risk Management (IRM) for all their assistance as I established the safety and waste management protocol of the research project. Thank you to Mr. Dan Mathers, the supervisor of the Analytical Lab for Environmental Science Research and Training (ANALEST) at the Department of Chemistry of the University of Toronto, for ad-hoc training of the analytical technology and kind support throughout my experimental analyses.

Finally, I would like to express my heartfelt appreciation to Mr. Robin Luong, the Environmental Technician of the Department of Civil Engineering at Ryerson University; who was beyond technical support throughout my academic career. He has taught me the fundamentals of quality research skills and the importance of perseverance, which I will take with me in my professional career and in life.

To my family, both near and far, thank you for all of your love throughout this incredible journey; I love you and cherish you always.

DEDICATION

TO MY PARENTS – LIDIJA + ZELJKO ALAICA.

Ja вас волим.

"THE ONLY WAY OUT IS THROUGH." – R. FROST.

PREFACE

This Dissertation is submitted for the degree of Doctor of Philosophy at Ryerson University. The research described herein was conducted under the direct supervision of Professor Dr. Grace K. Luk of the Department of Civil Engineering, Ryerson University, between September 2012 and August 2017.

This Dissertation is based on a four-phase research project, and is submitted as a manuscript-style document, composed of eight chapters and six appendices. Chapter 1 is the introduction and critical review of the experimental design of the research topic. Chapter 2 defines the study objectives and scope, document structure as well as the statement of authorship. Chapter 3 presents the analytical procedures and quality control measures implemented; which are consolidated for cohesion in the document. Chapters 4, 5, 6, and 7 are the manuscripts that discuss the significant findings of each phase of the research project. Chapter 8 provides the major conclusions and recommendations for future implementation of the technology in engineering practice. The appendices provide the details of all the experimental procedures and schedule (A), analytical technology operating procedure (B), as well as technical conference papers (C, D, E). Appendix F highlights a cover featured journal publication that investigates the capacity of natural zeolite to remove nutrients from wastewater; a former research endeavour investigated by the Ph.D. Candidate.

This research is to the best of knowledge original, expect where acknowledgements and references are made to previous work. Neither this, nor any substantially similar Dissertation has been or is being submitted for any other degree, diploma or other qualification at any other university. This Dissertation document contains less than 60,000 words, within 200 pages.

TABLE OF CONTENTS

LIST OF TABLES

LIST OF FIGURES

LIST OF NOMENCLATURE

LIST OF ABBREVIATIONS

HMI		Heavy Metallic Ion	
ICP-AES		Inductively Coupled Plasma – Atomic Emission Spectroscopy	
SEM/EDS		Scanning Electron Microscopy/Energy Dispersive X-Ray Spectroscopy	
GLWQA		Great Lakes Water Quality Agreement	
GAC		Granulated Activated Carbon	
Si/Al		Silica/Aluminium Ratio	
CEC		Cation Exchange Capacity	
FBR		Fixed-Bed Reactor	
PF		Plug Flow	
SBC		Slurry Bubble Column	
HNO$_3$		Concentrated Nitric Acid	
Pb^{2+}	**[P]**	Lead ion	Single-Component Lead System
Cu^{2+}	**[C]**	Copper ion	Single-Component Copper System
Fe^{3+}	**[F]**	Iron ion	Single-Component Iron System
Ni^{2+}	**[N]**	Nickel ion	Single-Component Nickel System
Zn^{2+}	**[Z]**	Zinc ion	Single-Component Zinc System
[D-xy]		Dual-Component System (xy)	
[T]		Triple-Component System	
[M]		Multi-Component System	
ANALEST		Analytical Lab for Environmental Science Research and Training	
SOP		Standard Operating Procedure	
QDL		Quantifiable Detection Limits	
%-RSD		%-Relative Standard Deviation	
CC		Correlation Coefficient	
SR		Selectivity Ratio	
PFO		Pseudo-First-Order Model	
PSO		Pseudo-Second-Order Model	
IPD		Intra-Particle Diffusion Model	
RDS		Rate-Determining Step	
BP		Breakthrough Point (Breakpoint)	
EP		Exhaustion Point	
MTZ		Mass Transfer Zone	
C1		Column 1	
C2		Column 2	
SC1		Sampling Chamber 1	
SC2		Sampling Chamber 2	
MODE		Sampling Mode (I, II, III)	

LIST OF SYMBOLS

Symbol	Description	Unit
%R	Percent removal	(%)
d_p	Particle size	(mm)
q_t	Sorption capacity of HMI at time t	(meq/g)
C_0	Influent HMI concentration in solution	(meq/L)
C_t	Effluent HMI concentration at time t	(meq/L)
t	Contact time	(min)
V	Batch-mode sample volume	(L)
M	Zeolite mass	(g)
q_{180}	Sorption capacity at 180-contact time	(meq/g)
q_e	Sorption capacity at equilibrium	(meq/g)
k_1	PFO rate constant	(min^{-1})
h	initial sorption rate	(meq/g·min)
k_2	PSO rate constant	(g/meq·min)
β	Elovich constant	(g/meq)
α	Initial sorption rate	(meq/g·min)
k_P	IPD rate constant	$(meq/g·min^{1/2})$
C	IPD constant	(meq/g)
r_A	Reaction rate of reactant	(meq/L·min)
$[A]_0$	Initial reactant concentration	(meq/L)
$[A]_t$	Reactant concentration at time t	(meq/L)
$k_{n=1}$	First-Order reaction rate constant	(min^{-1})
$k_{n=2}$	Second-Order reaction rate constant	(L/meq·min)
η	Column efficiency (degree of saturation)	---
C_{BP}	Breakthrough capacity of the bed	(meq/g)
C_{EP}	Maximum capacity at exhaustion of the bed	(meq/g)
V_{BP}	Effluent volume collected up to BP	(L)
V_{EP}	Effluent volume at which the EP is reached in the zeolite bed	(L)
ρ	Packing density of the bed	(g/cm^3)
H	Bed depth	(cm)
A	Bed cross-sectional area	(cm^2)
m_Z	Zeolite mass in the bed	(g)
η_{BP}	Total amount of HMI ions removed up to BP	(meq)
η_{EP}	Total amount of HMI ions removed up to EP	(meq)
EBCT	Empty Bed Contact Time	(min)
v	Feed solution velocity	(cm/min)
d	Column internal diameter	(cm)
Q	Volumetric flow rate	(mL/min)
v_U	Usage rate	(g/L)
k_T	Coefficient of permeability	(cm/s)
V_C	Quantity of water that has discharged and collected from the column	(cm^3)
L	Column height	(cm)
A_c	Column cross-sectional area	(cm^2)
H_C	Constant head of water on the column or the vertical distance between the feed head level and the column overflow level	(cm)
T	Time required to collect V_C	(seconds)

1. INTRODUCTION

1.1. Industrial Wastewater Effluents –
Characteristics, Impacts, and Treatment Methods

Water has been damaged by various anthropogenic sources over the past several decades, and such sources include but are not limited to municipal wastewater treatment plants, agricultural cultivation and fertilization activities, as well as mining and *industrial wastewater effluents* (Asubiojo and Ajelabi, 2009; Barakat, 2011; Fu and Wang, 2011; Tchounwou et al., 2012; Lata et al., 2015). Surface water, ground water, as well as municipal and industrial wastewater contain many different types of pollutants, such as organics and inorganics (i.e., anionic and cationic ions (heavy metallic ions; HMIs)), causing toxic effects on our ecosystem (Wang and Peng, 2010). Natural water systems are comprised of chemical and physical processes that affect both the distribution and circulation of pollutants. The hydrologic cycle has climatic and seasonal variations, which influences geo-chemical processes and may cause dissolution and chemical reactions with solids, liquids and gases. Anthropogenic interferences associated with industrial processing effluents may cause slight variations in these natural waters, directly causing an influx of pollutants, such as HMIs, which adsorb onto particulates and deposit onto sediments affect the overall balance of metals in the aquatic system (Yabe and de Oliveira, 2003).

Heavy metals are an environmental priority pollutant as they deteriorate water quality, and are a detrimental threat to our ecosystem (Alvarez-Ayuso et al., 2003; Inglezakis and Poulopoulos, 2006, p. 18; Fu and Wang, 2011). Because of their high solubility in the aquatic environment, heavy metals can impact living organisms (microorganisms, fish, and plants) (Kocasoy and Sahin, 2007; Barakat, 2011). Heavy metals are non-biodegradable pollutants which persist and remain intact in the environment (Asubiojo and Ajelabi, 2009) and once entered and transferred through the food chain (Kocasoy and Sahin, 2007), they trigger various diseases and disorders (Erdem et al., 2004; Akcil and Koldas, 2006; Sprynskyy et al., 2006; Inglezakis and Poulopoulos, 2006, p. 18; Acheampong et al., 2010; Barakat, 2011). The effects of heavy metals in wastewater effluents not only impact the environment, but are detrimental to humans also. The impact can be toxic (acute, chronic or sub-chronic), neurotoxic, carcinogenic,

mutagenic or teratogenic (Acheampong et al., 2009; Akpor et al., 2014). Lead is known as a designated substance, with carcinogenic consequences that affect every organ and system in the human body (OHSA, 2014; Martin and Griswold, 2009; Tchounwou et al., 2012). In addition to lead, nickel and zinc that are dissolved in water are acutely toxic at various levels, and cause numerous health complications; such as cardiovascular and nervous system function conflicts that result in death (Acheampong et al., 2009).

Being part of a very complex and dynamic system, there are many anthropogenic sources and sinks of heavy metals, which can be transported in their dissolved form in water or part of suspended sediments, volatilized to the atmosphere or stored in sediments (Curenature, 2018). The most common source of pollution is through the discharge of wastewater as a by-product of industrial processing. The increased demand for the production of commodities produced by various industries has triggered an accumulation of pollutants (i.e., heavy metals) (Barakat, 2011; Fu and Wang, 2011; Farouq and Yousef, 2015). Large quantities of wastewaters, residues, and sludge as hazardous wastes are generated, which require extensive waste management (Barakat, 2011). These pollutants put the entire ecosystem at risk, and therefore, it is imperative to remove them prior to their discharge into waterways (Asubiojo and Ajelabi, 2009; Barakat, 2011). *Industrial wastewater streams laden with heavy metals* include but are not limited to (Barakat, 2011; Fu and Wang, 2011; Tchounwou et al., 2012; Akpor et al., 2014):

- mining operations;
- metal surface treatment processing (i.e., electroplating, electroless depositions, conversion-coating, anodizing-cleaning, milling, and etching);
- inorganic pigment (tanneries, dye) manufacturing;
- petroleum refining;
- batteries and printed circuit board (PCB) manufacturing;
- paper and pesticides processing, as well as;
- fertilizer and wood processing.

The Canadian mining sector has invested heavily in exploration and development and is among the global leaders in mineral extraction and metal production/processing. As reported by the Ontario Mining and Exploration Directory (2015), there are 32 metal processing (i.e., gold, base metal, iron, platinum group) mines and 43 mines in total in this province alone. In particular, the towns of Timmins and Sudbury ('The Nickel Belt') are associated with industrial wastewater effluents and heavy metal processing pollutants. At just 300 km apart and in proximity to our great lakes, these industrial sites pose great concern to our revered fresh water source and prompts the discussion of the importance of treatment technology development to remove heavy metals, in order to meet stringent water/wastewater regulations (Kocasoy and Sahin, 2007).

The Great Lakes Water Quality Agreement (GLWQA), which originated in 1972, reflects the continued concern of the future direction and quality of the Great Lakes ecosystem (Rasmussen, 1979). As stated by the Canada-United States Collaboration for Great Lakes Water Quality, the purpose of the agreement is to address current and future challenges in source control, and "…to restore and maintain the chemical, physical, and biological integrity of the Waters of the Great Lakes". The GLWQA has evolved over the years with various amendments (1978, 1983, 1987, 2012) to address the problem of toxic substances in the lakes and the pollution from assorted land use activities, through the development and implementation of stricter water quality goals (Rasmussen, 1979), (water/wastewater) contingency planning and management. In particular, the 1978 GLWQA amendment initiated the concern of heavy metals. According to the International Joint Commission of the United States and Canada for the 1978 GLWQA amendment, the necessity for *industry-academia research* by means of 'development, interpretation and demonstration of advanced scientific knowledge for the resolution of issues' is stressed. Metals of persistent toxic concern were emphasized, with total concentrations in an unfiltered water sample to not exceed the thresholds to protect aquatic life and raw water for public supply; such concentrations include 10-25, 5, 25, 30, 50, 0.2, and 50 mg/L for lead, copper, nickel, zinc, arsenic, cadmium, chromium, respectively. As discussed by Rasmussen (1979), the agreement highlights the need for pollution prevention (P2), which would lead to less heavy metal discharge to control at the source of an industrial process. The agreement also introduces the requirements that joint source control research programs be cost-effective as a priority for our Great Lakes.

Industrial wastewater effluents are treated to meet federal and provincial thresholds by neutralizing free acidity, as well as removing suspended solids and metals (i.e., lead, copper, nickel, zinc, arsenic, cadmium). Provincial requirements are stricter in certain instances, while scientific fact and societal pressure continue to demand further reductions of acceptable metal concentrations for regulation (Dinardo et al., 1991). Based on the MOECC Water Management - Policies, Guidelines and Provincial Water Quality Objectives (1994) and the Provincial Water Quality Objectives (PWQO) (MOECC, 2016), the receiving-water effluent requirements for point source discharges to surface waterbodies have been established. Primary emphasis is on the treated effluent discharge limits from pollution point sources, such as industrial wastewater. Treatment technology-based effluent requirements are contained in a range of provincial and federal acts, regulations, guidelines and policies. For industrial point-source discharges, a concentration-based approach was incorporated into provincial effluent requirements on the basis of experience with municipal sewage treatment systems; and revised guidelines were developed for specific industrial sectors, based on the state of treatment technology for those sectors. Before any discharger-specific effluent requirements are specified, the impact of the treatment technology-based effluent on the receiving water body must be reviewed (MOECC, 2016). Water quality considerations take precedence when contaminant discharges exceed the assimilative capacity of the receiving waters, even if the discharged loadings are within the treatment technology-based effluent requirements based on the guidelines, regulations or policies. Receiving-water based effluent requirements also take precedence when ambient levels of toxic contaminants are above acceptable levels (MOECC, 2016). As outlined in **Table 1.1**, the heavy metal contamination of various anthropogenic influenced wastewater streams are subject to numerous national and international standards.

Table 1.1 Water Standards – Maximum Contaminant Level of Heavy Metals (mg/L)

Element	Water Quality Standards[X]	Drinking Water[X]	UN FAO Irrigation[Y]	US EPA Standard[Y]	Canadian Mining Effluent Limits[Z,d]
pH	6.5-8.5	---			
Lead	0.0025	0.015	---	0.015[c]	0.20
Copper	0.009	1.3	0.20	1.3[c]	0.30
Iron	---	---	5	0.3[b]	---
Nickel	0.052	0.1	0.20	0.1[a]	0.5
Zinc	0.117	---	2	5[b]	0.50
Arsenic	0.148	0.05	0.10	0.05[a]	0.50
Cadmium	0.0021	0.005	0.01	0.01[a]	
Chromium	0.027	0.1	0.10	0.10[a]	

[X](Benjamin, 2010, p.4); [Y](Rice et al., 2012); [Z](CMJ, 2014)
[a]Primary drinking water; [b]Secondary drinking water;
[c]90th percentile action level [Lead and Copper Rule – LCR];
[d]Maximum Authorized Monthly Mean Concentration

Innovative technology research and development for the reduction of water/wastewater toxicity has expanded, in order to meet evolving treatment standards caused by the various anthropogenic sources (Lata et al., 2015). Conventional and emerging (Dinardo et al., 1991) treatment technologies considered in the industry include chemical precipitation, ion-exchange, ion-exchange and solvent extraction, ion-exchange and precipitation, adsorption, bio-sorption, coagulation/flocculation, flotation, membrane filtration, ultrafiltration and electro-chemical remediation (Peric et al., 2004; Mohan and Chander, 2006; Han et al., 2006; Barakat, 2011; Fu and Wang, 2011; Margeta et al., 2013). Chemical (lime/limestone; hydroxide, sulphide) precipitation is most widely used (Dinardo et al., 1991; Barakat, 2011), as it is a relatively simple and inexpensive process; HMIs form insoluble precipitates, separated by sedimentation or filtration, where the treated water is discharged or reused. However, it is not a very economical process due to slow metal precipitation, poor settling, the aggregation of metal precipitates, and the long-term environmental impacts of managing and processing of residual chemicals and sludge (Barakat, 2011; Fu and Wang, 2011).

Various treatment technologies for the removal of heavy metals from industrial wastewater have focused on physico-chemical removal processes (Barakat, 2011). Among these, *sorption (adsorption/ion-exchange)* (Helfferich, 1962; Inglezakis and Poulopoulos, 2006) is considered as a promising treatment method (Motsi et al., 2011; Wang et al., 2009). These findings are also supported by Margeta et al. (2013), which highlight the removal efficiency of metal ions by natural zeolite from various sources of wastewater, and shows that sorption is superior compared to standard physical/chemical techniques. Industry has developed an interest for exploring sorption as a wastewater treatment method (Wang et al., 2009; Motsi et al., 2011), based on demonstrated heavy metal removal efficiency, industrial viability (ease of implementation), cost-effectiveness (Anari-Anaraki and Nezamzadeh-Ejhieh, 2015; Borandegi and Nezamzadeh-Ejhieh, 2015; Xu et al., 2013) (the use of naturally abundant materials) and environmental sustainability (regenerative potential and sludge-free operation) (Lata et al., 2015).

Ion-exchange is considered a very successful removal process for the removal of heavy metals from industrial wastewater effluent, associated with high treatment capacity, high removal efficiency and fast kinetics (Barakat, 2011; Fu and Wang, 2011). Ion-exchange has demonstrated both technical and economic feasibility of metal recovery from acid mine drainage, and is also a significant method for handling wastewaters in the metal finishing industry (Dinardo et al., 1991). *Adsorption* is also an effective and economic method, with design and operation flexibility, producing high-quality treated effluent. As a reversible process, this leads to the potential to regenerate the sorbent material (Fu and Wang, 2011). There are various advantages associated with physico-chemical treatment of inorganic effluents, which include being a relatively rapid process, with ease of operation and control, accommodates variability in input loads and flow (seasonal flows and complex discharge), as well as requiring lower space and installation costs. Drawbacks of this treatment method include higher operational and sludge disposal handling expenditures, which can be offset with the use of *low-cost adsorbent materials* (Barakat, 2011).

1.2.   Selection of Sorbent Material – Natural Zeolite Mineral Characteristics

Governmental policies and initiatives, such as the GLQWA, have impelled the continued interest by researchers to find cost-effective adsorbent material alternatives to replace conventionally considered and costly granulated activated carbon (GAC). Existing literature in the investigation of various alternatives for the uptake of heavy metals from industrial wastewater include natural minerals such as *zeolites* and clay minerals (i.e., bentonite, kaolin), biomaterials (i.e., biomass, moss, peat, sawdust), as well as agricultural wastes and industrial by-products (i.e., fly ash) (Babel and Kurniawan, 2003; Gunay et al., 2007; Wang and Peng, 2010; Fu and Wang, 2011). Among these different sorbent materials, zeolites appear as one of the most promising to perform metal purification processes (Alvarez-Ayuso et al., 2003). Zeolites are a low-cost, globally abundant natural mineral (Kocasoy and Sahin, 2007); considered relatively inexpensive ($0.03-0.12/kg-USD) compared to industrial grade GAC ($20-22/kg-USD); depending on the quality of the materials (Babel and Kurniawan, 2003).

Natural zeolites have garnered particular research interest due to their co-existing molecular sieve action, ion-exchange and catalytic properties (Wang et al., 2009; Tsitsishvili, 1988; Nezamzadeh-Ejhieh and Shirzadi, 2014), and are applied worldwide in various industries, which include agriculture, soil remediation, and energy (Wang, 2010), as well as the wastewater treatment industry. Wang and Peng (2010) reported that the global consumption of zeolite has grown from 3.98Mt in 2009 to reach 5.5Mt in 2010, and is on the rise. Among the 40 known types of natural zeolites, *clinoptilolite* is well-documented and relatively abundant, found in large deposits all over the world (Wingenfelder et al., 2005; Wang and Peng, 2010), and is extensively used on a global scale (Wang and Peng, 2010; Xu et al., 2013) in various sorption treatment studies of industrial effluent. Over the past decade, extensive research of natural zeolites has resulted in a substantial number of patents. As reported by Margeta et al. (2013), over 410 patents and well over 2,000 scientific research efforts have materialized for that of clinoptilolite alone. Due to its global abundance and cost-effectiveness, mineral zeolite has attracted a high level of interest in its use in future water treatment technology development by industrial wastewater processing sectors.

1.2.1. Chemical Composition and Structure

Zeolite is a hydro-aluminosilicate (Tsitsishvili, 1988) crystalline and is a member of the tecto-silicates group, similar to quartz and feldspar minerals (Mumpton, 1977). With a 'honeycomb-like structure' (Jha and Sigh, 2016), it is composed of a three-dimensional framework built of primary building units (tetrahydra) of silicon-oxygen and aluminum-oxygen, which encompass complex rings that create an open homogenous microporous structure of voids and channels (Mumpton, 1977; Tsitsishvili, 1988). The structure of zeolite contains cations (Na^+, Ca^{2+}, Mg^{2+}, K^+) (co-ions), and is represented by the general empirical formula shown in **Equation 1.1** (Mumpton, 1977; Wang, 2010):

$$M_{x/n}\left(Al_xSi_yO_{2(x+y)}\right) \cdot pH_2O \qquad (1.1)$$

where M is any alkali or alkaline earth cation (Na, K, Li and/or Ca, Mg, Ba, Sr), n is the cation charge, and the constant ratios of y/x and p/x ranging from 1-6 and 1-4, respectively. Exchangeable cations are represented as the ions in the first set of parentheses within the unit-cell formula; the ions in the second set of parentheses is (x+y), which refers to the oxygen content; which make up the tetrahedral framework. The ratio of the base to alumina is always equal to the value of y. As a true tecto-silicate, oxygen is connected to either a silicon or an aluminum ion with a ratio of (Al+Si):O of 1:2. The presence of silicon ions is greater than the tetrahedral aluminum ions, with the SiO_2: Al_2O_3 ratio greater than 2:1 (Mumpton, 1977). Quadrivalent silicon is replaced by trivalent aluminum, creating a positive charge deficiency to become negatively charged. A balance among charges is achieved through the addition of mono- and di-valent cations (Mumpton, 1977). The cations (or co-ions) which leave the zeolite's framework are replaced by an equivalent amount of counter-ions (HMIs). In order to meet its electro-neutrality requirement, when the counter-ion moves out into solution, the zeolite is left with an electric surplus charge to be compensated by taking up another counter-ion; the total counter-ion content (in equivalents) remains constant, regardless of ionic composition (Helfferich, 1962, p. 250).

Significant properties of zeolite, which vary depending on the source and type, include: physical (bulk density, specific gravity, CEC, SSA, void volume, pore radius), chemical (LOI, Si/Ai ratio), adsorption/ion-exchange (Si/Al ratio, selectivity), mineralogical and morphological (XRD, SEM/EDS), thermal (temperature resistance, stability, conductivity, heat capacity), acidic

stability (electronegativity equalization), crystal structure (chain, sheet, framework), framework structure (Si/Al ratio; CEC, channel dimensions, void volume, specific gravity) and surface structure (hydrophobic, hydrophilic) (Jha and Sigh, 2016). The conjugated pairs in cation exchanged zeolites are Lewis acids (extra framework protons cations) and Lewis bases (framework oxygens), where the alkali exchanged zeolites are designated as basic zeolites. The Lewis acidity and Lewis basicity in cation exchanged zeolites are affected by various factors, including the Si/Al ratio, bond angles and lengths, the location of Al, the crystallographic sitting of oxygen, as well as the electronegativity of the framework (Huang et al., 1995); the electronegativity referring to the tendency of an atom to attract electrons (Benjamin, 2010, p. 227). The *Si/Al ratio* influences the amount and distribution of the Si-O-Al groups within the crystalline structure. The greater the ratio, the more Si-O-Si than Si-O-Al linkages, which change the geometrical structure (bond angles and lengths around acid sites) of the zeolite. This influences the degree of H^+ adsorption selectivity and electrostatic potential and binding interaction strength of cations (i.e., HMI) on negative charge sites in the crystalline framework (Jha and Sigh, 2016). The Si/Al ratio in clinoptilolite is relatively high (4.25-5.25) (Breck,1974; Ouki and Kavanagh, 1997), which corresponds to a low volumetric capacity and relatively weak ionic field within the structure; such that the electrostatic interactions are not as significant as the hydration free energy. Therefore, the metals with the highest free energy of hydration (i.e., lead; –357.8 kcal/g·ion) (Inglezakis et al., 2003) should prefer to remain in dissolved form. The selectivity order is influenced by both physico-chemical and stereo-chemical factors (i.e., hydrated radii, cation hydration enthalpy, and micropore space requirements). The rejection of water molecules is related to the hydration enthalpies of the cations, which may explain the high selectivity of lead (Inglezakis et al., 2005). The analysis of natural zeolites for the treatment of mixed metal-contaminated effluents by Ouki and Kavanagh (1997) showed that based on the hydration energies, the selectivity series for the metals considered should be Pb > Cd > Co >Zn > Cu; with the greater selectivity of lead in keeping of the research presented in the Dissertation document.

There is a wide variety of zeolites, which depend on the environment from which they are derived. Their behaviour is dependent upon various factors, including the framework structure, cation species' nature (i.e., size, shape, and charge), the external electrolyte shape and solution ionic charge, cation species and solution concentration, as well as temperature (Mumpton, 1977;

Wang, 2010). The *clinoptilolite* zeolite mineral type is related to the heulandite category, as part of Group 7 ($T_{10}O_{20}$ units), with greater potassium and slightly greater silica contents. Like heulandite, its structural organization are sheets that are connected by bonds, of which are comparatively separated in a monoclinic crystal structure; contains 39% void volume, as well as an approximate specific gravity and ion-exchange capacity of 2.16 and 2.54 meq/g, respectively (Mumpton, 1977). Its framework structure consists of three channels. Channels A and B are 12-membered (0.75×0.31 nm) and 8-membered (0.46×0.361 nm) tedrahedral rings respectively, are parallel to each other. The third channel C is an 8-membered (0.47×0.28 nm) tedrahedral ring that intersects channels A and B (Çakıcğlu-Ozkan and Ülkü, 2008). **Figure 1.1** provides a view of the clinoptilolite structure, and its relationship with a counter-ion (i.e., HMI) to its framework.
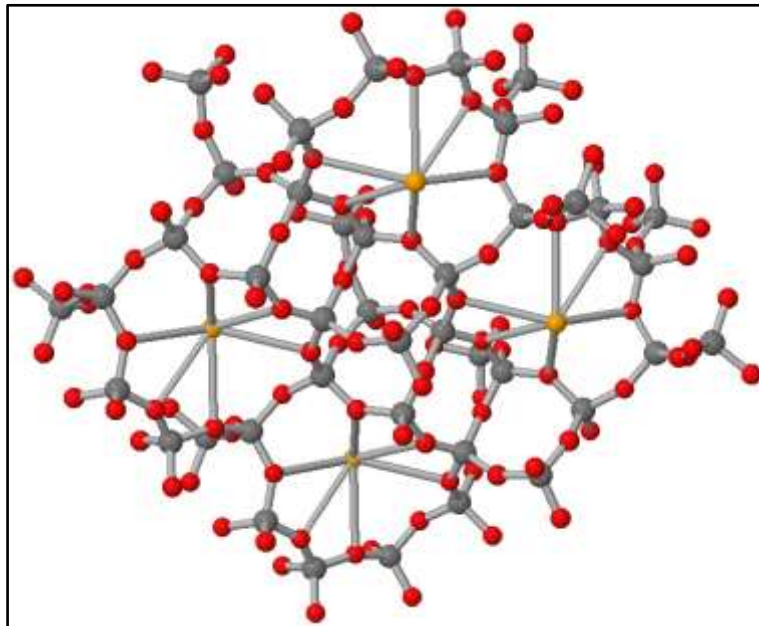
Figure 1.1 Relationship of the Clinoptilolite Framework and a Trapped Cation
(adapted from University of Liverpool, 2017)

The structure of zeolite is divided into three components (Mumpton, 1977; Wang, 2010): (1) alumino-silicate framework, (2) interconnected void spaces in a framework containing exchangeable cations (co-ions), and (3) zeolitic water (water molecules as an occluded phase) present at 10-20% (Margeta et al., 2013) of the dehydrated phase of the natural zeolites' structure. In addition, zeolite is comprised of various phases: (1) zeolite and the external sorbate solution, (2) molten salt and zeolite at equilibrium, and (3) the 'solvent vapour' (water), a thermodynamic reference point with profound effect on the reaction (i.e., attainment rate and exchange position at equilibrium). There are both thermodynamic and kinetic aspects to ion-

exchange, being a stoichiometric process between the phases to maintain electro-neutrality. The chemical reaction involves cations initially present in separate phases moving between two phases until equilibrium within each phase is achieved (Bekkum et al., 1991). Available exchange sites have been referred to as 'two-way traffic in a one-way street' (Helfferich, 1962, p. 186). The amount of solvent that the crystalline is able to uptake depends on the internal volume, defined by the lattice channels' width and intra-crystalline voids, and on the volume occupied by counter-ions found in solution.

The co-ions within the framework significantly influence the sorption and thermal properties of the zeolite (Çakıcğlu-Ozkan and Ülkü, 2008; Yörükoğulları et al., 2010). Three water types are recognized in zeolite: (1) water with crystal-water-like bonds, (2) water bound to the lattice by OH-bonds, and (3) 'typical'/zeolitic water (able to freely move into and out of the lattice without disruption (Van Reeuwijk, 1974). Water molecules occupy the large central cavities and entry channels (Ovsyuk and Goryaœnov, 2006; Çakıcğlu-Ozkan and Ülkü, 2008), which form hydration spheres around the exchangeable cations. The crystal structure of zeolite possesses a considerable void space within its simple, polyhedral building blocks and within larger frameworks formed by several polyhedral blocks. The pore sizes differ, ranging from 3-10 Å (Breck, 1974; Jha and Sigh, 2016), depending on the structure, channel and cavity systems, as well as effective entry opening (Mumpton, 1977). A considerable amount of water is given off continuously and reversibly by heating from room temperature to approximately 350°C. When water is removed, cations fall back into positions on the inner surface of channels and central cavities of the zeolite structure. Thermal/Dehydration treatment of zeolite is an endothermic process (Mumpton, 1977), which significantly impacts the mineralogical properties and specific sieve action requirements of the mineral; sorptive properties of the mineral depending greatly on its cell dimensions. Activation of 'stable' species (i.e., clinoptilolite) is often accompanied by discernible lattice deformations and phase transformations. The leading mechanism of the dehydration process refers to the reaction enthalpy; the sum of the energies required for the sub-reactions involved (i.e., volatilization of water (breaking bonds with cations), diffusion of water through the channels, re-arrangement of lattice), and depends on the temperature and water vapour pressure of the process (Van Reeuwijk, 1974). Dehydrated zeolite typically achieves void volumes of up to 50% (Mumpton, 1977). Given that water is selectively adsorbed by natural zeolite, it slows the sorption rate of the other molecules (Yörükoğulları et al., 2010).

In addition to global abundance, existing literature has shown that natural zeolites are resilient towards chemical, biological, mechanical or thermal modifications (Margeta et al., 2013). Most importantly, natural zeolites have a relatively high cation exchange capacity (CEC) (depending on its Si/Al ratio) (Nezamzadeh-Ejhieh and Shirzadi, 2014) and good selectivity (Inglezakis et al., 2002; Gunay et al., 2007), which are strong attributes for the removal of heavy metals (Ersoy and Celik, 2002).

1.2.2. Sorption – Adsorption and Ion-Exchange Capacity

Natural zeolites exhibit high adsorption of heavy metals in aqueous solutions, due to their combined adsorption and ion-exchange properties (Wang and Peng, 2010). They are able to neutralize acidic wastewater, as well as be regenerated and reused (Kocasoy and Sahin, 2007); which make them a favourable material for industrial wastewater loaded with heavy metals (Babel and Kurniawan, 2003). The term *sorption* refers to every type of capture of a substance from the external surface of solids, liquids or mesomorphs as well as from the internal surfaces of porous solids or liquids. It is a reversible phenomenon that depends on factors such as the molecular size, swelling pressure, sieve action, solution concentration, and temperature (Helfferich, 1962) and is classified as (Inglezakis and Poulopoulos, 2006, p. 31):

- Physical (Physiosorption) – no exchange of electrons occurs but rather intermolecular attractions between favourable energy sites and is independent of the electronic properties of the molecules involved;
- Chemical (Chemisorption) – exchange of electrons between specific surface sites and solute molecules, forming a chemical bond; stronger and more stable than physiosorption; and
- Electrostatic (Ion-Exchange) – attractions between ions and charged functional groups.

Adsorption, in particular, is referred to as the separation process where specific components of one phase of a fluid transfers onto the surface of a solid adsorbent. Adsorptive molecules transport through macropores to the mesopores and finally enter the micropores, where the micropores establish a majority of the internal surface and represent most of the total pore volume (Inglezakis and Poulopoulos, 2006, p. 33). This process involves molecules from a liquid phase that bind in a condensed layer onto a solid surface. The quantity adsorbed depends on temperature, pressure and composition of the solution (Masel, 1996). Zeolites possess unique adsorption properties, characterized as a synthetic molecular sieve. Large central cavities and

access channels are filled with water molecules to form hydration spheres around the exchangeable cations at normal conditions. Conditioning is achieved when water is removed by heating the material to 350-400°C for a few hours to overnight. The molecules with effective cross-sectional diameters small enough to pass through the channels are promptly adsorbed in both the dehydrated channels and cavities. Molecules that are too large to pass through the channels are excluded, demonstrating its molecular sieving property (Mumpton, 1977).

Ion-exchange capacity of zeolite is defined by degree of substitution of aluminum for silicon in the framework structure; the exchange of ions between a liquid and solid phase. The greater the substitution, the greater charge deficiency, such that a higher number of alkali or alkaline earth cations become required for electrical neutrality (Mumpton, 1977). Pure ion-exchange occurs at equimolar concentration, such that the ratio of the HMI(s) bound to the sorbent material and released should be equal to unity (Mohan and Chander, 2006). Ion-exchangers, such as zeolites, are able to uptake charged ions from the solution and release an equivalent amount of other ions into the solution. This ability is attributed to the charged framework in specific locations in the solid structure or in functional groups. This charge is balanced by the counter-ions that move in the framework and are replaced by other ions of equal charge (Inglezakis and Poulopoulos, 2006, p. 34). A major attribute of zeolites is their ability to exchange ions with external medium through an iso-morphous approach. This is expressed by the following **Equation 1.2** (Wang, 2010).

$$z_B A^{Z_A^+} + z_A BL_{Z_B} \rightleftharpoons z_A B^{Z_B^+} + z_B AL_{Z_A} \tag{1.2}$$

where z_A and z_B are the valences of respective cations, and L is the proportion of the zeolite framework holding unit negative charge. The solid phase (exchanger) is charged and balanced by the ions of an opposing charge, known as counter-ions. The exchanger containing ions A is immersed in the liquid phase (solution) containing ions B. Diffusion takes place due to the considerable concentration imbalance between the exchanger and solution; ions A diffuses out from and B diffuses into the exchanger. Equilibrium is established once the ions stabilize the existing concentration variation. Most importantly, it is the active charge of the solid phase that is directly related to the ion-exchange capacity of the solid phase in the system. The fact that the structure of natural zeolite contains exchangeable cations (Na^+, Ca^{2+}, Mg^{2+}, K^+) (co-ions) which are relatively innocuous to the ecosystem promotes its

13

potential in tertiary treatment of industrial wastewater (Vukojevic Medvidovic et al., 2006; Gaikwad et al., 2011).

The removal of HMIs is attributed to both adsorption (on the surface of the sorbents' micropores) and ion-exchange (through the sorbents' framework pores and channels) mechanisms (Curkovic et al., 1997). Both are a mass transfer process from a fluid to a solid phase, and the total charge sorbed and desorbed is explicitly the same as required by the electro-neutrality principle (Helfferich, 1962; Inglezakis and Poulopoulos, 2006). It is important to note that ion-exchange is very similar to sorption; however, it is a stoichiometric process where for every ion removed, another ion is replaced in the release into solution (Inglezakis and Poulopoulos, 2006, p. 34). *For practical applications, it is generally accepted to collect adsorption and ion-exchange as sorption for a unified treatment process* (Helfferich, 1962; Inglezakis and Poulopoulos, 2006).

Inglezakis (2005) reviews theoretical considerations and experimental methods, and distinguishes several types of capacity with respect to zeolite systems. The research demonstrates the need for unified terminology and standardized methodology in regards to zeolite capacity studies, and enforces that further contributions must be theoretically investigated and experimentally proven. The complexity in addressing 'real exchange capacity' when determining the concentration of exchangeable cations present in the sorbent is discussed. Inglezakis (2005) concludes by bringing the attention to metals, where they are not only exchanged but also adsorbed and precipitated onto the exchanger's surface. This presents a greater challenge when addressing zeolite capacity, such that it becomes the sum of both the active ion-exchange and adsorption sites. Inglezakis (2005) highlights the capacity terms defined by IUPAC as follows:

- Theoretical (Specific) – number of ionogenic groups per specified amount ion-exchanger;
- Apparent/Effective – number of exchangeable counter-ions per specified amount of material;
- Practical (Specific) – total amount ions taken up per gram ion-exchanger under specific (given) conditions; may be lower than the theoretical amount if conditions prevent full exchange;
- Useful – when equilibrium is unattainable, and;
- Breakthrough – utilized in column operations.

The theoretical exchange capacity refers to the maximum exchange level, and is expressed by the amount of exchangeable cations in a specific, fixed quantity of the mineral; which can be derived from its elemental composition (Oter and Akcay, 2007). Specifically to zeolites, there are no separate ionogenic groups. The tetrahedral lattice of SiO_4 and AlO_4 are common with their oxygen atom, providing a trivalent aluminum negative electric charge. This charge is balanced by alkali and alkaline earth cations and do not occupy fixed positions, but rather are free to move in the lattice framework such that the counter-ions are replaced by other cations. Consequently, the negative charge of zeolite is not localized but rather uniformly distributed and constant, known as the 'framework charge' (Inglezakis, 2005). Also expressed by Oter and Akcay (2007), the negative charges are compensated for by incorporating the cations (co-ions), which are not part of the actual tetrahedral framework, but rather exist in the internal channels. As the crystalline lattice absorbs the solution into its channels, one cation may be exchanged for another without influencing the mineral structure or electro-neutrality.

The apparent/effective capacity (including useful and breakthrough capacities; Inglezakis, 2005) is of more practical importance, as it refers to the amount of exchangeable cations of zeolite contained in a specific amount of the material (Oter and Akcay, 2007), which balance the 'framework charge' (Inglezakis, 2005). This capacity is dependent upon the experimental conditions, which include: (1) liquid-volume-to-solid-mass ratio (dosage), (2) batch systems (agitation rate and contact time), (3) column systems (volumetric flow rate and breakpoint concentration), and (4) temperature and normality (ionic concentrations) (Inglezakis, 2005). This points to the unique nature of natural zeolites and thereby generates a necessity to redefine the term 'capacity'. As such, Inglezakis (2005) proposes the following capacity terminology shown in the **Figure 1.2**. Based on the proposed terminology, the analysis showed the following capacity series: $TEC \geq REC \geq MEL \geq OC \geq EC, BC$. The research conducted has applied particular experimental conditions, contributing to the overall unified terminology predicament of the practical capacity category.
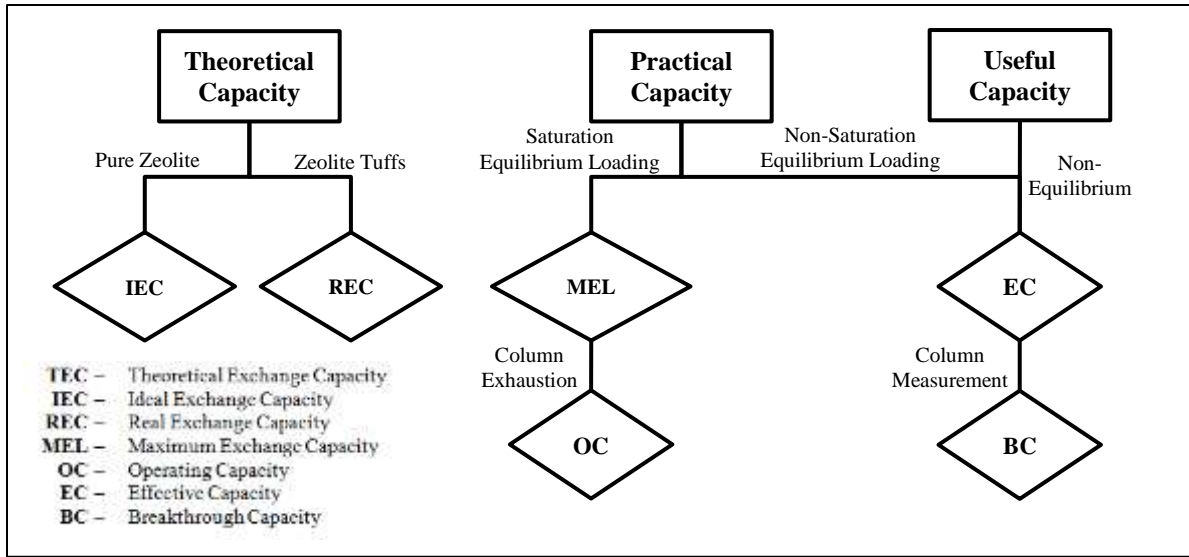
Figure 1.2 Capacity Terminology Considerations (adapted from Inglezakis, 2005)

The challenge to define 'real exchange capacity' is due to associated impurities and subsequent experimental errors. The inconsistency of experimental procedures and detection methods among researchers generates considerably inadequate comparability for a given system. *Consequently, the overall underlying message to the research stresses the importance of a proper experimental procedure and the further development of unified terminology*. The research presented in the Dissertation should be recognized as a '*proof-of-concept'*, as it contributes to the collection of data to further advance the understanding of these terminologies.

1.3. Selection of Experimental Influent Stock

The influent stock is of great importance to the experimental program in this research project. Existing literature targeting heavy metal removal introduce the discussion with an emphasis on the importance of the various industrial wastewater effluent streams previously described, which evidently all contain diverse constituents in solution. Previous studies have investigated the treatment capacity of zeolites with *synthetic simple solute solutions* or *simulated acidic mine waters* that are prepared by combining and dissolving various heavy metal analytical grade salts, with anions such as chloride, nitrate or sulphate, with either tap water or distilled water. However, research in the remediation of *actual industrial wastewater* is still very limited (Xu et al., 2013).

Table 1.2 provides a summary of several relevant literatures that showcase the various types of influent stock investigated in the removal of HMIs. In review, there is a distinct variety in the source and type of sorbent material used, experimental configurations, analytical methodology as well as the targeted heavy metals of interest. Although diverse in the design of their respective experimental programs, these literatures have concluded a comparatively consistent HMI removal trend. The review by Babel and Kurniawan (2003) reports a trend of Pb > Cd > Cu > Co > Cr > Zn > Ni > Hg, while Wingenfelder et al. (2005) states Pb > Cu, Zn > Cd,Sr > Co and Pb > Cd > Cs > Cu > Co > Cr > Zn > Ni > Hg; additional trends summarized in the **Table 1.2**. *This consistency of trends contributes to the persistent great interest by the scientific community, and importance of the methodical combination of the selected heavy metals investigated by the study presented in the Dissertation document.*

Table 1.2 Existing Trends in Influent Stock, Zeolite Material and Heavy Metals of Interest

Influent Stock Solution	Zeolite	HMI		Removal Trend	Reference
Synthetic Simple Solute	American 85-95% Clinoptilolite	Lead Iron Copper	Zinc Nickel	Pb >> Fe > Cu > Zn >> Ni	*This Study*
	American Zeolite (Clinoptilolite and Chabazite)	Lead Copper Zinc Nickel	Cadmium Chromium Cobalt	Pb > Cu > Cd > Zn > Cr > Co > Ni	Ouki and Kavannagh (1999)
	Mexican 70% Clinoptilolite	Lead Cadmium	Chromium Phenol	Pb > Cd > Cr	Vaca-Mier et al. (2001)
	Brazilian Zeolite (Scolecite)	Copper Zinc Lead	Nickel Cobalt Cadmium	Cu > Zn > Pb > Ni > Co > Cd	Bosso and Enzweiler (2002)
	Greek Zeolite (Natural Clinoptilolite)	Copper Cadmium Chromium	Nickel Zinc	Cu > Cr > Zn > Cd > Ni	Alvarez-Ayuso et al. (2003)
	Greek Clinoptilolite	Lead Copper	Iron Chromium	Pb > Cr > Fe > Cu	Inglezakis et al. (2002, 2003, 2004)
	Turkish 70% Clinoptilolite	Cobalt Copper	Zinc Manganese	Co > Cu > Zn > Mn	Erdem et al. (2004) Wang and Peng (2010)
	Ukrainian 75% Clinoptilolite	Lead Copper	Nickel Cadmium	Pb > Cu > Cd > Ni	Spryskyy et al. (2006)
	Sardinian 40–70% Clinoptilolite	Lead Copper	Cadmium Zinc	Pb > Cu > Cd $\cong$ Zn	Cincotti et al. (2006)
	Lignite	Iron Manganese Zinc		Fe > Zn > Mn	Mohan and Chander (2006)
	Turkish Clinoptilolite	Lead		---	Gunay et al. (2007)
	Turkish (Aegean) Clinoptilolite	Copper Iron Zinc		Cu > Fe > Zn	Kocasoy and Sahin (2007)
	Turkish Zeolite (Clinoptilolite and Heulandite)	Lead Zinc	Copper Nickel	Pb > Zn > Cu > Ni	Oter and Akcay (2007) Wang and Peng (2010)
	Turkish Zeolite	Copper		---	Aydin and Saygili (2009)
	Serbian Clinoptilolite	Lead Zinc		Pb > Zn	Nuic, Peric, Trgo, Vukojevic Medvidovic (2006-2016)
Simulated Acidic Mine Water	Slovakian Zeolite	Lead Cadmium	Zinc Iron	Pb > Fe > Zn > Cd	Wingenfelder et al. (2005)
	Turkish Clinoptilolite	Iron Zinc	Copper Manganese	Fe > Zn > Cu > Mn	Motsi et al. (2009)
Actual Industrial Wastewater	Turkish (Aegean) Clinoptilolite	Lead Copper Iron	Nickel Zinc	Cu > Zn > Fe	Kocasoy and Sahin (2007)
	Synthetic Zeolite	Lead Copper Iron Zinc	Nickel Arsenic Chromium	Fe > As > Pb > Zn > Cu > Ni > Cr	Rios et al. (2008)
	Fly Ash Zeolite	Lead Copper Iron Nickel Zinc	Barium Manganese Strontium Cadmium Chromium	Pb > Cd > Zn > Cu > Fe > Ni > Ba	Prasad and Mortimer (2011)
	American Clinoptilolite	Zinc Copper Iron	Aluminum Manganese	Fe > Al > Cu > Zn > Mg > Mn	Cui et al. (2006) Xu et al. (2010, 2012-2014)

The sorption of HMIs in multi-component systems is considered intricate due to solute-solute competition and solute-surface interactions (Wilson, 1994), and the complexity in the interpretation of these systems are influenced by the pH, HMI ionic radii, electronegativity, as well as active site availability on the sorbent material itself (Mohan and Chander, 2006). In addition, the existence of HMIs in industrial wastewater effluents is site-specific, and the concentrations differ and fluctuate extensively (Wilson, 1994). This is demonstrated in **Table 1.3**, which provides a summary of diverse industrial wastewater effluents, and evidently vast variations of metal concentrations. Helfferich (1962, p. 201) points out that for multi-component systems, the exchange rate may vary for the various counter-ions of HMIs in solution, with the possibility that the concentrations of certain species in either the sorbent or solution may fluctuate prior to attaining its balanced state. This reiterates that real-life fluctuations of HMIs in industrial wastewater effluents are widespread.

Confounding factors, such as the sorption phenomena, interactions along the migration pathway, or non-seasonal features, have an overriding impact on many industrial wastewater stream characteristics (Wilson, 1994). The Canada-Wide Survey of Acid Mine Drainage (Wilson, 1994) is based on a census of 30 mines from data acquisition of 75 stream records located across Canada. Various mine types, such as copper-zinc and nickel-copper, and waste from different sources that include mine water, tailings pond water, seepage/runoff/streams, tailings effluent, and treatment/collection systems, are reported. Based on metal processing mines at the time of this survey, the metals commonly found in acid mine drainage streams include lead, copper, iron, nickel, zinc, arsenic, cadmium, cobalt, aluminum, and manganese. This survey also reports that copper concentrations tend to be highest in the spring and lowest in the fall (both moderate trends); iron (weak trend) and lead (strong trend) concentrations tend to be highest in the winter; zinc concentrations tend to be highest in the spring (weak trend) and lowest in the summer and fall (strong trend). A moderate trend towards the occurrence of the highest concentration of sulphate occurs in the winter, and a strong trend towards the occurrence of the lowest concentration in the spring (Wilson, 1994). In addition to HMIs, other constituents such as the variations in minerals, micro-organisms, and (weather and seasonal) temperature all influence the quality and quantity of industrial waste streams (Motsi, 2010). A survey by Dinardo et al. (1991) selected acidic mineral effluents in Canada that contain high metal concentrations of copper, lead, zinc, nickel, aluminum, total iron and sulphate. The Canadian

19

Minister of Justice Metal Mining Effluent Regulations outline the authorized limits of deleterious substances (Schedule 4) (CMJ, 2014), for arsenic, cyanide, lead, copper, lead, nickel, and zinc. This regulation also highlights the need for effluent water quality monitoring based on the concentrations of aluminum, cadmium, iron, mercury, selenium, ammonia, and nitrate. Lead in particular is considered an acute toxic priority (OHSA, 2014). Due to a greater presence in Ontario mines presented by Wilson (1994), the strict limitations required by the Canadian Government (CMJ, 2014), and most importantly, the metals of persistent toxic concern as emphasized by the Great Lakes Water Quality Agreement 1978 amendment, *this research study focuses on the presence of lead (Pb^{2+}), copper (Cu^{2+}), iron (Fe^{3+}), nickel (Ni^{2+}) and zinc (Zn^{2+}) ions that are commonly found in industrial wastewater effluents.*

A majority of previous research on sorption capacity of zeolite has investigated synthetic simple solute solutions spiked in single-component systems, and has demonstrated greater removal compared to investigating actual industrial wastewater effluents (Motsi et al., 2009; Xu et al., 2013). *However, there is still a disparity in research that limits the understanding of sorption capacity by zeolite for heavy metals and the associated mechanisms when in various multi-component systems* (Inglezakis et al., 2003; 2004). Additional research is needed to address this research gap on HMIs in their simultaneous sorption, and to quantify the uptake interference by zeolite of these HMIs in combination (Borandegi and Nezamzadeh-Ejhieh, 2015); in order to utilize the mineral's potential in tertiary industrial treatment processes (Vaca-Mier, 2001) for technology development.

A well-referenced review by Wang and Peng (2010) highlights the recent developments of natural zeolites as adsorbents in water and wastewater treatment, where the influent characteristics (i.e., synthetic, simulated or actual wastewater) vary substantially. With this in mind, it is important to note that the mining industry reference pertaining to the four chapter manuscripts embodied in the Dissertation document does not preclude the fact that the findings are also transferable to other industries and applications. The synthetic simple HMI solute permitted the analysis in a *controlled environment for improved quantification, and identification of the important trends* established by the dual-column system prototype; which was the fundamental goal and major contribution of this research project.

Table 1.3 Metal Concentrations of Various Industrial Wastewater Effluents (mg/L)

Metal	Batter Factory Waste Sample[a]	Electrolytic Copper Industrial Wastewater Tank Sample[b]		British Columbia Highway 97C Acid Rock Drainage[c]	Typical Gold Mine Wastewater[d]	Wheal Jane Mine[e]	Electroplating Rinse Waters[f]	Pretreatment Requirement for Discharge to POTW[f]	Copper Production Plant Scrubber[g]
		Equalization	Neutralization						
pH	3.8-5.8	---	---	---	7.4	---	5-12	5.5-12	1.81
Pb	4.0-13	2.4	3.8	---	0.140	---	0.7	2	---
Cu	<0.0033-0.38	404	1806	0.17	5.063	12	3	3	0.65
Fe	0.02-20	42.5	206	0.82	0.114	200	---	---	---
Ni	0.07-0.38	78.3	436	---	---	---	3	2.5	0.01
Zn	0.6-17	49.5	307	101.2	0.042	85	2	5	18.4
Cd	0.02-0.12	---	---	---	---	1	0.5	0.5	0.73
As	---	---	1.9	---	7.35	9	---	1	---
Cr	<0.0044-0.08	---	---	---	---	---	3	2.75	---
Co	---	---	1.26	---	---	---	---	---	---
Mn	0.04-0.6	---	1.3	10.7	---	15	---	---	0.08
Si	---	---	---	44.2	---	---	---	---	---
Al	0.2-7.0	4.3	---	22.6	---	15	---	---	0.35
Ca	83-255	620	610	204	---	---	---	---	71.7
Na	---	210	565	181	---	---	---	---	9.2
K	---	3.1	6.3	---	---	---	---	---	1.4
Mg	15-26	---	---	52.3	---	---	---	---	22.2
Sb	---	1.8	4.8	---	---	---	---	---	0.25
Sn	---	---	6.6	---	---	---	---	---	---
Se	---	---	---	---	---	---	---	---	1.27
B	---	---	---	---	---	---	---	---	0.12

[a](Yabe and de Oliveira, 2003); [b](Kocasoy and Sahin, 2007); [c](Cui et al., 2006); [d](Acheampong et al., 2009); [e](Motsi et al., 2009); [f](Benjamin, 2010, p.4); [g](Beyazit, 2013)

1.4. Techniques and Challenges of Current Treatment Technology Research

As emphasized previously, heavy metals must be removed by advanced treatment methods prior to discharge (Stylianou et al., 2007a; Stylianou et al., 2007b; Asubiojo and Ajelabi, 2009; Barakat, 2011; Xu et al., 2012; Nuic et al., 2013; Markovic et al., 2015). The advancement of treatment processes requires the development and optimization of new operations that incorporate low-cost raw materials with favourable removal efficiency (Markovic et al., 2015), with an overall simple, resilient and cost-effective strategy (Vaca-Mier et al., 2001; Margeta et al., 2013). However, the feasibility of migration control becomes a challenge due to the site-to-site variability and complex industrial wastewater effluents (Akcil and Koldas, 2006); in addition to the strict limitations imposed by wastewater discharge water regulations (Bektas and Kara, 2004) of local water recipients (Markovic et al., 2015). This is a reoccurring proclamation by all industry that must address effluents which contain heavy metals.

Innovative treatment technologies are a challenge for all related industries, which include but are not limited to high associated economic costs and pollutant specific methods. Consequently, the conversion of inorganic ion-exchangers into hybrid fibrous or nanoscale ion-exchangers is considered to be the latest development of the water treatment industry. These materials are gaining attention, as they demonstrate a high efficiency and rate of sorption with short diffusion path towards environmental pollutants. Among metal-containing nanoparticles, carbonaceous materials and dendrimers, zeolites are considered as one of the most progressive functional and nano-sized materials of the millennium. The prospects of this natural mineral are promising, and its unique position is attributed to its sorption properties particularly through their surface treatment. Nanoscale science and engineering developments are providing extraordinary opportunities to develop more cost effective and environmentally acceptable water purification processes (Chmielewská et al., 2008).

Columns are a convenient approach for industrial-scale treatment applications (Vukojevic Medvidovic et al., 2013), and are frequently implemented in sorption studies such as in Inglezakis et al. (2004), Mohan and Chander (2006), Peric et al. (2009), Aydin and Saygili (2009), and Nuic et al. (2016). The continuous-mode process demonstrates an efficiency in treating large effluent volumes (Nuic et al., 2016), which requires less investment and operational costs, and is more economically feasible than in a batch-mode configuration (Nuic et

22

al., 2016) (i.e., single-stirred tanks, series of mixed vessels) (Cui et al., 2006). The general classification of columns or 'multi-phase reactors' consist of three major categories: (1) trickle bed reactors, (2) fluidized bed reactors, and (3) bubble column reactors (Kantarci et al., 2005). The overall performance and practicality of a reactor is influenced by the sorbent material (zeolite), as well as the efficiency of the sorption process (equilibrium and kinetics); all of which depends on the unsteady state process of the space and time distribution relationship to the mass transfer mechanisms between phases (liquid, solid, gas) (Nuic et al., 2016).

As presented in the packed-bed reactor theory by Nuic et al. (2016), the trickle bed reactor is such that the sorbent material particles are fixed and the concentration gradient is constant (the feed solution with the same concentration enters the column continuously); it is also known as a fixed-bed reactor (FBR). The overall sorption process rate is controlled by mass transfer, and is influenced by the concentration profile over time. The transport into and out of the reactor volume are due to the same mechanisms, which include dispersion (a function of turbulence; random fluctuations in the movement of fluid transport of dissolved and suspended matter) and diffusion (random motion of molecules) (Droste, 1997, p. 244). In a packed bed, the sustained axial flow encompasses diffusion-convection interactions; there is no sustained radial flow and therefore radial molecular diffusion and convective dispersion may be considered independent random motions (Gunn, 1987).The mass transfer process depends fundamentally on: (1) convection (flow of solution through the zeolite layer, a pathway for the binding of HMIs onto the zeolite particle surface), and (2) axial dispersion (flow of solution by-passing around the zeolite particle in the column direction). At the point of inflection, the controlling mechanism changes from convection (through the liquid phase) to dispersion (through the zeolite particle itself). As highlighted by Cui et al. (2006), fixed-bed reactors are at an advantage by providing little axial dispersion, operating very similar to a plug flow (PF) hydraulic regime. In a PF regime, the water flows through the reactor in a series of plugs. There is no transfer of contents between plugs; consistent with vertical and lateral mixing (excluding longitudinal) (Droste, 1997, p. 245). A steady state flow situation exists, and there is no mixing between adjacent planes in the reactor (Droste, 1997, p. 258).

A bubble column reactor is essentially a vessel with a gas distributor at the base, such that the gas is sparged into either a liquid or liquid-solid suspension; known as a slurry bubble

column (SBC) in the presence of a solid phase (zeolite) (Kantarci et al., 2005). The solid phase particles are relatively small in size and are suspended by very vigorous relative motion influenced by the superficial gas velocity (Cui et al., 2006). This reactor category demonstrates excellent heat and (external and internal) mass transfer characteristics (Kantarci et al., 2005; Cui et al., 2006). In comparison to FBR, Cui et al. (2006) demonstrates that a SBC provides a shorter residence time (faster uptake) required for sorption, as well as an ease of sorbent replacement to the column for regeneration.

The process effectiveness of industrial wastewater treatment by zeolite depends on the quality of the clinoptilolite and the initial composition of the effluent (Xu et al., 2014). The critical review of literature has demonstrated the application of numerous natural zeolite deposit sources in the removal technology development of industrial wastewater contaminants such as HMIs; including the United States (Ciosek and Luk, 2017), Mexico (Vaca-Mier, 2001), Serbia (Nuic, Peric, Trgo, Vukojevic Medvidovic, 2006-2016), and Greece (Inglezakis et al., 2001-2010). Margeta et al. (2013) summarizes the chemical composition of natural zeolites from different deposits, expressed as mass fraction of oxide components; which highlight the complex mineralogical composition depending on the country of origin. Once again, the summary of influent stock and zeolite diversity (clinoptilolite source, content and mineralogical properties/quality) highlights the consistency among HMI removal capacity and selectivity trends; which lends to an additional challenge to the unity of terminology (i.e., capacity), *the advancement of source control treatment technology development being a worthwhile pursuit.*

With technical feasibility in mind in terms of operation and maintenance, the treatment method of sorption may be considered expensive compared to current treatment methods. However, the revenue generated from the recovered metals may offset the associated costs and offers significant environmental benefits due to the recovered, reusable form of the metals of interest (Dinardo et al., 1991). In addition, to date, many research efforts have employed zeolite in the various multi-phase reactor configurations described above. *This prompted the motivation to explore a new treatment system configuration that would provide a different perspective on how to remove the heavy metals, with the potential for future optimization in the removal-regeneration-recovery process.*

2. RESEARCH MOTIVATION AND AUTHORSHIP

2.1. Research Objectives and Scope

To date, significant industrial interests have established numerous research groups for the investigation of the natural mineral zeolite as a sorbent material in treatment technology process development; such groups include but are not limited to Inglezakis et al. (2001-2010), Motsi (2009-2010), Nuic et al. (2013-2016), Peric et al. (2004, 2009), Vukojevic Medvidovic et al. (2006-2013), and Xu et al. (2010, 2012-2014). Based on the trends of the critical review presented in **Chapter 1**, the following research gaps define the problem statement that is addressed by this research endeavour:

1. The investigation of the *zeolite mineral in its natural state*, without modification or pre-treatment, as a more industry-viable, environmentally-conscious material alternative in the development of sorption treatment technology;

2. The greater understanding of the *removal capacity by zeolite for heavy metals* and the associated mechanisms and uptake interferences when in *various HMI multi-component systems*, and;

3. The design of a FBR treatment system to incorporate *automation and adaptable modules*.

The fundamental goal of this research project is to investigate the zeolite mineral and the sorption process of HMIs that are commonly found in industrial wastewater effluent, with the development of a sorption system prototype as the fundamental contribution. The scope of this research involves the mineral in its natural state and indicates lead (Pb^{2+}), copper (Cu^{2+}), iron (Fe^{3+}), nickel (Ni^{2+}) and zinc (Zn^{2+}) as the HMIs of interest, to be combined in various (single, dual-, triple-, multi-) component systems. The specific objectives of the study are outlined in **Figure 2.1**, detailing the four journal manuscripts that pertain to the phases of the research project.

Table 2.1 Dissertation Chapters – Research Project Phases and Focus

	DISSERTATION CHAPTER		FOCUS
4	Effects of Operation Parameters on Heavy Metallic Ion Removal from Mine Waste by Natural Zeolite	→	To demonstrate the effects of operation parameters (particle size, sorbent-to-sorbate dosage, influent concentration, contact time, set-temperature, heat pre-treatment) on the sorption process.
5	Lead Removal from Mine Tailings with Multiple Metallic Ions	→	To investigate the systematic increase of HMIs in various (single, dual, triple, multi-) component system combinations. To demonstrate the effects on zeolite selectivity (order) of lead (Pb^{2+}) uptake.
6	Kinetic Modelling of the Removal of Multiple Heavy Metallic Ions from Mine Waste by Natural Zeolite Sorption	→	To investigate the associated mechanisms and rate of the sorption process in various component system combinations. To demonstrate the representation of kinetic models; reaction-type and diffusion-type on the uptake of HMIs by zeolite.
7	An Innovative Dual-Column System for Heavy Metallic Ion Sorption by Natural Zeolite	→	To design and construct a packed, fixed-bed, dual-column sorption system containing natural zeolite. To investigate the performance of the sorption system. To demonstrate the system treatability (i.e., empty bed contact time, breakthrough curve, usage rate).

The major contributions of this research to the scientific community include:

1. A *methodical experimental design* to evaluate removal trends in various HMI component system combinations, furthering the understanding of the effects on the sorption capacity of *zeolite in its natural state*;

2. The kinetic analysis of the sorption rate of the HMIs of interest, that are methodically combined in various component systems;

3. Consistent removal selectivity trends in batch-mode, with the *trend validation* in continuous-mode configuration and supporting literature;

4. The innovative design of a dual-column sorption system prototype, with *proven on-trend removal performance*, and;

5. Exclusive automated, variable-flow prototype configuration with a custom sampling technique potential; a platform for the further *advancement of intelligent process controls*.

The removal of heavy metals and other industrial waste pollutants is regarded as a very complex process. Nevertheless, there is still a great need for continued advances in treatment technology to achieve industry remediation goals and to meet government regulations. *The fundamental contributions of 'proof-of-concept' and the thought-provoking development of technology design in the research endeavour presented in the Dissertation document is certainly a worthwhile pursuit.*

2.2.   Dissertation Structure

This Dissertation is based on a four-phase research project, and is submitted as a manuscript-style document, composed of eight chapters and six appendices. A summary of each chapter is presented as follows:

Chapter 1
A critical review of previous research efforts in the treatment of industrial wastewater of heavy metals with natural zeolite is presented in the introductory chapter, in order to expose existing research gaps and to outline the experimental program.

Chapter 2
This chapter defines the objectives and scope of the research project, as well as proclaim the major contributions to the scientific community. The document structure as well as the statement of authorship are also provided.

Chapter 3
This chapter outlines the fundamental aspects to the experimental methodology and quality control protocol that have been implemented in the research; which present the consolidated 'Materials and Methods' for cohesion in the document.

The following four chapters are the manuscripts that discuss the significant findings of each phase of the research project.

Chapter 4
The effects of preliminary parameters and operative conditions (particle size, sorbent-to-sorbate dosage, influent concentration, contact time, set-temperature, and heat pre-treatment) are demonstrated.

Chapter 5
The selectivity of natural zeolite for lead (Pb^{2+}) ion in the presence of competitive ions is evaluated.

Chapter 6
The modelling of removal kinetics using 'reaction-type' and 'diffusion-type' models is discussed.

Chapter 7
The design and removal performance of a packed, fixed-bed, dual-column sorption system prototype is investigated.

Chapter 8
This chapter presents a summary of the fundamental conclusions of the research project, and the recommendations for further study in the engineering practice are discussed.

Appendices
The appendices provide the details of all the experimental procedures and schedule (A), analytical technology operating procedure (B), as well as technical conference papers (C, D, E). Appendix F highlights a cover featured journal publication that investigates the capacity of natural zeolite to remove nutrients from wastewater; a former research endeavour investigated by the Ph.D. Candidate.

2.3. Statement of Authorship

Amanda L. Alaica-Ciosek *conceived and designed all experiments*, with feedback from Dr. Grace K. Luk. Alaica-Ciosek *designed and constructed* the sorption system prototype, *performed all experiments and analytical simulations*, as well as *analyzed all the data*. The journal *manuscripts were written by Alaica-Ciosek* with input from Luk. The following chapter specifications provide the journal manuscripts and publication details pertaining to this Dissertation document.

Chapter 4
Effects of Operation Parameters on Heavy Metallic Ion Removal from Mine Waste by Natural Zeolite
International Journal of Environmental Pollution and Remediation

Published: 07 February 2018.
doi:10.11159/ijepr.2018.002.

Chapter 5
Lead Removal from Mine Tailings with Multiple Metallic Ions
International Journal of Water and Wastewater Treatment

Published: 19 January 2017.
doi:10.16966/2381-5299.134.

Chapter 6
Kinetic Modelling of the Removal of Multiple Heavy Metallic Ions from Mine Waste by Natural Zeolite Sorption
Water – Special Issue – Treatment of Wastewater and Drinking Water through Advanced Technologies

Journal Citation Reports ® (Clarivate Analytics) Impact Factor: 1.832 (5-Year: 2.056)
CiteScore (Scopus): 2.05; Rankings: 34/88 (Q2) in 'Water Resources' category.

Published: 01 July 2017.
doi:10.3390/w9070482.

Chapter 7
An Innovative Dual-Column System for Heavy Metallic Ion Sorption by Natural Zeolite
Applied Sciences – Special Issue – Wastewater Treatment and Reuse Technologies

Journal Citation Reports ® (Clarivate Analytics) Impact Factor: 1.679 (5-Year: 1.913)
Rankings: 150/275 (Q3) in "Materials Science, Multidisciplinary", 91/166 (Q3) in "Chemistry, Multidisciplinary", and 75/147 (Q3) in "Physics, Applied" categories.

Published: 05 August 2017.
doi:10.3390/app7080795.

3. EXPERIMENTAL RESEARCH DESIGN

The methodology presented in this chapter is the consolidation of the 'Materials and Methods' subsections pertaining to the four journal manuscripts presented in **Chapters 4** to **7**; as identified in the **Preface** and **Chapter 2**, in accordance with of the manuscript-style structure of the Dissertation document.

3.1. Experimental Methodology

Table 3.1 outlines the fundamental experimental factors (i.e., analytical method, sample size, contact period, cleaning cycle, etc.) that were kept constant throughout the experimental work.

Table 3.1 Established Experimental Factors throughout Analysis

Factor	Description	Reference
Elemental Analysis	Perkin Elmer Optima 7300 ICP-AES *Triplicate Combination*	University of Toronto ANALEST Centre
Sorbent Cleaning Cycle	Sieve Debris – DDW Rinse Moisture – Dry 24 hr at 80°C	Inglezakis et al. (2001)
Filtration	Syringe via 0.45 um Filter	Rice et al. (2012)
Acidification Preservation	pH Level to 2 via HNO_3 acid	Rice et al. (2012)
Agitation Method*	Thermo-Fischer Scientific MaxQ 4450 Orbital Shaker *Triple Eccentric Drive Platform – 400 rpm*	Ryerson University Environmental Engineering Lab
Contact Time (min)*	<5, 10, 15, 30, 45, 60, 90, 120, 180>	Motsi et al. (2009) Sprynskyy et al. (2006)
Sample Volume (mL)*	100	Ouki and Kavannagh (1999) Motsi et al. (2009)

*Chapters 4 to 7 in Batch-Mode Configuration

The various experimental procedures are provided in **Appendix A**. The following subsections elaborate on the zeolite mineral particle size and cleaning cycle, influent stock preparations, as well as elemental analysis selection and sorption capacity calculations.

3.1.1. Sorbent Material

This study employed a natural zeolite mineral sample composed primarily of 85-95% clinoptilolite (CAS No. 12173-10-3) with traces of opaline silica, and is sourced from a deposit located in Preston, Idaho (Bear River Zeolites, 2012; 2017). The natural zeolite sample specifications are provided in **Table A.2**. Typical elemental analysis indicated the presence of various elements, including sodium, calcium, magnesium, and potassium, as well as lead, copper, iron, and zinc. No significant concentrations of toxic trace elements were present in its composition, nor are trace metal elements water soluble. The low-clay content unique to this sample ensured good hydraulic conductivity, low dust content, and a harder and more resistant structure (Bear River Zeolites, 2012; 2017). **Figure 3.1** is a view of the natural zeolite mineral sample employed in this research, as presented in the Dissertation document.
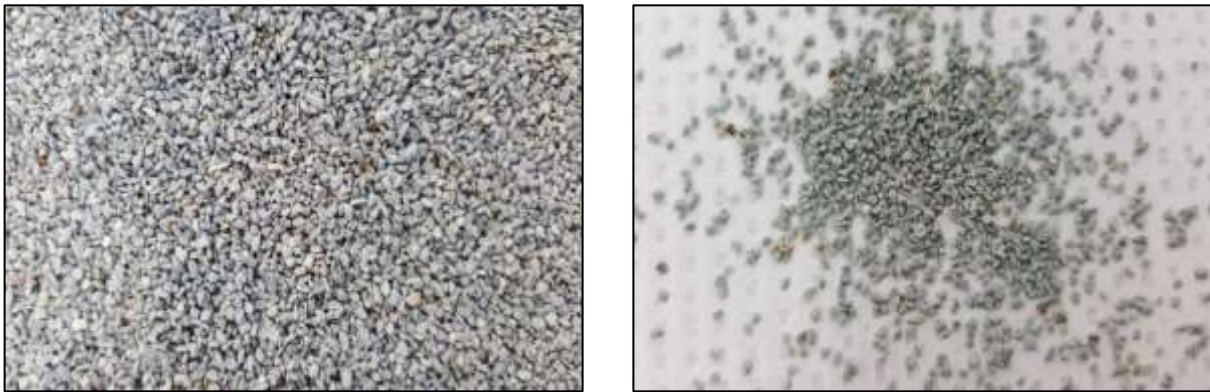
Figure 3.1 Granular View of Natural Zeolite Sample

Preliminary analysis of the raw zeolite mineral supply involved a particle size range within the standard mesh fractions of -8+40, -14+40, and -30+60; discussed with greater detail in **Appendix A.6**. The particle size range from 1.41 mm (pass No. 14) to 0.420 mm (retain No. 40) is divided into sizes A ($d_{p,A}$) (1.190-1.410 mm), B ($d_{p,B}$) (0.707-0.841 mm), C ($d_{p,C}$) (0.420-0.595 mm) and D ($d_{p,D}$) (0.841-1.19 mm); with standard mesh sieves and a mechanical shaker. Overall, these four divisions were selected to provide a distinct variance, based on the approximate distribution of the +14-40 material source, as displayed in **Table 3.2**.

Table 3.2 Preliminary Distribution of +14-40 Zeolite Supply

	Test Sample Size (g)		1006.60
	Sieve Gradations	**Sample Distribution**	
		(g)	(%)
	#14 Retain	76.5	7.60
A	#14 Pass | #16 Retain	200	19.9
D	#16 Pass | #18 Retain	181	18.0
	#18 Pass | #20 Retain	151	15.0
B	#20 Pass | #25 Retain	119	11.8
	#25 Pass | #30 Retain	94.0	9.34
C	#30 Pass | #35 Retain	68.1	6.77
	#35 Pass | #40 Retain	48.3	4.80
	#40 Pass (PAN)	57.9	5.75
	SUM	996.0	98.93
	LOST	10.8	1.07

The particle size operation parameter is investigated in **Chapter 4** of the Dissertation document. All subsequent phases of the research employed the $d_{p,D}$ size exclusively, with a geometric mean diameter of 1.00 mm (Mullin, 2001); which demonstrated the greatest percent yield within the +14-40 source and also, being a broader, coarser size range, is of interest to this study; being a more conservative, viable range. As suggested by the laboratory-scale packed bed system investigations by Inglezakis et al. (2001b), a zeolite fraction of 0.8 mm to 1 mm nominal diameter is recommended for the continuous-mode (columns) to ensure the full exploitation of the material but also to prevent considerable pressure drop during the analysis period.

Low-cost and readily available raw materials without any further economic investment (i.e., pre-treatment) are very useful for any industrial use (Markovic et al., 2015). Therefore, the zeolite mineral sample was applied in its natural state, without any chemical modifications, to minimize all associated costs and environmental impacts of this study. The sieved zeolite was exposed to a cleaning cycle, which involved rinsing in deionized distilled water to remove debris and dust, and drying at 80 ± 3°C (Isotemp® Oven Model 630G; Fisher Scientific, USA) for 24 hours to remove any residual moisture (Inglezakis et al., 2001a).

3.1.2. Sorbate Solution

3.1.2.1. *Heavy Metallic Ion Concentration*

Heavy metals are elements with atomic weights between 63.5 to 200.6, and a specific gravity greater than 5.0 (Inglezakis and Poulopoulos, 2006, p. 24; Fu and Wang, 2011; Tchounwou et al., 2012). They are classified as either: (1) toxic (i.e., Pb, Cu, Ni, Zn, Cd, Cr, Co, As, Hg, Sn), (2) precious (i.e., Pd, Pt, Ag, Au, Ru), or (3) radionuclides (i.e., U, Th, Ra, Am) (Acheampong et al., 2009). Total metals found in industrial wastewater effluents are composed of both dissolved and suspended fractions, defined as dissolved (unacidified sample passing a 0.45 μm filter), suspended (unacidified sample retained by a 0.45 μm filter), and total metals (unfiltered sample defined by digestion (dissolved and suspended) (Rice et al., 2012). *This research focused on lead (Pb^{2+}), copper (Cu^{2+}), iron (Fe^{3+}), nickel (Ni^{2+}) and zinc (Zn^{2+}) metals in dissolved fraction, known in their ionic form as HMIs.*

The simple synthetic HMI solutions were prepared from analytical grade nitrate salts in deionized distilled water, namely $Pb(NO_3)_2$, $Cu(NO_3)_2 \cdot 3H_2O$, $Fe(NO_3)_3 \cdot 9H_2O$, $Ni(NO_3)_2 \cdot 6H_2O$, and $Zn(NO_3)_2 \cdot 6H_2O$, respectively, and combined equally to maintain a total normality of 0.01 N (10 meq/L) (Inglezakis et al., 2002, 2003; Kocasoy and Sahin, 2007); charge equivalents (Benjamin, 2010, p. 13). The NO_3^- anions in the aqueous solution do not influence the ion-exchange process, since they do not form any metal-anion complexes and do not hydrolyze in solution (Peric, 2004; Minceva et al., 2008). The corresponding HMI concentrations are approximately 1036 mg/L for Pb^{2+}, 318 mg/L for Cu^{2+}, 186 mg/L for Fe^{3+}, for 293 mg/L Ni^{2+}, and 327 mg/L for Zn^{2+}; discussed with greater detail in **Appendix A.5** with supporting calculations in **Table A.2**. It is important to note that this study methodically increased the HMI combinations to develop a more comprehensive understanding of how the presence of multiple HMIs influences the sorption process, as follows:

- single-component system – 10 meq/L per metal, (lead [P], copper [C], iron [F], nickel [N], zinc [Z]);

- dual-component system [D] – 5.0 meq/L per metal (lead-copper [D-PC], lead-iron [D-PF], lead-nickel [D-PN], lead-zinc [D-PZ], copper-iron [D-CF], copper-nickel [D-CN], iron-zinc [D-FZ], nickel-zinc [D-NZ]);

- triple-component system [T] – 3.3 meq/L per metal (lead-copper-iron), and;

- multi-component system [M] – 2.0 meq/L per metal (all five metals).

To examine the effect of competitive HMIs in solution, the appropriate mass of its nitrate salt was dissolved to produce a competitive cation concentration of 0.01N; with the concentration ratio (CR) aimed to 1. The CR refers to the ratio of competitive cation concentration to metal concentration, all in the eq/L scale. As ion-exchange is a stoichiometric process, the effect of cations should be investigated under equal normality (CR=1) for all metals and cations (Inglezakis et al., 2005). The removal efficiency order is indicative of how the adsorptive nature of zeolite for each ion varies among the different component systems (Inglezakis et al., 2003). Overall, this selectivity or preference of zeolite for one cation compared to another (at given equilibrium conditions and composition) (Bekkum et al., 1991) is stronger for the counter-ion of higher valence, increasing with dilution of solution and strongest with ion-exchange of high internal molality. The counter-ions' valences affect the 'electro-selectivity' of zeolite. The preference is also stronger for smaller solvated equivalent volumes, and forms stronger ionic bonds with fixed ionic groups (Helfferich, 1962). The cations present in the sorbent have valences that differ from those in solution. Consequently, as the dilution increases, the selectivity of the sorbent for the ion with a higher valence also increases. Accordingly, comparative analysis of various metal ions should be conducted at the same normality and temperature, in order to minimize the changes observed in isotherm configuration with dilution (Inglezakis et al., 2003).

As discussed in **Chapter 1**, the concentrations of HMIs in industrial wastewater effluents are complex and diverse. With that being said, the five HMIs of interest are combined to a total 10 meq/L aqueous solution concentration to maintain an efficient, conservative structure and controlled environment, in order to draw meaningful, quantifiable analysis to this research endeavour presented in the Dissertation document.

3.1.2.2. *pH Levels*

It is important to note that the pH range under which sorption takes place should be specified (Styianou et al., 2007b) and attentively monitored. The removal of multiple HMIs from aqueous solutions by the sorption of natural zeolite is a complex process consisting of predominately adsorption and ion-exchange. However, at a high initial pH, this process could be accompanied by precipitation and the metal ion hydroxo-complexes formed can be sorbed on zeolite surface sites that encompass different sorption affinity (Peric, 2004). Research has demonstrated (Ouki and Kavannagh, 1999; Ersoy and Celik, 2002; Inglezakis et al., 2003) that

the sorbate solution pH affects the uptake of metals, and this is particularly the case for the HMIs that have low preference by zeolite. The uptake mechanism shifts from ion-exchange/adsorption in the acidic region to adsorption/complexation and possible precipitation in the basic region (Minceva et al., 2008). Influential factors include the metal ion speciation and natural stability, as well as the electro-kinetic properties of zeolite in aqueous solutions. At a low pH level, the hydrogen cation (H^+) is considered as a competitive ion to the HMI during the ion-exchange process (Inglezakis et al., 2003). Decationization (exchange of co-cations with H^+ ions) and dealumination of the zeolite structure may occur under acidic conditions (Xu et al., 2014). Evidently, the adsorption/ion-exchange process is preferred at higher pH levels, which should be less than the minimum pH of precipitation (Styianou et al., 2007a) of the respective metal ions (Mohan and Chander, 2006).

The process of adsorption from the sorbate to the surface of the zeolite mineral is followed by ion-exchange, then hydrolysis; which is detected by the pH level and electric conductivity of the sorbent-sorbate solution (Margeta et al., 2013). The pH of the effluent solution decreases, depending on the metal removed (Styianou et al., 2007b); as a function of metal concentration, likely due to two equilibria: (1) ion-exchange, and (2) water hydrolysis (Mohan and Chander, 2006). The two-way reversible relationship between the hydrolysis and hydration of metals is presented in **Equation 3.1**, which is affected by the acidity of the solution (Inglezakis et al., 2003). At a lower pH, the reaction is shifted to the left and more highly charged metal complexes are formed (Inglezakis et al., 2003), with inorganic ligands such as OH^- (Ouki and Kavannagh, 1999); which encourages the sorption processes.

$$[M(H_2O)]^{n+} + H_2O \rightleftharpoons [M(H_2O)_{x-1}(OH)]^{(n-1)+} + H_3O^+ \qquad \text{(3.1)}$$

However, this condition is not favourable as the hydrogen cation is considered as a competitive ion to the targeted HMIs in solution during the sorption process, adversely affecting the overall uptake (Inglezakis et al., 2003). The degree of metal complex formation depends on the pH level as well as the ionic composition and HMI of interest. Accordingly, the metal speciation influences the removal efficiency of the sorbent and the preference for a given metal is affected by the metal complex characteristics (Inglezakis et al., 2003) that predominate at a given pH level (Ouki and Kavannagh, 1999). Since the hydrolyzed cations (co-ions) within in the voids and channels are connected by relatively weak electrostatic bonds to the aluminium-silicate

lattice framework of the zeolite, these co-ions are mobile to exchange with the cations (counter-ions) from the sorbate. The relative size and charge of cations (co-ions, counter-ions), solution cation concentration and ionic strength, temperature and pH level, solvent properties as well as zeolite characteristics all influence the quantity of ions and inevitably the rate of exchange (Margeta et al., 2013).

The natural acidity (controlled only by the hydrolysis of metals and not by the addition of acid) of the respective metal solution and stability constants of metal complexes are significant (Inglezakis et al., 2003). The acidity effects on the uptake of Pb^{2+}, Cu^{2+}, Fe^{3+}, Cr^{3+} investigated by Inglezakis et al. (2003) reports the natural acidities as 4, 3, and 2 for that of Pb^{2+}, Cu^{2+}, and Fe^{3+}, respectively, and determined that the Pb^{2+} ion uptake in particular remained stable in a pH range of 2 to 4; which is an indication of the high preferential level by zeolite. The kinetic study conducted by Kocaba et al. (2007) investigated a pH range of 1 to 10 on the removal of Cd^{2+}, Cu^{2+}, and Ni^{2+}. The sorption percentages were increased sharply after a pH of 4 for all HMIs. The sorption of Ni^{2+} remains almost constant up to a pH of 2, and increased sharply beyond this level. The uptake of Ni^{2+} reached 86.5% at a pH of 6, to a maximum uptake of 91.9% at a pH of 10. The sorption of Cu^{2+} increased sharply after a pH of 4 to reach 75.4% uptake, then increased gradually to 88.9% at a pH of 6 then 97.6% at a pH 10. The pH of 6 was chosen by Kocaba et al. (2007) as the optimum studying pH to avoid precipitation of HMIs. Generally, it was observed that sorption of HMIs increased by increasing the pH value. Most of the HMIs tend to form precipites at pH higher than 6, which limits this process greatly. Bektas and Kara (2004) reported that the removal of lead ions by clinoptilolite occurs by ion-exchange and physical adsorption when the pH level is below 6, and the precipitation of Pb^{2+} ions in the form of $Pb(OH)_2$ increases above this pH level. Therefore, the sorption of HMIs by zeolite is challenging to quantify at a pH level greater than 6, and the actual sorption could be masked by precipitation (Kocaba et al., 2007).

Natural zeolites are known to raise the pH in acidic aqueous solutions, due to: (1) the ion-exchange of H^+ ions, (2) the binding of H^+ ions to the Lewis basic sites linked to the oxygen atoms in the zeolite framework, and (3) the OH^- ions in solution deriving from hydrolysis of some species present in the zeolite (Stylianou et al., 2007a). The pH level of the aqueous solution controls the overall sorption process; adsorption of the HMI at the solid–water interfaces as well

as the ion-exchange of cations within the zeolite structure. Stylianou et al. (2007b) points out that for all minerals, a decrease in the ion-exchange capacity of HMIs occurs for a pH range of 1 to 2. However, very low pH levels may positively influence the sorption process with the hydrolysis of the HMIs in solution (Stylianou et al., 2007a). Also, the pH level may influence the ionization degree of the sorbate (HMI solution) and the surface property of the sorbent (zeolite mineral) (Minceva et al., 2008). The structural stability of the sorbent should not be compromised; for once the pH reaches below 1, the structure of clinoptilolite breaks down in a process termed 'dealumination'. However, zeolites exhibit good structural stability, even in acidic conditions (Motsi, 2010).

Research conducted by Ersoy and Celik (2002) investigated the zeta potential of clinoptilolite, and demonstrates its electro-kinetic properties (i.e., isoelectric point, potential determining point) in aqueous solutions, which are critical to the understanding of adsorption mechanisms of the solid-solution interface. The CEC of clinoptilolite is largely due to the imbalance of charges within the mineral framework. This imbalance is caused by the isomorphous substitutions of Al^{3+} for Si^{4+} in the tetrahedral lattice framework (Oter and Akcay, 2007), which enables some exchangeable co-cations, such as the hydrogen ion, to account for the surface charge. These exchangeable co-cations are able to enter into the channels to compensate the positive charge deficiencies (negative charge) of the mineral lattice. Consequently, the pH level of the system is predicted to affect the sorption behaviour. The potential determining ions were verified to be H^+ and OH^- for the cations of interest. The isoelectric point refers to when the sum of all interactions (i.e., H^+ and OH^- adsorption, dissolved lattice ions distribution, etc.) occurring at the mineral-water interface has a net zero charge. Ersoy and Celik (2002) demonstrated that at a pH level of 2, the zeta potential of the clinoptilolite surface is approximately −18 mV; showing a permanent net negative charge at very acidic conditions, which provides an advantage during electrostatic interactions of inorganic cationic contaminants in wastewater.

At lower pH levels, the HMI is more soluble which favours its removal (Xu et al., 2012). Evidently, the initial pH of the solution must be selected attentively; the aim is to avoid precipitation, for once precipitated, the ions of interest cannot be sorbed (Inglezakis et al.; 2003). Based on the Mine Environment Neutral Drainage (MEND) Program of Canada, typical

wastewater pH levels range from 1.8 to 3.9 in the study of acidic mineral effluents and metals (Dinardo et al., 1991), and a range of 2 to 5 based on the census of the Canada-Wide Survey of Acid Mine Drainage Characteristics (Wilson, 1994). Yabe and de Oliveira (2003) reported a pH range of 3.8 to 5.8 from battery processing effluent, while electroplating rinse waters exhibit a range of 5 to 12 (Benjamin, 2010, p. 4). Evidently, depending on the industrial process, the pH of industrial wastewater effluents vary. *Hence, this research project was conducted in a conservative manner, such that all pH levels documented were on the acidic end for a controlled experimental program in the analysis of the HMI sorption capacity trends.*

The pH level of every sample (stock solution and sorbent-solution contact) was attentively measured for all operation parameters investigated, using the accumet Basic AB15 pH Meter (Fisher Scientific; CAT No. 13 636 AB15). The measurements were conducted before and after contact, and before dilution (following 24 hour storage) preparation for calibration. The influent stock is acidified via commercially high-purity nitric (HNO_3) acid (3 mL 1+1 HNO_3/L sample) (CAS No. 7697-37-2) to a pH of below 2 (Rice et al., 2012); to prevent precipitation of the metal ions (Wang et al., 2009; Inglezakis et al., 2003). Additional trials verified that the filtered and unfiltered HMI influent stock concentrations are the same, indicating both effective dilution practices and complete solubility. Therefore, the concentration of each HMI before and after sorption were exclusively in soluble form. All samples were stored at approximately $4^{o}C$ to prevent volume change due to evaporation; which can be kept stable at ppm levels for up to 6 months (Rice at al., 2012); consistently prepared for all HMI component system combinations.

3.1.3. Analytical Methodology

The analytical detection method of the HMI concentration in samples prior to and after zeolite treatment is crucial to the success of the research performed in this project.

The selection of a preferred analytical method is based on solution chemistry (i.e., potential interferences, site-specific samples) and its efficiency (i.e., re-productivity, time and cost). This complexity is attributed to various factors, such as continuous reliability, solution recycling, routine monitoring, minimal by-products, operation of site-specific climatic conditions, solution chemistry, and discharge requirements (Kuyucak et al., 2013). The analytical method selected is determined by the relevance of the method to Canadian standards (Standard Methods for the Examinatoin of Water and Wastewater, 22nd Edition; Rice et al., 2012), the ease and speed of

detection, the material and equipment costs, and the expected presence of any interfering chemicals.

Analytical methods are categorized as colorimetric and instrumental, which include atomic absorption (AA) spectrometry (flame, electro-thermal, hydride, cold-vapour), flame photometry, inductively coupled plasma (ICP) (atomic emission, mass), and anodic stripping voltammetry (Rice et al., 2012). Among the various atomic spectrometry techniques (i.e., Flame AA, Graphite Furnace AA, ICP-MS), *ICP Atomic Emission Spectroscopy (ICP-AES)* allows the complete atomization of the elements in a given sample, which minimizes the potential for chemical interferences. It is considered as a true multi-element technique with exceptional sample throughput, and with a very wide range of analytical signal intensity (Perkin Elmer Inc., 2011).

Plasma emission spectroscopy offers many advantages, including lower vulnerability to chemical interference (high excitation temperatures), as well as strong emission spectra outcomes for most elements (which provides multi-elemental analysis with simultaneous recording). This method also provides detectable concentration ranges within several orders of magnitude. With the many emission lines that are associated with this source, this is an advantage for qualitative information but does pose a risk for spectral interferences during quantitative analysis (Skoog et al., 2007).

The plasma consists of an electrically conductive cation-electron based gaseous mixture. Argon gas is primarily used, where the ions absorb sufficient power from the external source to maintain extreme temperatures (of up to $10,000^\circ$K), where further ionization indefinitely sustains the plasma state. The ICP is one of three primary types of high-temperature plasmas. Its external source is generated by a torch, which is comprised of three concentric quartz tubes where the argon gas flows. The argon gas consumption occurs at a rate between 5-20 L/min, which varies with the torch design. A water-cooled induction coil surrounds at the top of the largest tube, which is powered by a radio-frequency generator oscillating at 27.12 MHz (Skoog et al., 2007; Rice et al., 2012). The flowing argon is ionized by a spark from a Tesla coil, where the created ions and associated electrons interact with the variable magnetic field created by this coil. The ion-electron interaction causes a flow in the close annular paths, and their resistance cause ohmic heating of the plasma. The heat generated requires thermal isolation of the outer quartz cylinder, which is achieved by the argon flowing tangentially around the tube walls. The torch design is

viewed by both radial and axial geometry. The sample is introduced to the ICP unit through a concentric glass nebulizer and spray chamber, in the form of an aerosol by the argon flowing at approximately 1 L/min (Skoog et al., 2007; Rice et al., 2012).

ICP-AES is applicable to a wide array of elements, which vary in their corresponding detection limits and wavelength lines along the emission spectrum; and is faced with interferences in both the spectral (light emission from spectral sources affect net signal intensity) and non-spectral form (Skoog et al., 2007). Chemical interferences and matrix effects are minimal, but background emissions at low analyte concentrations become an issue when the argon ions significantly recombine with electrons. This issue is addressed by either applicable software auto-corrections or by the operator. Given that the ICP spectrum is abundant for many elements, spectral interferences may arise. Along with a strong spectral line database, current software provides the means to address these issues through wavelength and concentration calibration, spectral analysis, as well as deconvolution of overlapping lines (Skoog et al., 2007) (i.e., data reprocessing).

Based on the single- and multi-component systems of the HMIs selected for this research endeavour, ICP was implemented as the method for elemental analysis (Rice et al., 2012). Mr. Dan Mathers was contacted during experimental design development; who at the time of experimental development and analysis was the Supervisor of the Analytical Lab for Environmental Science Research and Training (ANALEST) (Department of Chemistry – University of Toronto, Canada). The ANALEST centre offers the most current technology with their ICP-AES equipment (Optima 7300 DV, Part No. N0770796, Serial No. 077C8071802, Firmware Version 1.0.1.0079; Perkin Elmer Inc.; Waltham, MA, USA), providing rapid, simultaneous measurement of 5,000 emission lines and dual (axial and radial) views, with corresponding WinLab32 Software (Version 4.0.0.0305). The facility provides an ad-hoc training protocol that is instrument specific, which is required for potential users to access the equipment. Self-directed learning computer modules for the application of interest were completed in December 2014 by the Ph.D. Candidate, which was followed by hands-on equipment monitoring and training (3-hours) by ANALEST staff in January 2015. The Standard Operating Procedure (SOP) compiled for the ICP-AES and WinLab32 Software during this hands-on training is presented in **Appendix B**.

The analyte primary wavelengths of each HMI element targeted are 327.393 (Cu), 238.204 (Fe), 231.604 (Ni), 220.353 (Pb), and 206.200 (Zn), respectively; with Quantifiable Detection Limits (QDL) corresponding to 0.05 ug/mL for Cu, Fe, Ni, and Zn, and 0.10 ug/mL for Pb, respectively (per Dan Mathers, ANALEST, 2015). As a measure of electromagnetic radiation (light photons) emission, the light intensity signal is proportional to the specific element analyte wavelength concentration based on calibration. These wavelengths were selected on the basis that they have the strongest emission and provide the best detection limits.

Analysis was conducted with a plasma setting in radial view (to concentrations of greater than 1 mg/L), auto sampling of 45 seconds normal time at a rate of 1.5 mL/min, and a processing setting of 3 to 5 points per peak with 2 point spectral corrections. The calibration curve was generated by applying a stock blank and a multi-element Quality Control Standard 4 with 1, 10, 50, 90, and 100 mg/L concentrations; as per Standard Methods Part 3000 (Rice et al., 2012). Calibration was conducted through 'linear calculated intercept', and verified 'through zero' that a majority of the trace ions detected are within acceptable QDL levels. Triplicate readings of the HMI aqueous solution and their mean concentrations in calibration units are generated in mg/L by the corresponding WinLab32 Software. The sorbed amount of HMI was calculated from the difference between the starting concentration and its concentration in the 0.45 µm syringe-filtered samples' supernatant.

The sorption capacity is a significant parameter in the batch-mode analyses and kinetic modelling process. Based on the zeolite mass to a 100 mL HMI solution volume, the sorption uptake is calculated by the mass balance expressed by **Equation 3.2** (Inglezakis et al., 2003; Bektas and Kara, 2004; Erdem et al., 2004; Sprynskyy et al., 2006; Gunay et al., 2007; Motsi et al., 2009; Zolgharnein and Shahmoradi, 2010; Beyazit, 2013; Farouq and Yousef, 2015); applied to the capacity calculations of **Chapters 4** to **6**:

$$q_t = \frac{V \times (C_O - C_t)}{M} \tag{3.2}$$

where q_t (in meq/g) is the sorbed uptake of HMI at time t (in min), C_O and C_t are the HMI concentrations in solution (in meq/L) initially and after time t, respectively, V is the solution volume (in L), and M is the zeolite mass (in g).

Qualitative analysis of the natural zeolite was conducted to observe the surface morphology over time, by a high-resolution Scanning Electron Microscopy (SEM) technology (6380LV, JEOL, USA), equipped with Oxford energy dispersive X-ray spectroscopy (EDS) and electron backscatter diffraction (EBSD) capacity; accessed at the Department of Mechanical Engineering of Ryerson University. These images are evaluated in **Chapter 4** and **5** of the Dissertation document. It is important to note that this study focused on the removal of HMIs from solution, of which the variations in concentrations were detected by the ICP-AES equipment as described in this chapter. For analysis of composition, surface properties and minerology, the use of time-of-flight-secondary-ion mass-spectroscopy (TOF-SIMS), X-Ray Fluorescence (XRF), and X-Ray Diffraction (XRD) are required. *Future research on the optimization of the treatment system prototype should incorporate these additional qualitative and quantitative analytical techniques.*

3.2. Quality Control (QC) Protocol

Quality control is of the utmost importance to any and every aspect of research and development. This section to the Dissertation document will point out the substantial efforts made and significant clarifications.

3.2.1. Experimental Sampling and Statistical Considerations

The US EPA document (US EPA QA/G-5S, 2002) established a thorough guide in selecting a sampling design protocol. Sampling design (i.e., protocol, handling, quality assurance) is an essential aspect of data collection for the scientific development of decision-making. The key objective is to ensure that the data collected is sufficient to draw overall conclusions about the contamination level in the environment; accurately representing the population by the sample(s). Considerations include the appropriateness, accuracy, and quality (i.e., sample collection, handling methods, and laboratory analysis), effect of measurement error, as well as data representativeness to the study objectives.

There are two sampling design techniques: 1) non-probabilistic (judgmental), and 2) probabilistic. For the purposes of this research, the protocol reflects the latter. It consists of the following sampling forms: simple random, stratified, systematic and grid, ranked set, adaptive cluster, and composite. A 'Data Quality Objectives Process' is a systematic planning approach, with seven key steps:

1. State the Problem
2. Identify the Decision
3. Identify the Inputs
4. Define the Study Boundaries
5. Develop a Decision Rule
6. Specify Tolerable Decision Error Limits
7. Optimize Design for Data Acquirement

In order to determine the ideal sampling design, various factors must be taken into consideration:

1. Information Regarding the Process/Area of Concern
   a. Secondary data (previous pilot studies)
   b. Conceptual model (size/breadth and media of concern, variability sources, chemical/physical properties and distribution of contaminant)
2. Data Quality Information
   a. Purpose of data collection
   b. Spatial/Temporal Boundaries
   c. Preliminary variance estimates
   d. Statistical parameter of interest
   e. Tolerance for Potential Decision Errors
   f. Overall Precision Requirements
3. Constraints
   a. Sampling/Analysis
   b. Time/Schedule
   c. Budget

The number of sampling points must be established to ensure a strong (i.e., 95%) confidence level of data correlation to represent the population with respect to the various experimental parameters and conditions to be analyzed. As such, the software spectrometer setting for each ICP-AES sample during every analytical sequence was selected to perform analytical combinations in triplicate. Ideally, it would be to extract three (3) sub-samples in triplicate. Due to budget limitations, the former methodology was applied as the most resource-effective design for the research project.

3.2.2. Validation Check Parameters

Triplicate readings and their mean concentrations in calibration units are generated in mg/L by the ICP-AES software. During every ICP-AES analytical session, several quality control methods were applied, and evaluated to assess the calibration quality (Perkin Elmer Inc., 2010):

1. The triplicate concentrations of the median calibration standard (50 mg/L) (selected as an additional sample to act as a reference point of the data sample set) was within 5% of the known value;

2. The relative standard deviation (%-RSD) was well within the <3% limit recommended; as well as the;

3. The correlation coefficient (CC) of each HMI analyte primary wavelength reported an average very close to unity.

These three parameters verified that the data are relatively accurate, highly reproducible, and the experimental replicates were reliable based on the calibration relationship established.

It is important to note that for purposes of cohesion, the validation of the QC protocol has been consolidated from each manuscript for each chapter study of the Dissertation document.

3.2.3. Influent Concentration Detection Trends

   Appendix A.5 outlines the procedure employed to prepare the HMI influent stock for all (single-, dual-, triple-, multi-) component system combinations. Based on the chemical and physical properties of the selected analytical grade nitrate salts (**Table A.2**), the conversion of the total influent concentration of 0.01 N (10 meq/L) to mg/L for each HMI was determined (**Table A.5**). These theoretical initial HMI concentration values are supported by various research efforts of current literature (Inglezakis et al., 2002; Inglezakis et al., 2003; Inglezakis et al., 2004; Stylianou et al., 2007a).

   It is important to note that the experimentally determined HMI concentrations presented in mg/L varied slightly from those theoretically expected. For all five HMIs combined in the major component systems (single-, dual-, triple-, multi-), the average %-RSD of the experimental initial concentrations was approximately 2.45%, which demonstrates laboratory consistency. Overall, the experimental initial concentrations were approximately 17.3% greater than that of the theoretically expected values. This discrepancy may be attributed to various factors, including the significantly small analytical grade nitrate salt mass (of less than 1 g) required, the trace elements present in the concentrated nitric acid used for acidification, as well as the ICP-AES equipment settings (i.e., argon gas tank pressure, peristaltic pump maintenance, tubing, etc.), standards calibration and sample preparations. Interestingly, the multi-component [M] system combination concentrations had the lowest %-RSD, and were closest to the theoretical influent concentrations; only one 50% (DIL1) dilution for sample preparations is required (**Appendix A.9**). This trend points to the influence of dilution protocol. During every experimental laboratory session, the pH meter, analytical scale and pipettes (0.1-1 mL; 2-10 mL) were calibrated on a standard, routine basis to minimize any associated impacts to the experimental data. Overall, consistency was demonstrated by all calculations conducted and results presented in the Dissertation document.

4. EFFECTS OF OPERATION PARAMETERS

Fundamental components of this chapter were also presented as a paper at the WEAO2017 Technical Symposium ('Industrial Treatment A' Session); referenced in **Appendix D** of the Dissertation document.

Abstract

This study investigates the effects of particle size (0.420-1.1410 mm), dosage (40, 80 g/L), influent concentration (total 10 meq/L, 400 mg/L), contact time (5-180, 270, 360 min), set-temperature ($20\text{-}32^{o}C$), and heat pre-treatment ($200, 400, 600^{o}C$) of natural zeolite on the removal efficiency of heavy metallic ions (HMIs); lead (Pb^{2+}), copper (Cu^{2+}), iron (Fe^{3+}), nickel (Ni^{2+}), and zinc (Zn^{2+}). The sorption process is performed in batch-mode with a 100 mL aqueous solution, acidified to a pH level of 2 with concentrated nitric (HNO_3) acid. For all experimental parameter conditions examined, the removal efficiency order follows: $Pb^{2+} >> Fe^{3+} > Cu^{2+} > Zn^{2+} > Ni^{2+}$; the zeolite mineral exhibits the greatest preference towards the Pb^{2+} ion in all parameter trends. Overall, the removal efficiency is increased with decreasing particle size, as well as increasing dosage, contact time, and set-temperature. The operation is influenced by the studied parameters in the order of: influent concentration > heat pre-treatment level > dosage > particle size > contact time > set-temperature.

4.1. Introduction

The industry holds great interest in the physico-chemical influential factors that dictate sorption efficiency of zeolite; which include particle size, initial concentration, pH level, and contact time. A smaller particle size of the sorbent material provides greater contact surface area, which improves the performance of the sorption process (Inglezakis et al., 2003; Acheampong and Meulepas, 2010); which may be attributed to diffusion as the rate-determining step (RDS) of the overall ion-exchange mechanism in the sorption process (Inglezakis et al., 2003). The effect of the dosage (solid-mass-to-solution-volume) on the uptake of heavy metal ions is well-established. An increase in dosage translates to an increase in the rate of uptake; although the amount sorbed per unit mass decreases, there is a higher availability of active sorption sites which sorb more HMIs from the solution (Motsi et al., 2009).

The initial concentration influences the removal efficiency due to the availability of functional groups on the specific surface to bind with the HMIs. This is primarily the case at higher concentrations, demonstrating a higher overall uptake given that the concentration difference is the driving force to overcome mass transfer resistance to metal ion transport between the solution and the sorbent surface (Acheampong and Meulepas, 2010). The pH influences the dissociation of the sorbent and solution chemistry, and affects surface charge of the sorbents and degree of ionization of different pollutants (Acheampong and Meulepas, 2010). This influence of acidity is particularly the case for HMIs that are in a rather low preference by zeolite; the initial pH must be attentively selected to ensure a balance among all ionic species. The goal is to avoid precipitation; for once precipitated, the ions of interest cannot be sorbed (Inglezakis et al., 2003).

The state of equilibrium is altered throughout the sorption process. Room temperature is preferred for analysis, although higher temperatures are assumed to enhance sorption with increased surface activities and solute kinetic energy (Motsi et al., 2009; Acheampong and Meulepas, 2010). Thermal treatment may enhance the sorption capacity, by removing the 'zeolitic water' present in the framework (Motsi et al., 2009); however, the dehydration of zeolite is an endothermic process, thereby causing 'activation' of the material (Mumpton et al., 1977) to a certain threshold, after which may lead to the structural collapse of the mineral (Motsi et al., 2009).

The contact time is an important factor in the relationship of pollutants and sorbents. The rapid uptake of pollutants and equilibrium is established in a specific and limited period, which demonstrates efficiency of the sorbent for treatment. The mechanism study conducted by Sprynskyy et al. (2006) states that the sorption of HMIs by natural zeolite is a heterogeneous process with three distinct stages: (1) rapid uptake within the first 30 minutes of contact, (2) inversion due to desorption prevalence, and (3) slower increase in uptake. In the kinetic studies conducted by Motsi et al. (2009), the initial stage of rapid adsorption occurs within the first 40 contact minutes; when all of the adsorption sites are available for cations to interact, and when the concentration difference between the influent stock and sorbent–solution interface is very high. Inglezakis et al. (2002) tributes this period to ion-exchange in the micropores on the zeolite particles' surface. The predominance of desorption is most likely caused by slower diffusion of exchangeable cations within the internal zeolite crystalline structure, and consequently these preferred ions occupy the available exchange positions on the zeolite surface. During the third stage, the gradual deceleration of sorption in the micropores is caused by poor access as well as by more intensive sorption in comparison to the particles' surface. All of these factors are significant towards establishing the performance of any sorbent material (Acheampong and Meulepas, 2010).

In feasible treatments of industrial waste, it is essential to classify the degree of influence of each operational parameter on the overall system performance (Inglezakis et al., 2004). Therefore, the objective of this phase of the research project is to assess the sorption capacity of natural zeolite for the removal of the five HMIs selected, combined in various component systems. The operative conditions of particle size, zeolite dosage, influent concentration, contact time, set-temperature and heat pre-treatment level are investigated. This is of great importance, in order to harness the full potential of zeolite in tertiary treatment processes.

4.2.   Materials and Methods

Refer to **Chapter 3** for the consolidated experimental methodology; sorbent material, sorbate solution, and analytical procedure. All analyses are conducted in batch-mode, creating the synthetic simple solute HMI solution in the various component system combinations at a 100-mL sorbate volume.

Table 4.1 summarizes the parameters investigated to determine their influence on the overall removal of the selected HMIs in this study. The heat pre-treatment was conducted by placing the cleaned zeolite into a pre-heated muffle furnace (NEY M-525 SII; Serial No. AKN 9403-108; 120 V; 50/60 Hz; 12.5 A; 1500 W; Barkmeyer Division, USA) at the three selected temperatures of 200°C, 400°C, and 600°C (Motsi et al., 2009), for 1-hour; as outlined in the hydrothermal pre-treatment procedure in **Appendix A.7**.

Table 4.1 Operation Parameters and Conditions

Parameter	Conditions
Particle Size	Single-Component Systems: [P], [C], [F], [N], [Z] **A** *1.140-1.190mm (pass No. 14, retain No. 16)* **B** *0.707-0.841mm (pass No. 20, retain No. 25)* **C** *0.420-0.595mm (pass No. 30, retain No. 40)*
Dosage	Single-Component Systems: [P], [C], [F], [N], [Z] Particle Size: **D** (0.841-1.19 mm) *Dosage: 4 g/100 mL, 8 g/100 mL*
Influent Concentration	Systems: [P], [T], [M] Particle Size: D *Concentrations: total 10 meq/L, 400 mg/L*
Contact Time	Systems: [P], [D-PC], [D-PF], [T], [M] Particle Size: D *Contact Time: 180, 270, 360 minutes*
Set-Temperature	Systems: [T], [M] Particle Size: D Contact Time: 180 minutes *Set Temperature: 20°C, 24°C, 28°C, 32°C*
Heat Pre-Treatment	Systems: [P], [T], [M] Particle Size: D *Heat Pre-Treatment: 200°C, 400°C, 600°C*

4.3. Quality Control (QC) Protocol

For all analytical sessions in this chapter, the triplicate concentration of the median standard (50 mg/L) detected an average of 51.37 mg/L, and is within 5% of the known value; the percent relative standard deviation (%-RSD) reported an average of 0.494%, which is well within the ≤3% limit; the correlation coefficient of each HMI analyte primary wavelength generated an average of 0.9997, which is very close to unity.

4.4. Analysis

4.4.1. Particle Size and Dosage

The particle size and dosage parameters are of paramount significance to this study, as well as to the industry that adopt sorption as a treatment method. **Figure 4.1** displays the uptake of each HMI at 180 minutes of contact with zeolite. As expected, with a reduction in the particle size (d_p) from A to C, the uptake and percent removal increases. This trend is most prevalent for the HMI Pb^{2+}, with a 45.6% decrease in concentration or a 15.2% increase in uptake from $d_{p,A}$ (0.1872 meq/g) to $d_{p,B}$ (0.2157 meq/g). However, this trend is not as prevalent from $d_{p,B}$ to $d_{p,C}$, with only a 3.98% in improved HMI uptake. This may be due to the greater particle size gradation range between $d_{p,A}$ and $d_{p,B}$ specifically, as well as a 40.5% decrease in nominal geometric mean diameter of 1.30 mm ($d_{p,A}$) to 0.77 mm ($d_{p,B}$). Based on the sieve distribution presented in **Table 3.4** of **Chapter 3**, an average of 10% per mesh range was detected for particle sizes B and C. In order to eliminate skater/variability, and to maintain a controlled environment, the particle size selected to observe the other experimental parameters is selected between A and B, denoted hereon in as size D ($d_{p,D}$). Based on these initial observations in the removal trends by particle size, the $d_{p,D}$ was considered a more feasible and conservative range moving forward; with a nominal geometric mean diameter of 1.00 mm (Mullin, 2001).
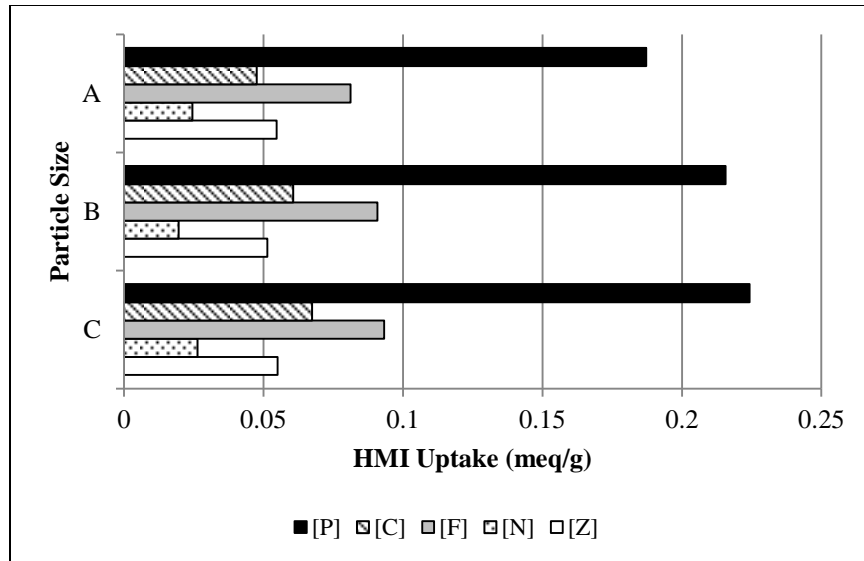
Figure 4.1 HMI Uptake based on Particle Size Parameter

Figure 4.2 displays the overall percent removal of each HMI (in single-component solutions) at 180 minutes of contact with natural zeolite by increasing the sorbent dosage from 4 g to 8 g, for every 100 mL of sorbate volume. As illustrated, when the dosage increases (doubled), the percent removal increases substantially; which is attributed to higher site uptake availability (Oter and Akcay, 2007). The HMI effluent concentration at a contact time of 180 minutes is reduced for Cu^{2+} at 19.9%, Fe^{3+} at 35.9%, and significantly for Pb^{2+} at 82.4%. Additionally, the overall removal efficiency of the selected $d_{p,D}$ falls within the range achieved of $d_{p,A}$ and $d_{p,B}$; demonstrating experimental continuity.
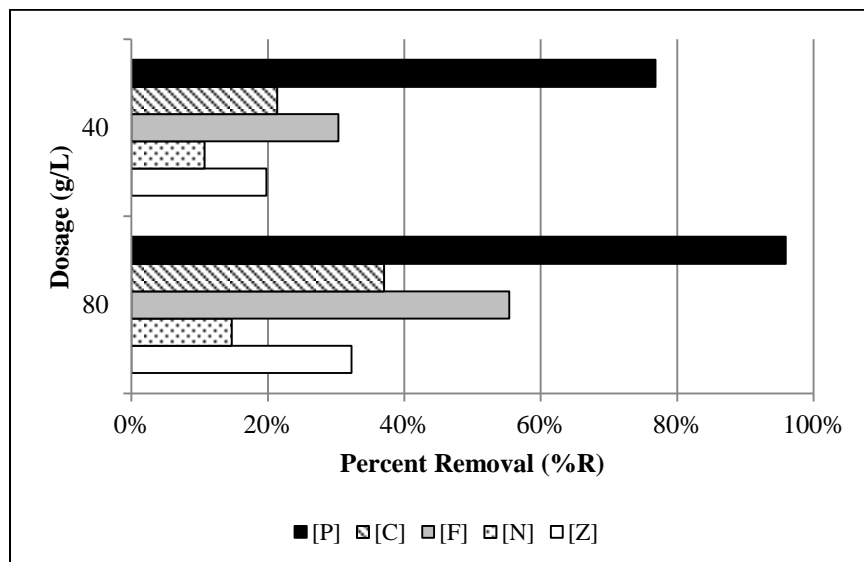
Figure 4.2 HMI Percent Removal based on Dosage Parameter

Kinetic modelling is a powerful tool to assess the performance of sorbent materials and to better comprehend the fundamental mechanisms involved in the sorption process. The sorption rate depends on the amount of ions on the sorbent surface at time t and what is sorbed when an equilibrium state is reached. The models are classified as either reaction-type or diffusion-type (film, intra-particle) (Oter and Akcay, 2007); both models have been thoroughly investigated and have demonstrated strong correlation (Bektas and Kara, 2004; Ho and Ofomaja, 2006; Oter and Akcay, 2007; Qiu et al., 2009).

The reaction-type known as the pseudo-second-order (PSO) kinetic model has well-demonstrated this rate process of various contaminants, including metal ions and organic substances in an aqueous state (Qiu et al., 2009; Jovanovic et al., 2012). This model implies that the RDS is by chemical adsorption (chemisorption). It is represented in **Equation 4.1** and by applying the boundary conditions of $t = 0 \rightarrow q_t = 0$ and $t = t \rightarrow q_t = q_t$, its linearized form is presented in **Equation 4.2** (Sprynskyy et al., 2006; Ho and Ofomaja, 2006; Qiu et al., 2009; Motsi et al., 2011):

$$\frac{dq_t}{dt} = k_2(q_e - q_t)^2 \qquad (4.1)$$

$$\frac{t}{q_t} = \frac{t}{q_e} + \frac{1}{k_2 q_e^2} \qquad (4.2)$$

where $h = k_2 q_e^2$ is the initial sorption rate (in meq/g·min) as t approaches zero (Ho and Ofomaja, 2006), and k_2 is the PSO rate constant (in g/meq·min). These constants are determined by a plot of the linearized form of t/q_t versus t (Ho and Ofomaja, 2006; Qiu et al., 2009). The PSO rate constants and correlation coefficients are summarized in **Table 4.2** and **Table 4.3** for the particle size and dosage parameters, respectively. Based on the linearized form of **Equation 4.2**, the slope (m) and y-intercept (b) values are interpreted to determine the theoretical sorption at equilibrium (q_e in meq/g). The experimental sorption at 180 minutes (q_{180} in meq/g) of contact is also presented.

Table 4.2 PSO – Particle Size Data

System	q_{180}	CC	m	b	q_e
Size A					
[P]	0.1872	0.9840	4.374	216.46	0.2286
[C]	0.0476	0.8193	12.780	1445.40	0.0782
[F]	0.0813	0.9741	11.002	372.35	0.0909
[N]	0.0245	0.9141	31.057	969.75	0.0322
[Z]	0.0548	0.7413	9.569	1420.10	0.1045
Size B					
[P]	0.2157	0.9970	3.856	147.15	0.2594
[C]	0.0607	0.9866	13.611	626.99	0.0735
[F]	0.0908	0.9934	10.190	202.53	0.0981
[N]	0.0196	0.9872	47.121	298.41	0.0212
[Z]	0.0514	0.9623	16.317	795.49	0.0613
Size C					
[P]	0.2242	0.9964	3.783	110.79	0.2644
[C]	0.0674	0.9700	13.942	373.99	0.0717
[F]	0.0933	0.9976	10.067	155.73	0.0993
[N]	0.0263	0.9942	37.924	274.89	0.0264
[Z]	0.0550	0.9646	17.211	430.21	0.0581

Table 4.3 PSO – Dosage Data

System	q_{180}	CC	m	b	q_e
Dosage 40					
[P]	0.1919	0.9926	4.098	217.01	0.2440
[C]	0.0533	0.9291	15.750	836.09	0.0635
[F]	0.0757	0.9708	11.872	419.08	0.0842
[N]	0.0268	0.9806	34.919	739.14	0.0286
[Z]	0.0494	0.9147	15.237	1106.10	0.0656
Dosage 80					
[P]	0.1198	0.9986	7.343	174.00	0.1362
[C]	0.0463	0.9821	17.211	926.12	0.0581
[F]	0.0691	0.9899	12.893	344.90	0.0776
[N]	0.0184	0.9967	50.300	655.14	0.0199
[Z]	0.0403	0.6369	13.507	1771.00	0.0740

As demonstrated by the coefficients (CC), a strong correlation is established for all HMIs for both parameters. For all HMIs on average, the particle size q_{180} reaches the theoretical q_e uptake of 92.3% for $d_{p,A}$, 86.9% for $d_{p,B}$, and 93.5% for $d_{p,C}$; the dosage q_{180} reaches the theoretical q_e uptake on average of 84.3% for dosage 40 g/L and 80.7% for dosage 80 g/L. The particle size

uptake rate trends in **Table 4.2** are systematically consistent; with the $q_{e,[P]}$ within 5% of the theoretical maximum 0.25 meq/g threshold for total HMIs.

The dosage level is not directly proportional to the sorption removal efficiency. The removal efficiency of Pb^{2+} improves from 76.8 to 95.9%; however, the q_{180} uptake has decreased from 0.1919 to 0.1198 meq/g, and the theoretically anticipated q_e uptake at equilibrium decreases from 0.2440 to 0.1362 meq/g, comparing a dosage of 40 to 80 g/L, respectively. This may be attributed to the very rapid uptake of the first stage of sorption. The two HMIs preferred by zeolite in this study exhibit a faster initial sorption rate (h); for Pb^{2+}, the rate increases from 0.0046 to 0.0057 meq/g·min and for Fe^{3+}, this rate increases from 0.0024 to 0.0029 meq/g·min; comparing dosage 40 to 80 g/L, respectively. This finding in conjunction with the lower overall expected uptake at equilibrium demonstrates that the dosage 80 (8 g/100 mL) has reached its threshold of available active sorption sites. A higher removal at a faster rate comes at a cost of consuming more zeolite material; with the dosage 40 (4 g/100 mL) considered more economically feasible (Beyazit, 2013).

In accordance with the fundamental principles of sorption (adsorption and ion-exchange), when intra-particle diffusion (IPD) as considered as the rate-determining step, the sorption rate is proportional to $\overline{D}/d_p^2$; where $\overline{D}$ is the diffusion coefficient of a specific HMI. Since the d_p should not affect either the equilibrium state or the $\overline{D}$, higher sorption rates should be observed for smaller particle sizes. However, smaller particle sizes may exhibit lower rates, due to lower effective $\overline{D}$ values, caused by structural problems or pore clogging (Inglezakis et al., 2004). It is important to note that the natural (as-received) zeolite mineral sample is put through a systematic cleaning cycle, thoroughly washing before use. Therefore, pore clogging is not expected to affect the diffusion coefficients which are considered to be constant regardless of particle size. Then, with intra-particle diffusion considered as the controlling step, the exchange rate should be increased by decreasing particle size (Inglezakis et al., 2004); as demonstrated. *Based on the trends observed under the testing conditions, the ideal levels of these two parameters are selected moving forward in this study.*

4.4.2. Influent Concentration

In addition to maintaining a total 10 meq/L initial concentration, this component of the study is also conducted at 400 mg/L for each HMI, based on the median range of conversion from meq/L to mg/L concentrations for a majority of the HMI investigated throughout this research endeavour; or single-lead [P], triple- [T], and multi- [M] component system combinations (**Table 4.4**).

Table 4.4 The HMI Removal Variation by Influent Concentration

System	HMI	Total 10 meq/L			400 mg/L per HMI	
		q_{180}		%R	q_{180}	%R
		mg/g	meq/g		mg/g	
[P]	Pb^{2+}	23.31	**0.192**	76.8	9.36	95.1
[T]	Pb^{2+}	9.01	0.075	90.2	7.35	79.9
	Cu^{2+}	0.64	0.016	19.0	1.04	11.4
	Fe^{3+}	0.85	0.041	49.5	1.73	18.3
	TOTAL	–	**0.132**	–	–	–
[M]	Pb^{2+}	5.52	0.047	94.0	7.62	79.7
	Cu^{2+}	0.41	0.011	21.9	0.75	8.42
	Fe^{3+}	0.58	0.028	56.2	1.51	15.6
	Ni^{2+}	0.15	0.005	9.10	0.18	1.84
	Zn^{2+}	0.30	0.008	16.5	0.41	4.58
	TOTAL	–	**0.099**	–	–	–

The difference in the removal of each HMI investigated when the influent concentration is set to meq/L versus mg/L is evident. The trends observed are consistent with the literature; the amount in mg of Pb^{2+} ions available for uptake by zeolite decreases, theoretically from 1036 mg/L to 400 mg/L and the amount of the other four ions (in mg) has increased with this conversion of influent concentration. Oter and Akcay (2007) demonstrated consistent findings, as the initial concentration increases, the amount of sorbed HMI increases, while the percent of sorbed HMI decreases for all ions.

Inglezakis et al. (2003) demonstrated that dilution leads to an increase in the volume of treated solution to breakthrough (5-10% of the influent concentration) in continuous column configuration; the magnitude of which depends on the specific metal exchanged. This finding can be attributed to the increase of selectivity in the ion-exchange mechanism of sorption by dilution. The valences of the exchanging cations have a strong effect on ion-exchange at equilibrium, and consequently on the removal efficiency. This attribute is referred to as the "concentration-valency effect". It is theoretically recognized that when the exchanging ions are

not of equal valence, the equilibrium is a function of the total concentration; at higher concentrations, this process prefers the uptake of the lower charged cations and subsequently excludes higher charged cations from the sorbent (Inglezakis et al., 2003). The cations present in the sorbent have valences that differ from those in solution. Consequently, as the dilution increases, the selectivity of the sorbent for the ion with a higher valence also increases. Accordingly, comparative analysis of various metal ions should be conducted at the same normality and temperature, in order to minimize the changes observed in isotherm configuration with dilution (Inglezakis et al., 2003).

4.4.3. Contact Time and Set-Temperature

With [P], [T], and [M] component system combinations at total 10 meq/L influent concentration: (1) the contact time was extrapolated from 3 hours to 4.5 and 6 hours (**Table 4.5**), and (2) the set-temperature was evaluated to an adjusted range of 20 to 32°C at 180 contact minutes (**Table 4.6**).

Table 4.5 The HMI Removal Variation by Contact Time at 22°C Set-Temperature

		Contact Time (mins)					
System	**HMI**	**180**		**270**		**360**	
		q_{180}	%R	q_{270}	%R	q_{360}	%R
[P]	Pb^{2+}	**0.2106**	84.4	**0.2235**	89.5	**0.2299**	92.1
[PC]	Pb^{2+}	0.116	92.9	0.119	95.3	0.120	96.5
	Cu^{2+}	0.025	19.7	0.031	24.9	0.034	27.3
	TOTAL	**0.1405**	–	**0.1500**	–	**0.1546**	–
[PF]	Pb^{2+}	0.109	87.1	0.114	91.7	0.118	94.3
	Fe^{3+}	0.054	43.3	0.060	47.7	0.064	51.5
	TOTAL	**0.1629**	–	**0.1740**	–	**0.1820**	–
[T]	Pb^{2+}	0.076	91.7	0.079	94.7	0.080	96.0
	Cu^{2+}	0.018	21.4	0.022	26.8	0.025	29.8
	Fe^{3+}	0.041	48.9	0.046	55.4	0.049	58.6
	TOTAL	**0.1347**	–	**0.1471**	–	**0.1534**	–
[M]	Pb^{2+}	0.047	95.1	0.048	96.6	0.049	97.3
	Cu^{2+}	0.013	26.4	0.015	30.0	0.016	32.9
	Fe^{3+}	0.029	58.8	0.031	62.5	0.033	67.0
	Ni^{2+}	0.005	9.60	0.005	9.81	0.005	10.0
	Zn^{2+}	0.011	21.6	0.013	25.2	0.014	27.8
	TOTAL	**0.1055**	–	**0.1118**	–	**0.1172**	–

Table 4.6 The HMI Removal Variation by Set-Temperature at 180 Contact Minutes

HMI		Set-Temperature ($^{\circ}$C)							
		20		24		28		32	
		q_{180}	%R	q_{180}	%R	q_{180}	%R	q_{180}	%R
[T]	Pb^{2+}	0.075	90.5	0.076	91.8	0.076	91.8	0.077	92.8
	Cu^{2+}	0.018	21.8	0.019	23.2	0.020	24.4	0.022	26.7
	Fe^{3+}	0.041	49.6	0.041	49.0	0.043	51.8	0.045	53.7
	TOTAL	**0.1347**	–	**0.1366**	–	**0.1398**	–	**0.1442**	–
[M]	Pb^{2+}	0.047	94.8	0.048	95.3	0.048	95.3	0.048	95.7
	Cu^{2+}	0.013	25.4	0.014	27.6	0.014	28.0	0.015	30.0
	Fe^{3+}	0.030	60.0	0.030	60.0	0.031	61.6	0.031	62.8
	Ni^{2+}	0.006	12.7	0.007	13.4	0.007	13.4	0.007	13.3
	Zn^{2+}	0.011	22.0	0.012	24.9	0.013	25.1	0.014	27.3
	TOTAL	**0.1074**	–	**0.1106**	–	**0.1117**	–	**0.1144**	–

When the initial concentration data of **Table 4.4** is compared to the contact time comparison in **Table 4.5** at 180 contact minutes, the removal efficiency is similarly on trend. Only a 5.94% average percent difference in the uptake of total HMIs of [P], [T], and [M] is detected. When this same comparison is made with 20°C uptake of [T] and [M] data of **Table 4.6** (a temperature below the controlled 22°C), only a 4.85% average percent difference in the uptake of total HMIs is detected; these observations demonstrate continuity and repeatability of the experimental procedure. To visualize the influence of both operating parameters, **Figure 4.3** and **Figure 4.4** display the total HMI uptake (meq/g) with respect to extrapolated contact time and set-temperature, respectively.
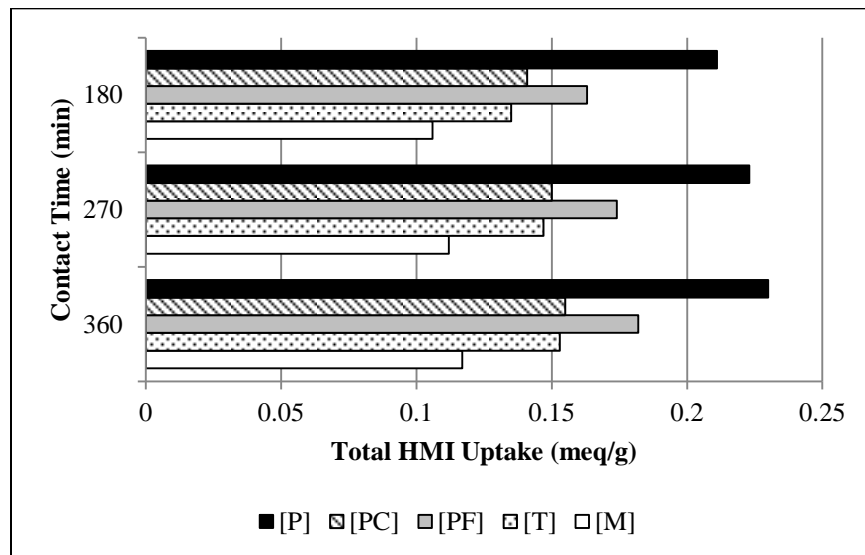
Figure 4.3 Total HMI Uptake based on Contact Time Parameter
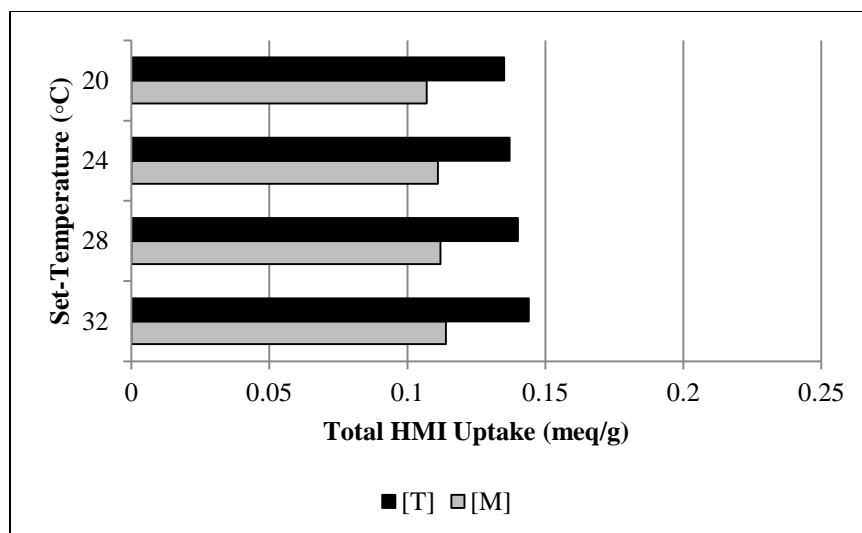
Figure 4.4 Total HMI Uptake based on Set-Temperature Parameter

A greater increase in uptake of the total HMIs occurs from 180 to 270 minutes by, on average 0.010 meq/g compared to 0.006 meq/g from 270 to 360 minutes. This demonstrates the expected proportionality between uptake and contact time. For Pb^{2+}, the theoretical $q_{e,[P]}$ of 0.2440 meq/g by the PSO model (**Table 4.3**) is experimentally supported by the q_{360} of 0.230 meq/g. Research conducted by Oter and Akcay (2007) demonstrates that equilibrium is attained for Cu^{2+} and Zn^{2+} in approximately 6 contact hours, while more rapidly for Pb^{2+} and Ni^{2+} at only 1 contact hour. As such, the uptake threshold quickly approaches equilibrium at 360 minutes of contact.

The results in **Table 4.6** are on trend, with a direct proportionality between the systematic increase in set-temperature and uptake. This supports the fact that the sorbent's structure and surface functional groups are influenced by temperature between 20-35°C, observed by the overall sorption capacity (Sprynskyy et al., 2006). However, the impact of set-temperature is not as significant within this selected range of study conditions.

4.4.4. Hydrothermal Pre-Treatment

The hydrothermal stability of zeolites establishes the operational lifetime of a material, as well as degradation and regeneration conditions (Kostandyan et al., 1982). It is a measure of the structural changes that occur when exposed to water vapour at high temperatures and pressures (Kostandyan et al., 1982). This characteristic depends primarily on the type of zeolite, the Si/Al ratio, as well as the divalent/monovalent ratio and nature of cations entering the framework (Kostandyan et al., 1982; Langella et al., 2003). The total dehydration of zeolite occurs at a temperature that significantly exceeds the boiling point of water. This process is therefore associated with considerable expenditures of energy used to break bonds holding water molecules in the intra-crystalline channels of zeolite as well as to overcome the diffusion energy barrier of water molecules in the crystal framework channels (Kostandyan et al., 1982). The structural changes that occur are influenced by the degree of participation of water molecules in the energy balance of zeolite. Therefore, water molecules positioned in cavities and channels of the framework contribute to the compensation of the non-uniformly distributed charge of the silicate framework and cations. When water is separated from the crystalline lattice, the charge distribution breaks down. This leads to a deformation of the framework and variation in the mobile cations' positions (Kostandyan et al., 1982).

Motsi et al. (2009) investigated the uptake efficiency of natural zeolite for the HMIs of Fe^{3+}, Cu^{2+}, Mn^{2+} and Zn^{2+}. The effects of heat pre-treatment were examined with exposure to a muffle furnace at $200^{o}C$, $400^{o}C$, and $800^{o}C$ for 30 minutes. The pre-treated zeolite was then in contact with the HMIs in single-component solutions for 6 hours. It was observed that the specific surface area is improved when treated at $200^{o}C$. An increase in both the adsorption rate and capacity due to this thermal treatment is caused by the removal of water from internal channels, which leave them vacant. However, this trend is minimized beyond this temperature threshold. The structure collapses and the porosity inevitably decreases. The rate of adsorption by calcined zeolite is faster compared to untreated zeolite, but the efficiency decreases for zeolite exposed to very high temperatures (Motsi et al., 2009).

Water is removed continuously and reversibly, both partially and completely (Kostandyan et al., 1982; Langella et al., 2003), when exposed to heat from air at room temperature. When exposed to heat at approximately 350-400°C (Mumpton, 1977; Breck, 1974; Yörükoğulları et al., 2010), the water is eliminated, and the cations fall back into positions on the inner surface of channels and central cavities of the zeolite structure. Dehydration of zeolite is an endothermic process, thereby causing 'activation' of the material (Mumpton, 1977) between 250-400°C (Kostandyan et al., 1982), at approximately 350°C (Breck, 1974); with a structural stability of up to 750°C (Breck, 1974; Margeta et al., 2013). Research has also revealed that the relationship between the dehydration mechanism of zeolite and positions occupied by aluminum and cations in its structure have an effect on the thermal stability. Thermal treatment of zeolite between 500-600°C causes the loss of one H_2O molecule from two nearby OH^- or one H_2O molecule for every two tetrahedral Al atoms in its structure. This temperature range instigates a loss of oxygen atoms in the framework, producing structural vacancies (Langella et al., 2003). Beyond this thermal threshold, the crystalline structure breaks down and the clinoptilolite becomes an amorphous solid (Breck, 1974; Kostandyan et al., 1982).

Langella et al. (2003) investigated the three thermal behavioural types of zeolites. This work emphasizes that reversible dehydration with minimal framework contraction would be observed upon heating up to approximately 230°C (Type-1) and 280°C (Type-2), while irreversible structural changes hinders rehydration at a range of 230-260°C (Type-1) and 280-400°C (Type-2). Also, heat pre-treatment greater than 450°C (Type-1) and 550°C (Type-2) causes a thermally induced collapse of the zeolite structure. Behavioural Type-3 exhibits continuous reversible dehydration with only very small structural contraction; the framework is not destroyed at an exposure of up to 750°C. High aluminum and alkaline-earth contents give rise to Type-1. An increase in silicon and/or alkaline-earth cations leads to a progressive change in thermal behavior in the order of Type-1 to -2 to -3. The study presented in the Dissertation document is also comparable with the findings of Langella et al. (2003), as the temperature levels analyzed exhibit Type-2 behaviour (Ciosek and Luk, 2017b).

4.4.4.1. Heavy Metallic Ion Pre-Treatment Trends

Table 4.7 provides the HMI uptake at 180 minutes (q_{180} in meq/g) of contact for non-heated and heat-pre-treated zeolite in the triple-[T] and multi-[M] component systems. With each heat pre-treatment level, the same trend is maintained among the various component systems. Once again, for all operation parameters investigated in this study, zeolite has the highest affinity and favoured uptake for Pb^{2+} ion (Ouki and Kavannagh, 1997; Inglezakis et al., 2002, 2003, 2004; Sprynskyy et al., 2006; Ciosek and Luk, 2017a) followed by Fe^{2+} and Cu^{2+}, with a lower affinity for Zn^{2+} then Ni^{2+}. A significant loss in crystallinity and hence catalytic activity are common with this pre-treatment process (Akkoca et al., 2013). Dehydration temperature as well as micropore volume and transitional porosity development are directly proportional (Kostandyan et al., 1982). It is important to increase surface area, porosity and sorption capacities of natural zeolites without crystallinity loss (Akkoca et al., 2013). The percent removal of the Pb^{2+} ion in [M] is 94.0%, while only 56.7% in [M-600]. The percent removal of the total HMIs reduces from 16.5 to 3.68% going from non-heat-pre-treated to $600^{o}C$ exposure. This demonstrates the extreme temperature effects on the zeolite's sorption capacity to the HMIs of interest.

Table 4.7 HMI Uptake (meq/g) by Heat Pre-Treatment Level

Heat Level	Non-Heated		$200^{o}C$		$400^{o}C$		$600^{o}C$	
System	[T]	[M]	[T]	[M]	[T]	[M]	[T]	[M]
HMI								
Pb^{2+}	0.075	0.047	0.073	0.047	0.057	0.040	0.038	0.028
Cu^{2+}	0.016	0.011	0.015	0.011	0.008	0.006	0.006	0.003
Fe^{3+}	0.041	0.028	0.036	0.025	0.024	0.017	0.026	0.017
Ni^{2+}	–	0.005	–	0.004	–	0.004	–	0.003
Zn^{2+}	–	0.008	–	0.008	–	0.004	–	0.002
TOTAL HMI	**0.1320**	**0.0986**	**0.1239**	**0.0937**	**0.0882**	**0.0712**	**0.0703**	**0.0523**

Figure 4.5 displays the effects of each heat pre-treatment level, with respect to the percentage of non-heated zeolite uptake. Evidently, the presence of each HMI in solution impacts the uptake of the other; as seen by the interference of the Ni^{2+} and Zn^{2+} ions to the [M] component system uptake of the Cu^{2+}, Fe^{3+}, and Pb^{2+} ions in the [T] system. Comparing [T] to [M], the uptake of the Pb^{2+} ion is reduced by 36.2, 30.4 and 25.9% at the heat pre-treatment levels of 200, 400, and $600^{o}C$, respectively, and 37.5% without heat pre-treatment. When heat-pre-treated to $600^{o}C$, the total HMI uptake is reduced by approximately 47.0% in both systems.
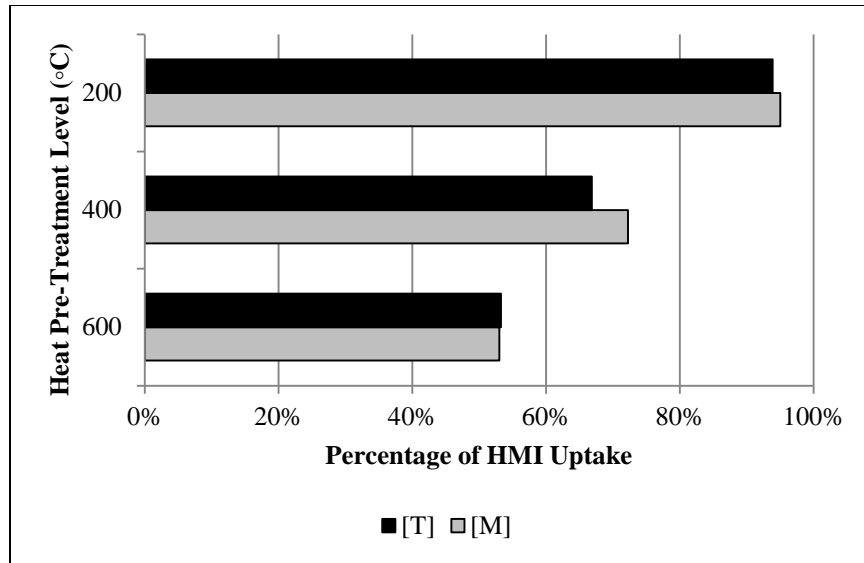
Figure 4.5 Percentage of Non-Heated Level Total HMI Uptake

Figure 4.6 displays the total HMI uptake over the 3-hour contact period for each heat pre-treatment level, for the [T] (4.6.a) and [M] (4.6.b) component systems, respectively. This study is consistent with the three distinct stages discussed by Sprynskyy et al. (2006). As expected, there is a slightly greater uptake in the [T] over time; attributed to the interference of the additional two HMIs in the [M]. The rate of uptake for both component systems is not significantly affected by the 200°C heat exposure. The first 45-minute period is very similar for [M-200], compared to the non-heated. Consistent with the findings of Motsi et al. (2009), a substantial reduction of HMI uptake occurs at the 400°C threshold.
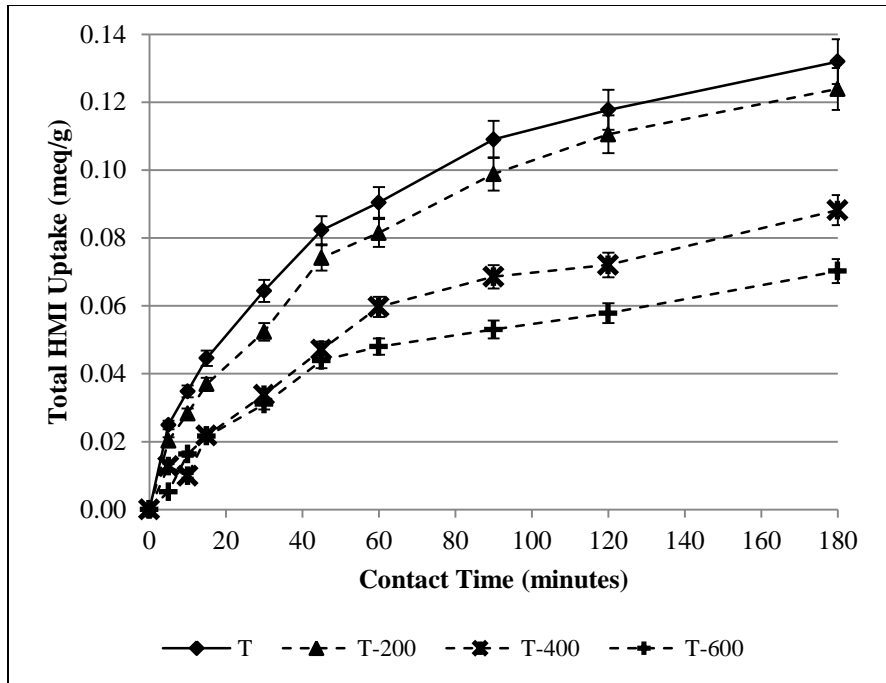
a. Triple-Component System
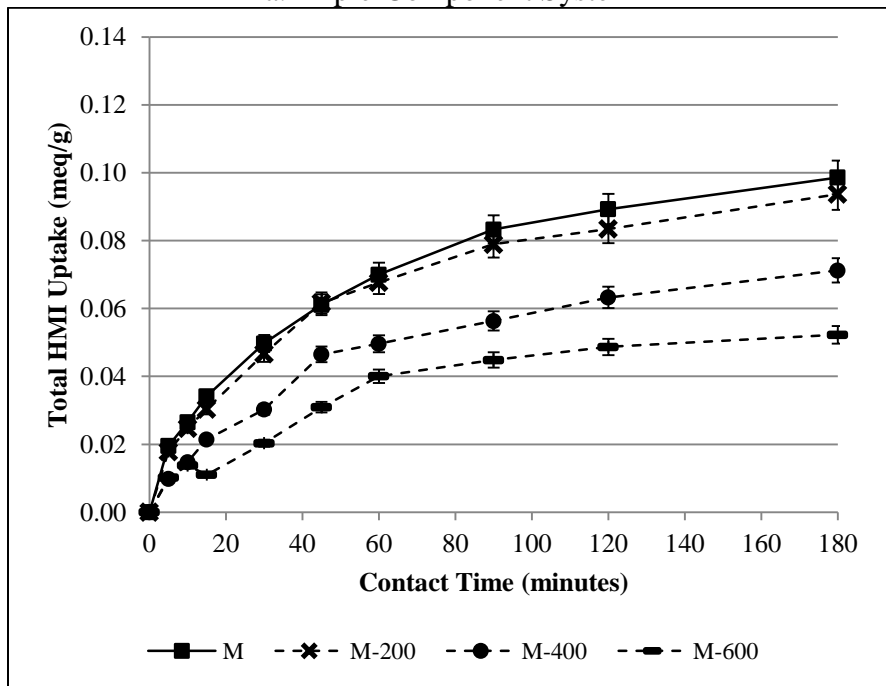
b. Multi-Component System

Figure 4.6 Heat Pre-Treatment Variation of Total HMI Uptake over Time
(adapted from Ciosek and Luk, 2017b)

4.4.4.2. Qualitative Pre-Treatment Trends

Once the cleaning cycle of the raw zeolite sample was complete, the as-received pale green colour was sustained. Following the progressive heat pre-treatment exposure, this colour transitioned to a pink, pale pink, then light brown colour (Ciosek and Luk, 2017b). **Figure 4.7** provides SEM images obtained by the high-resolution microscope, taken at ×5000 magnification (5 μm scale bar). Subtle physical changes of the surface structure are observed when comparing the raw granules (shown in 4.7a) to those exhibited to the cleaning cycle (shown in 4.7b). The images of the zeolite exposed to heat pre-treatment of 200, 400, and 600°C are shown in 4.7c, 4.7d, and 4.7e, respectively. To point out once again, a substantial reduction of HMI uptake occurs within the 400-600°C temperature range of this study (Motsi et al., 2009). The non-heated uptake in [T] and [M] is achieved by 93.9 and 95.0% in [T-200] and [M-200], respectively. This is qualitatively observed in Figures 4.7b and 4.7c, with the visual similarity. The 400 and 600°C exposures are not as texturally complex in Figures 4.7d and 4.7e, respectively.
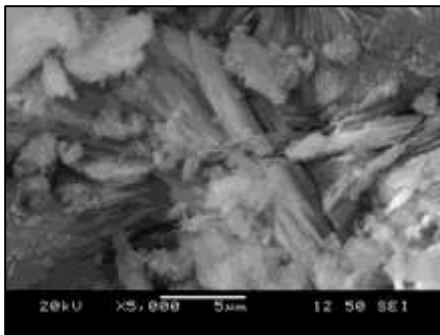
a. Natural Zeolite – As Received   b. Cleaning Cycle
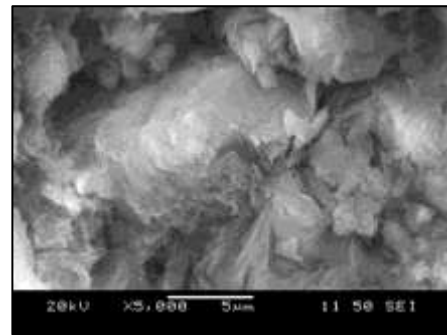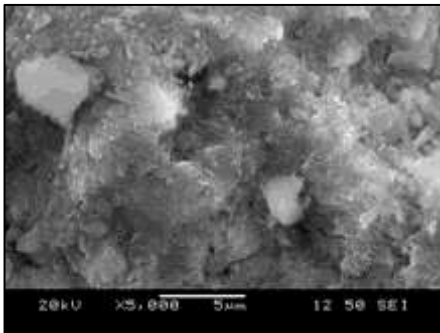
c. Heat Pre-treated at 200°C   d. Heat Pre-treated at 400°C   e. Heat Pre-treated at 600°C
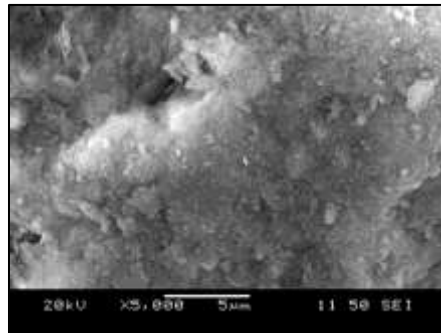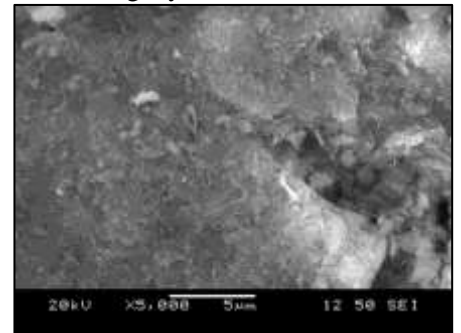
Figure 4.7 SEM Images of Natural Zeolite Exposure to Heat-Pre-treatment
(adapted from Ciosek and Luk, 2017b)

As seen in **Table 4.7**, the sorption capacity is significantly compromised at the 400 and 600°C exposures; which is supported by the lack of textural complexity in Figures 4.7d and 4.7e, respectively. It is visually evident that the raw sample possesses textured granularity and significant detail, which is subsequently diminished with heat-pre-treatment towards the inter-granular spaces and mineral crevasses. This provides additional knowledge into how the structure of the zeolite mineral has been modified. However, the process of dehydration requires a considerable amount of energy, which practically outweighs the interest to 'activate' the structure of the mineral sample. Both the quantitative and qualitative observations demonstrate that there is no economic benefit to the hydrothermal pre-treatment of the zeolite mineral, under the testing conditions.

4.4.5. Acidity Observations

It is important to note that the pH level of every sample (stock solution and sorbent-solution contact) was measured for all operating parameters investigated; utilizing the accumet Basic AB15 pH Meter (Fisher Scientific; CAT No. 13 636 AB15). This was conducted after batch-mode contact, and before dilution (following 24 hour storage) preparation for calibration. The set-up of the initial stock pH was kept consistent throughout all experiments, with an average of 1.85 measured. The average maximum and minimum values between the batch bottle and stored supernatant samples are summarized in **Table 4.8**.

Table 4.8 The Average pH Level Data

	pH Sample	
Observation	**Batch Contact**	**Storage Filter**
Maximum	2.18	2.14
Minimum	1.90	1.89

This data is based on a dosage 40 ratio (4 g/100 mL); excluding the pH observations for the dosage 80 (8 g/100 mL) parameter. At 45 minutes of contact for all HMIs at dosage 80 conditions, the effluent becomes more basic to reach a maximum of just above 2.20. Overall, the samples collected show an average pH maximum and minimum of 2.39 and 1.91, respectively. This level is still quite acidic, and brings attention to the fact that the H^{+} ions are in competition with the HMI of interest. The doubled dosage provides greater active sites availability for sorption to occur. The decision to proceed with particle size D ($d_{p,D}$) as the controlled parameter moving forward in the analysis is once again justified, given that the pH was consistent throughout this study.

65

4.5. Conclusions

The removal efficiency of heavy metallic ions by natural zeolite increases by:

- Decreasing particle size and influent concentration;
- Increasing dosage level, contact time and set-temperature, and by;
- Maintaining the heat-pre-treatment level below the activation threshold.

The efficiency is improved depending on the specific metal and the parameter observed, it can be qualitatively speculated that other heavy metals would be equally influenced (Ouki and Kavannagh, 1997). The removal efficiency order (or selectivity series) is consistent for all examined experimental conditions: $Pb^{2+}>>Fe^{3+}>Cu^{2+}>Zn^{2+}>Ni^{2+}$ (Ciosek and Luk, 2017a; 2017b).

The sorption uptake of HMIs by natural zeolite is complex, due to the aqueous chemistry of the elements and the nature of the sorbent mineral (Oter and Akcay, 2007). However, this research provides a greater understanding into how the presence of multiple metallic ions and various operative parameters impact the overall removal efficiency under the testing conditions, and indicates how the sorption properties of zeolite influence the overall selectivity trends. This is a significant contribution to the current knowledge-base, and how these parameters impact the removal capacity of natural mineral in batch-mode configuration.

4.6. Future Works

This study demonstrates that the zeolite mineral exhibits the greatest preference towards the lead (Pb^{2+}) ion, regardless of how the operation parameters or conditions are altered. This prompts the interest to further investigate how the other HMIs influence the removal of Pb^{2+} when combined, and to further develop a better understanding of the interactive trends associated in the sorption process. Given that lead is considered a designated substance of toxic priority, the focus of this next chapter is of significance to the industry and the peripheral environment at risk.

5. LEAD REMOVAL CAPACITY AND SELECTIVITY

Lead Removal from Mine Tailings with Multiple Metallic Ions

Fundamental components of this chapter were also presented as a paper at the WEAO2016 Technical Symposium ('Industrial Treatment A' Session); referenced in **Appendix C** of the Dissertation document.

Abstract

This study investigates the ionic effects of Cu^{2+}, Fe^{3+}, Ni^{2+} and Zn^{2+} on the sorption of the target metal ion Pb^{2+} by natural zeolite in the form of clinoptilolite. The batch testing configuration consisted of a synthetic nitrate salt solution maintained at 10 meq/L system total concentration, acidified to a pH of 2 by HNO_3 acid, with an adsorbent dosage of 40 g/L. The aqueous solution was agitated for a contact period of 5 to 180 minutes by means of a triple-eccentric drive orbital shaker operating at 400 r/min. The objective is to determine the overall sorption of the target metal lead and the selectivity of clinoptilolite to the various heavy metallic ions (HMIs) combined in aqueous phase. Elemental analysis concludes that after 3 contact hours, the lead ion is removed by 76.8% in the single-lead system. In the dual-lead system, Pb^{2+} is removed by 88.3, 79.5, 89.1, and 88.5% when combined with copper, iron, nickel, and zinc, respectively. Finally, Pb^{2+} is removed by 90.2 and 94.0% in the triple-(lead-copper-iron) and multi-component systems, respectively. As the HMIs are introduced to the system with a 10 meq/L total concentration, the uptake of the Pb^{2+} ion in the single-system of 7.68 meq/L is decreased by 75.6% to 1.88 meq/L in the multi-component system. Overall, the total HMIs removed decreases from 7.68 meq/L in the single-system to 3.95 meq/L with the subsequent addition of ions in the multi-component system.

5.1. Introduction

This chapter focuses on the heavy metallic ion lead (Pb^{2+}). This particular HMI is known as a designated substance, with carcinogenic consequences that affect every organ and system in the human body (OHSA, 2014). Based on the Canada-Wide Survey of Acid Mine Drainage Characteristics (Wilson, 1994), the annual-seasonal average levels for lead (Pb^{2+}) is 0.50 mg/L, exceeding the mean monthly effluent limit of 0.20 mg/L (CMJ, 2014) by 150%. The Occupational Health and Safety Act (OHSA, 2014) has identified lead as a designated substance of acute toxic priority (Kragovic et al., 2013) that poses a great risk to our ecosystem, with carcinogenic consequences that affect every organ and system in the human body (OHSA, 2014). As discussed in **Chapter 4**, the effects of operating conditions investigated in the first phase of the research project demonstrate that regardless of condition, the trend among the five (5) HMIs selected is consistent. Compared to the other HMIs, Pb^{2+} is superior in uptake as it is not composed of complex, hydrated compounds and thereby demonstrates a significantly higher selectivity by clinoptilolite (Ouki and Kavannagh, 1997; Inglezakis et al., 2003). This particular HMI was chosen to further the understanding of zeolite's affinity and selectivity, and how the other HMIs affect the removal uptake when combined.

5.2. Materials and Methods

Refer to **Chapter 3** for the consolidated experimental methodology; sorbent material, sorbate solution, and analytical procedure. All analyses were conducted in batch-mode, creating the synthetic simple solute HMI solution in the various component system combinations at a 4-g sorbent mass to 100-mL sorbate volume dosage.

5.3. Quality Control (QC) Protocol

Several measures were applied to ensure quality control (QC) of the experimental investigations carried out in this study. During the preliminary stages of investigation, all of the batch sorption experiments were conducted twice. Filter separation was investigated with 5 and 180 minutes effluent samples, with a first then second filter pass. Only a maximum of 1.50% difference among the filtered sets was measured, and supports that the agitation method in triple-

eccentric drive for adsorbent-adsorbate contact is effective. These preliminary findings demonstrated that the protocol established is repeatable and moving forward, all other tests were run once per sample. Furthermore, each sample concentration was read in triplicates as set in the ICP-AES system software for validation purposes. Quality control checks were applied to both the calibration standards and the sorption results.

Table 5.1 summarizes the QC checks conducted on the calibration standard of 50 mg/L for the various component systems. The %-RSD values are considerably lower than the 3% targeted limit, and a majority of detected concentrations fall well within 5% of the 50 mg/L theoretical value.

Table 5.1 Calibration Standard 50 QC Check of Various Component Systems

Sample ID	Analyte	%-RSD (Corr Int)	Triplicate Mean (Calib) (mg/L)	Corr Coef
SINGLE [P]	Cu 327.393	0.81	52.98	0.999729
	Fe 238.204	0.90	53.91	0.999745
	Ni 231.604	1.06	54.28	0.999731
	Pb 220.353	0.40	53.87	0.999710
	Zn 206.200	1.36	54.69	0.999675
DUAL [D]	Cu 327.393	0.13	50.78	0.999867
	Fe 238.204	0.19	51.32	0.999909
	Ni 231.604	0.18	51.18	0.999916
	Pb 220.353	0.58	51.43	0.999838
	Zn 206.200	0.19	50.66	0.999960
TRIPLE [T] MULTI [M]	Cu 327.393	0.32	52.12	0.999966
	Fe 238.204	0.45	52.50	0.999953
	Ni 231.604	0.61	52.48	0.999948
	Pb 220.353	0.75	52.06	0.999900
	Zn 206.200	0.96	52.01	0.999968

5.4.   Analysis

5.4.1. Quantitative Observations – Acidity and Heavy Metallic Ion Levels

Table 5.2 provides a summary of the sample preparations involved for elemental analysis. The 'Sample ID' column outlines each component system, and their respective influent stock (S) and contact times, which ranged from 5 to 180 minutes. The number of 50% dilutions are indicated in the column 'DIL', which is required to keep all concentrations within the calibration range of 0-100 mg/L. Based on the established sorbent-to-sorbate ratio of 4 g to 100 mL, the measured 'Zeolite Mass' is provided for each sample. Finally, the 'pH Level' verification results are provided for both directly from sample on the day of zeolite exposure, and the day after of the filtered sample. Following sorbate-sorbent contact, the pH is observed to be steady throughout the ion-exchange process, with a maximum of 0.20 pH difference after 3 contact hours. The pH of the prepared influent stock and filtered effluent are also observed to be consistent during refrigerated storage prior to dilution preparation for elemental analysis.

The quantitative results of the various systems are summarized in **Table 5.3**. The primary wavelengths, given in Column 1, to the ICP-AES model were applied for all five metal ions to generate the Relative Standard Deviation (%-RSD) as shown in Column 3. Triplicate readings and their mean concentrations in calibration units are presented in mg/L, and given in Column 4. Based on the dilution factors presented in **Table 5.2**, the corresponding HMI concentrations and percent removal after 3 hours were calculated and provided in Column 5 and 6, respectively. Overall, the %-RSD values are low and all within $\leq 3\%$, which is indicative that the data are accurate and the experimental replicates are reliable (Perkin Elmer Inc., 2010). A significant observation is made for that of the target metal ion. The overall removal of the lead ion is highest compared to the four other HMI investigated. In addition, this removal level is consistently high regardless of the component system. This is a first glimpse in this study of zeolite's preference for lead, and the overall impact of the presence of the other ions.

Table 5.2 Sample Preparation with pH Level Verification

DIL	Sample ID	Zeolite Mass	Expose	Filter	DIL	Sample ID	Zeolite Mass	Expose	Filter	DIL	Sample ID	Zeolite Mass	Expose	Filter
4	[P]-S	---	---	1.82		[D-PC]-S	---	---	1.87		[D-PN]-S	---	---	1.70
	[P]5	4.0018	1.92	1.84		[D-PC]5	4.0049	1.94	1.89		[D-PN]5	4.0043	1.90	1.84
	[P]10	4.0013	1.94	1.88	**3**	[D-PC]10	4.0063	1.98	1.91	**3**	[D-PN]10	4.0070	1.98	1.93
	[P]15	4.0088	1.95	1.93		[D-PC]15	4.0048	2.01	1.92		[D-PN]15	4.0044	2.00	1.97
	[P]30	4.0042	2.02	1.95		[D-PC]30	4.0072	2.03	1.97		[D-PN]30	4.0036	2.04	2.00
3	[P]45	4.0041	2.03	1.99		[D-PC]45	4.0045	2.08	2.05		[D-PN]45	4.0025	2.09	1.99
	[P]60	4.0084	2.04	1.98		[D-PC]60	4.0069	2.12	2.09		[D-PN]60	4.0072	2.14	2.05
	[P]90	4.0055	2.07	2.01	**2**	[D-PC]90	4.0041	2.19	2.13	**2**	[D-PN]90	4.0068	2.10	2.04
	[P]120	4.0061	2.09	2.01		[D-PC]120	4.0067	2.15	2.13		[D-PN]120	4.0084	2.17	2.10
	[P]180	4.0025	2.10	2.04		[D-PC]180	4.0062	2.18	2.15		[D-PN]180	4.0075	2.18	2.11
2	[T]-S	---	---	1.88		[D-PF]-S	---	---	1.79		[D-PZ]-S	---	---	1.83
	[T]5	4.0083	1.97	1.90		[D-PF]5	4.0061	1.89	1.82		[D-PZ]5	4.0063	1.85	1.85
	[T]10	4.0090	2.01	1.94	**3**	[D-PF]10	4.0076	1.92	1.84	**3**	[D-PZ]10	4.0088	1.94	1.94
	[T]15	4.0073	2.03	1.92		[D-PF]15	4.0088	1.96	1.93		[D-PZ]15	4.0027	1.99	1.97
	[T]30	4.0060	2.07	1.96		[D-PF]30	4.0074	2.01	1.98		[D-PZ]30	4.0068	2.02	2.01
1	[T]45	4.0026	2.11	2.01		[D-PF]45	4.0012	1.99	1.99		[D-PZ]45	4.0081	2.06	2.00
	[T]60	4.0014	2.11	2.03		[D-PF]60	4.0059	2.06	2.06		[D-PZ]60	4.0082	2.14	2.06
	[T]90	4.0005	2.17	2.09	**2**	[D-PF]90	4.0077	2.10	2.08	**2**	[D-PZ]90	4.0045	2.10	2.04
	[T]120	4.0045	2.15	2.08		[D-PF]120	4.0068	2.11	2.12		[D-PZ]120	4.0038	2.15	2.06
	[T]180	4.0073	2.19	2.08		[D-PF]180	4.0075	2.14	2.11		[D-PZ]180	4.0038	2.17	2.10
1	[M]-S	---	---	1.85										
	[M]5	4.0050	1.93	1.90										
	[M]10	4.0082	1.97	1.89										
	[M]15	4.0081	2.00	1.92										
	[M]30	4.0064	2.05	1.99										
0	[M]45	4.0030	2.07	2.00										
	[M]60	4.0071	2.09	1.93										
	[M]90	4.0049	2.10	2.01										
	[M]120	4.0045	2.13	2.01										
	[M]180	4.0076	2.17	2.04										

Table 5.3 ICP-AES HMI Results of Various Component Systems

1	2	3	4	5	6	1	2	3	4	5	6
Analyte	Sample ID	%-RSD (Corr Int)	Concentration (mg/L)		% Removal	Analyte	Sample ID	%-RSD (Corr Int)	Concentration (mg/L)		% Removal
			Triplicate Mean (Calib)	DIL					Triplicate Mean (Calib)	DIL	
Pb 220.353	[P]-S	0.24	75.93	1214.81	76.8	Pb 220.353	[T]-S	1.27	100.05	400.21	90.2
	[P]180	0.59	35.20	281.63			[T]180	0.21	19.66	39.32	
Pb 220.353	[D-PC]-S	0.13	75.47	603.79	88.3	Cu 327.393	[T]-S	1.16	33.76	135.03	19.0
	[D-PC]180	0.59	17.68	70.73			[T]180	1.58	54.70	109.40	
Cu 327.393	[D-PC]-S	0.11	24.18	193.44	12.2	Fe 238.204	[T]-S	0.59	17.23	68.92	49.5
	[D-PC]180	0.61	42.44	169.77			[T]180	1.81	17.40	34.80	
Pb 220.353	[D-PF]-S	0.42	75.98	607.82	79.5	Pb 220.353	[M]-S	0.53	117.76	235.52	94.0
	[D-PF]180	0.54	31.19	124.77			[M]180	0.67	14.20	14.20	
Fe 238.204	[D-PF]-S	0.31	13.01	104.11	37.7	Cu 327.393	[M]-S	1.96	37.58	75.16	21.9
	[D-PF]180	0.45	16.21	64.82			[M]180	0.99	58.74	58.74	
Pb 220.353	[D-PN]-S	0.82	77.16	617.29	89.1	Fe 238.204	[M]-S	2.26	20.52	41.03	56.2
	[D-PN]180	0.68	16.81	67.22			[M]180	1.24	17.97	17.97	
Ni 231.604	[D-PN]-S	0.86	21.05	168.37	7.40	Ni 231.604	[M]-S	0.56	32.87	65.75	9.10
	[D-PN]180	0.12	38.99	155.94			[M]180	1.48	59.76	59.76	
Pb 220.353	[D-PZ]-S	1.01	76.78	614.22	88.5	Zn 206.200	[M]-S	2.23	35.99	71.98	16.5
	[D-PZ]180	0.50	17.68	70.72			[M]180	1.63	60.12	60.12	
Zn 206.200	[D-PZ]-S	0.92	23.46	187.65	11.0						
	[D-PZ]180	0.83	41.75	166.98							

5.4.2. Qualitative Observations

Figure 5.1 displays the SEM images of the natural zeolite taken at ×1000 magnification (10 µm scale bar). The physical changes of the surface structure are illustrated when comparing the raw granules (shown in 5.1a) and those exposed to the cleaning cycle of debris and moisture removal (shown in 5.1b). Once cleaned, the zeolite mineral has greater detailed textured granularity of its inter-granular spaces and mineral crevasses; providing visual evidence that the zeolite has been prepared for the sorption process.

a. Raw Zeolite	b. Cleaned Zeolite
c. 3 hr (M180) Solution Exposure	d. 6 hr (M360) Solution Exposure
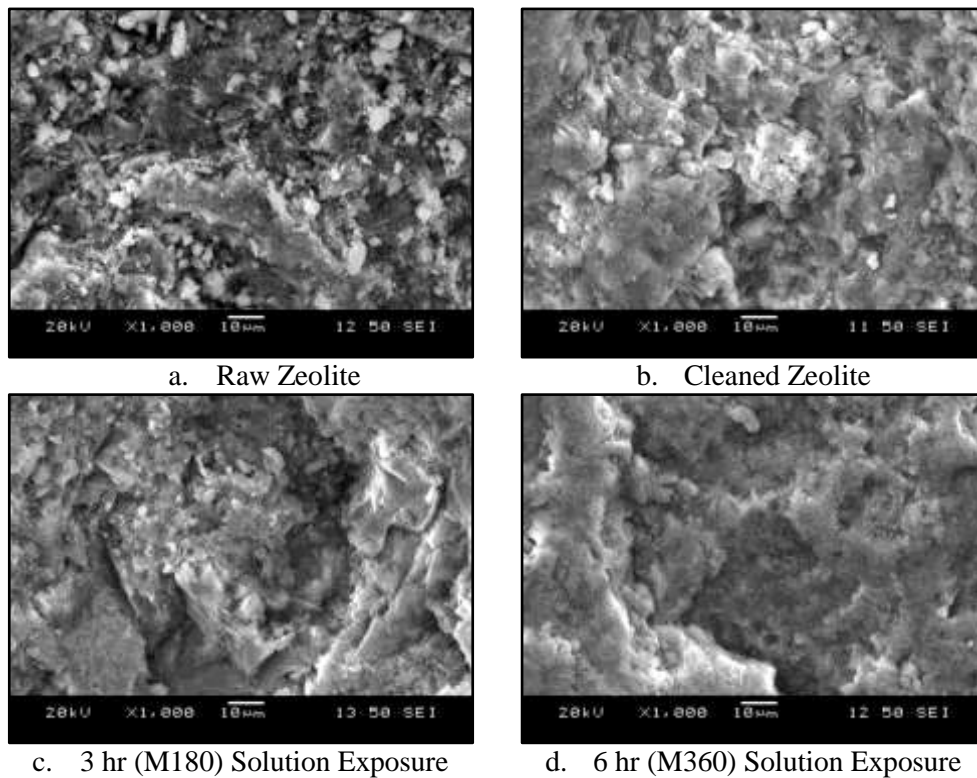
Figure 5.1 SEM Images of Natural Zeolite Exposure to Multi-Component Solution Over Time (adapted from Ciosek and Luk, 2017b)

The images of the zeolite exposed to the multi-component solution containing all metals over 3 and 6 hours of contact are shown in Figures 5.1c (M180) and 5.1d (M360), respectively. The spectrum of x-ray energy versus counts were evaluated by EDS to determine the elemental composition of the samples exposed to the multi-component solution, and presented in **Figure 5.2** based on a 25 μm scale of the samples. As expected, a majority of the zeolite is composed of oxygen, silicon, and aluminum, as well as the co-cations. The presence of lead (Pb) has more than doubled (0.6 to 1.7 Wt%) with the additional 3 contact hours; further solidifying the strong preference of zeolite towards this particular heavy metal.
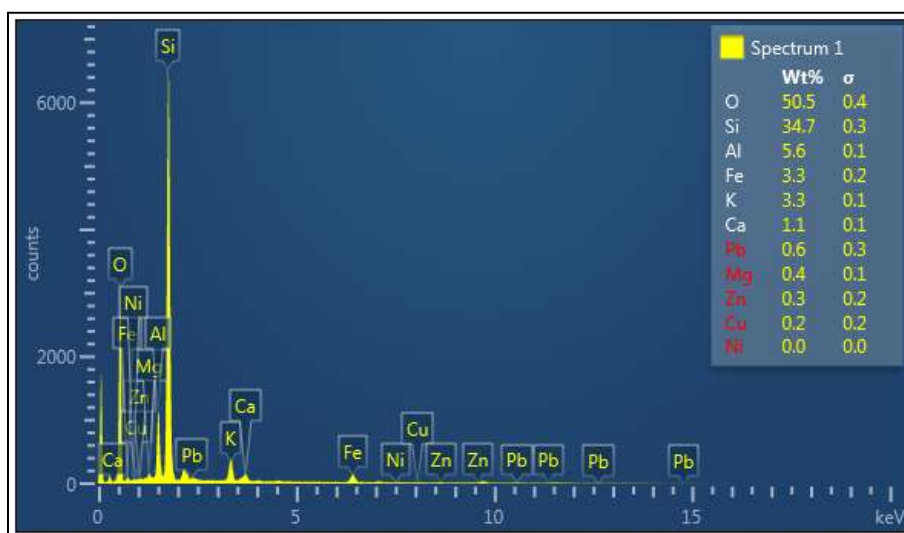
a.   3 hr (M180) Solution Exposure
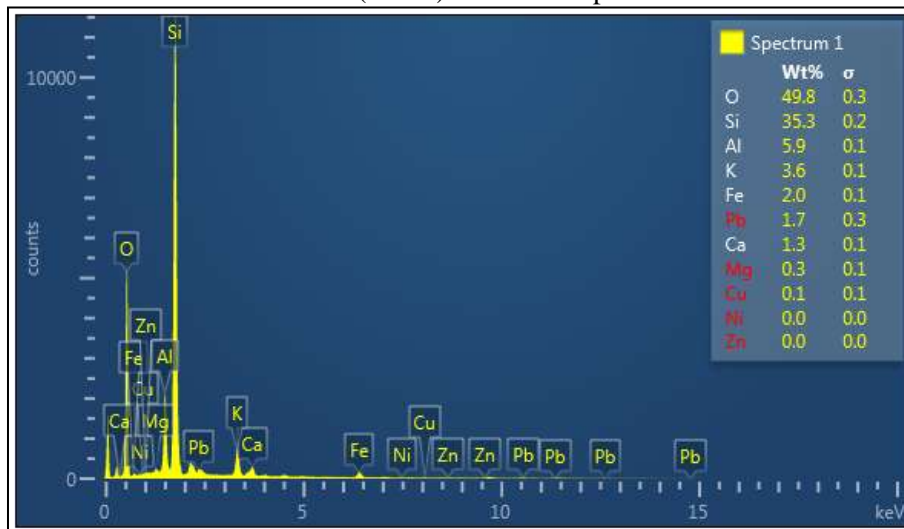
b.   6 hr (M360) Solution Exposure

Figure 5.2 EDS Spectrum of Zeolite Sample Exposure to Multi-Component Solution

5.4.3. Percent Removal by Sorption

Figure 5.3 displays the percent removal trend of lead over time, and how it varies among the various HMI component systems. The elemental analysis results have indicated that after just 3 hours of contact with natural zeolite, the target metal ion lead is removed by 76.8% in the single-lead system. In the dual-lead system, the lead ion is removed by 88.3, 79.5, 89.1, and 88.5% when combined with copper [D-PC], iron [D-PF], nickel [D-PN], and zinc [D-PZ], respectively. The targeted lead ion is removed by 90.2 and 94.0% in the triple-(lead-copper-iron) [T], and multi-component [M] systems, respectively. In the multi-component system involving all five metals, the percent removal observed for Pb^{2+}, Cu^{2+}, Fe^{3+}, Ni^{2+}, and Zn^{2+} are 94.0, 21.9, 56.2, 9.10, and 16.5%, respectively. The corresponding removal trends of each HMI in the [M] system are illustrated in **Figure 5.4**. Zeolite's preference towards each metal ion is also observed in the triple-component system, with percent removals of 90.2, 19.0, and 49.5% for that of Pb^{2+}, Cu^{2+}, and Fe^{3+}, respectively.
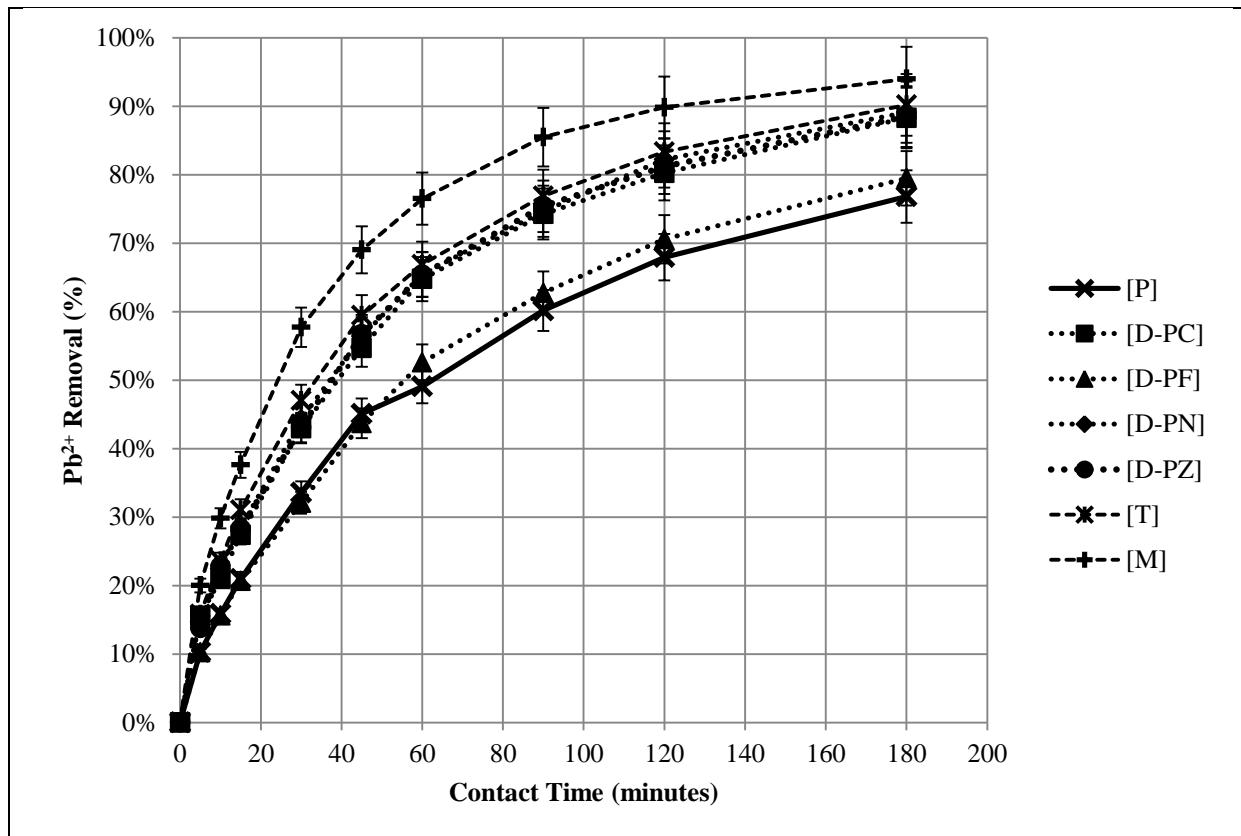
Figure 5.3 Percent Removal of Lead in the Various Component Systems
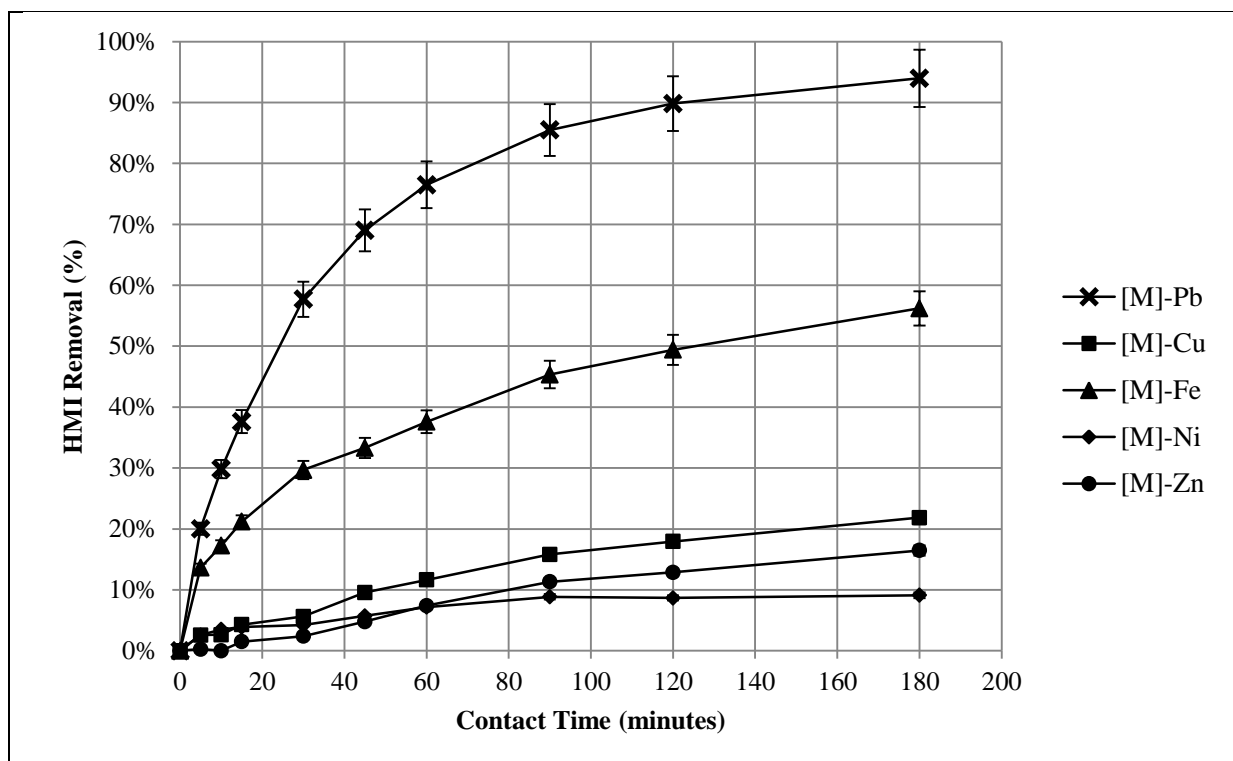
Figure 5.4 Percent Removal of HMIs in the Multi-Component System

Additional observations are revealed when the percent removal of each HMI of the various component systems is investigated further. With Pb^{2+} as the ion of interest in this study, **Table 5.4** shows that only 1.88 meq/L out of a possible 2.0 meq/L in the multi-component system versus 7.68 meq/L of 10 meq/L in the single-component system. Zeolite's highest affinity is for lead, and is followed by iron. In the dual-iron [D-PF] system, 3.97 meq/L of 5.0 meq/L is removed and in the triple [T] system, 3.01 meq/L of 3.3 meq/L is removed once Cu^{2+} ion is introduced.

Table 5.4 The HMI Removal (meq/L) in the Various Component Systems Relative to the Lead Ion

System			HMI	TOTAL	System		HMI	TOTAL
[P]		Pb^{2+}	**7.68**		TRIPLE [T]	Pb^{2+}	3.01	5.29
						Cu^{2+}	0.63	
	[PC]	Pb^{2+}	4.41	5.03		Fe^{3+}	1.65	
		Cu^{2+}	0.61					
	[PF]	Pb^{2+}	3.97	5.86		Pb^{2+}	**1.88**	**3.95**
		Fe^{3+}	1.89			Cu^{2+}	0.44	
DUAL	[PN]	Pb^{2+}	4.46	4.82	MULTI [M]	Fe^{3+}	1.12	
		Ni^{2+}	0.37			Ni^{2+}	0.18	
	[PZ]	Pb^{2+}	4.42	4.97		Zn^{2+}	0.33	
		Zn^{2+}	0.55					

5.4.4. Selectivity Determination

The removal efficiency order is indicative of how the adsorptive nature of zeolite for each ion varies among the different component systems. Based on the sorbent-to-sorbate ratio of 4 g to 100 mL, the HMI uptake is calculated by applying **Equation 3.2** and presented in **Table 5.5**. For a HMI pair evaluated as A/B, the selectivity ratio (SR) is determined by **Equation 5.1** and presented in **Table 5.6**, where q_t is the uptake at time t (in meq/g) (Inglezakis et al., 2003):

$$SR = \frac{q_{t,A}}{q_{t,B}} \qquad \textbf{(5.1)}$$

As HMIs are introduced into the system, the overall uptake of the lead ion and the total HMIs are decreased. An uptake of lead ions by zeolite is reduced by approximately 75.6%, going from 0.1919 meq/g in the single-component [P] system to 0.0469 meq/g in the multi-component [M] system. Also, in the presence of highly competitive ions, the removal of Pb^{2+} is hindered. This is indicative of zeolite's selectivity, where the Pb/Fe ratio is the lowest and the Pb/Ni as the highest, with a greater uptake of lead in combination of Ni^{2+} than with Fe^{3+}. Furthermore, Cu^{2+} is seen as the third ion of appeal to that of zeolite. When introduced in the triple-component system, it is observed that the overall uptake of HMIs is reduced from 0.1462 meq/g in the [PF] system to 0.1320 meq/g in the [T] system. These key trends are indicative of the selectivity of zeolite for the various HMIs in solution.

Table 5.5 The HMI Uptake in the Various Component Systems by Zeolite

System		HMIs	Uptake (meq/g)		System	HMIs	Uptake (meq/g)	
			HMI	TOTAL			HMI	TOTAL
[P]		Pb^{2+}	0.1919		TRIPLE [T]	Pb^{2+}	0.0750	
DUAL	[PC]	Pb^{2+}	0.1102	0.1255		Cu^{2+}	0.0158	0.1320
		Cu^{2+}	0.0153			Fe^{3+}	0.0412	
	[PF]	Pb^{2+}	0.0992	0.1462				
		Fe^{3+}	0.0471		MULTI [M]	Pb^{2+}	0.0469	
	[PN]	Pb^{2+}	0.1112	0.1204		Cu^{2+}	0.0109	
		Ni^{2+}	0.0092			Fe^{3+}	0.0281	0.0986
	[PZ]	Pb^{2+}	0.1105	0.1243		Ni^{2+}	0.0045	
		Zn^{2+}	0.0138			Zn^{2+}	0.0082	

Table 5.6 Selectivity Ratios (SR) of the Various Component Systems Relative to Lead Uptake

HMI Pair	DUAL (5.0 meq/L)	TRIPLE (3.3 meq/L)	MULTI (2.0 meq/L)
Pb/Cu	7.22	4.75	4.30
Pb/Fe	2.11	1.82	1.67
Pb/Ni	12.1	---	10.3
Pb/Zn	8.04	---	5.71

Figure 5.5 represents the total uptake of HMI in the various component systems over the 3-hour analysis period. It is evident that equilibrium has yet to be reached based on the established experimental conditions; however, a curve-to-plateau is detected and can be indicative of the long-term trends. As demonstrated by Motsi et al. (2009), the initial stage of rapid adsorption occurs within the first 40 minutes of contact. This is when all of the adsorption sites are available for cation interaction to occur, and when the concentration difference between the influent stock and sorbent-solution interface is very high. Inglezakis et al. (2002) credits this period to ion-exchange in the micropores on the zeolite particles' surface. Slower sorption follows, which is attributed to slower diffusion of the cations in solution into the internal network of the zeolite, such that these cations must occupy the exchangeable sites within the channeled structure (Motsi et al., 2009).
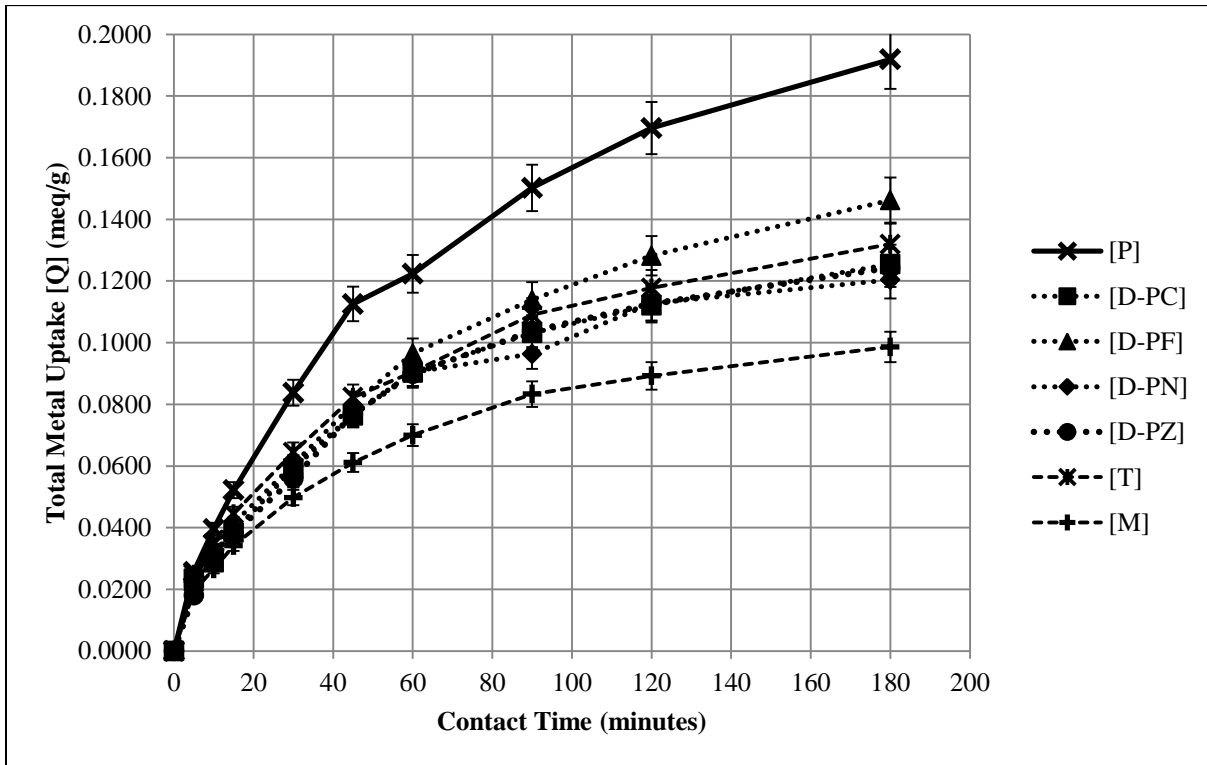
Figure 5.5 Total HMI Uptake in the Various Component Systems over Time

The presence of each HMI in solution impacts the uptake of lead; however, the removal efficiency trend is maintained throughout the various component systems. Once again, the sorbent mineral zeolite has a favoured uptake for that of the Pb^{2+} ion, followed by Fe^{3+}, Cu^{2+}, Zn^{2+}, and then Ni^{2+}. The selectivity study conducted by Anari-Anaraki and Nezamzadeh-Ejhieh

(2015) involved surface surfactant modified clinoptilolite nanoparticles, with Pb^{2+} ion dual-component systems and interfering cations; supporting reported literature trends as: $Pb^{2+}> Cd^{2+}>$ $Cs^+ > Cu^{2+}> Co^{2+}> Cr^{3+}> Zn^{2+}> Ni^{2+}$. This selectivity series is also consistent with the results obtained by Inglezakis et al. (2003), which investigated the trends of lead, copper, iron and chromium ions in various component systems as well as the findings of Ouki and Kavannagh (1997, 1999), who studied the selectivity and removal performance of lead, copper, cadmium, zinc, chromium, cobalt and nickel in a mixed system. Their research has determined that both physicochemical and stereochemical factors (i.e., micropore spacing constraints, hydrated radii (ion-to-pore ratio), cation hydration enthalpy) influence the removal efficiency.

Ouki and Kavannagh (1997) emphasize that clinoptilolite is comprised of a: (1) high Si/Al ratio, (2) low volumetric capacity, and (3) weak ionic field, within the structure. Therefore, the cation hydration free energy (a measure of water molecule rejection) (Inglezakis et al., 2003) is considered more significant than the electrostatic interactions within the framework during the sorption process. The HMIs with higher hydration energy prefer to remain in solution, where their hydration conditions are well-fulfilled. The hydration energy of Pb^{2+} (−357 kcal/mol) compared to Cu^{2+} (−502 kcal/mol) and Fe^{3+} (−1053 kcal/mol) suggests that lead is superior in uptake to the other ions as it is not composed of complex, hydrated compounds and thereby demonstrates the significantly higher selectivity of lead by clinoptilolite (Ouki and Kavannagh, 1997; Inglezakis et al., 2003); this general observation is further substantiated by the contribution of this present study.

It is important to note that sorption equilibria is strongly affected by complexation of co-ions, counter-ions, and neutral molecules with one another; as a highly specific interaction, it may influence the selectivity of a given sorbent material (Helfferich, 1962, p. 202). Heavy metals are able to form stable complexes due to their electrostatic structure; Cu^{2+}, Fe^{3+}, and Ni^{2+} form stable complexes with water molecules, where these complexes are charged and give colour to their solutions (Inglezakis et al., 2004) (for the HMIs above, blue, orange/yellow, and green, respectively). As the metal concentration increases, metal ions which can no longer form outer-sphere complexes (e.g. ion-exchange) as a purely electrostatic attraction are forced into internal sites and start to form inner-sphere complexes (Xu et al., 2013) that are site-specific to the sorbent surface. This type of complexation is said to affect the reversibility of sorption reactions,

given that inner-sphere complexation appears to be irreversible, due to the formation of covalent bonds (Xu et al., 2013). Specifically for the lead ion (Pb^{2+}) of interest to this study, the fact that the sorbent material prefers this counter-ion, which associates less strongly (least tendency to form strong complexes), compared to the co-ions in its framework is of importance. Consequently, the selectivity order observed in this study may be due to the fact that large and stable inorganic complexes may be mechanically excluded from the zeolitic structure by its unique sieve action properties. This may be the basis for the preferential uptake by the zeolite mineral for lead (Inglezakis et al., 2004).

In practical applications of industrial wastewater effluent, the presence of multiple HMIs in solution affects the overall treatment process. This study has demonstrated that the natural zeolite clinoptilolite is effective in the uptake of the target metal lead. Finally, further knowledge and quantitative details have been presented for using the sorption process as a valuable asset to wastewater treatment.

5.5. Conclusions

This study investigated the predominant heavy metallic ions found in mine waste streams, and how in combination, the removal specifically of lead (Pb^{2+}) is affected with their presence over time. The significant findings from this research are as follows:

1. Existing literature all agree that the Pb^{2+} ion can be removed by zeolite sorption; however, there are limitations on addressing the effect on this removal when other HMIs are present in the waste.
2. Qualitative observations by SEM/EDS imagery display that zeolite is influenced by the exposure to various heavy metallic ions in multi-component aqueous solutions.
3. While maintaining the 10 meq/L total HMI influent concentration, the removal of Pb^{2+} decreases from that in a single- to the multi-component system by approximately 75.6%.
4. The systematic introduction of copper, iron, nickel and zinc to the system decreases the overall uptake of the total HMIs in solution.

This removal method may be a predictive indicator for the removal of other metallic ions from other industrial effluents. The findings presented are significant both the mining and related environmental industry, which contribute to the advancement in the design of treatment systems through experimentation, modelling, and simulation.

5.6.   Future Works

This study verifies that the zeolite mineral exhibits the greatest preference towards the lead (Pb^{2+}) ion with a selectivity series of $Pb^{2+} > Fe^{3+} > Cu^{2+} > Zn^{2+} > Ni^{2+}$ and provides an understanding of how the HMIs affect the removal trends when combined. The next chapter addresses the gap in existing research that kinetic analysis is still very limited (Oter and Akcay, 2007; Motsi et al., 2011) in the number of HMIs of various multi-component system combinations, with sorption by zeolite in its natural form (Panayotova and Velikov, 2002; Inglezakis et al., 2003; Bektas and Kara, 2004; Wang and Peng, 2010).

6. KINETIC MODELLING TRENDS

Kinetic Modelling of the Removal of Multiple Heavy Metallic Ions from Mine Waste by Natural Zeolite Sorption

Abstract

This study investigates the sorption of heavy metallic ions (HMIs), specifically lead (Pb^{2+}), copper (Cu^{2+}), iron (Fe^{3+}), nickel (Ni^{2+}) and zinc (Zn^{2+}), by natural zeolite (clinoptilolite). These HMIs are combined in single-, dual-, triple-, and multi-component systems. The batch-mode experiments consist of a total initial concentration of 10 meq/L normality for all systems, acidified to a pH of 2 by concentrated nitric (HNO_3) acid. A zeolite dosage of 4 g per 100 mL of synthetic nitrate salt aqueous solution is applied, for a contact period of 5 to 180 min. Existing kinetic models on HMIs sorption are limited for multi-component system combinations. Therefore, this study conducts kinetic analysis by both reaction and diffusion models, to quantify the sorption process. The study concludes that the process correlates best with the pseudo-second-order (PSO) kinetic model. In the multi-component system combining all five HMIs, the initial sorption rate and theoretical equilibrium capacity are determined as 0.0033 meq/g·min and 0.1159 meq/g, respectively. This provides significant insight into the mechanisms associated with the sorption process, as well as contributing to the assessment of natural zeolite as a sorbent material in its application in industrial wastewater treatment.

6.1. Introduction

The demand for proper evaluation and predication of water quality has grown, in order to protect surrounding water resources (Muttil and Chau, 2007; Wang et al., 2014). Environmental management is significant in any industry, which is a controlling factor for economic advancement, profitable development and the protection of the water resources at risk of future contamination (Wang et al., 2014). The environmental impact assessment (EIA) of large developments, such as industrial mining, is of great importance. The ecological, environmental, and socio-economic effects of these developments must be thoroughly evaluated. With this in mind, the EIA must establish both quantitative and qualitative standards with regards to modelling predication (Zhao et al., 2006).

In recent years, the study of sorption kinetics has attracted a lot of interest among researchers due to its importance in sorbent material assessment and subsequent application in the wastewater treatment industry (Qiu et al., 2009). Predicting the rate at which pollutant removal takes place in a given solid-solution system is crucial to establish an effective sorption system design (Plazinski et al., 2009). Many attempts have been made to generate an expression(s) to describe sorption kinetics on solid surfaces (i.e., natural zeolite, activated carbon, bio-sorbents, etc.) for solid-solution phase sorption systems (Ho and McKay, 1998a). Sorption kinetics defines the reaction pathways and uptake rates, along with residence times at which the equilibrium point is reached at the solid-solution interface (Beyazit, 2013). The physical as well as chemical composition of the sorbent material influences the sorption kinetics and controlling mechanisms (Kocaoba et al., 2007). A proper understanding of the mechanisms involved is not complete without experimental data on the simultaneous sorption of the heavy multi-metallic ions that are prevalent in industrial effluent, and an analysis on the uptake and rate of interference of these HMIs in combination (Helfferich, 1962; Borandegi and Nezamzadeh-Ejhieh, 2015). With the significant sorption research that has been undertaken, however, data is still very limited on kinetic analysis (Oter and Akcay, 2007; Motsi et al., 2011) of the number of HMIs in different multi-component system combinations, with sorption by zeolite in its natural form (Panayotova and Velikov, 2002; Inglezakis et al., 2003; Bektas and Kara, 2004; Wang and Peng, 2010). In light of this, the objective of the current study is to investigate the use of kinetic modelling to study the rate of the overall sorption process of the five (5) HMIs in this research

project, by natural zeolite. To better understand how the removal of various ions may be affected by the presence of other HMIs, the experimental investigation will be carried out in increasing complexities, by combining the ions in single-, dual-, triple-, and multi-component aqueous solution systems. Various kinetic models, based on the reaction and diffusion concepts, will be considered in this study. It is envisaged that this kinetic analysis of the experimental data consisting of multiple HMIs in different combinations will provide significant insight into the mechanisms associated with the sorption process for industrial wastewater treatment (Qiu et al., 2009).

6.2.   Materials and Methods

Refer to **Chapter 3** for the consolidated experimental methodology; sorbent material, sorbate solution, and analytical procedure. All analyses are conducted in batch-mode, creating the synthetic simple solute HMI solution in the various component system combinations at a 4-g sorbent mass to 100-mL sorbate volume dosage. The following subsections discuss the associated principles of sorption kinetics and the model selection rationale for this study.

6.2.1.   Sorption Kinetics Principles

The accuracy of modelling prediction is dependent on the various open boundary conditions, model parameters selected, and numerical method(s) implemented. The variation in sorption kinetics is attributed to the specific crystalline structure (physical as well as chemical composition) of the sorbent material, and is controlled by various mechanisms (Helfferich, 1962; Bekkum et al., 1991; Kocaoba et al., 2007; Motsi et al., 2011). Kinetic modelling is a powerful tool to assess the performance of sorbent materials and to comprehend these fundamental mechanisms involved in the sorption process. This is classified as follows (Qiu et al., 2009; Motsi et al., 2011), where either one sole-step or multiple phases have a predominate impact (Fierro et al., 2008):

1. Reaction-Type Model
   Chemisorption – chemical reaction at the sites of the functional ionic groups within the zeolite and focuses on the process as a whole.

2. Diffusion-Type Model
   a. Film Diffusion – diffusion of counter-ions in the adherent layer surrounding the zeolite (between the external solution and crystal surface).

   b. Intra-Particle Diffusion – diffusion of counter-ions in the solute within the zeolite pores and/or along the pore walls.

   c. Mass Action – sorption or desorption between the active sites and the sorbate material.

Both reaction-type and diffusion-type sorption kinetic classifications have been investigated; correlations between the sorption uptake of the HMIs with respect to time were analyzed specifically in this study. The most prevalent models (Ho and McKay, 1998a; Bektas and Kara, 2004; Sprynskyy et al., 2006; Fierro et al., 2008; Qiu et al., 2009; Palzinski et al., 2009; Motsi et al., 2011; Jovanovic et al., 2012; Olu-Owolabi et al., 2014; Farouq and Yousef, 2015; Largitte and Pasquier, 2016) considered in the model selection process are discussed in the following subsections.

6.2.1.1.   Reaction-Type Models

Pseudo-First-Order (PFO) Rate Equation

This model is considered to be earliest to represent the liquid-solid phase sorption process, relating the capacity to rate (Qiu et al., 2009). The general relationship is given in **Equation 6.1**. By applying the boundary conditions of $t = 0 \rightarrow q_t = 0$ and $t = t \rightarrow q_t = q_t$, its solution and linearized form are given in **Equation 6.2** and **Equation 6.3**, respectively (Ho and McKay, 1998a; Bektas and Kara, 2004; Qiu et al., 2009; Farouq and Yousef, 2015):

$$\frac{dq_t}{dt} = k_1(q_e - q_t) \tag{6.1}$$

$$k_1 t = \ln\left(\frac{q_e}{q_e - q_t}\right) \tag{6.2}$$

$$\log(q_e - q_t) = \log q_e - \left(\frac{k_1}{2.303}\right)t \tag{6.3}$$

where q_e and q_t are sorption capacity (the amount of HMI sorbed per unit weight of sorbent) (in meq/g) at equilibrium and at time t (in min), respectively; and k_1 is the pseudo-first order rate constant (in min^{-1}). According to this model, a plot of $\log(q_e - q_t)$ versus t would provide a linear trend (Fierro et al., 2008).

Pseudo-Second-Order (PSO) Rate Equation

This model implies that the rate-determining (RDS) step is by chemical adsorption (chemisorption), involving valent forces through sharing or electron exchange between the sorbent material and the HMIs in solution. The sorption rate depends on the amount of ions on the sorbent surface at time t and what is sorbed at equilibrium (Qiu et al., 2009). The general relationship is given in **Equation 6.4**. By applying the boundary conditions of $t = 0 \rightarrow q_t = 0$ and $t = t \rightarrow q_t = q_t$, its linearized form is given in **Equation 6.5** and rearranged in **Equation 6.6** (Ho and McKay, 1998a; Bektas and Kara, 2004; Sprynskyy et al., 2006; Qiu et al., 2009; Motsi et al., 2011; Farouq and Yousef, 2015):

$$\frac{dq_t}{dt} = k_2(q_e - q_t)^2 \tag{6.4}$$

$$\frac{t}{q_t} = \frac{t}{q_e} + \frac{1}{k_2 q_e^2} \tag{6.5}$$

$$q_t = \frac{k_2 q_e^2 t}{[1 + k_2 q_e t]} \tag{6.6}$$

where $h = k_2 q_e^2$ is the initial sorption rate (in meq/g·min) as t approaches zero (Ho et al., 2006), and k_2 is the PSO rate constant (in g/meq·min). These constants are determined by a plot of the linearized form (**Equation 6.5**) of t/q_t versus t (Bektas and Kara, 2004; Ho et al., 2006; Kocaoba et al., 2007; Qiu et al., 2009).

The Elovich Equation

This model was developed to predominately describe the sorption interactions between the gas phase onto a heterogeneous solid surfaces (Plazinski et al.; 2009; Qiu et al., 2009; Farouq and Yousef, 2015), but has also represented sorption of contaminants from aqueous solutions (Fierro et al., 2008). The general relationship is given in **Equation 6.7**. By applying the boundary conditions of $t = 0 \rightarrow q_t = 0$ and $t = t \rightarrow q_t = q_t$, and the assumption that $\alpha\beta t \gg 1$,

its linearized form is given in **Equation 6.8**. (Ho and McKay, 1998a; Fierro et al., 2008; Qiu et al., 2009; Olu-Owolabi et al., 2014; Farouq and Yousef, 2015; Largitte and Pasquier, 2016):

$$\frac{dq_t}{dt} = \alpha \cdot \exp(-\beta dq_t) \tag{6.7}$$

$$q_t = \left(\frac{1}{\beta}\right)[\ln(t)] + \left(\frac{1}{\beta}\right)[\ln(\alpha\beta)] \tag{6.8}$$

where q_t is the amount sorbed at time t, β is the Elovich constant (in g/meq) (Wu et al., 2009) (relating to the extent of surface coverage (site availability) (Fierro et al., 2008) and activation energy for chemisorptions) (Farouq and Yousef, 2015), and α is the initial sorption rate (in meq/g·min) (Ho and McKay, 1998a; Wu et al., 2009). According to this model, a plot of q_t versus $\ln(t)$ would provide a linear trend (Ho and McKay, 1998a; Fierro et al., 2008).

6.2.1.2. *Diffusion-Type Models*

Sorption kinetics may be described from a systematic point of view. Of the three steps involved in the diffusion kinetic category described, mass action is very rapid, and therefore considered negligible in kinetic analysis (Qiu et al., 2009). The Weber–Morris intra-particle diffusion (IPD) model and its parameters provide significant information in order to determine whether film diffusion or intra-particle diffusion is the RDS. The IPD model demonstrates that in numerous sorption studies, the ion solute uptake varies almost proportionately with $\sqrt{t}$ rather than with time t (Bektas and Kara, 2004; Kocaoba et al., 2007; Qiu et al., 2009). If diffusion is the sorption mechanism, then the plot of q_t versus $\sqrt{t}$, as expressed in **Equation 6.9**, is linear (Bektas and Kara, 2004; Kocaoba et al., 2007; Fierro et al., 2008; Qiu et al., 2009; Zolgharnein and Shahmoradi, 2010; Olu-Owolabi et al., 2014):

$$q_t = k_P \cdot \left(\sqrt{t}\right) + C \tag{6.9}$$

where k_P (in meq/g·min$^{1/2}$) is the intra-particle diffusion rate constant, and C (in meq/g) is a constant representing the thickness of the boundary layer (Fierro et al., 2008; Olu-Owolabi et al., 2014); the greater the C value, the greater the boundary layer effect. Further, the intra-particle diffusion mechanism specifically is the RDS when this plot intersects the origin (Fierro et al., 2008; Qiu et al., 2009). When the sorption process is controlled by more than one diffusion mechanism, then the data plot deviates from the origin with a multi-linear trend; the mechanism

of sorption is complex and both external and intra-particle diffusion play a role in the actual sorption process (Zolgharnein and Shahmoradi, 2010). The initial steep phase implies that the external resistance to mass transfer surrounding the particles is significant, representing macropore and mesopore diffusion. The second gradual phase implies micropore intra-particle diffusion as the RDS (Fierro et al., 2008).

6.2.2. Kinetic Model Selection

The mechanism study conducted by Sprynskyy et al. (2006) demonstrates that the sorption of HMIs (Pb^{2+}, Cu^{2+}, Ni^{2+}, Cd^{2+}) by natural zeolite is a heterogeneous process with three distinct stages. First, a very fast (instantaneous) uptake occurs within the first 30 minutes, observed for four HMIs at three different concentrations. This is followed by inversion due to desorption prevalence, observed predominantly for Ni^{2+} at all concentrations and overall increases for all four HMIs at higher metal concentrations. Finally, a slower uptake increase of all four HMIs is observed, with a majority of Ni^{2+} occurring in the first stage. In the kinetic studies of HMI uptake (Fe^{3+}, Cu^{2+}, Mn^{2+}, Zn^{2+}) by natural zeolite conducted by Motsi et al. (2009), the initial stage of rapid adsorption occurs within the first 40 minutes of contact. This is when all of the adsorption sites are available for cation interaction to occur, and when the concentration difference between the influent stock and sorbent–sorbate interface is very high. Inglezakis et al. (2002) credits this period to ion-exchange in the micropores on the zeolite particles' surface. During the second stage, desorption prevalence is most likely caused by slower diffusion of exchangeable co-ions within the internal network (Ca^{2+}, Na^+, K^+) of the zeolite crystalline framework, and consequently occupies the exchange positions on the surface to the counter-ions (HMIs) in solution. During the third stage, a gradual sorption in the micropores within the crystalline occurs. Deceleration in the close micropores within the framework is connected by poor access as well as by more intensive sorption in comparison with in the surface micropores.

Under the testing conditions of this study, the sorption capacity at equilibrium (q_e) was not experimentally determined (due to the 3-hour contact time limitation); which must be known in order to fit the data to the PFO model equation. In addition, previous research efforts have demonstrated that the equation does not fit the data as well for the complete contact time range (Bektas and Kara, 2004; Fierro et al., 2008; Zolgharnein and Shahmoradi, 2010; Olu-Owolabi et al., 2014). The Elovich equation can be associated with the model of a strongly heterogeneous solid surface. However, recent studies show that the PSO and Elovich equations exhibit very similar behaviour under the assumption that the system is not close to equilibrium (Plazinski et al., 2009). The PSO model assumes: (1) sorption only occurs on localized sites and involves no interaction between the sorbed ions; (2) the energy of adsorption is not dependent on surface coverage; (3) maximum adsorption corresponds to a saturated mono-layer of adsorbates on the adsorbent surface, (4) the concentration of the sorbate is considered to be constant, and (5) the metal ion uptake on the activated carbons is governed by a second-order rate equation. The Elovich model differs in the first two assumptions in that: (1) sorption only occurs on localized sites and there is inter-action between the sorbed ions; and (2) the energy of adsorption increases linearly with the surface coverage (Largitte and Pasquier, 2016).

The PSO model has effectively demonstrated the sorption process of various contaminants, including metal ions, and organic substances in an aqueous state (Fierro et al., 2008; Qiu et al., 2009; Zolgharnein and Shahmoradi, 2010; Jovanovic et al., 2012; Olu-Owolabi et al., 2014). Several literature review findings of kinetic models of the removal *specifically* of *heavy metals* from *aqueous solutions* by *natural clinoptilolite* were considered by Jovanovic et al. (2012), which widely described by researchers that the sorption process by the *PSO model* is the best representation. However, the system specific presumptions of system variables (Ho and McKay, 1998a) (operation conditions) (i.e., sorbent particle size, counter-ions' initial concentration, temperature, pH level, degree of agitation, etc.) must be stated, which affect the mechanisms involved. The experimental data that fits to the PSO model indicates that chemisorption (chemical reaction) is the rate-determining step (RDS), which is the case if the rate coefficient is constant for each operative condition. If any of these conditions are not satisfied, chemisorption is not the RDS even if the data fits the PSO kinetic model well (Motsi et al., 2011). Motsi et al. (2011) determined that intra-particle diffusion is the primary RDS in the uptake of HMIs (Fe^{3+},

Cu^{2+}, Mn^{2+}, Zn^{2+}) by natural zeolite and suggested that electric transference during intra-particle diffusion is a significant event in the sorption process.

Based on the above discussion and preliminary research findings, the study presented in this paper will be carried out with these two selected models: (1) the PSO reaction model and (2) the IPD model. The objective is to observe the various uptake rates and mechanisms associated of the two models, thereby resulting in an assessment and comparison of the final performance of the two kinetic models developed from distinctly different premises.

6.3. Quality Control (QC) Protocol

For all analytical sessions, the triplicate concentration of the median standard (50 mg/L) detected an average of 51.62 mg/L, and is within 5% of the known value; the percent relative standard deviation (%-RSD) reported an average of 0.597%, which is well within the ≤3% limit; the correlation coefficient of each HMI analyte primary wavelength generated an average of 0.9998, which is very close to unity.

6.4. Analysis

6.4.1. Acidity Levels

Following sorbate-sorbent contact, the pH is observed to be steady throughout the sorption process. The maximum recorded pH values are 2.16, 2.21, 2.19, and, 2.17 for the single-, dual-, triple-, and multi-component systems, respectively; for both at day of zeolite exposure and the day after of filtered sample. The pH levels of the prepared influent stock and filtered effluent are also observed to be constant during refrigerated storage prior to dilution preparation for elemental analysis. This present study was conducted in the conservative manner, with all pH values documented to be below reported ranges and within comparability. By maintaining very low pH levels in the batch experiments and the use of highly soluble nitrate salts, the precipitation of the HMIs is avoided. Additional trials verified that the filtered and unfiltered HMI influent stock concentrations are the same, indicating both effective dilution practices and

complete solubility. Therefore, the concentration of each HMI before and after batch sorption was exclusively in soluble form.

6.4.2. Heavy Metallic Ion Levels

The ICP-AES results of the various component systems at 3 contact hours are summarized in **Table 6.1.** to **Table 6.3**. The primary wavelengths 'Analyte' are given in Column 1, and the 'Sample ID' in Column 2 provides the systems' influent stock (S) and 180 contact minute data. In order to keep all concentrations within the calibration range of 0–100 mg/L, the samples are diluted by 50% with deionized distilled water, indicated by the superscript value. As observed in the quality control measures for the calibration standard, the %-RSD values are low and all within <3% as given in Column 3, which is indicative that the data is accurate and the experimental replicates are reliable (Perkin Elmer Inc., 2010). Triplicate readings and their mean concentrations in calibration units in mg/L are presented in Column 4. The dilution factors in Column 2 are applied to the triplicate concentrations, and the corresponding HMI concentrations are given in Column 5. By applying **Equation 3.2**, the uptake sorption capacity is given in Column 6. The percent removal after 180 contact minutes is calculated in Column 7. Before kinetic analysis is conducted, the overall removal efficiency order indicates that the Pb^{2+} ion is highest compared to the four other HMIs investigated. This order is consistently high regardless of the component system combinations (Panayotova and Velikov, 2002; Oter and Akcay, 2007).

Figure 6.1 presents the percent removal of the total HMIs found in the single-lead [P], triple-(lead-copper-iron) [T], and multi-[M] component systems over the 3 hour analysis period. The HMIs are progressively added to the aqueous solution while maintaining the total HMI concentration of 10 meq/L. The overall uptake is reduced from [P] to [T] by 0.0599 meq/g or 31.2%, and from [T] to [M] by 0.0334 meq/g or 25.3%. It is visually evident that each HMI in solution distinctively impacts the overall uptake. An equilibrium state has yet to be reached based on the established experimental conditions. Yet, the curve-to-plateau trend shows three distinct stages, where rapid uptake is observed within the first 45 contact minutes; as demonstrated by Sprynskyy et al. (2006) and Motsi et al. (2009). This is a first glimpse in this study of zeolite's preference for the HMIs to be investigated, indicative of the long-term trends.

Table 6.1 ICP-AES HMI Results of the Single-Component Systems

1	2	3	4	5	6	7
			Concentration (mg/L)			
Analyte	**Sample ID**	**%-RSD**	Triplicate Mean (Calib)	DIL	**meq/g**	**%R**
Pb 220.353	[P]-S[4]	0.24	75.93	1214.81	0.1919	76.8
	[P]180[3]	0.59	35.20	281.63		
Cu 327.393	[C]-S[2]	0.40	105.37	421.49	0.0533	21.4
	[C]180[2]	0.16	82.84	331.37		
Fe 238.204	[F]-S[1]	0.53	105.83	211.65	0.0757	30.3
	[F]180[1]	0.55	73.73	147.46		
Ni 231.604	[N]-S[2]	0.32	87.30	349.19	0.0268	10.7
	[N]180[2]	0.36	77.92	311.69		
Zn 206.200	[Z]-S[2]	1.10	104.67	418.68	0.0494	19.8
	[Z]180[2]	0.74	83.94	335.77		

Table 6.2 ICP-AES HMI Results of the Dual-Component Systems

1	2	3	4	5	6	7
			Concentration (mg/L)			
Analyte	**Sample ID**	**%-RSD**	Triplicate Mean (Calib)	DIL	**meq/g**	**%R**
Pb 220.353	[D-PC]-S[3]	0.13	75.47	603.79	0.1102	88.3
	[D-PC]180[2]	0.59	17.68	70.73		
Cu 327.393	[D-PC]-S[3]	0.11	24.18	193.44	0.0153	12.2
	[D-PC]180[2]	0.61	42.44	169.77		
Pb 220.353	[D-PF]-S[3]	0.42	75.98	607.82	0.0992	79.5
	[D-PF]180[2]	0.54	31.19	124.77		
Fe 238.204	[D-PF]-S[3]	0.31	13.01	104.11	0.0471	37.7
	[D-PF]180[2]	0.45	16.21	64.82		
Pb 220.353	[D-PN]-S[3]	0.82	77.16	617.29	0.1112	89.1
	[D-PN]180[2]	0.68	16.81	67.22		
Ni 231.604	[D-PN]-S[3]	0.86	21.05	168.37	0.0092	7.40
	[D-PN]180[2]	0.12	38.99	155.94		
Pb 220.353	[D-PZ]-S[3]	1.01	76.78	614.22	0.1105	88.5
	[D-PZ]180[2]	0.50	17.68	70.72		
Zn 206.200	[D-PZ]-S[3]	0.92	23.46	187.65	0.0138	11.0
	[D-PZ]180[2]	0.83	41.75	166.98		
Cu 327.393	[D-CF]-S[1]	0.90	95.76	191.51	0.0283	22.7
	[D-CF]180[1]	0.58	74.06	148.13		
Fe 238.204	[D-CF]-S[1]	2.75	50.61	101.21	0.0534	42.8
	[D-CF]180[1]	0.70	28.95	57.90		
Cu 327.393	[D-CN]-S[1]	0.50	94.92	189.85	0.0361	28.9
	[D-CN]180[1]	0.40	67.46	134.92		
Ni 231.604	[D-CN]-S[1]	0.23	80.53	161.06	0.0125	10.0
	[D-CN]180[1]	0.48	72.48	144.96		
Fe 238.204	[D-FZ]-S[1]	2.31	51.15	102.30	0.0546	43.7
	[D-FZ]180[1]	0.20	28.78	57.56		
Zn 206.200	[D-FZ]-S[1]	2.69	90.55	181.09	0.0236	18.9
	[D-FZ]180[1]	0.22	73.43	146.85		
Ni 231.604	[D-NZ]-S[1]	1.22	80.15	160.31	0.0067	5.4
	[D-NZ]180[1]	3.49	75.85	151.71		
Zn 206.200	[D-NZ]-S[1]	1.30	89.51	179.02	0.0244	19.6
	[D-NZ]180[1]	3.84	71.99	143.99		

Table 6.3 ICP-AES HMI Results of the Triple- and Multi-Component Systems

1	2	3	4	5	6	7
			Concentration (mg/L)			
Analyte	**Sample ID**	**%-RSD**	Triplicate Mean (Calib)	DIL	**meq/g**	**%R**
Pb	[T]-S[2]	1.27	100.05	400.21	0.0750	90.2
220.353	[T]180[1]	0.21	19.66	39.32		
Cu	[T]-S[2]	1.16	33.76	135.03	0.0158	19.0
327.393	[T]180[1]	1.58	54.70	109.40		
Fe	[T]-S[2]	0.59	17.23	68.92	0.0412	49.5
238.204	[T]180[1]	1.81	17.40	34.80		
Pb	[M]-S[1]	0.53	117.76	235.52	0.0469	94.0
220.353	[M]180[0]	0.67	14.20	14.20		
Cu	[M]-S[1]	1.96	37.58	75.16	0.0109	21.9
327.393	[M]180[0]	0.99	58.74	58.74		
Fe	[M]-S[1]	2.26	20.52	41.03	0.0281	56.2
238.204	[M]180[0]	1.24	17.97	17.97		
Ni	[M]-S[1]	0.56	32.87	65.75	0.0045	9.10
231.604	[M]180[0]	1.48	59.76	59.76		
Zn	[M]-S[1]	2.23	35.99	71.98	0.0082	16.5
206.200	[M]180[0]	1.63	60.12	60.12		
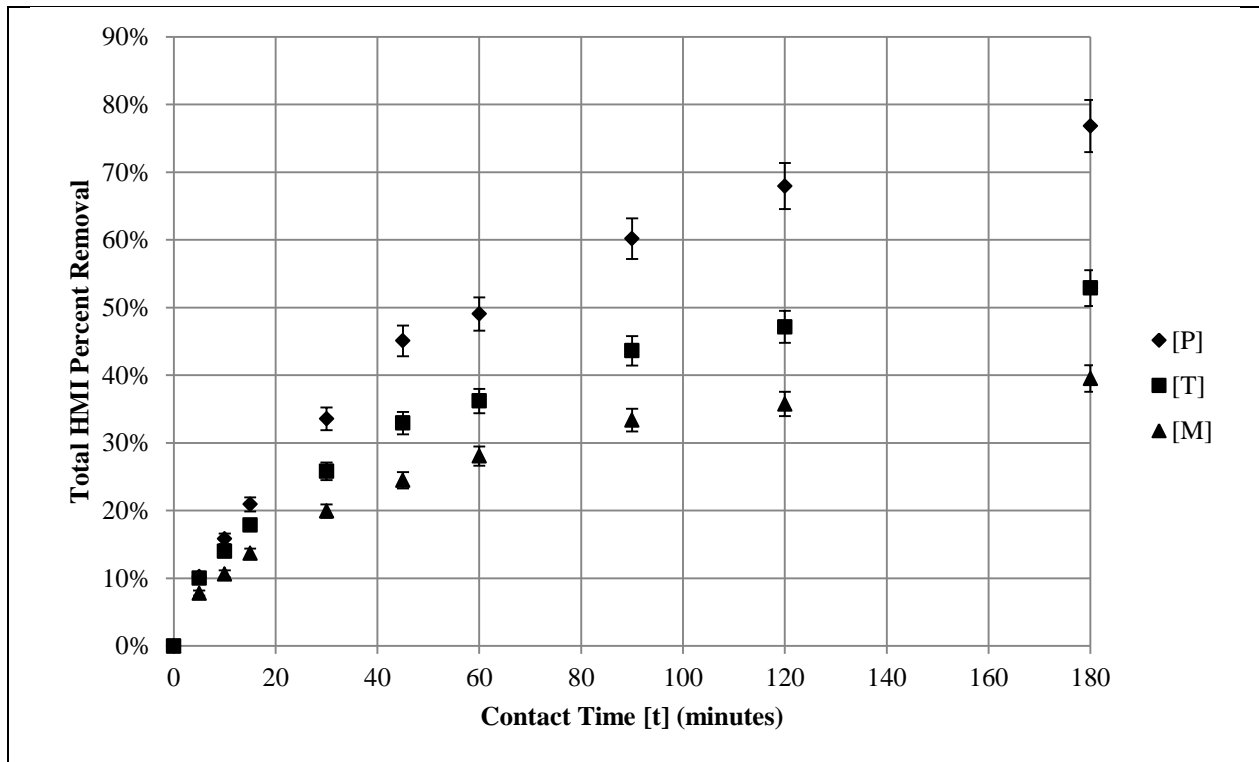
Figure 6.1 Total HMI Percent Removal versus Contact Time

93

6.4.3. Sorption Kinetics

The selected kinetic relationships are analyzed for all five HMIs and component systems, in both their individual and total combinations. The PSO rate constants and correlation coefficients are summarized in **Table 6.4**. Based on the linearized form of **Equation 6.5**, the slope (m) and y-intercept (b) values are interpreted to determine the theoretical sorption at equilibrium (q_e), overall sorption rate constant (k_2), and initial sorption rate (h). The IPD rate constants and correlation coefficients are summarized in **Table 6.5**. Based on **Equation 6.9**, the slope and y-intercept represent the corresponding diffusion rate constant (k_P) and boundary constant (C), respectively.

An impressive performance is observed in the correlation coefficient (CC) for both models of all the component system combinations. For the PSO model, 64.1% of the data falls within 0.95–1.0 CC range (excellent), while 84.6% has a CC of over 0.90 (good), and 87.2% has a CC over 0.85 (acceptable). For the IPD model, **Equation 6.9** is applied in two scenarios with respect to the origin. Good linearization of the data is observed for the initial phase of the reaction, in accordance with expected behaviour if intra-particle diffusion is the rate-determining step (Ho and McKay, 1998b; Zolgharnein and Shahmoradi, 2010). For the first scenario (at origin[A]), 64.1% of the data falls within the excellent range, while 82.1% within the good range and 87.2% within the acceptable range. For the second scenario (deviation from origin[B]), 79.5% of the data falls within the excellent range, while 94.9% within the good range. It is important to note that the boundary constant (C) values observed are very small and considered negligible, with 35.9% of the data showing a negative value with no physical meaning (Fierro et al., 2008; Olu-Owolabi et al., 2014). When comparing the diffusion rate constant (k_P) values, an average of positive C values differs by only 0.0004 meq/g·min between the two scenarios, demonstrating that the slopes (k_P) are very similar. Although a stronger CC is observed when deviation from the origin, it may be stated with confidence that intra-particle diffusion is the leading diffusion mechanism to represent the sorption process. Of the excellent CC range, the data correlated at 0.99 or above to unity is only 4.00% (1 of 25) by the IPD model while 48.0% (12 of 25) by the PSO model. As observed by Bektas and Kara (2004), a stronger correlation is observed by the PSO kinetic rate expression.

Table 6.4 Pseudo-Second-Order (PSO) Data

SYSTEM	$m = \left(\dfrac{1}{q_e}\right)$	$b = \left(\dfrac{1}{k_2 \cdot q_e^2}\right)$	CC	Equilibrium Sorption q_e (meq/g)	Sorption Rate Constant k_2 (g/meq·min)	Initial Sorption Rate $h = k_2 q_e^2$ (meq/g·min)
[P]	4.098	217.01	0.9926	0.244	0.077	0.0046
[C]	15.750	836.09	0.9291	0.063	0.297	0.0012
[F]	11.872	419.08	0.9708	0.084	0.336	0.0024
[N]	34.919	739.14	0.9806	0.029	1.650	0.0014
[Z]	15.237	1106.10	0.9147	0.066	0.210	0.0009
[D-PC]-Pb	7.474	299.43	0.9941	0.134	0.187	0.0033
[D-PC]-Cu	55.217	2840.90	0.9282	0.018	1.073	0.0004
[D-PC]	6.596	269.78	0.9906	0.152	0.161	0.0037
[D-PF]-Pb	7.692	448.41	0.9904	0.130	0.132	0.0022
[D-PF]-Fe	18.375	727.45	0.9703	0.054	0.464	0.0014
[D-PF]	5.489	275.71	0.9837	0.182	0.109	0.0036
[D-PN]-Pb	7.465	284.48	0.9957	0.134	0.196	0.0035
[D-PN]-Ni	109.750	3126.00	0.5378	0.009	3.853	0.0003
[D-PN]	6.976	254.36	0.9914	0.143	0.191	0.0039
[D-PZ]-Pb	7.436	293.22	0.9973	0.134	0.189	0.0034
[D-PZ]-Zn	40.653	5898.50	0.4358	0.025	0.280	0.0002
[D-PZ]	6.534	280.74	0.9946	0.153	0.152	0.0036
[D-CF]-Cu	21.169	2683.00	0.9629	0.047	0.167	0.0004
[D-CF]-Fe	16.655	581.48	0.9750	0.060	0.477	0.0017
[D-CF]	10.297	488.73	0.9703	0.097	0.217	0.0020
[D-CN]-Cu	21.936	1271.30	0.9453	0.046	0.379	0.0008
[D-CN]-Ni	72.008	1686.80	0.9498	0.014	3.074	0.0006
[D-CN]	17.329	747.04	0.9471	0.058	0.402	0.0013
[D-FZ]-Fe	16.438	502.40	0.9778	0.061	0.538	0.0020
[D-FZ]-Zn	28.869	3101.00	0.6387	0.035	0.269	0.0003
[D-FZ]	11.140	451.04	0.9554	0.090	0.275	0.0022
[D-NZ]-Ni	133.600	999.38	0.9731	0.007	17.860	0.0010
[D-NZ]-Zn	19.459	3808.80	0.3642	0.051	0.099	0.0003
[D-NZ]	24.852	1452.00	0.9113	0.040	0.425	0.0007
[T]-Pb	11.194	394.10	0.9980	0.089	0.318	0.0025
[T]-Cu	48.524	3252.90	0.9141	0.021	0.724	0.0003
[T]-Fe	21.496	721.14	0.9807	0.047	0.641	0.0014
[T]	6.438	237.29	0.9918	0.155	0.175	0.0042
[M]-Pb	18.593	465.67	0.9990	0.054	0.742	0.0021
[M]-Cu	58.274	6429.20	0.8600	0.017	0.528	0.0002
[M]-Fe	31.695	989.38	0.9830	0.032	1.015	0.0010
[M]-Ni	190.820	5086.10	0.9747	0.005	7.159	0.0002
[M]-Zn	−51.894	2,5482.00	0.1723	-0.019	0.106	0.0000
[M]	8.630	303.14	0.9931	0.116	0.246	0.0033

Table 6.5 Intra-Particle Diffusion (IPD) Data

SYSTEM	Diffusion Rate Constant [A] k_P (meq/g·min$^{1/2}$)	CC^A	SYSTEM	Diffusion Rate Constant [B] k_P (meq/g·min$^{1/2}$)	Boundary Constant [B] C (meq/g)	CC^B
[P]	0.015	0.9818	**[P]**	0.016	−0.004	0.9828
[C]	0.004	0.9882	**[C]**	0.004	−0.000	0.9883
[F]	0.006	0.9548	**[F]**	0.005	0.006	0.9747
[N]	0.002	0.6930	**[N]**	0.002	0.007	0.9629
[Z]	0.004	0.9729	**[Z]**	0.004	−0.003	0.9846
[D-PC]-Pb	0.009	0.9597	[D-PC]-Pb	0.009	0.004	0.9627
[D-PC]-Cu	0.001	0.9658	[D-PC]-Cu	0.001	0.000	0.9669
[D-PC]	0.010	0.9662	**[D-PC]**	0.010	0.004	0.9690
[D-PF]-Pb	0.008	0.9790	[D-PF]-Pb	0.008	−0.004	0.9827
[D-PF]-Fe	0.004	0.9860	[D-PF]-Fe	0.003	0.003	0.9951
[D-PF]	0.012	0.9873	**[D-PF]**	0.012	−0.001	0.9876
[D-PN]-Pb	0.009	0.9569	[D-PN]-Pb	0.009	0.005	0.9622
[D-PN]-Ni	0.001	0.4479	[D-PN]-Ni	0.001	0.002	0.5521
[D-PN]	0.010	0.9527	**[D-PN]**	0.009	0.007	0.9616
[D-PZ]-Pb	0.009	0.9542	[D-PZ]-Pb	0.009	0.004	0.9576
[D-PZ]-Zn	0.001	0.9088	[D-PZ]-Zn	0.001	−0.002	0.9378
[D-PZ]	0.010	0.9639	**[D-PZ]**	0.010	0.003	0.9649
[D-CF]-Cu	0.002	0.9523	[D-CF]-Cu	0.002	−0.004	0.9933
[D-CF]-Fe	0.004	0.9666	[D-CF]-Fe	0.004	0.005	0.9902
[D-CF]	0.006	0.9923	**[D-CF]**	0.006	0.001	0.9925
[D-CN]-Cu	0.003	0.9888	[D-CN]-Cu	0.003	−0.001	0.9915
[D-CN]-Ni	0.001	0.6540	[D-CN]-Ni	0.001	0.003	0.9089
[D-CN]	0.004	0.9795	**[D-CN]**	0.004	0.002	0.9843
[D-FZ]-Fe	0.005	0.9332	[D-FZ]-Fe	0.004	0.007	0.9906
[D-FZ]-Zn	0.002	0.9303	[D-FZ]-Zn	0.002	−0.002	0.9494
[D-FZ]	0.006	0.9777	**[D-FZ]**	0.006	0.005	0.9907
[D-NZ]-Ni	0.001	−0.2510	[D-NZ]-Ni	0.000	0.003	0.6264
[D-NZ]-Zn	0.002	0.9348	[D-NZ]-Zn	0.002	−0.004	0.9801
[D-NZ]	0.002	0.9605	**[D-NZ]**	0.002	−0.000	0.9605
[T]-Pb	0.006	0.9434	[T]-Pb	0.006	0.005	0.9536
[T]-Cu	0.001	0.9747	[T]-Cu	0.001	−0.001	0.9826
[T]-Fe	0.003	0.9622	[T]-Fe	0.003	0.004	0.9900
[T]	0.011	0.9668	**[T]**	0.010	0.008	0.9761
[M]-Pb	0.004	0.8584	[M]-Pb	0.004	0.007	0.9130
[M]-Cu	0.001	0.9473	[M]-Cu	0.001	−0.001	0.9851
[M]-Fe	0.002	0.9465	[M]-Fe	0.002	0.003	0.9886
[M]-Ni	0.000	0.8566	[M]-Ni	0.000	0.001	0.9251
[M]-Zn	0.001	0.8479	[M]-Zn	0.001	−0.002	0.9720
[M]	0.008	0.9585	**[M]**	0.008	0.007	0.9713

[A] $q_t = k_P \cdot (\sqrt{t})$; [B] $q_t = k_P \cdot (\sqrt{t}) + C$

A significantly low correlation is observed for the singular uptake of the Zn^{2+} ion in the [D-PZ], [D-FZ], [D-NZ], and [M] component systems when observed by the PSO model. The Ni^{2+} ion in the [N], [D-PN], [D-CN] and [D-NZ] component systems also demonstrates a weaker correlation in its singular uptake when observed by the IPD model. However, due to zeolite's lower selectivity to these ions, the overall uptake in each combined component system is not significantly affected by these incurred outliers. Based on the initial sorption rate determined by the PSO kinetic model given in **Table 6.4**, the single-component system of lead (Pb^{2+}) [P] achieves the greatest rate at 0.0046 meq/g·min among the HMI investigated. In the dual-component systems, the overall uptake of HMI containing Pb^{2+} was on average 0.0037 meq/g·min. For the dual-component systems without Pb^{2+}, the uptake rate was on average 0.0016 meq/g·min. The initial sorption rates in the triple- and multi-component systems were observed as 0.0042 and 0.0033 meq/g·min, respectively. This kinetic analysis has demonstrated that the initial uptake rate of total HMIs is most improved with the presence of lead.

Although the Elovich equation was not selected as the primary model of consideration to represent the reaction-type chemisorption relationship associated with the sorption process, the comparison between initial sorption rates is a valued discussion. In the kinetic analysis of lead removal from aqueous solution by natural clinoptilolite by Gunay et al. (2007), the Elovich equation produced trends that the initial sorption rate (related to chemisorption) increased with an increase in initial concentration, while the β constant (related to surface coverage) decreased with an increase in initial concentration and increased with an increase in mass of sorbent (site availability). With reference to **Table 6.6** of this study, the overall influence of the total HMI removal on each component system is consistent between each model, with the initial sorption rate of α being on average 0.0039 meq/g·min greater than that of h (Largitte and Pasquier, 2016). The data shows a stronger correlation with the PSO model compared to that of the Elovich Equation; validating the model selection rationale of this study.

Table 6.6 Pseudo-Second-Order (PSO) and Elovich Data Comparison

SYSTEM	PSO		Elovich				
	CC	Initial Sorption Rate $h = k_2 q_e^2$ (meq/g·min)	CC	$m = \left(\dfrac{1}{\beta}\right)$	$b = \left(\dfrac{1}{\beta}\right)[\ln(\alpha\beta)]$	Elovich Constant β (g/meq)	Initial Sorption Rate α (meq/g·min)
[P]	0.9926	**0.0046**	0.9742	0.0486	-0.0697	20.58	**0.0116**
[C]	0.9291	0.0012	0.9104	0.0118	-0.0151	84.75	0.0033
[F]	0.9708	0.0024	0.9606	0.0165	-0.0162	60.61	0.0062
[N]	0.9806	0.0014	0.9614	0.0049	-0.0002	204.08	0.0047
[Z]	0.9147	0.0009	0.9208	0.012	-0.0188	83.33	0.0025
[D-PC]	0.9906	0.0037	0.9730	0.0309	-0.0382	32.36	0.0090
[D-PF]	0.9837	0.0036	0.9636	0.0361	-0.0496	27.70	0.0091
[D-PN]	0.9914	0.0039	0.9767	0.0294	-0.0336	34.01	0.0094
[D-PZ]	0.9946	0.0036	0.9794	0.0315	-0.0409	31.75	0.0086
[D-CF]	0.9703	0.0020	0.9564	0.0189	-0.0243	52.91	0.0052
[D-CN]	0.9471	0.0013	0.9165	0.0109	-0.012	91.74	0.0036
[D-FZ]	0.9554	0.0022	0.9174	0.0166	-0.0162	60.24	0.0063
[D-NZ]	0.9113	0.0007	0.9164	0.0075	-0.0099	133.33	0.0020
[T]-Pb	0.9980	0.0025	0.9880	0.0186	-0.0214	53.76	0.0059
[T]	0.9918	0.0042	0.9809	0.0314	-0.0354	31.85	0.0102
[M]-Pb	0.9990	0.0021	0.9869	0.0113	-0.0097	88.50	0.0048
[M]	0.9931	0.0033	0.9815	0.0236	-0.0257	42.37	0.0079

The trendlines' equations displayed in **Table 6.4** and **Table 6.5** are applied to the kinetic models for the total HMI uptake of the various component systems, and shown for visual comparisons in **Figures 6.2** to **6.4**. **Figure 6.5** presents the uptake (q_t) of all five HMIs in the [M] multi-component system over the three-hour contact period, with both kinetic models applied in linearized form based on **Equation 6.6** and excluding the boundary constant of **Equation 6.9**. It is observed that even for this most complicated system containing all five HMIs [M], it is evident that a stronger correlation, at a CC of 0.9931, is achieved with the PSO rate model.
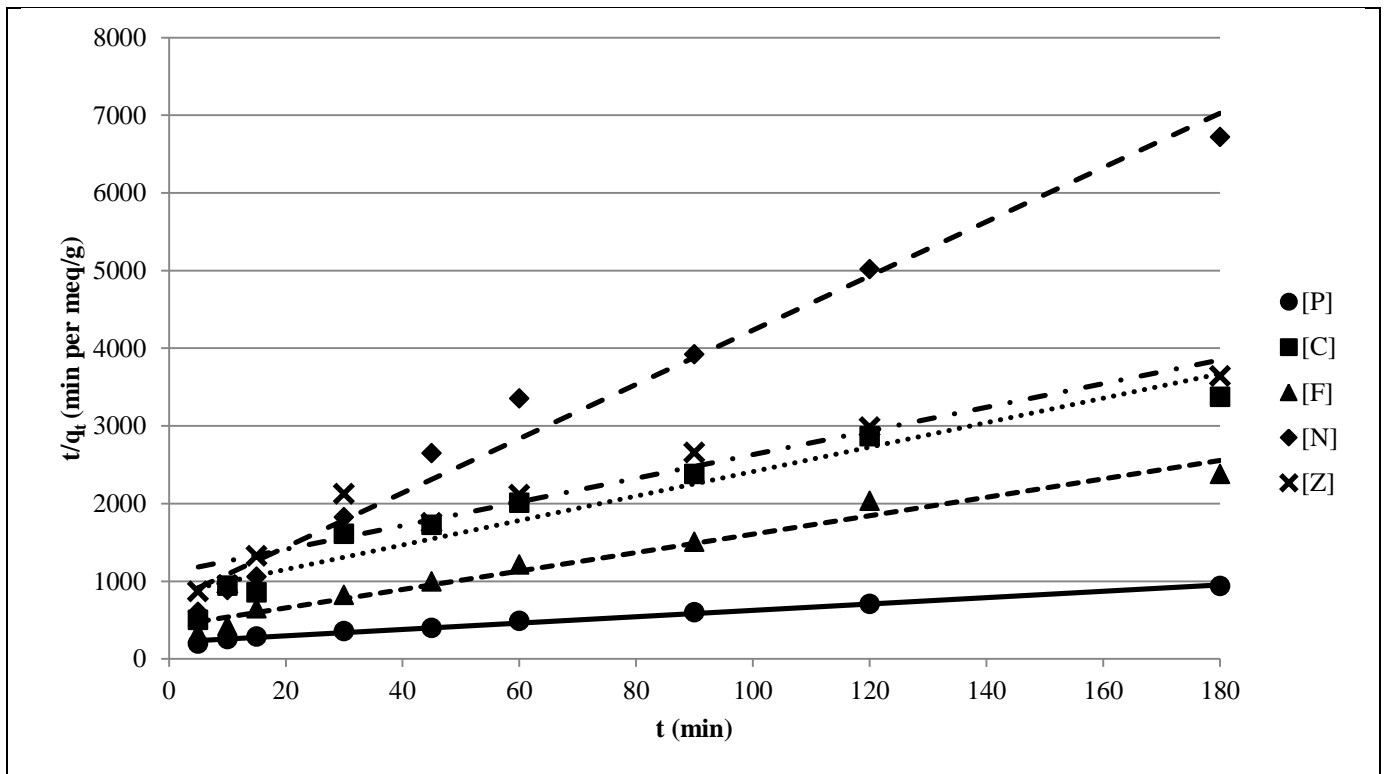
a.
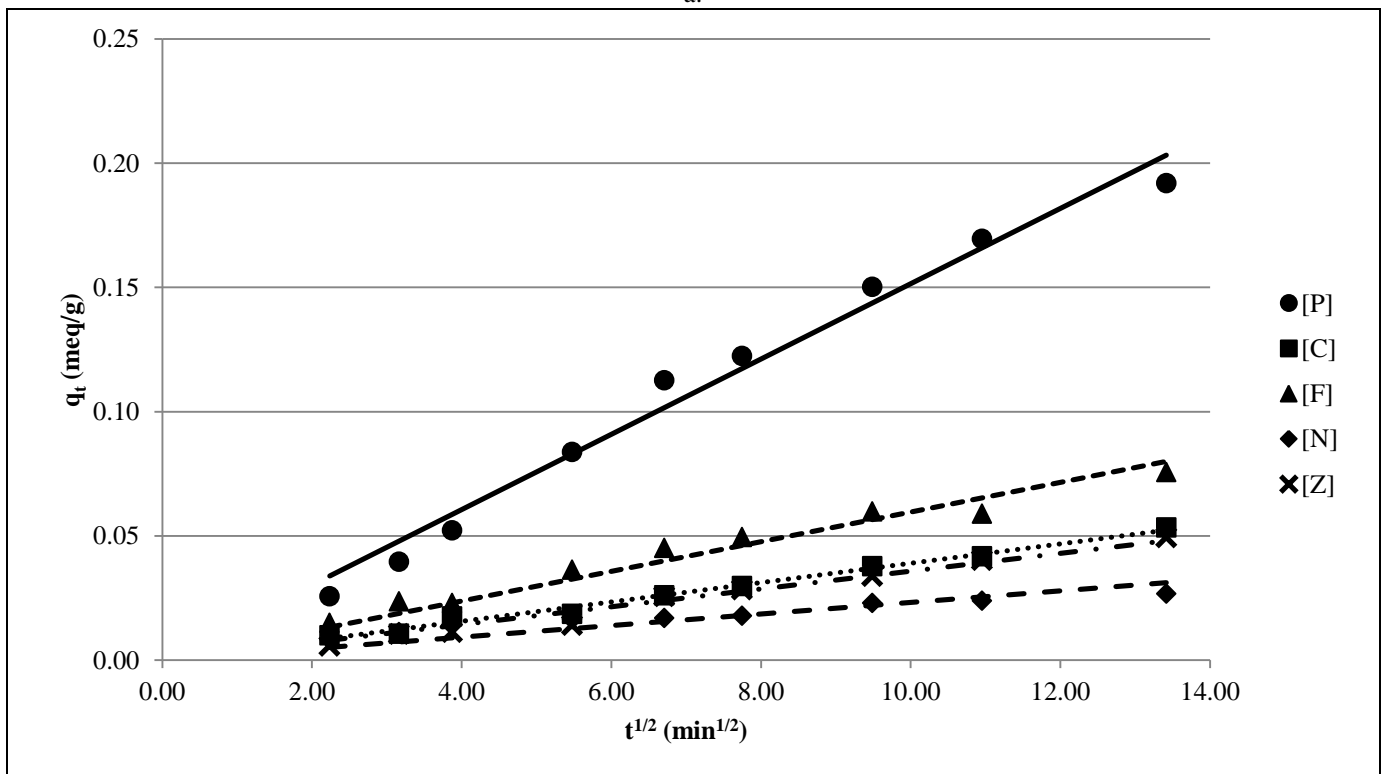
b.

Figure 6.2 Single-Component System Kinetic Model Plots
a. pseudo-second-order; b. intra-particle diffusion
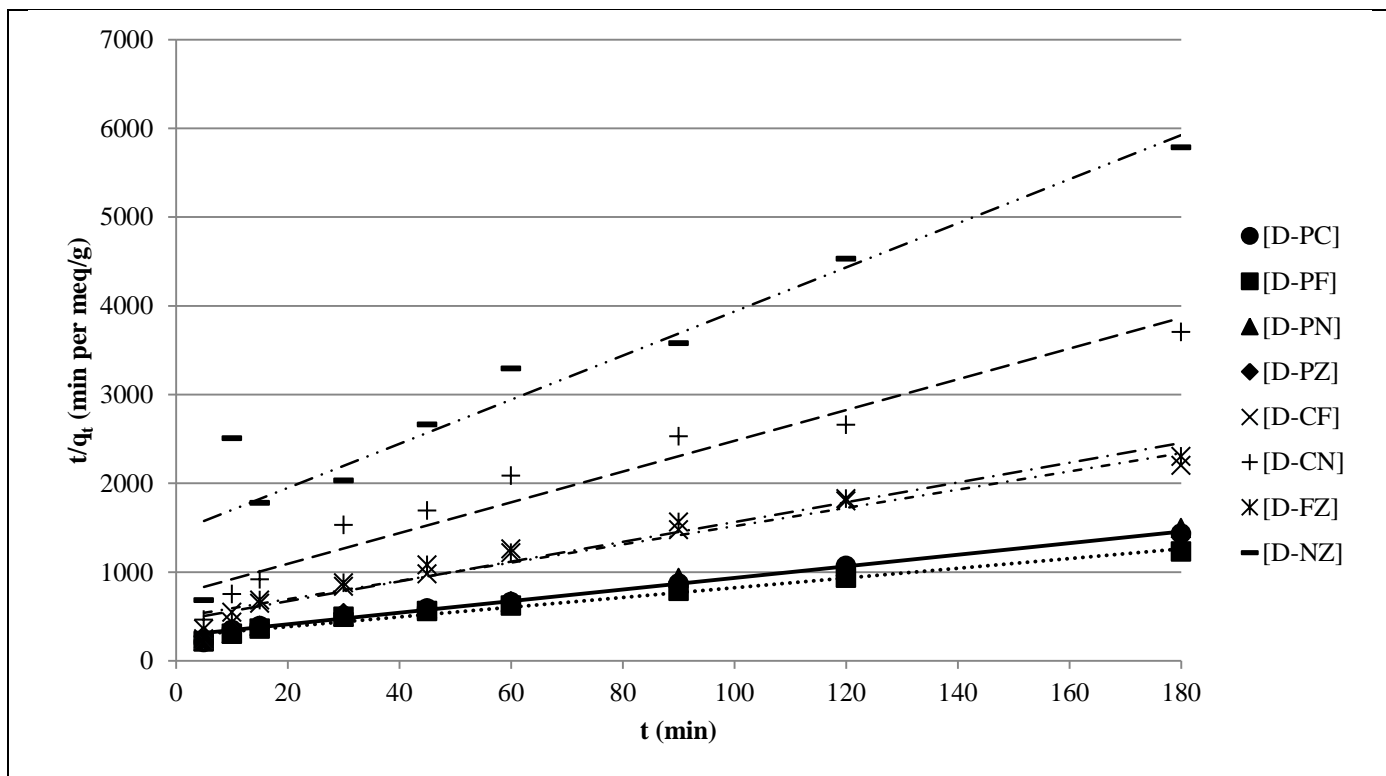
a.
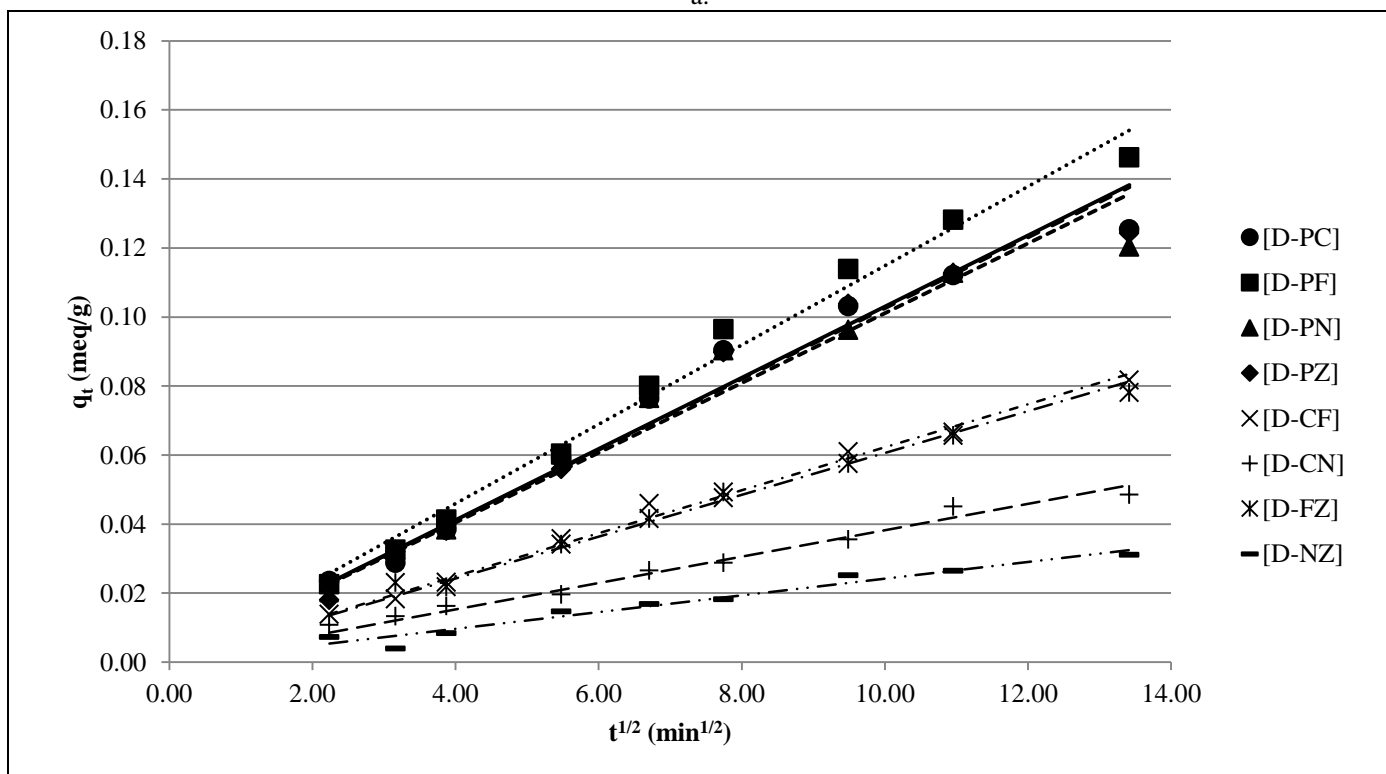
b.

Figure 6.3 Dual-Component System Kinetic Model Plots
a. pseudo-second-order; b. intra-particle diffusion
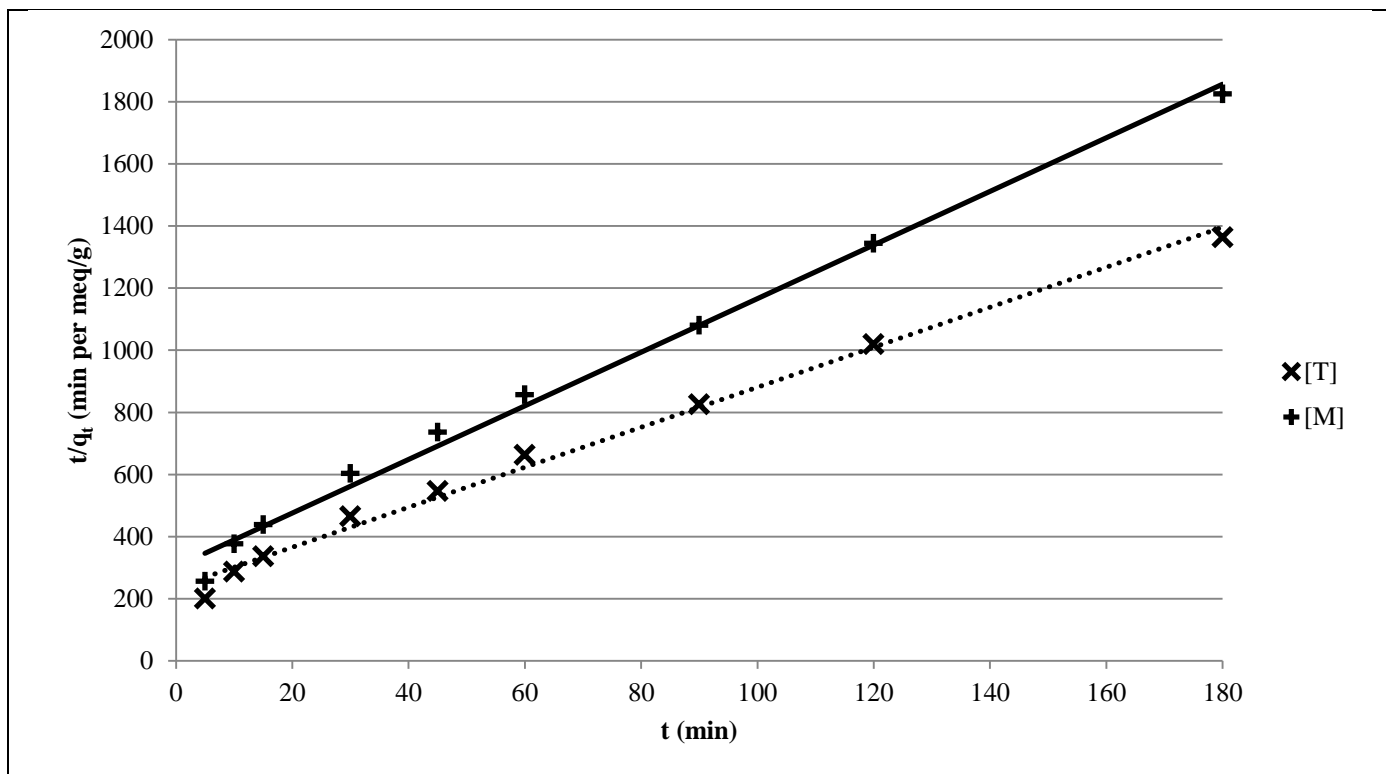
a.
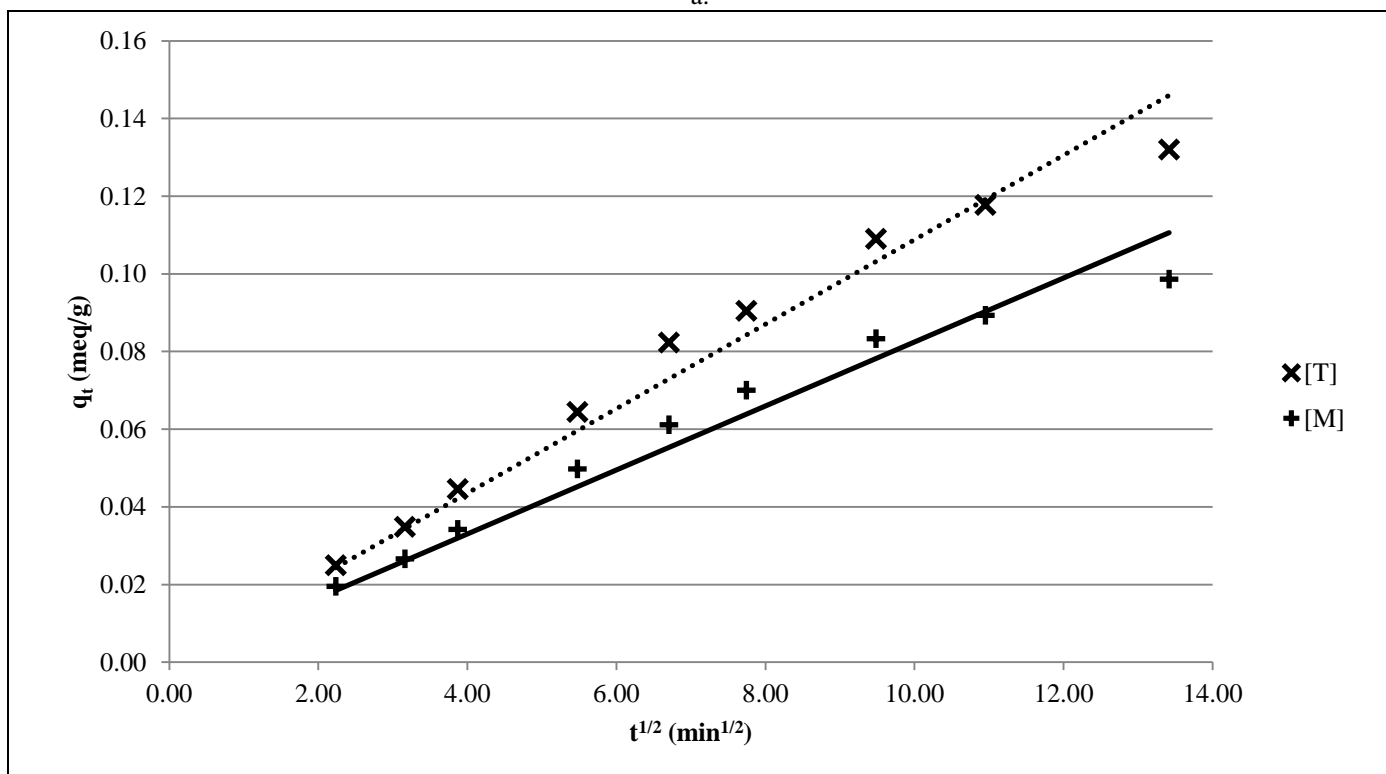
b.

Figure 6.4 Triple- and Multi-Component System Kinetic Model Plots
a. pseudo-second-order; b. intra-particle diffusion
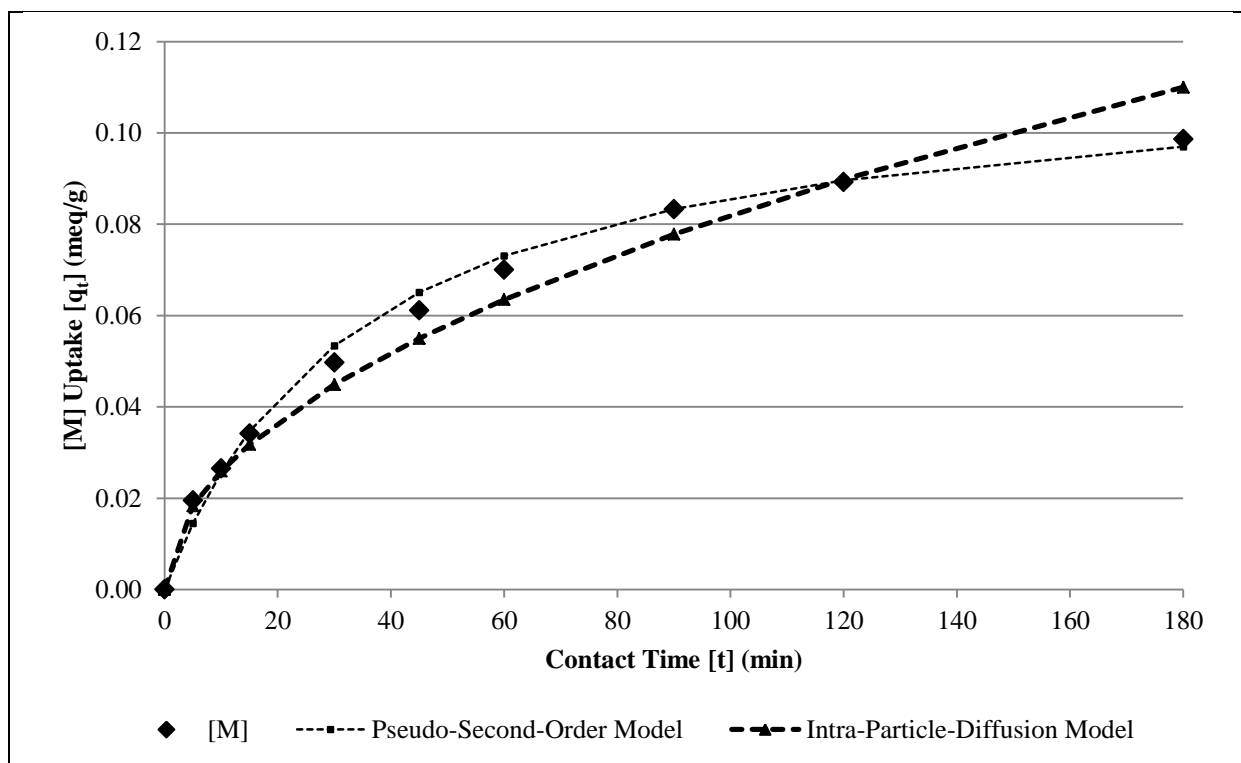
Figure 6.5 Multi-component System – Uptake Over Time alongside Kinetic Models

The data presented in **Table 6.7** provides compelling trends into the removal efficiency and the zeolite's selectivity to the five HMIs investigated in this study. When comparing the total HMI uptake at 3 contact hours to the theoretical equilibrium values generated by the PSO model of each system, an average of 83.5% of the equilibrium uptake is achieved. In the single-component systems, the uptake of [P] is highest, followed by [F], [C], [Z], and [N]. Only 78.7% of [P] at equilibrium is achieved, whereas 93.5% of [N] at equilibrium is observed. At the opposite end of removal efficiency, there is this significant difference in overall uptake. In the dual-component systems, the [D-PF] is the greatest uptake and the [D-NZ] is the least. The overall HMI uptake is increased by an average of approximately 0.0778 meq/g or 152% when combined with Pb^{2+}; when comparing [C], [F], [N], and [Z] to [D-PC], [D-PF], [D-PN] and [D-PZ], respectively. For the dual-systems without Pb^{2+}, the presence of Fe^{3+} improves the uptake in [D-CF] and [D-FZ] by 53.2 and 58.1%, respectively; the Ni^{2+} hinders the overall uptake in [D-CN] and [D-NZ] by 9.00 and 37.1%, respectively. The combination of lead, copper and iron in the triple-component system increases the [D-PC] and [D-CF] by 5.20 and 61.5%, respectively; but the inclusion of Cu^{2+} decreases the [D-PF] by 9.80%. Once again, the Pb^{2+} ion has the greatest improvement to the overall uptake of total HMI of a given system. In the multi-

102

component system, the introduction of Ni^{2+} and Zn^{2+} impedes on the total HMI uptake in the triple system [T] by 25% for both the experimental and theoretical equilibrium data. This demonstrates that each HMI impacts the zeolite's ability to sorb those co-ions in solution.

As reported in **Table 6.7**, the zeolite removal efficiency order based on the experimental and theoretically derived equilibrium HMI uptake data is observed as $Pb^{2+} \gg Fe^{3+} > Cu^{2+} > Zn^{2+} > Ni^{2+}$. This selectivity trend is also observed in other experimental findings, including Wang and Peng (2010), and Inglezakis et al. (2002; 2003). Current research on the HMI sorption capacity of natural zeolites and other sorbent materials is summarized in **Table 6.8**. Accordingly, the natural zeolite employed in this study compares favourably and within trend based on the major findings of current research endeavours.

Table 6.7 Experimental Total and Theoretical Equilibrium HMI Uptake System Observations

SYSTEM		(meq/g) q_{180}	q_e	% Achieved of q_e at 3 contact hours	OBSERVATION			
SINGLE HMI	[P]	0.1919	0.2440	78.7	Highest Single Uptake of 76.8% for q_{180} [P]			
	[C]	0.0533	0.0635	84.0				
	[F]	0.0757	0.0842	89.8				
	[N]	0.0268	0.0286	93.5	Lowest Single Uptake of 10.7% for q_{180} [N]			
	[Z]	0.0494	0.0656	75.3				
DUAL [D]	[PC]	0.1255	0.1516	82.7				
	[PF]	0.1462	0.1822	80.3	Highest [D] Uptake of 58.5% for q_{180} [PF]			
	[PN]	0.1204	0.1433	84.0				
	[PZ]	0.1243	0.1530	81.2				
	[CF]	0.0817	0.0971	84.1				
	[CN]	0.0486	0.0577	84.1				
	[FZ]	0.0782	0.0898	87.1				
	[NZ]	0.0311	0.0402	77.3	Lowest [D] Uptake of 12.4% for q_{180} [NZ]			
TRIPLE [T]		0.1320	0.1553	85.0	[D-PC] Increased 5.2% 2.5% [D-PF] Decreased 9.8% 14.7% [D-CF] Increased 61.5% 59.9%			
MULTI [M]		0.0986	0.1159	85.1	[D-PC] Decreased 21.4% 23.6% [D-PF] Decreased 32.6% 36.4% [D-CF] Increased 20.7% 19.3% [T] Decreased 25.3% 25.4%			
							q_{180}	q_e

Table 6.8 The Sorption Trends of Heavy Metallic Ions on Various Sorbent Materials

Sorbent Material	HMI	Sorption Trends		Reference
		q_{180} (meq/g)	q_e	
American 85–95% Clinoptilolite	Pb^{2+}	0.1919	0.2440	This Study
	Fe^{3+}	0.0757	0.0842	
	Cu^{2+}	0.0533	0.0635	
	Zn^{2+}	0.0494	0.0656	
	Ni^{2+}	0.0268	0.0286	
		$Pb^{2+} \gg Fe^{3+} > Cu^{2+} > Zn^{2+} > Ni^{2+}$		
Brazilian Zeolite (Scolecite)	Cu^{2+}	130 µeq/g		Bosso and Enzweiler (2002)
	Zn^{2+}	64 µeq/g		
	Pb^{2+}	56 µeq/g		
	Ni^{2+}	31 µeq/g		
	Co^{2+}	7.8 µeq/g		
	Cd^{2+}	3.2 µeq/g		
		$Cu^{2+} \gg Zn^{2+} > Pb^{2+} > Ni^{2+} > Co^{2+} > Cd^{2+}$		
Turkish 70% Clinoptilolite	Co^{2+}	77.96% (0.448 meq/g)		Erdem et al. (2004) Wang and Peng (2010)
	Cu^{2+}	66.10% (0.282 meq/g)		
	Zn^{2+}	45.96% (0.268 meq/g)		
	Mn^{2+}	19.84% (0.153 meq/g)		
		$Co^{2+} > Cu^{2+} > Zn^{2+} > Mn^{2+}$		
Ukrainian 75% Clinoptilolite	Pb^{2+}	27.7 mg/g		Sprynskyy et al. (2006)
	Cu^{2+}	25.76 mg/g		
	Ni^{2+}	13.03 mg/g		
	Cd^{2+}	4.22 mg/g		
		$Pb^{2+} > Cu^{2+} > Cd^2 > Ni^{2+}$		
Sardinian 40–70% Clinoptilolite	Pb^{2+}	0.34 meq/g		Cincotti et al. (2006)
	Cu^{2+}	0.27–1.2 meq/g		
	Zn^{2+}	0.1 meq/g		
	Cd^{2+}	0.05-0.19 meq/g		
		$Pb^{2+} > Cu^{2+} > Cd^{2+} \cong Zn^{2+}$		
Turkish Zeolite (Clinoptilolite and Heulandite)		Single-	Multi-	Oter and Akcay (2007) Wang and Peng (2010)
	Pb^{2+}	0.730 meq/g	0.299 meq/g	
	Zn^{2+}	0.251 meq/g	0.108 meq/g	
	Cu^{2+}	0.227 meq/g	0.022 meq/g	
	Ni^{2+}	0.173 meq/g	0.017 meq/g	
		$Pb^{2+} > Zn^{2+} > Cu^{2+} > Ni^{2+}$		
Turkish Clinoptilolite	Fe^{3+}	6.41 mg/g		Motsi et al. (2009)
	Zn^{2+}	1.60 mg/g		
	Cu^{2+}	0.44 mg/g		
	Mn^{2+}	0.37 mg/g		
		$Fe^{3+} > Zn^{2+} > Cu^{2+} > Mn^{2+}$		
Brine Sediments	Zn^{2+}	4.85 mg/g		Fu and Wang (2011)
	Cu^{2+}	2.58 mg/g		
Sawdust Materials	Zn^{2+}	4.69 mg/g		
	Cu^{2+}	2.31 mg/g		
Dried Marine Green Macroalga Algal Biomass	Cu^{2+}	1.46 mmol/g		
	Zn^{2+}	1.97 mmol/g		
Rhizopus Oryzae Fungi Biomass	Cu^{2+}	19.4 mg/g (Natural) 43.7 mg/g (NaOH-treated)		

6.4.4. Experimental Evaluation of Reaction Rate Kinetics

The concurrent assessment of reaction rate constants and the orders of reaction with respect to all relevant entities under a variety of experimental conditions (i.e., concentrations) would require extensive experimentation and data analyses. Therefore, an abridged approach to evaluate one entity at a time is applied, by limiting the experimental conditions to assume that the reaction is irreversible and the concentrations of all but one entity remain approximately constant throughout the experiment. In this case, the reaction rate is assumed to follow a power law, approximated by the following expression in **Equation 6.10** (Benjamin, 10, p. 97):

$$r_A = -k_n[A]^n \tag{6.10}$$

where [A] refers to the one reactant (i.e., HMI) whose concentration changes significantly during the experiment, such that the concentration is typically analyzed in a batch-mode reactor. To evaluate the experimental data, the *integral method* is a common approach in determining rate constants. Assuming that the reaction is the only process that alters [A], the rate of change of [A] is equated with the reaction rate as seen in **Equation 6.11** (Benjamin, 10, p. 98):

$$r_A = \frac{d[A]}{dt} \rightarrow \int_{[A]_0}^{[A]_t} \frac{d[A]}{r_A} = \int_0^t dt \tag{6.11}$$

where $[A]_0$ and $[A]_t$ refer to the initial reactant concentration and the reactant concentration at time t (HMIs in meq/L), respectively. By predicting the order of the reaction (n), the substitution for r_A is made into **Equation 6.11** to generate the integrated expression. The expressions for first-, second-, and n^{th}- order reactions are presented in **Table 6.9**.

Table 6.9 Rate Expressions for Reactant A Concentration in a Batch-Mode Reactor System (adapted from Benjamin, 2010, p. 100)

Rate Expression		Reaction Order (n)		
		1	2	n^{th}
Differential Form		$r_A = \frac{d[A]}{dt} = -k_{n=1}[A]$	$r_A = \frac{d[A]}{dt} = -k_{n=2}[A]^2$	$r_A = \frac{d[A]}{dt} = -k_n[A]^n$
Integral Form		$\int \frac{d[A]}{[A]} = -k_{n=1}\int dt$	$\int \frac{d[A]}{[A]^2} = -k_{n=2}\int dt$	$\int \frac{dc_A}{c_A^n} = -k_n \int dt$
Integrated Expression	$k_i t$	$k_{n=1}t = \ln\left(\frac{[A]_0}{[A]_t}\right)$	$k_{n=2}t = \frac{1}{[A]_t} - \frac{1}{[A]_0}$	$k_n t = \left(\frac{1}{n-1}\right)([A]_t^{1-n} - [A]_0^{1-n})$
	$[A]_t$	$[A]_t = [A]_0 \cdot \left(e^{-k_{n=1}t}\right)$	$[A]_t = \left(\frac{1}{[A]_0} + k_{n=2}t\right)^{-1}$	$[A]_t = ([A]_0^{1-n} + (n-1) \cdot k_n t)^{\frac{1}{1-n}}$

By plotting $\ln([A]_t)$ versus t for a first-order reaction (Chemistry LibreTexts, 2015), a slope of $-k_{n=1}$ (in min^{-1}) (Benjamin, 2010, p. 98) and y-intercept of $\ln([A]_0)$ (Chemistry LibreTexts, 2015) is generated. By plotting $\frac{1}{[A]_t}$ versus t for a second-order reaction, a slope of $k_{n=2}$ (in L/meq·min) and y-intercept of $\frac{1}{[A]_0}$ (in L/meq) are generated (Benjamin, 2010, p. 100). If the reaction order prediction is correct, then the plot versus t would be linear with a strong correlation (CC value close to 1.0). *However, an assumed rate expression will not always reproduce the experimental observations*. If this is the case (i.e., a non-linear relationship is observed), then an alternative reaction order integer predication is made and the process is repeated. The integral method was applied to evaluate the experimental data of each HMI entity in this study, in each (single-, dual-, triple-, multi-) component system combination. The corresponding reaction rate data (reaction rate constants, predicated initial concentrations, and correlation coefficients) is presented in **Table 6.10**.

As reported in Benjamin (2010, p. 98), the first-order reaction rate plot of $\ln\left(\frac{[A]_t}{[A]_0}\right)$ versus t also generates a slope of $-k_{n=1}$ (in min^{-1}). For each HMI entity in **Table 6.10**, only an average percent difference of 0.07% between the $k_{n=1}$ slope values is observed, with a stronger overall correlation (CC^Y) in the $\ln([A]_t)$ versus t plot. The initial predication of a first-order reaction ($n = 1$) generates a reasonable linear correlation, with 17.2% of the CC values below the acceptable range (0.85) and 41.1% above the excellent range (0.95-1.0). This prompted the decision to repeat the process and predict a second-order reaction ($n = 2$), which shows that 69.0% of the CC values are above the excellent range. With the HMI single-component system combinations as an example, **Figure 6.6** illustrates the strong linear relationships of both reaction orders with the respective rate decay profiles (Benjamin, 2010, p. 99). In keeping with the zeolite selectivity order and regardless of which reaction order, the lead ion (Pb^{2+}) shows the strongest correlation and the nickel ion (Ni^{2+}) shows the weakest correlation. However, the predicated initial concentrations of $[A]_0$ for the Pb^{2+} ion in the dual-, triple-, and multi-component system combinations at $n = 2$ are off-trend; such that the theoretically expected values of 5.0, 3.33, and 2.0 meq/L for each component system, respectively, are exceeded by those concentrations predicated. Although a slightly stronger correlation is observed at $n = 2$, it is proposed that the sorption reaction rate of the Pb^{2+} ion is best represented by the first-order reaction rate, such that

the concentration is only dependent on the one reactant (a unimolecular reaction). This analysis thereby demonstrates that *the rate of sorption changes for each HMI as additional HMIs are introduced into solution,* under the testing conditions of the various component system combinations.

Table 6.10 Reaction Rate Data

SYSTEM	First Order n = 1					Second Order n = 2		
	$-m = k_{n=1}$ (min^{-1})	CC^X	$-m = k_{n=1}$ (min^{-1})	$[A]_0$ (meq/L)	CC^Y	$m = k_{n=2}$ (L/meq·min)	$[A]_0$ (meq/L)	CC^Z
[P]	0.0092	0.9358	0.0081	8.85	0.9719	0.0018	10.2	0.9969
[C]	0.0016	0.7928	0.0012	9.63	0.9409	0.0001	9.64	0.9559
[F]	0.0025	0.6235	0.0018	9.27	0.8785	0.0002	9.29	0.9080
[N]	0.0008	0.0588	0.0005	9.63	0.7651	0.0001	9.62	0.7800
[Z]	0.0014	0.8535	0.0012	9.72	0.9409	0.0001	9.74	0.9539
[D-PC]-Pb	0.0134	0.9450	0.0119	4.24	0.9751	0.0080	7.26	0.9774
[D-PC]-Cu	0.0009	0.7135	0.0007	4.88	0.9101	0.0001	4.88	0.9202
[D-PF]-Pb	0.0099	0.9548	0.0089	4.49	0.9783	0.0042	5.47	0.9940
[D-PF]-Fe	0.0032	0.7322	0.0024	4.59	0.9218	0.0006	4.61	0.9544
[D-PN]-Pb	0.0139	0.9459	0.0123	4.21	0.9762	0.0087	7.89	0.9758
[D-PN]-Ni	0.0006	0.1422	0.0004	4.88	0.5693	0.0001	4.88	0.5728
[D-PZ]-Pb	0.0136	0.9383	0.0121	4.21	0.9704	0.0083	7.19	0.9831
[D-PZ]-Zn	0.0008	0.8591	0.0007	4.94	0.9156	0.0001	4.94	0.9231
[D-CF]-Cu	0.0016	0.9130	0.0014	4.89	0.9527	0.0003	4.90	0.9664
[D-CF]-Fe	0.0038	0.6898	0.0028	4.49	0.9097	0.0008	4.52	0.9506
[D-CN]-Cu	0.0023	0.8368	0.0018	4.76	0.9438	0.0004	4.78	0.9623
[D-CN]-Ni	0.0008	0.1051	0.0005	4.82	0.7680	0.0001	4.82	0.7789
[D-FZ]-Fe	0.0040	0.6208	0.0029	4.41	0.8970	0.0008	4.44	0.9424
[D-FZ]-Zn	0.0013	0.9114	0.0011	4.90	0.9678	0.0002	4.90	0.9756
[D-NZ]-Ni	0.0005	-0.7590	0.0002	4.85	0.4677	0.0001	4.85	0.4720
[D-NZ]-Zn	0.0014	0.9171	0.0012	4.91	0.9519	0.0003	4.92	0.9628
[T]-Pb	0.0146	0.9395	0.0129	2.76	0.9737	0.0146	5.77	0.9733
[T]-Cu	0.0014	0.8438	0.0011	3.24	0.9413	0.0004	3.24	0.9528
[T]-Fe	0.0046	0.7071	0.0035	2.93	0.9132	0.0015	2.96	0.9601
[M]-Pb	0.0183	0.9073	0.0158	1.51	0.9553	0.0422	12.5	0.9760
[M]-Cu	0.0016	0.9192	0.0014	1.96	0.9590	0.0008	1.96	0.9700
[M]-Fe	0.0056	0.7110	0.0042	1.71	0.9156	0.0034	1.74	0.9695
[M]-Ni	0.0007	0.3354	0.0005	1.94	0.7790	0.0003	1.94	0.7869
[M]-Zn	0.0011	0.9694	0.0011	2.00	0.9695	0.0006	2.00	0.9752

$^X \ln\left(\frac{[A]_t}{[A]_0}\right)$ versus t ; $^Y \ln([A]_t)$ versus t; $^Z \frac{1}{[A]_t}$ versus t
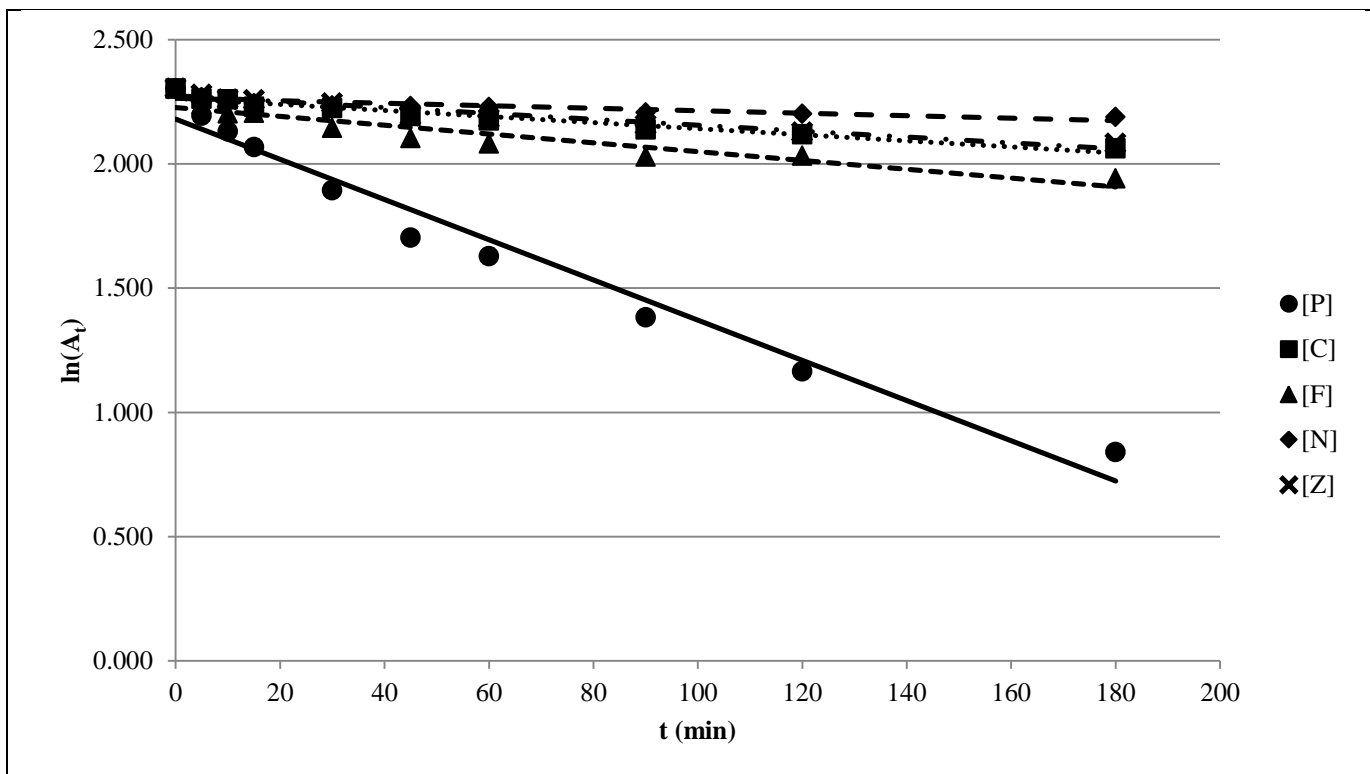
a.
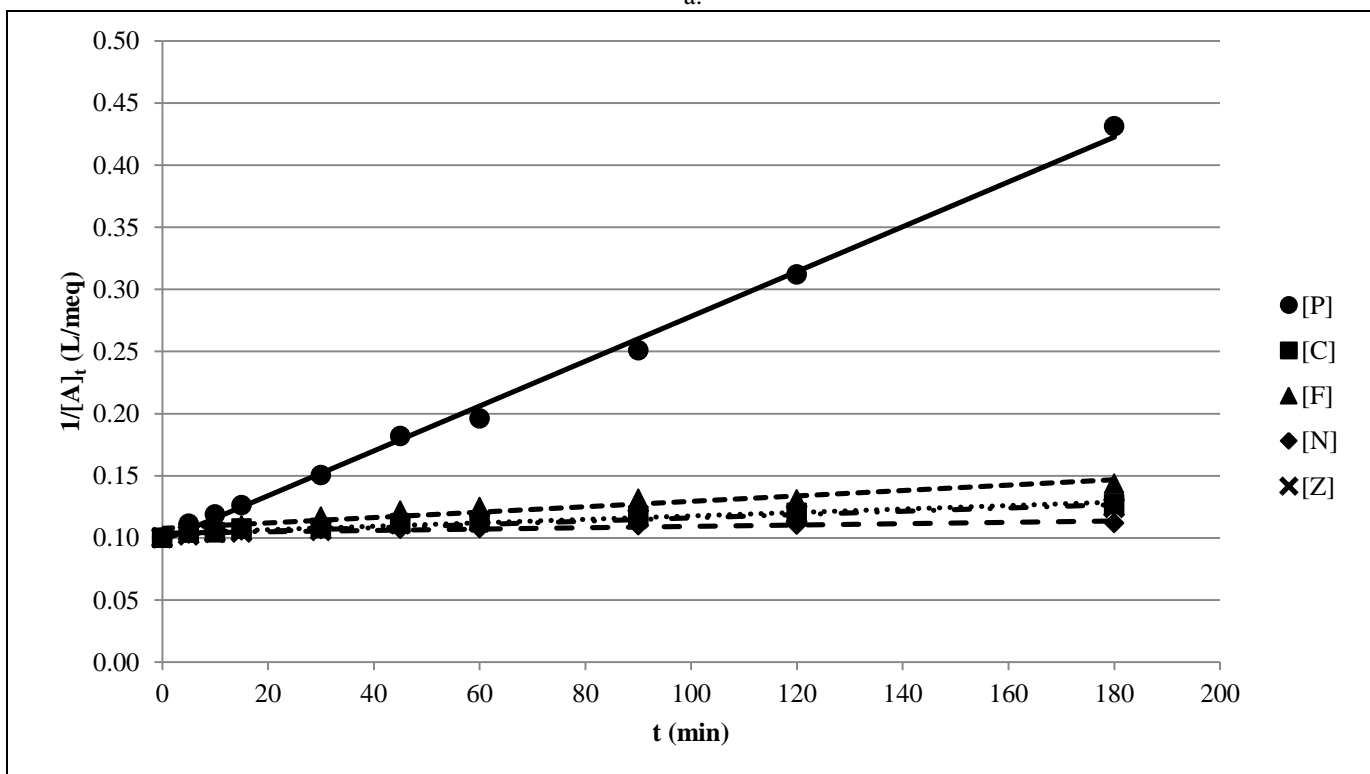
b.

Figure 6.6 Single-Component System Reaction Rate Decay Profiles
a. First-Order; b. Second-Order

6.4.5. Sensitivity Analysis Considerations of Model Parameters

In the assessment of the sensitivity of the experimental parameters in each non-linear form of a kinetic model, it is observed that the amount of HMI sorbed at equilibrium (q_e; meq/g) and the rate constant (k_2; g/meq·min) for the pseudo-second-order (PSO) model are critical variables; consistent with the findings presented by Dridi-Dhaouadi et al. (2011). The research conducted by Dridi-Dhaouadi et al. (2011) investigates the sorption of inorganic (heavy metal; Pb^{2+}) and organic pollutants by biomass, in both single- and dual-component systems; demonstrating a strong correlation with the PSO model, the analysis indicates that the q_e uptake is more sensitive than the k_2 constant. The study presented in the Dissertation document demonstrated that the zeolite mineral exhibits the greatest preference towards the lead ion (Pb^{2+}); considered in its single-component system [P], with reference to **Table 6.4** and **Figure 6.2a** of this chapter, a strong correlation of 0.9926 is observed based on the plot of t/q_t versus t under the specified testing conditions. As discussed in the previous subsection in the evaluation of the experimental data, the lead ion exhibits a different reaction rate compared to the other HMIs when combined in the various component systems. Accordingly, the quality control protocol discussed in **Section 3.3.** prompts the *need to allocate thoughtful attention to the influent concentration parameter when a kinetic model and reaction rate assessment are conducted, in order to predict the sorption of the Pb^{2+} ion by natural zeolite.*

It is important to note that the process variables of the zeolite source and particle size, sorbent-sorbate dosage, initial concentration, pH level, set-temperature as well as agitation speed are kept constant in this study. This was maintained in order to create a purposeful experimental design, with feasibility, to best observe the impact of the heavy metallic ions in combination. Although the pseudo-second-order kinetic model has demonstrated the strongest representation of the data in uptake over time, to declare the reaction based mechanism of chemisorption as the overall rate-determining step is not the objective of this study. Accordingly, it is recommended that the variation of the process variables would be required to make that final statement. Rather, this study has investigated simultaneous sorption of the HMIs, with the quantification of uptake and rate of interference of these HMIs in numerous component system combinations. The selected reaction and diffusion kinetic models demonstrated in this study have provided a stronger understanding into the associated mechanisms prior to equilibrium of the overall sorption process.

6.5. Conclusions

The sorption kinetics of the multiple heavy metallic ions (HMIs) predominantly found in mine wastewater has been investigated. With the systematic experimental design of five HMIs and zeolite in its natural state, the sorption uptake rate and subsequent interference of these HMIs in combination has been quantified and modelled. Both the pseudo-second-order (PSO) and intra-particle diffusion kinetic model demonstrate a very strong correlation of the extensive experimental data. However, the PSO model demonstrated a stronger performance, and further contributed to the assessment of the zeolite mineral performance and the fundamental mechanisms associated with the sorption process. Usually, the equilibrium sorption capacity is unknown. The process of chemisorption is significantly slow, and the sorbed amount is smaller than that at equilibrium. Study limitations include the fact that the time required to reach equilibrium is very long in various sorption systems. Although rapid uptake was observed in the first 45 minutes, the desired balanced state is achieved beyond the analysis period of kinetic analysis. A significant improvement to this study would be to extend the 3-hour contact time, in order to associate the equilibrium state capacity experimentally and theoretically, as well as evaluate various operative conditions to generate further insight into associated mechanisms. Nevertheless, the PSO model provides important information of the sorption capacity, initial sorption rate and overall rate coefficients devoid of any parameter in advance (Ho and Ofomaja, 2006).

6.6. Future Works

Further investigations in the variation of operation parameters are needed from this phase to develop a greater understanding of the kinetic reaction relationships. Through modeled kinetics, the prediction of sorption rate is significant for batch system design, in order to determine the solute uptake required for optimal conditions of full-scale processes. To be presented in **Chapter 7**, future work on this research project focuses on the interaction of heavy metallic ions combined in the multi-component system using natural zeolite in continuous-mode, with the design of a dual-column, fixed bed reactor, treatment system prototype.

7. DUAL-COLUMN SORPTION SYSTEM PERFORMANCE

An Innovative Dual-Column System for
Heavy Metallic Ion Sorption by Natural Zeolite

Fundamental components of this chapter were also presented as a paper at the WEAO2018 Technical Symposium ('Industrial Treatment B' Session); referenced in **Appendix E** of the Dissertation document.

Abstract

This study investigates the design and performance of a novel sorption system containing natural zeolite. The apparatus consists of packed, fixed-bed, dual-columns with custom automated controls and sampling chambers, connected in series and stock fed by a metering pump at a controlled adjustable distribution. The purpose of the system is to remove heavy metallic ions commonly found in industrial wastewater effluent, including lead (Pb^{2+}), copper (Cu^{2+}), iron (Fe^{3+}), nickel (Ni^{2+}) and zinc (Zn^{2+}), combined in equal equivalence to form an acidified total 10 meq/L aqueous solution. Reported trends on the zeolite's preference to these heavy metallic ions is established in the system breakthrough curve, as $Pb^{2+} \gg Fe^{3+} > Cu^{2+} > Zn^{2+} \gg Ni^{2+}$. Within a 3-hour contact period, Pb^{2+} is completely removed from both columns. Insufficient Ni^{2+} removal is achieved by either column with the promptest breakthrough attained, as zeolite demonstrates the least affinity towards it; however, a 49.0% removal is observed in the cumulative collection at the completion of the analysis period. The empty bed contact times for the first and second columns are 20 and 30 minutes, respectively; indicating a higher bed capacity at breakthrough and a lower usage rate of the zeolite mineral in the second column. This sorption system experimentally demonstrates the potential for industrial wastewater treatment technology development.

7.1. Introduction

The performance of columns or fixed-bed reactors (FBR) is convenient for industrial scale applications (Vukojevic Medvidovic et al., 2013), which requires less investment and operational costs, and is more economically feasible than its discontinuous batch-mode counterparts (Nuic et al., 2016). FBR columns have demonstrated performance efficiency in treating large volumes, and are frequently implemented in sorption studies. Operations are affected by equilibrium (isotherm and capacity), kinetic (diffusion and convection coefficients) and hydraulic (liquid holdup, geometric analogies and mal-distribution) factors (Inglezakis, 2010a). In practice, the influence of operative conditions on the overall system performance is not fully experimentally verified (Curkovic et al., 1997; Erdol Aydin and Nasun Saygili, 2009; Inglezakis et al., 2001a), but are extremely important to large-scale development. Although the FBR system is highly valuable, its analysis is unpredictably multi-faceted (Inglezakis, 2010a; 2010b) and even more so with the presence of numerous interfering ions. Complications due to ion competition and solute-surface interactions (Mohan and Chander, 2006), as well as the unique affinity sequences and sorbent material selectivity (Nuic et al., 2015), have been reported.

The first three phases of this research project (**Chapters 4** to **6**)were conducted in batch-mode, which reveal a key trend among the HMIs selected as lead (Pb^{2+}) >> iron (Fe^{3+}) > copper (Cu^{2+}) > zinc (Zn^{2+}) > nickel (Ni^{2+}). The findings of these preliminary phases have established a platform for the design of the sorption system in continuous mode, presented in this chapter.

Existing column experimental designs involve various limitations, including:
1. The evaluation of predominantly single- or dual-component HMI system combinations;
2. The implementation of primarily slender column aspect ratios (i.e., bed depth/particle diameter, column height/diameter), causing a challenge to eventual scale-up design;
3. The use of inconsistent and/or vague sorbent compaction techniques, and;
4. The application of simple, idealized flow patterns (i.e., set single and continuous flow rate).

The objective of this final research phase is to develop a novel dual-column sorption system to overcome some of these shortcomings. Important design factors such as the zeolite compaction, column dimensions and aspect ratios, flow control, sampling and analytical procedure, will be taken into consideration. *The exclusivity of this prototype is attributed to an*

automated, variable-flow configuration with a custom sampling technique. In contrast to most previous single-component sorption set-ups, this study evaluates the simultaneous sorption process by natural zeolite of five commonly occurring HMIs found in industrial wastewater effluent. This study will demonstrate the effectiveness and the removal efficiency in a continuous-flow FBR system over a 3-hour contact duration from the dual columns, providing insights on HMIs selectivity and treatment system breakthroughs. It is envisaged that this research will provide much-needed information to the wastewater treatment industry for the design and implementation of innovative sorption technologies.

7.2.   Materials and Methods

Refer to **Chapter 3** for the consolidated experimental methodology; sorbent material, sorbate solution, and analytical procedure. All analyses are conducted in continuous-mode, creating the synthetic simple solute HMI solution in the multi-[M] component system combination. The following subsections discuss the associated breakthrough and exhaustion principles as well as the treatment system prototype design details for this study.

7.2.1. Packed Fixed-Bed Column Design Considerations

When the concentration of the effluent reaches 5-10% of the influent, this point on a typical S-shaped breakthrough curve is commonly referred to as the 'breakthrough point' or 'breakpoint' (BP) (Beyazit, 2013). The point of column exhaustion (EP) is when the effluent reaches maximum capacity to 90-95% of its influent concentration value (Nuic et al., 2013; Vukojevic Medvidovic et al., 2006). The efficiency of the column performance is related to the bed capacity at breakthrough and at exhaustion, represented by the following relationship (Nuic et al., 2013; Vukojevic Medvidovic et al., 2006):

$$\eta = \frac{C_{BP}}{C_{EP}} \tag{7.1}$$

where η is the column efficiency (degree of saturation), C_{BP} is the breakthrough capacity of the bed (in meq/g), and C_{EP} is the maximum capacity at exhaustion of the bed, defined by the total amount of HMI ions bound in the zeolite (or exchanged in the packed fixed-bed) (in meq/g).

The breakthrough capacity and equilibrium capacity are further expressed in **Equation 7.2** and **Equation 7.3**, respectively (Nuic et al., 2013; Vukojevic Medvidovic et al., 2006):

$$C_{BP} = \frac{\int_0^{V_{BP}}(C_0 - C_t)\,dV}{\rho HA} = \frac{C_O \cdot V_{BP}}{m} = \frac{\eta_{BP}}{m_Z} \tag{7.2}$$

$$C_{EP} = \frac{\int_0^{V_{EP}}(C_0 - C_t)\,dV}{\rho HA} = \frac{\int_0^{V_{EP}}(C_O - C_t)\,dV}{m} = \frac{\eta_{EP}}{m_Z} \tag{7.3}$$

where V_{BP} is the effluent volume collected up to breakthrough point (BP) (in L), V_{EP} is the effluent volume at which the exhaustion point (EP) is reached in the zeolite bed (in L), C_O is the influent concentration (in meq/L), C_t is the effluent concentration (in meq/L), ρ is the packing density of the bed (in g/cm^3), H is the bed depth (in cm), A is the bed cross-sectional area (in cm^2), m_Z is the zeolite mass (in g); where η_{BP} and η_{EP} is the total amount of HMI ions removed up to BP and EP (in meq), respectively.

The empty bed contact time (EBCT) is a primary design variable (Droste, 1997, p. 489), which represents the length of time a liquid stream is in contact with the bed without sorbent. It is related to the removal kinetics of the column treatment system medium (Reed et al., 1996; Jarvie et al., 2005). This is represented by the following relationship between the bed depth (H) in the column and the feed solution velocity (v) (Droste, 1997, p. 478; Nuic et al., 2015; Vukojevic Medvidovic et al., 2006):

$$EBCT = \frac{H}{v} = \frac{H}{(Q/A)} = \frac{d^2 \pi H}{4Q} \tag{7.4}$$

Research conducted by Vukojevic Medvidovic et al. (2006) demonstrates that the breakthrough curve results reveal that the flow through the column determines the EBCT; with the same initial concentration, the increase in flow rate decreases the contact time and increases the mass transfer zone (MTZ) height. The MTZ is the restricted area where the exchange process occurs, and is defined as the zeolite layer height between the equilibrium zone and the unused bed zone (Vukojevic Medvidovic et al., 2006); where the effluent concentration varies from 5-95% of the influent concentration (Nuic et al., 2015). As the HMI solution is fed through the packed fixed-bed, the MTZ moves in the direction of flow and eventually reaches the exit (Nuic et al., 2013; Vukojevic Medvidovic et al., 2006). Peric et al. (2009) distinctly demonstrates the

importance of the column bed depth on the removal of lead from aqueous solutions. The results show that as the bed depth increases, a delay in breakthrough and exhaustion occurs, with an increase of the MTZ height. The higher the bed depth, the longer the service time at various breakthrough points due to the increase in binding sites on the sorbent material (zeolite mineral) (Han et al., 2006). Adequate wetting of the zeolite, and ideal contact time between the zeolite and solution interface are important for mass transfer and equilibrium conditions based on the selection of the flow rate and particle size. To minimize possible wall and axial dispersion effects in the fixed-bed column, the bed depth-to-particle diameter ratio (H/d_p) must be greater than 20. At a higher H/d_p ratio, the breakthrough point appears later and the curve is steeper.

The usage rate (v_U, in g/L) determines the rate at which the sorbent would be exhausted and how often it must be replaced or regenerated, and is expressed in the following relationship (Jarvie et al., 2005; Mohan and Chander, 2006; Nuic et al., 2015):

$$v_U = \frac{m_Z}{V_{BP}}$$

(7.5)

where m_Z is the zeolite mass in the bed (in g) and V_{BP} is the volume of the effluent treated at breakthrough (BP) (in L) (Nuic et al., 2015). Inglezakis (2010a) states that it is extremely difficult to model multi-component system interactions, as numerous time-consuming data are required and the process involves significant mathematical complexity. Breakthrough and exhaustion thresholds of specific HMIs within a fixed-bed are important for experimental specific conditions. In order to optimize the liquid-solid contact time and removal capacity, it is necessary to develop a greater understanding of these relationships, between EBCT and usage rate (Inglezakis, 2010a).

7.2.2. Sorption Treatment System Design

Based on qualitative observations, the uptake of counter-ions in a continuous column system is favoured by various factors, including: a strong preference of the zeolite for the HMI counter-ions in solution, low concentration of HMI counter-ions, small and uniform particle size, high volume capacity and low degree of cross-linking, elevated temperature and low flow rate, as well as a high column height or aspect ratio (Helfferich, 1962, p. 427). The apparatus development considered an extensive material and equipment selection process, with numerous stages of optimization in order to maintain flow continuity and repeatability. The prototype development is highlighted in **Appendix A.10** of the Dissertation document.

The final design was adopted in consideration of the following factors:

- Zeolite Compaction Technique
  - Regulated Layers of Dry Mass
  - Systematic Tampered Compaction
- Column Dimensions
  - Modular Design
  - Internal Diameter (1 in)
  - Sorption Column Height (1 ft)
- Flow Configuration
  - Upflow Distribution
  - Dual-Column Series Connection
  - Methodical Flow Rate Variability

- Pump Type
  - Diaphragm Metering
- Sampling Method
  - Automated Mode Controls
  - Customized Sampling Chambers
  - Modes' Interchange
    in Five (5)-minute Intervals
- Analysis Period
  - Three (3)-hour Contact Period

Based on these critical parameters, the sorption system design was finalized. **Figure 7.1** is a schematic representation of the constructed prototype, detailing the flow paths through the system. The fundamental components include:

- HMI Multi-Component Influent Stock
- Metering Pump
- Silicon Tubing and
  Polyvinyl chloride (PVC) Connections
- Check Valves
- Automatable Solenoid Valves (symbol S)

- Packed Fixed-Bed Sorption Columns
- Custom Sampling Chambers
- Sampling Ports
- Effluent Collection Basin
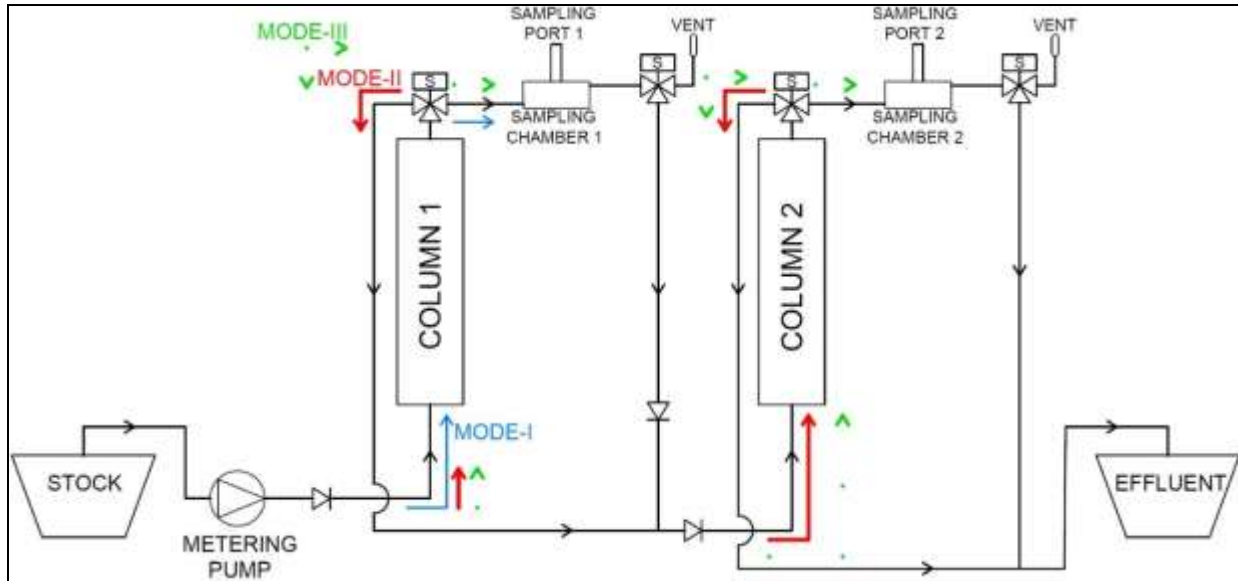
Figure 7.1 Schematic of Automated Sorption System Prototype Flow Path Layout
(adapted from Ciosek and Luk, 2017d)

7.2.2.1. *Column Dimensions*

The column was made of a circular section of clear PVC SCH-40 pipe (Part No. r4-1000; Fabco Plastics; Maple, ONT, Canada), 30.48 cm in height with 2.61 cm internal diameter. In order to minimize potential effects of wall and axial dispersion in the columns, the bed depth-to-particle diameter ratio should be kept greater than 20 (Peric et al., 2009). Using the average nominal zeolite diameter of 1.00 mm as a reference, this ratio translated to over 300 for the design. The cleaned and dry zeolite particles were added to the column at nine layers applied at 20-mL or 16.9 g amounts. Each layer was compacted with medium force, pounding six times with a customized PVC plunger of a diameter equal to the internal diameter of the column; such that the column height and the zeolite bed depth are equivalent. Inert plastic mesh with a smaller size than the minimum zeolite particle gradation of 0.841 mm was used to contain the zeolite material, and permitted sample flow through the columns. This mesh was set at each end of the column, within the two halves of a PVC SCH-80 socket union fitting incorporating a viton o-ring (Part No. 897010; Fabco Plastics; Maple, ONT, Canada), connected to a nominal $1 \times 1/2$-inch PVC SCH-40 reducer bushing (Part No. 438130 (slip $\times$ FPT); Fabco Plastics; Maple, ONT, Canada). All components were connected to 1/4-inch silicon tubing and with corresponding adapters and nipples fittings.

7.2.2.2. *Flow Rate and Configuration*

As a dual-stage system, the two columns were connected in a serial-flow arrangement, such that the first column received the original stock with a higher HMI concentration and the second column received the effluent from the first column. The upflow configuration ensures an overall better quality of flow, with a low liquid hold-up and a good stock feed distribution across the column cross sectional area (Inglezakis, 2010a); enabling the media to move upward and fall away separately from the filter, swirling the solution within the system to yield a longer contact time (Andoh, 2014). In contrast, for the downflow mode, an increase in pressure drop and flooding of the column bed is more probable (Inglezakis, 2010a). Consequently, the stock was fed in an upflow direction to ensure proper and thorough distribution to the column beds and to minimize the need for backwashing (Gregory, 2010) and head loss effects.

A critical parameter in the design process is the flow rate. Existing research demonstrates that lower flow rates result in high detention times in the column, which is needed due to the relatively slow uptake rate of zeolite (Inglezakis et al., 2002; 2004). The HMI solution volume element is in contact with a given zeolite bed layer for only a limited period of time. Consequently, equilibrium is not usually achieved and results in a lower overall uptake of HMIs from the influent stock solution. Preliminary testing involved a peristaltic pump, using the corresponding silicon rubber tubing. Significant back pressure was observed and the capacity of the peristaltic pump was hindered. Consequently, the required flow rate was unachievable; the rotational speed and strength decreased for the feed to completely traverse through the entire system. Subsequently, a diaphragm-type metering pump (No. 950218125-C Plus, max 45-LPD, 80-psi, 125-AC, 50/60-Hz; PULSAtron; Punta Gorda, FL, USA) was employed in the final design, which mechanically facilitates the desired stock feeding rate. Based on the 45-LPD (31.25 mL/min) capacity of the metering pump, preliminary flow rate testing of the pump set to 100% stroke (mechanically pumped volume) and 50% rate established an initial, repeatable, point-of-reference flow rate of 6.36 ± 0.32 mL/min. This stroke-rate setting was maintained and is comparable to the lower end of the 6-18 mL/min range recommended by Inglezakis et al. (2002; 2004), to provide sufficient detention time in the system.

7.2.2.3.   Sampling Method

Another critical component to the design is the sampling method, and how to maintain continuous flow through the system while sampling the effluent of both columns. Due to the relatively slow feeding rate selected for this study, the time to collect the desired sample volume for dilution and ICP-AES analysis would require residual sample volume and minutes of valuable contact time. Therefore, three-way solenoid valves (No. 00457979, 0124-C, 1/8-FKM-PP, NPT-1/4, max 145-psi, 24-V, 60-Hz, 8-W, 38-mL; burkert; Ingelfingen, Germany) were implemented as a device to ensure that while a sample volume is collected at the desired sampling time, both columns would still be fed continuously by unique the modes of operation. The MODE valves and custom fabricated rotating 30-mL sampling chambers were attached to the top exit of each sorption column, with accessible sampling ports. A second three-way solenoid VENT valve was included at the exit of each sampling chamber to introduce an air vent to assist in rapid sample extraction by preventing vacuum pockets within the sample chamber and discharge tubing. A multi-turn valve was included at the exit of the vent for the first column to introduce minor back pressure similar to that of the second column, so as to not significantly alter the flow characteristics through the first column. Check valves were placed at critical locations throughout the hydraulic circuit to prevent back flows.

7.2.2.4. *System Modes of Operation*

The sorption system presented in this paper is comprised of three distinct modes of operation that are controlled by the MODE valves for each column, in the following sequence:

- **MODE-I**
    - Activate System
        - Prime Inlet Tubing and Check Valve
        - Fill Inlet Connection Cavity
    - Fill Sorption Column 1 (8:39 min:s to fill)
    - Fill Sample Chamber 1 (3:40 min:s to fill)
- **MODE-II**
    - Divert Flow from Sampling Chambers
    - Activate VENT Valve
        - Collect Column 1 Sample (C1-A at 18:50 min:s)
    - 'Circulate' Flow through Sorption Columns
    - Fill Sorption Column 2 (8:27 min:s to fill)
- **MODE-III**
    - 'Pulse' Flow between Sampling Chambers
        - Divert 100% flow, 50% time per Timer Setting
    - Fill Sampling Chambers
- **MODE-II**
    - Detour Flow from Sampling Chambers
    - Activate VENT Valve
        - Collect Samples from Sorption Columns (C1-B and C2-B at 42:50 min:s)
    - 'Circulate' Flow through Sorption Columns
- **>INITIATE MODE-II/III SEQUENCE<**

Figure 7.2 presents the arrangement of the prototype components, including an adjustable bi-stable timer which determines the time division modulation of the MODE and VENT solenoid valves.

Activating the process in Mode-I, the fluid element was mechanically pumped from the acidified 3-L multi-component influent stock. Once the pump is turned on, the inlet tubing was primed with the influent stock and passed the column check valve at the system inlet. The fluid element passed through the mesh-union fitting and reached the base of the first column (C1), and traversed up through the sample chamber entry solenoid valve to the first sampling chamber. Once the 30-mL sample chamber was filled, the fluid element began to drip at its exit against the multi-turn valve, which was an indication to switch the sample chamber entry solenoid MODE valves to Mode-II using the automated mode controls.

In Mode-II, the fluid element by-passes the first sampling chamber (SC1), continued to traverse through column 1 (C1) and began to fill column 2 (C2). The fluid element did not cross-circuit back towards the exits of first column, due to the connection of additional check valves connection located at the entry of the second column. While the fluid element traversed up both columns C1 and C2, the sampling chamber exit solenoid VENT valve was switched from closed to open. The sampling port tube was uncapped, twisted using the custom rotating handle and inverted to draw a 30-mL sample. The VENT valve was then turned off (closed from atmosphere). It is important to note that the inlet-outlet offset of the sampling chambers guarantees a highly repeatable sample volume. It is designed to minimize cross-contamination, for when the chamber is rotated from the vertical upward (sample collection in Mode-III) to downward (sample dispense in Mode-II and VENT) position, the chamber contents are completely void.

Once C2 was filled, both MODE valves of the sampling chambers were switched from Mode-II to Mode-III. The fluid element now simultaneously traverses through C1 and C2, while filling SC1 and SC2, dividing the flow rate and maintaining a continuous flow through the system. Once both sampling chambers were filled, the MODE valves were switched from Mode-III back to Mode-II, such that the fluid element by-passes the sample chambers and only traverses through the columns. At this time, the VENT valves were switched from closed to open, and the samples were taken from the sampling ports of both SC1 and SC2. Once both samples were collected, the VENT valves were closed and the MODE valves were once again switched back to pulse in Mode-III until SC1 and SC2 were filled. This sequence was repeated at approximately 5-minute increments between Mode-II and Mode-III, for a total analysis period of just over 3-hours. The prototype was secured to a sturdy, level frame that included supporting clamps for the packed fixed-bed columns and a removable sampling chamber lock mechanism for maintenance accessibility.
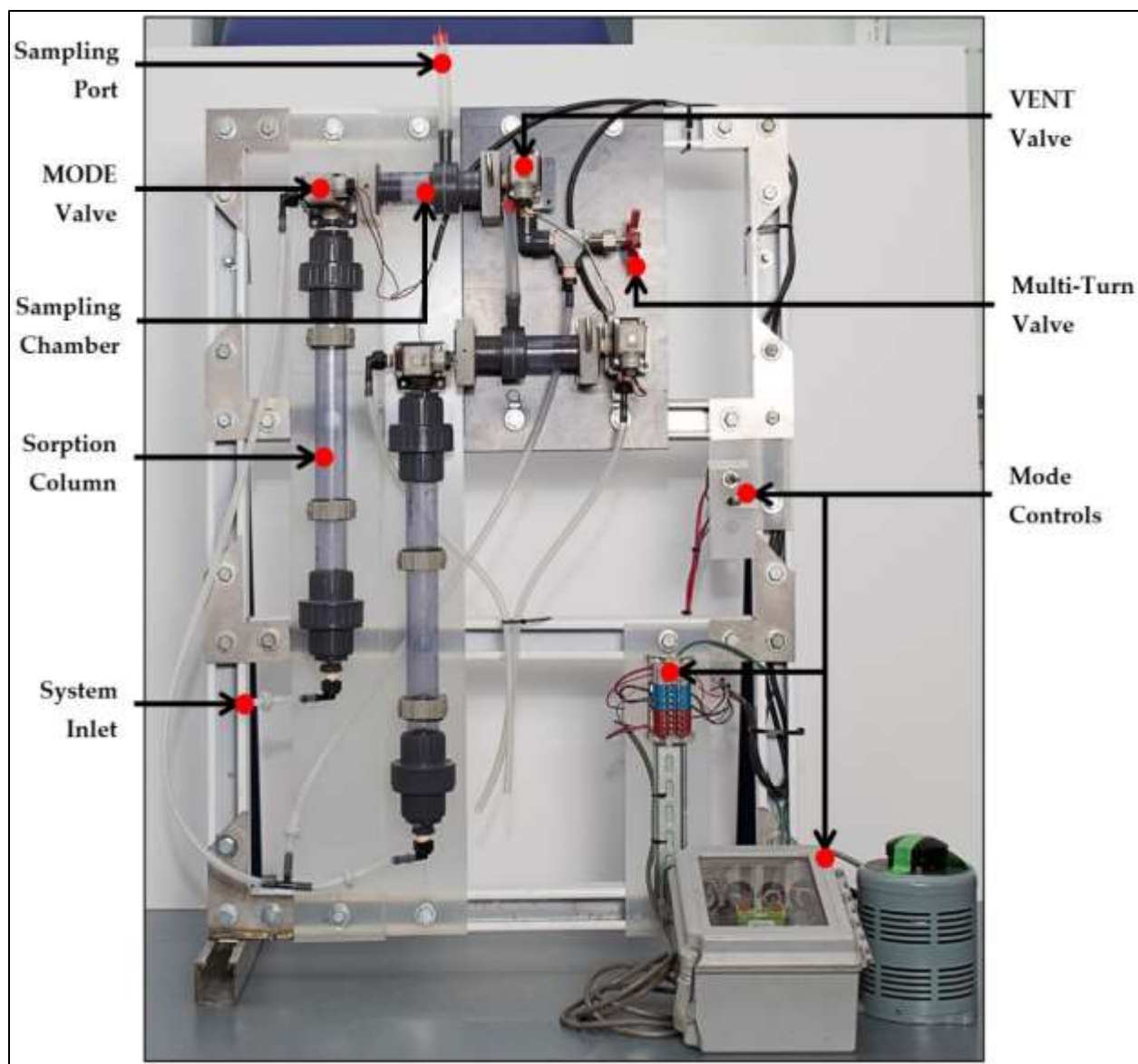
Figure 7.2 Image of Automated Sorption System Prototype Design
(adapted from Ciosek and Luk, 2017d)

It is important to note that the sample chambers were fabricated to a 30-mL capacity, to ensure that the 25-mL required volume is attained, to be filtered for dilution in preparation of ICP-AES analysis. This influences the time to collect the sample volume, based on the selected pump flow rate of this study. Also, the spacing of the prototype components influences the tubing connection lengths. The dual-column sorption system design presented in **Figure 7.1** and **Figure 7.2** provides the opportunity to analyze higher flow rates and/or prolonged sample collection in Mode-III in future research endeavours.

7.3. Quality Control (QC) Protocol

For all analytical sessions, the triplicate concentration of the median standard (50 mg/L) detected an average of 49.26 mg/L, and is within 5% of the known value; the percent relative standard deviation (%-RSD) reported an average of 0.433%, which is well within the $\leq 3\%$ limit; the correlation coefficient of each HMI analyte primary wavelength generated an average of 0.999977, which is very close to unity.

The multi-component stock was created by diluting the respective HMI nitrate salts of three 1-L stock solutions, acidified to a pH of 2.0 ± 0.1, and then re-combined. These 3 stocks (denoted as X, Y, Z) were diluted by one 50% step to be within the 0–100 mg/L calibration range, analyzing each separately and combined (denoted as [M]). The five metals in a multi-component system of 2.0 meq/L per metal corresponded to concentrations of approximately 207 mg/L for Pb^{2+}, 64 mg/L for Cu^{2+}, 37 mg/L for Fe^{3+}, 59 mg/L for Ni^{2+}, and 65 mg/L for Zn^{2+}, respectively. The consistency in stock preparation is demonstrated in **Table 7.1**.

Table 7.1 ICP-AES Generated Multi-Component Stock Concentration.

Sample ID	Analyte	Int (Corr)	RSD (Corr Int)	Conc (Calib) (mg/L)
	Cu 327.393	188,070.71	0.27	34.26
	Fe 238.204	79,641.94	0.39	19.18
M-X	Ni 231.604	41,071.22	0.50	29.81
	Pb 220.353	32,330.16	0.52	105.28
	Zn 206.200	55,015.91	0.38	32.31
	Cu 327.393	186,885.03	0.74	34.04
	Fe 238.204	79,083.95	0.90	19.04
M-Y	Ni 231.604	40,721.53	0.48	29.55
	Pb 220.353	31,973.87	0.31	104.12
	Zn 206.200	54,758.60	1.09	32.16
	Cu 327.393	202,742.71	0.91	36.93
	Fe 238.204	85,771.53	1.02	20.65
M-Z	Ni 231.604	44,652.28	3.73	32.41
	Pb 220.353	35,199.76	3.77	114.63
	Zn 206.200	60,176.84	4.12	35.34
	Cu 327.393	192,776.82	0.63	35.11
	Fe 238.204	81,419.80	0.80	19.60
M[M]	Ni 231.604	41,667.28	0.38	30.24
	Pb 220.353	32,738.45	0.40	106.61
	Zn 206.200	56,170.16	0.94	32.99

The average diluted concentrations of the X, Y, and Z influent stocks for Cu^{2+}, Fe^{3+}, Ni^{2+}, Pb^{2+}, and Zn^{2+} are 70.15, 39.25, 61.18, 216.02, and 66.54 mg/L, respectively. The diluted concentration of the M influent stock for Cu^{2+}, Fe^{3+}, Ni^{2+}, Pb^{2+}, and Zn^{2+} are 70.22, 39.21, 60.48,

213.2, and 65.98 mg/L, respectively. A maximum difference of 2.80 mg/L, equivalent to 1.30%, is detected for the Pb^{2+} stock. Also, the corresponding HMI concentrations in mg/L are comparable to the theoretically expected values, based on the selected total 10 meq/L initial concentration; only a 0.05% difference between the average of all initial concentrations of the theoretical and combined M stock is detected. Overall, this demonstrates that strong quality control has been implemented.

7.4. Analysis

7.4.1. Preliminary Batch-Mode Trends

Detailed analysis on the selected HMIs of this study was conducted by Ciosek and Luk (2017a; 2017c) in batch-mode configuration (as presented in **Chapter 5** and **6** of the Dissertation document), consisting of a synthetic nitrate salt solution at 10 meq/L total concentration, acidified to a pH of 2 by concentration HNO_3 acid, with a zeolite dosage of 4 g per 100-mL HMI solution. The aqueous solution was agitated within a contact period 180 minutes by means of a triple-eccentric drive orbital shaker operating at 400 r/min set to 22°C. The five (5) HMIs were methodically combined in single-, dual-, triple-, and multi-component systems. Elemental analysis by ICP-AES concluded that after 3 hours, a total HMI uptake of 0.0986 meq/g is achieved the multi-component system. The percent removal of Pb^{2+}, Cu^{2+}, Fe^{3+}, Ni^{2+} and Zn^{2+} are 94.0, 21.9, 56.2, 9.10, and 16.5%, respectively. The zeolite's preference among the HMIs is demonstrated by the selectivity series, which was established as $Pb^{2+} >> Fe^{3+} > Cu^{2+} > Zn^{2+} > Ni^{2+}$. One of the objectives of this current study is to investigate how these HMIs interact and affect the removal uptake in a continuous-mode, dual-column flow settling.

7.4.2. Automated Column Sorption System

7.4.2.1. Sampling Sequence and Flow Rate

Table 7.2 provides the timeline of modes in the system set-up sequence. Once the inlet tubing and check valve are primed, the pump starts to fill the inlet connection cavity. At full flow rate in Mode-I, it required approximately 8:39 min:s to travel from the base to the top of column 1 (C1). After approximately 3:40 min:s, sample chamber 1 (SC1) was filled, and Mode-II (circulation) was initiated while the first sample (C1-A) was collected. In the continuous flow of

Mode-II, and it required approximately 8:27 min:s for the flow to travel from the base to the top of column 2 (C2). The flow was then switched to Mode-III (pulse), which divides the flow to fill both sample chambers SC1 and SC2. Once the 30-mL volumes were filled, Mode-III is switched back to Mode-II and the samples C1-B and C2-B were collected at 42:50 min:s.

Table 7.2 Sorption System Set-Up Sequence

MODE	Function	Flow Description	Time (min:s)
I	Fill C1	Primed Inlet to C1 Base	2:26
		C1 Base to C1 Top	11:05
		C1 Top to SC1 Drip	15:10
	Fill SC1	Sample C1-A	18:50
II	Fill C2	C2 Inlet to C2 Base	24:08
		C2 Base to C2 Top	32:35
		C2 Top to SC2 Drip	36:14
III	Fill SC1 and SC2		
II		Sample C1-B and C2-B	42:50
III	Fill SC1 and SC2		48:04
II		Sample C1-1 and C2-1	54:27

Once the system is set-up, there is an orderly switch between Mode-II (circulation) and Mode-III (pulse). **Table 7.3** summarizes this sampling sequence. Altogether, there are twenty-nine 30-mL samples collected throughout the analysis period. During the system set-up, the collection of the first sample (C1-A) was followed by the second column 1 sample (C1-B) and first column 2 sample (C2-B). The orderly sequence began at the collection of Cx-1 (48:04 min:s), for a total of two samples for each of the thirteen (13) runs. A total waste (TW) sample in the collection basin of the sorption system was also collected half-way through sampling (115:45 min:s) and at the end of the analysis period (195:00 min:s). The final influent stock and total effluent volumes were approximately 1.45-L and 550-mL, respectively.

Table 7.3 Sorption System Sampling Sequence

Sample	MODE	Start Time (min:s)	End Time (min:s)	
			SC1	SC2
C1-A	I	15:10	18:50	-
	II	18:50		
Cx-B	III	36:40	42:42	42:49
	II	42:50		
Cx-1	III	48:04	54:10	54:27
	II	54:27		
Cx-2	III	59:39	66:15	66:34
	II	66:34		
Cx-3	III	71:37	77:55	78:19
	II	78:20		
Cx-4	III	83:24	89:56	89:56
	II	89:57		
Cx-5	III	95:05	101:32	101:45
	II	101:46		
Cx-6	III	106:52	112:53	113:10
	II	113:11		
TW1		115:45		
Cx-7	III	118:10	123:45	123:56
	II	123:57		
Cx-8	III	129:00	136:07	136:19
	II	136:20		
Cx-9	III	141:22	147:29	147:34
	II	147:35		
Cx-10	III	152:40	158:35	158:45
	II	158:46		
Cx-11	III	163:45	169:40	169:45
	II	169:46		
Cx-12	III	174:50	181:06	181:04
	II	181:10		
Cx-13	III	186:11	192:08	192:36
	II	PUMP OFF		
TW2		195:00		

The flow patterns were continuous and methodically kept consistent throughout the analysis period. Once samples C1-B and C2-B were collected, an average time of 6:26 min:s passed to switch from Mode-III to Mode-II, and 5:05 min:s from Mode-II to Mode-III. When the flow is divided in Mode-III, the average sampling acquisition time of 6:19 min:s was required to fill the 30-mL chambers, which was then collected for the filtering and dilution of the 25-mL sub-sample. The adjustable bi-stable timer at an approximate 50% duty setting automatically toggles the pulsing in Mode-III, to maintain a relatively consistent division of flow between the two columns, creating partial diversion to the two sampling chambers. This is demonstrated in relation to the start and end times of the sampling sequence.

It is important to note that the first sorption column (C1) received a continuous inlet flow rate, as observed by the Mode-I filling rate of 8.18 mL/min for SC1 sample C1-A. Immediately after SC1 was filled and before 30-mL collection, the switch to Mode-II diverted the flow to begin filling the second sorption column (C2). Once both columns were filled, the flow was divided in Mode-III at the top outlet of C1, between SC1 and SC2, while maintaining consistent contact throughout the system. Again, during Mode-III, C1 received the same inlet flow rate, but the sampling chambers SC1 and SC2 received this division of flow. It is column C2 that received a variable flow rate during the analysis period, set by the adjustable division timer. Based on the filling start time (36:40 min:s) of C1-B and C2-B, and the end time of collection (192:36 min:s) for C1-13 and C2-13, a geometric mean flow rate between Mode-II and Mode-III in C2 is established as 5.39 mL/min. With these unique flow rates recognized for both columns, their corresponding EBCTs are established by **Equation 7.4** to yield:

$$EBCT_1 = \frac{d^2\pi H}{4(Q_{C1})} = \frac{(2.61 \text{ cm})^2 \pi (30.48 \text{ cm})}{4(8.18 \text{ cm}^3/\text{min})} \cong 20{:}00 \text{ min: s}$$

$$EBCT_2 = \frac{d^2\pi H}{4(Q_{C2,AVG})} = \frac{(2.61 \text{ cm})^2 \pi (30.48 \text{ cm})}{4(5.39 \text{ cm}^3/\text{min})} \cong 30{:}20 \text{ min: s}$$

As reported by Reed et al. (1996) in the study of GAC column removal of lead, the void volume in columns is typically ~45%, which corresponds to a true residence time between the solution being treated and the sorbent particles of approximately double the EBCT. For a given sorbent material, the optimum EBCT occurs at which point no further improvement in column process efficiency (i.e., η) occurs (Reed et al., 1996). With that being said, due to the relatively slow kinetics of zeolites, long residence times are required. Any solution volume-element in contact with a given zeolite bed layer is for only a limited time period, which is usually insufficient to reach the equilibrium state. The failure of zeolite to attain local equilibrium causes a lower uptake of HMIs from solution (Stylianou et al., 2007b). The detention time that the fluid element is in contact with the fixed-bed per sorption column is a result of the flow rate selected in this present study. This trend between the columns provides insight into the overall treatment availability of the zeolite material in this very unique configuration.

7.4.2.2. Acidity Levels

Table 7.4 presents the pH levels of the effluent for both columns, of equally distributed selected time-step checkpoints of Cx-3, Cx-6, Cx-9, and Cx-13. When the acidified influent stock is combined to a 3-L volume, the average multi-component MM pH has a value of 1.90. By maintaining a very low initial pH and the use of highly soluble nitrate salts, the precipitation of the HMIs is avoided. Additional trials verified that the filtered and unfiltered HMI influent stock concentrations are the same, indicating both effective dilution practices and complete solubility.

Table 7.4 The pH Levels of Selected Sorption Column Samples

Sample	pH Level	
	SC1	SC2
C1-A	6.34	-
Cx-3	4.79	6.84
Cx-6	3.99	6.72
TW1	6.05	
Cx-9	3.86	6.33
Cx-13	3.60	5.76
TW2	5.44	

As the sample traverses through the first column C1, the H^+ ions are captured by the zeolite, resulting in an increase in the pH to 6.34 from the first sample C1-A. There is an interesting observation between the columns' pH levels, which is a direct reflection of the zeolite's removal capacity for both the HMIs of interest and the competitive H^+ ions in solution. The pH level gradually decreases in both columns, with the levels of C2 being slightly greater than that of C1. The total waste (TW) collects in the effluent basin throughout the analysis period, and its pH level decreases from the half-way check point of 6.05 (115:45 min:s) to 5.44 at the final collection (195:00 min:s). This is a clear indication that the zeolite capacity is becoming exhausted for the competing H^+ ions, as well as hindering the sorption process of the HMIs.

Zeolites are able to neutralize the solution acidity; when the point of saturation is reached, the ability of zeolite to neutralize decreases and the pH of the solution decreases back towards its initial pH level (Kocasoy and Sahin, 2007). This is also demonstrated by the research conducted by Vukojevic Medvidovic et al. (2006); the pH values changed during the uptake process, following the opposite shape of the typical breakthrough curves. At breakpoint, a drastic change in the pH occurred, which corresponded with a rapid Pb^{2+} concentration increase. The maximum

pH is reached at the breakthrough point, due to the absence of HMIs in the effluent. The minimum pH is reached at the exhaustion point, due to the increase of the concentration of HMIs in the effluent and due to their hydrolysis in solution. After the exhaustion point, the pH is constant (Nuic et al., 2013). These findings suggest that the continuous monitoring of pH levels is important and considerably contributes to the prediction of breakthrough and exhaustion points (Vukojevic Medvidovic et al., 2006; Stylianou et al., 2007b; Nuic et al., 2013); in order to monitor the progress of the service life and inevitably regeneration (adsorption/desorption cycles), both of which are very significant for practical industrial applications (Vukojevic Medvidovic et al., 2006).

It should be noted that while low pH levels prevent precipitation, the competitive H^+ ions present would hinder the sorption of HMIs. Therefore, it is to be expected that future field installations for the treatment of industrial wastewater effluents should potentially demonstrate even higher removal efficiencies. However, care should be taken in the design of industrial applications to incorporate pre-treatment processes to reduce particulates prior to applying the waste to any sorption system, to avoid flow obstruction in the sorption columns.

7.4.2.3.   *Hydraulic Conductivity Considerations*

Following HMI uptake analysis, the columns were drained to sit overnight. The standard test method for permeability of granular soils (constant head) (ASTM D2434-68) was adopted to determine the variance in the overall hydraulic conductivity between the sorption columns. The hydraulic coefficient of permeability is given by adapting the standard test in the following relationship:

$$k_T = \frac{V_C \cdot L}{A_c \cdot H_C \cdot T} \tag{7.6}$$

where k_T is the coefficient of permeability (in cm/s), V_C is the quantity of water that has discharged from the column and collected (in cm^3), L is the column height (in cm), A_c is the column cross-sectional area (in cm^2), H_C is the constant head of water on the column or the vertical distance between the feed head level and the column overflow level (in cm), and T is the time required (in seconds) to collect the V_C volume. With a plumb tank clamp support system, the water was fed in upflow mode from its base. The collection volume (V_C) was set to 50-mL by a graduated cylinder, with a column height (zeolite bed depth) and cross-sectional area of 30.48

cm and 5.37 cm^2, respectively. Based on an 18°C detected water temperature, the viscosity correction factor of $n_T/n_{20} = 1.0508$ is applied to reveal the hydraulic conductivity of columns C1 and C2 as 4.08×10^{-4} m/s and 3.89×10^{-4} m/s, respectively. With a 4.84% difference to the average between the columns, this demonstrates a consistency in the overall executed compaction method.

7.4.2.4.   *Heavy Metallic Ion Concentration Analysis*

Table 7.5 provides the results of the HMI concentrations (C_t) in both sorption columns based on triplicate readings obtained by the ICP-AES software. The percent removal (%R) values are presented with respect to the 2.0 meq/L influent concentrations of each HMI. During the experimental sequence of sample collection, C2-11 was lost due to improper handling when transferring from the sampling port to filtration at 169:45 min:s. However, this sample is of a lower HMI concentration and the overall removal trend has been well-established by the time this sample is collected. The first major observation is that throughout the analysis period, Pb^{2+} is not detected in both column effluents as well as the total waste, indicating a complete removal of the ion. The C1-13 sample for Cu^{2+}, Fe^{3+}, and Zn^{2+} reports a removal of 18.1, 82.5, and 10.7%, respectively, from the first column. The dual-column configuration provides a substantial improvement on the removal as observed with the second pass in sample C2-13, to achieve a final removal of Cu^{2+}, Fe^{3+}, and Zn^{2+} of 80.1, 99.98, and 51.5%, respectively. This improvement is also attributed to the unique feeding rate and design of the second column C2; the additional EBCT of approximately ten minutes is available for the sorption process to occur as well as the slightly higher pH levels (and therefore lower presence of competitive H^+ ions). The final total waste (TW2) effluent concentrations report very good removal for all ions except for Ni^{2+}, with a removal of 49.0%. This removal trend is also consistent with the batch analyses conducted by Ciosek and Luk (2017a; 2017c). This is significant, as it proves that results from complex experimental batch studies, which are in high abundance, are useful in providing information on the sorption performance (i.e., removal efficiency, selectivity, and kinetics) in industrial applications where the process is run in a continuous flow-feeding configuration. In summary, the results demonstrate for the first time the effectiveness of multiple HMIs sorption by zeolite in a dual-column system with continuous flow.

130

Table 7.5 The HMI Concentration (meq/L) and Percent Removal (%R) in the Sorption Columns

Sample		Cu^{2+}		Fe^{3+}		Ni^{2+}		Pb^{2+}		Zn^{2+}	
		meq/L	%R	meq/L	%R	meq/L	%R	meq/L	%R	meq/L	%R
	C1-A	0.000	100	0.000	100	0.007	99.7[BP]	0.0003	99.98	0.002	99.9[BP]
	C1-B	0.129	93.6[BP]	0.000	100	0.911	54.5	0.0006	99.97	0.541	72.7
	C1-1	0.517	74.2	0.000	100	1.483	25.9	0.0004	99.98	0.974	51.3
	C1-2	0.938	53.1	0.001	99.9	1.906	4.7	0.0006	99.97	1.320	34.0
	C1-3	1.221	38.9	0.011	99.5	2.116	0.00	0.0003	99.98	1.507	24.7
	C1-4	1.369	31.5	0.030	98.5	2.231	0.00	0.0006	99.97	1.622	18.9
	C1-5	1.431	28.5	0.052	97.4	2.269	0.00	0.0004	99.98	1.671	16.4
C1	C1-6	1.468	26.6	0.072	96.4	2.273	0.00	0.0005	99.97	1.703	14.8
	C1-7	1.584	20.8	0.102	94.9[BP]	2.316	0.00	0.0005	99.98	1.816	9.20
	C1-8	1.563	21.9	0.118	94.1	2.199	0.00	0.0005	99.98	1.751	12.4
	C1-9	1.543	22.8	0.138	93.1	2.174	0.00	0.0004	99.98	1.730	13.5
	C1-10	1.571	21.4	0.167	91.6	2.134	0.00	0.0004	99.98	1.739	13.0
	C1-11	1.598	20.1	0.209	89.6	2.123	0.00	0.0004	99.98	1.752	12.4
	C1-12	1.604	19.8	0.268	86.6	2.096	0.00	0.0001	100	1.750	12.5
	C1-13	1.638	18.1	0.349	82.5	2.130	0.00	0.0002	99.99	1.786	10.7
	C2-B	0.00	100	0.0004	99.98	0.002	99.9	0.0003	99.99	0.002	99.9
	C2-1	0.00	100	0.0003	99.98	0.002	99.9	0.0003	99.99	0.001	99.9
	C2-2	0.00	100	0.0003	99.98	0.012	99.4	0.0004	99.98	0.001	99.6
	C2-3	0.00	100	0.0002	99.99	0.046	97.7	0.0006	99.97	0.001	99.7
	C2-4	0.00	100	0.0002	99.99	0.131	93.4[BP]	0.0002	99.99	0.001	99.9
	C2-5	0.00	100	0.0002	99.99	0.285	85.6	0.0002	99.99	0.009	99.6
C2	C2-6	0.00	100	0.0003	99.98	0.505	74.8	0.0003	99.99	0.049	97. 6
	C2-7	0.00	100	0.0002	99.99	0.835	58.3	0.0003	99.98	0.155	92.2[BP]
	C2-8	0.004	99.8	0.0002	99.99	1.163	41.9	0.0003	99.99	0.312	84.4
	C2-9	0.029	98.6	0.0002	99.99	1.444	27.8	0.0004	99.98	0.455	77.2
	C2-10	0.085	95.8[BP]	0.0003	99.99	1.675	16.3	0.0004	99.98	0.597	70.2
	C2-12	0.289	85.6	0.0002	99.99	2.126	0.00	0.0006	99.97	0.895	55.2
	C2-13	0.399	80.1	0.0003	99.98	2.198	0.00	0.0004	99.98	0.969	51.5
TW1		0.0514	97.4	0.0004	99.98	0.3077	84.6	0.0004	99.98	0.1107	94.5
TW2		0.1659	91.7	0.0057	99.72	1.0207	49.0	0.0000	100	0.4088	79.6

7.4.2.5.   Breakthrough Curve, Capacity and Usage Rate Analysis

The breakthrough curve is displayed in **Figure 7.3**, as a plot of the solute outlet concentration (C_t) from **Table 7.5** normalized to the inlet concentration (C_o) (Vukojevic Medvidovic et al., 2006). This normalized ratio trend over the service time of analysis (Nuic et al., 2013; 2015) at which the sampling chambers (SC1, SC2) are extracted is presented for each of the five HMIs combined in the multi-component solution; for both the first sorption column (C1) and second sorption column (C2). The breakthrough point (BP) and exhaustion point (EP) of each HMI in each column are indicated. The first observation to be had is that the breakthrough curves of the first column C1 do not have a defined S-shape. However, in the second sorption column C2, the curves take on this typical shape. Vukojevic Medvidovic et al. (2006) points out that the shape-change may be attributed to an improved solid-solution phase contact for sorption to take place.
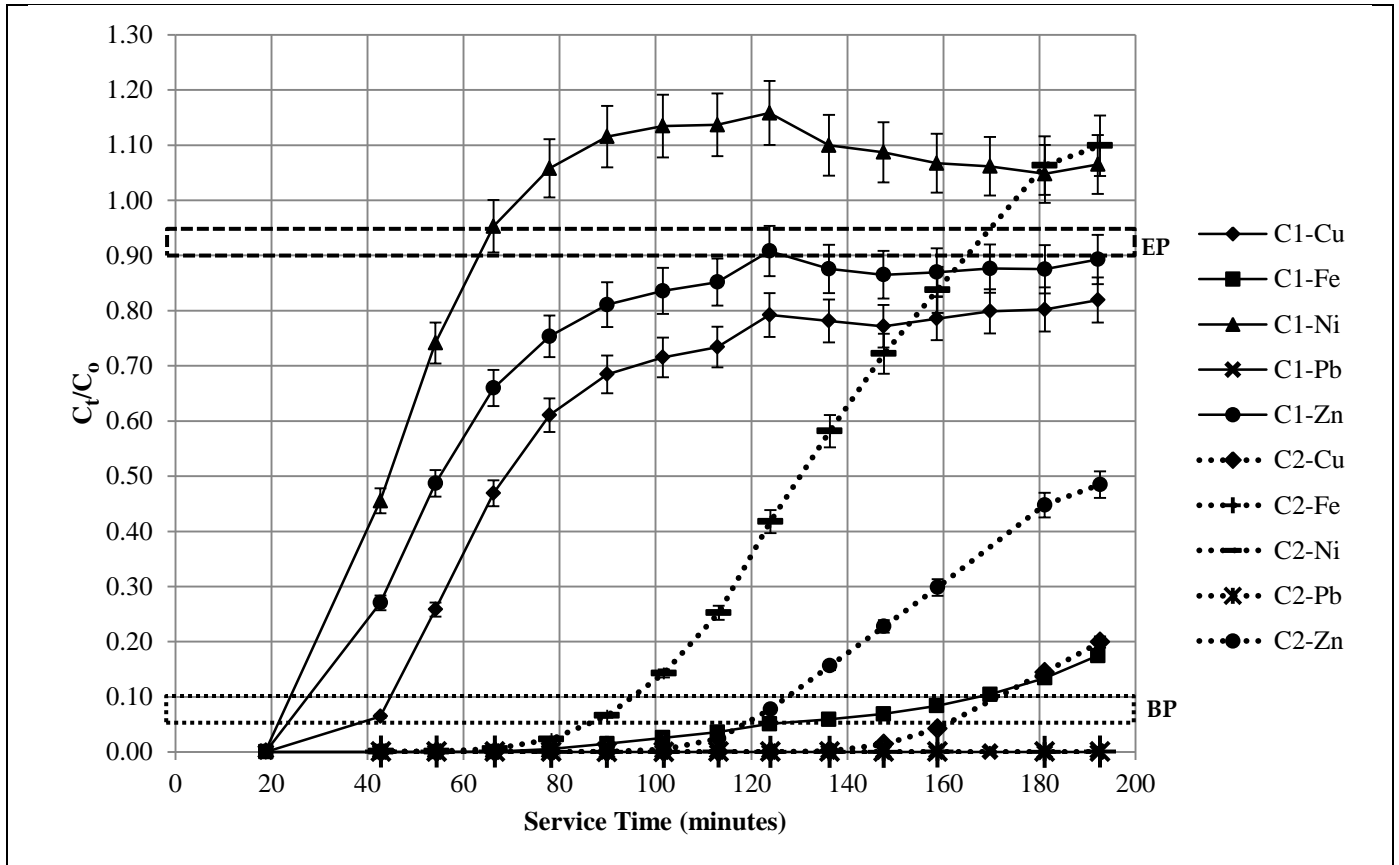

Figure 7.3 The Multi-Component System Breakthrough Curve

The influent stock concentration of the Ni^{2+} ion is exceeded in the effluent solution, where the normalized C_t/C_o ratio surpasses 1 to reach an approximate maximum of 1.16 at 125 minutes and 1.10 at 190 minutes of service time, in sorption columns C1 and C2, respectively. The final ratio readings plateau at the end of service to approximately 5-10% of the value of 1, given the nature of this experimental investigation. The effluent concentration that overshoots the influent concentration translates to concentration wave extremes inside the column (Naja and Velosky, 2006). Nuic et al. (2013) investigated the breakthrough curves of Pb^{2+} and Zn^{2+} ions in dual-component solutions by natural zeolite; a similar trend was observed compared to this present study, where the C_t/C_o ratio even reaches a value of 2 for one set of operation conditions. This is attributed to the displacement of the bound Zn^{2+} by the Pb^{2+} from the influent, which is supported by a lower breakthrough capacity and higher exhaustion capacity in favour of the Pb^{2+} ion, specifically (Nuic et al., 2013). It is important to note that the ion-exchange mechanism that attributes to the sorption process of HMIs transpires through the zeolite's framework of pores and channels. The presence of stronger binding HMIs, such as Pb^{2+}, weaken the chemical bonds between the functional group on the surface of zeolite and the weaker HMIs, such as Ni^{2+} ions (Han et al., 2006). Given that zeolite demonstrates its highest preference towards Pb^{2+}, sorption site availability has reached its threshold, which may cause the leaching out of ions that zeolite holds a lower preference towards during this process. Therefore, careful screening on the selectivity of HMIs by zeolite should be conducted prior to adaptation.

In summary, the major trends observed from the breakthrough curves are as follows:

1. The zeolite holds the greatest preference towards to Pb^{2+} ion, based on its complete removal throughout the analysis period;

2. The zeolite demonstrates the least preference towards the Ni^{2+} ion;
   a. A more sudden breakpoint occurring after just 25 min and 90 min of service time in columns C1 and C2, respectively;
   b. An approximate exhaustion point after just 65 min and 165 min of service time in columns C1 and C2, respectively;

3. The Fe^{3+} ion is removed entirely and sustained throughout the analysis period in C2, and;

4. The removal of both the Cu^{2+} and Zn^{2+} ions begin to plateau at 120 min of service time in C1, acting in parallel and do not reach the lower threshold of the exhaustion point in both columns throughout the analysis period.

The breakthrough curves provide significant information from a perspective of sorption process performance, feasibility and optimization, which are vital for scaling-up the sorption system for industrial applications (Naja and Velosky, 2006; Inglezakis, 2010a).

The overall column performance efficiency and its relationship between breakthrough capacity (C_{BP}) and exhaustion capacity (C_{EP}) of each sorption column are unique to the individual HMIs selected. As observed in the data displayed **Table 7.5** and the trends visualized in **Figure 7.3**, the EP is only attained by Ni^{2+}; the remaining four HMIs have yet to reach this point due to the constraints of the 3-hour analysis period. Evidently, the optimization of future works would be to prolong the service time in order to quantify the overall columns' performance efficiency. Qualitatively speaking, for both columns' effluent and total waste (TW), the Pb^{2+} ion is completely removed throughout the analysis period, demonstrating the utmost efficiency; neither BP nor EP are attained. On the opposite end of the spectrum, the Ni^{2+} ion reaches exhaustion quite rapidly.

The volume of the effluent treated at breakthrough (V_{BP}) is determined with the use of the mean flow rates of 8.18 mL/min (Q_{C1}) and 5.39 mL/min (Q_{C2}) for the sorption columns C1 and C2, respectively. These flow rates are applied to the time data of **Table 7.3**, at which BP (approximately 95% removal or 5% of the 2.0 meq/L influent concentration per HMI) is observed; as indicated by the superscript in **Table 7.5**. The 2:26 min:s time required for inlet priming to the base of C1 as well as the 24:08 min:s time observed for solute contact to the base of C2 are deducted from these BP times. As summarized in **Table 7.6**, the approximate effluent volumes treated at BP (V_{BP}) are provided for both sorption columns and each HMI selected; based on the zeolite mass in each bed (m_Z) of 152.10 g, **Equation 7.2** and **Equation 7.5** are employed to determine the corresponding breakthrough capacity (C_{BP}) and usage rate (v_U), respectively.

Table 7.6 System Breakthrough Point Performance

HMI	Sorption Column 1			Sorption Column 2		
	$V_{BP,1}$ (L)	$C_{BP,1}$ (meq/g)	$v_{U,1}$ (g/L)	$V_{BP,2}$ (L)	$C_{BP,2}$ (meq/g)	$v_{U,2}$ (g/L)
Cu^{2+}	0.3295	0.0043	461.7	0.7257	0.0095	209.6
Fe^{3+}	0.9926	0.0131	153.2	---	---	---
Ni^{2+}	0.1342	0.0018	1134	0.3547	0.0047	428.8
Pb^{2+}	---	---	---	---	---	---
Zn^{2+}	0.1342	0.0018	1134	0.5380	0.0071	282.7

The Pb^{2+} and Fe^{3+} ions are completely removed in sorption column C2, which essentially transforms the influent stock of a five HMI multi-component solution to a triple-component solution containing Cu^{2+}, Ni^{2+}, and Zn^{2+} ions within the 3-hour analysis period. The zeolite does not have to address the competition of the two preferred HMIs, which provides greater sorption site availability for the three HMIs remaining in solution. It is important to develop a relationship between the EBCT and usage rate. The time that the fluid element is in contact with the zeolite bed in sorption column C2 is ten minutes greater than the detention time in C1. This thereby demonstrates a stronger overall treatment availability in C2; reflected in the average 195% increase of bed capacity at breakthrough and the average 63.9% decrease in usage rate of the zeolite between the columns; based on the trends observed for the Cu^{2+}, Ni^{2+} and Zn^{2+} ions detected in solution.

Evidently, the columns' usage rate provides significant information into the operation and management required for this unique sorption system. It has a direct impact on the financial viability of performing either replacement (disposal) or regeneration (on- or off-site), and is affected by factors that include HMI influent concentration, zeolite bed depth, and flow rate. Research into other sorbent materials demonstrates that the order of usage rate is consistent with the sorption capacity (Othman et al., 2001). Due to the unique automated variable influent feeding rate and sampling technique proposed in this study, the usage rate and performance efficiency are very complex (Inglezakis et al., 2010a). However, the major removal trend of Pb^{2+} $\gg Fe^{3+} > Cu^{2+} > Zn^{2+} \gg Ni^{2+}$ is well-established and supports previous results (Inglezakis et al., 2001b; Inglezakis et al., 2003; Inglezakis et al., 2004; Wingenfelder et al., 2005; Wang and Peng, 2010; Ciosek and Luk, 2017a; Ciosek and Luk, 2017c), providing significant validation of this design.

The use of natural zeolites as sorbents in industrial wastewater treatment and environmental management is motivated by the non-toxicity of these minerals, their abundant global availability, and economic feasibility. The removal and recovery processes of HMIs from aqueous solutions by natural zeolites take into consideration the regeneration potential of the zeolite bed to be reused in multiple cycles, as well as the use of the recovered metals (Sprynskyy et al., 2006) in applicable industrial applications. Metal processing effluents contain high concentrations of recoverable metals, triggering a movement towards technologies to recover

these metals from industrial wastewater effluents, such as acid mine drainage waste (Zinck, 2005). The removal-regeneration-recovery process has the potential to generate additional revenue streams with the use of metals of value (Dinardo et al., 1991); such as the HMIs investigated in this innovative study.

7.5. Conclusions

This research has demonstrated the performance of natural zeolite (clinoptilolite) to remove multiple heavy metallic ions (HMIs) commonly found in industrial wastewater effluents. With the design and development of a novel dual-column sorption system, the lead (Pb^{2+}) ion is removed completely and sustained throughout the analysis period. The relationships between empty bed contact time (EBCT), breakthrough capacity, and usage rate are evident. The additional ten minutes of EBCT in the second sorption column contributes to an enhancement in overall removal for Cu^{2+}, Fe^{3+}, and Zn^{2+} by 75.7, 99.9, and 45.7%, respectively, from the first sorption column. This improvement is also apparent in the greater breakthrough capacity and lower usage rate in the second column, and visualized in an improved S-shape to the characteristic breakthrough curve. Based on the multi-component influent stock of 10 meq/L total concentration, the second column demonstrates a removal of 99.98, 99.98, 80.1, 51.5, and 0.00%, for Pb^{2+}, Fe^{3+}, Cu^{2+}, Zn^{2+}, and Ni^{2+}, respectively; and the final cumulative collection of effluent reports a removal of 100, 99.7, 91.7, 79. 6 and 49.0%, for Pb^{2+}, Fe^{3+}, Cu^{2+}, Zn^{2+}, and Ni^{2+}, respectively at the completion of the analysis period. These HMI sorption removal trends confirm the consistency between batch- and continuous-mode operations.

The modular design inventively incorporated a 'circulation-pulse' method to distribute the flow, rather than operating on a more commonly implemented fixed flow rate. With the consideration of this unique stock feed method, the findings of the service time and flow rate with respect to the removal trends are both interesting and significant. The potential for variable flow rate operation and automatic adjustable sampling in a packed fixed-bed dual-column sorption design reveals practicality for treatment applications. This study has provided greater insight into the immense potential that the natural mineral zeolite holds for the future of industrial wastewater treatment.

7.6. Future Works

Forthcoming works in this research project include the investigation of regeneration cycles and service life, with further design development and optimization in various prospective configurations. In addition, the investigation from synthetic simple solute to actual wastewater effluent samples would provide a greater understanding of the system potential in practical engineering application. To be discussed in the Recommendations of the Dissertation document (with reference to **Appendix E**), an improvement to this system prototype is to place an emphasis on the removal-regeneration-recovery process in sorption removal technology development.

8. CONCLUSIONS AND RECOMMENDATIONS

8.1. Fundamental Conclusions

The predominant presence of heavy metals in industrial wastewater effluents pose extreme environmental and health risks, owing to their highly toxic and dangerous nature, that is significantly complex to control. This Dissertation reports the fundamental findings of a four-phase research project to investigate the sorption removal capacity of natural zeolite of five heavy metallic ions (HMIs); lead (Pb^{2+}), copper (Cu^{2+}), iron (Fe^{3+}), nickel (Ni^{2+}), and zinc (Zn^{2+}); combined in various component systems. In keeping of existing literature and as 'proof-of-concept', this research has demonstrated that natural zeolite is an effective sorbent material in the removal of HMIs commonly found in industrial wastewater under the testing conditions, and has contributed to the thought-provoking development of treatment system technology. The key findings to each phase of the project are provided in the following subsections.

8.1.1. Effects of Operation Parameters

Consistent with existing trends in literature, the removal of heavy metallic ions by natural zeolite increases with decreasing particle size, as well as increasing dosage, contact time, and set-temperature. The studied parameters influence the process in the order of: influent concentration > heat pre-treatment level > dosage > particle size > contact time > set-temperature. The removal efficiency order (or selectivity series) is consistent for all examined experimental conditions as: $Pb^{2+}>>Fe^{3+}>Cu^{2+}>Zn^{2+}>Ni^{2+}$.

Based on preliminary investigations of existing critical performance trends (Acheampong et al., 2009; Motsi et al., 2009, 2011, Inglezakis, et al., 2002, 2003, 2004, 2005; Sprynskyy et al., 2006), the experimental conditions presented in **Table 3.2** were established for the analyses of all operation parameters and conditions; as summarized in **Table 4.1**. The particle size and dosage operation parameters were investigated in single-component system combinations of all five HMIs, which are significant parameters that form the basis for the remaining conditions. The analysis of the influent concentration at a total 10 meq/L is a subset of the kinetic modelling investigations found in **Chapter 6**, while the 400 mg/L condition for each HMI was included and selected on the basis that when converting from meq/L to mg/L, this is the median range for a majority of the HMIs selected. The heat pre-treatment operation parameter was a stand-alone

investigation, with a systematic increase from single-[P] to triple-[T] to multi-[M] component system HMI combinations, to quantitatively and qualitatively demonstrate the effects of heat on the zeolitic structure. The contact time conditions were to extrapolate from the 180 contact minutes established by preliminary investigations, which discusses the period at which sorption equilibrium is achieved with support of existing literature. Finally, the set-temperature conditions were set to develop a greater understanding of its influence of zeolite sorption selectivity.

Various factors (i.e., operation parameters, conditions) affect the overall removal efficiency, either positively or negatively. However, the efficiency may not be influenced by each factor individually. Unless the efficiency among all the factors is systematically arranged, the optimal combination of factors is not straightforwardly recognized. In order to reach the optimal combination of factors, those which positively influence the removal efficiency ought to be identified and investigate a refined combination of these factors with respect to the efficiency. Ideally, this aspect of the research project would be improved by investigating all six (6) operation parameters with all HMI component-system combinations. However, these combinations are fundamentally selected based on laboratory feasibility and hence, are the rationale towards the selection of the parameters presented.

8.1.2. Lead Removal Capacity and Selectivity

Zeolite cation exchange selectivity depends on the zeolite type, distance between anionic sites, cationic radii, hydrated cationic radii, and cationic hydration energy. The unhydrated ions are able to pass through the three-dimensional framework, but the hydrated ions may exchange only with faced obstacles. The Pb^{2+} ion has the smallest hydrated cationic radius and may pass effortlessly through this network. The cations with larger hydration energies prefer the sorbate (solution) phase, while the cations with the least hydration energies prefer the sorbent (zeolite) phase. As such, the lower hydration energy of Pb^{2+} implies that it loses its hydration shell more readily than other ions (Inglezakis et al., 2003); demonstrated by the high affinity and selectivity of clinoptilolite towards the Pb^{2+} ion (Oter and Akcay, 2007). In addition, the Pb^{2+} studied typically does not have a strong tendency to form strong complexes, and gives reasoning for its preferential uptake by natural zeolite (Inglezakis et al., 2004).

Under the testing conditions of this study, the methodical introduction of copper, iron, nickel and zinc to the component system decreases the overall uptake of the total HMIs in solution.

139

However, as previous work suggests (Wingenfelder et al. 2005; Prasad and Mortimer, 2011), the cation competition does not affect the preferential uptake of zeolite for the Pb^{2+} ion.

8.1.3. Kinetic Modelling Trends

The accuracy of modelling prediction is dependent on the various open boundary conditions, model parameters selected, and numerical method(s) implemented. The study of sorption kinetics holds great importance in sorbent material assessment and subsequent application in wastewater treatment (Qiu et al., 2009); it defines the reaction pathways and uptake rates, along with residence times at which the equilibrium point is reached at the solid–solution interface. Both the pseudo-second-order (PSO) and intra-particle diffusion kinetic model demonstrated a very strong correlation of the experimental data; however, the PSO model demonstrated a stronger performance, and further contributed to the assessment of the zeolite mineral performance and the fundamental mechanisms associated with the sorption process under the testing conditions.

The variation in sorption kinetics is attributed to the specific crystalline structure (physical as well as chemical composition) of the sorbent material, and is controlled by various mechanisms (Helfferich, 1962; Bekkum et al., 1991; Kocaoba et al., 2007; Motsi et al., 2011); best understood with experimental data of the simultaneous sorption of the HMIs of interest, and an analysis on the uptake and rate of interference of these counter-ions in combination (Helfferich, 1962; Borandegi and Nezamzadeh-Ejhieh, 2015). Therefore, kinetic modelling is considered as a powerful tool to assess the performance of sorbent materials and to comprehend these fundamental mechanisms involved in the sorption process.

8.1.4. Dual-Column Sorption System Performance

This study successfully demonstrated the performance of natural zeolite to remove multiple heavy metallic ions (HMIs) commonly found in industrial wastewater effluent, with the HMI sorption removal trends confirming the consistency between batch- and continuous-mode configuration operations. The modular design of a novel dual-column sorption system inventively incorporated a unique stock feed 'circulation-pulse' method to distribute the flow. The lead (Pb^{2+}) ion was removed completely and sustained throughout the analysis period. The additional ten minutes of empty bed contact time (EBCT) in the second sorption column lends to the removal enhancement from the first sorption column; which demonstrated greater

breakthrough capacity and lower usage rate. The relationships between EBCT, breakthrough capacity, and usage rate are significant, and the potential for variable flow rate operation and automatic adjustable controls in the packed fixed-bed dual-column sorption design reveals practicality for future treatment applications.

8.2. Future Recommendations

The ecosystem is a fragile network which requires a proactive rather than a reactive approach to dealing with industrial process pollution. Therefore, the advancement of treatment technologies is vital to minimizing the impact of pollutants on the environment. The selection of the most suitable treatment technology for inorganic metal-contaminated effluents is influenced by environmental impact and legislation/regulations, complacency and socio-economic constraints, existing process flow-schematics and site-specific logistics (i.e., technical applicability), lifecycle management and associated economics (cost-effectiveness, capital investment, operation and maintenance costs), overall water balance and climatic conditions, as well as wastewater effluent complexity (i.e., composition, pH, initial metal concentration) and notably, the overall treatment performance compared to other technologies (Johnson and Hallberg, 2005; Adams, 2008; Barakat, 2011; Fu and Wang, 2011). In addition, the treatment system lifecycle is of increasingly great importance, with respect to disposal, the removal-remediation-recovery cycle and the potential for financial return (Johnson and Hallberg, 2005). Lata et al. (2015) points out that the evaluation should be based on performance (removal efficiency) and cost, as well as the level of 'appropriateness', which reflects the robustness, quality and quantity output, (site-specific) condition suitability, and adaptability of a given treatment system. The design of a field-implemented prototype for the future must also take several technical complexities into account. A strong understanding must be had of all the bio-geo-chemical and physical processes taking place within the effluent (Ritcey, 2005). The hydrologic parameters such as detention time, flow rate, and volume capacity for the development of the treatment unit are also significant (Kuyucak et al., 2013). *Future optimization of the prototype would be to critically analyze these myriad of complex parameters, which will influence the overall treatment performance of the system, in order to practically and economically implement on an industrial scale.*

It is important to note that studies analyzing synthetic simple solute influent solutions have demonstrated greater removal performance compared to investigating actual wastewater (Motsi et al., 2009; Xu et al., 2010, 2013). This is largely due to the site-specific complexity (i.e., pH levels, HMI trace concentrations, various solution constituents). The study conducted by Prasad and Mortimer (2011) of actual acid mine drainage with fly ash and fly ash zeolite prompts the discussion of the importance of the solution pH level. The addition of the mineral to a relatively neutral pH solution may increase the pH level to reach the threshold of solubility of the metal hydroxides. This means that the removal may be partially attributed to precipitation (or sorption/co-precipitation) rather than just sorption (ion-exchange) (Wingenfelder et al. 2005; Prasad and Mortimer, 2011). This is echoed by the research conducted by Xu et al. (2014) using natural clinoptilolite as the sorbent material of an actual acid mine drainage sample; the pH level increase is caused by neutralization, attributing to the HMI removal primarily by precipitation, co-precipitation and adsorption. The proportions of interchangeable co-cations in the zeolite framework and those constituents in an actual sample that may hydrolyze have an impact on the overall presence of mineral species when in contact with the zeolite mineral. Xu et al. (2014) demonstrated in the study of adsorption/co-precipitation on Al-colloids that a final pH level of solution below 4 does not result in co-precipitates with colloids. This finding is in accordance with Inglezakis et al. (2003), whose synthetic simple influent solutions are acidified with nitric acid to a pH level of 2, to avoid hydroxide precipitation during the removal of Pb^{2+}, Cu^{2+}, Fe^{3+} and Cr^{3+} by clinoptilolite (Xu et al., 2014); in keeping of the experimental design of the research presented in the Dissertation document, under the testing conditions. As seen in **Table 7.4** of **Chapter 7**, the pH level of the total waste at the end of analysis (TW2) is just below 6. The NO_3^- anions in the synthetic aqueous solution in this study do not influence the ion-exchange process, since they do not form any metal-anion complexes and do not hydrolyze in solution (Peric, 2004; Minceva et al., 2008) under these controlled conditions of this study. However, various anionic ligands, which include NO_3^-, SO_4^2, and Cl^-, are present in actual AMD. As demonstrated by Xiu et al. (2014), SO_4^{2-} is said to form inner-sphere complexes with active sites and to increase the net negative charge at the surface of the zeolite, encouraging the processes of metal adsorption as well as dealumination. *Hence, further investigation of actual industrial wastewater effluent and the impacts of colloidal processes (although site-specific) are needed for the practical implementation of the system prototype.*

The synthetic simple solute solution used in this study was free of any suspended solids, and therefore, there was no need to fluidize/backwash the bed, during the analysis period under the testing conditions. However, with actual wastewater, the presence of suspended solids is another factor which influences the efficiency of a treatment system. The concentrations vary among industry, such as 4.1 mg/L for a copper production plant (Beyazit, 2013) or 22 mg/L for typical gold mine wastewater (Acheampong et al., 2009). The surfaces of suspended solids can occasionally acquire an electrical charge, much as dissolved species. This surface charge can either improve or impede the adsorption of ions from solution (Benjamin, 2010, p. 773). In addition to its influences in the chemisorption process (Benjamin, 2010, p. 774), suspended solids may also inhibit the hydraulic performance in the system. *As a recommendation, clogging should be addressed in an established operation and maintenance plan following further optimization of the prototype design.*

The natural zeolite clinoptilolite is considered as a strong candidate for the removal of HMIs from wastewater (Ersory and Celik, 2002; Alvarez-Ayuso et al., 2003). In addition to being a low-cost, globally abundant natural mineral (Kocasoy and Sahin, 2007), they hold the potential for regeneration, HMI recovery and reuse (Mohan and Chander, 2006; Lata et al., 2015) in relevant industrial applications. Metals cannot be destroyed and unless recovered, they become a recurring disposal problem. Consequently, an emphasis has shifted to treatment technologies which facilitate the recovery of metal pollutants; with economically attractive alternatives (Dinardo et al., 1991). In the ion-exchange study conducted by Riveros and Wong (1995), the extraction of Sb, Cd, Cu, Ni, and Zn from acid mine drainage solutions were analyzed in batch- and continuous-mode (column tests). An annual cost of full neutralization to pH level of 11 followed by re-acidification to pH level of 7 was compared to lime neutralization to pH level of 6 followed by adsorption onto zeolite (clinoptilolite). Based on an all-year operation at a flow rate of 10,000 m^3/day and an initial pH level of 2.1, the annual cost of lime was reduced from $1,560,375 to $1,178,950, and a total annual reduction in reagents of approximately $313,877.00. There are various limitations in cost, performance and market readiness of existing industrial wastewater technologies. As such, the implementation of natural zeolite as an alternative presents additional benefit of metal recovery potential (Zinck et al., 2005).

The regeneration/desorption of sorbent materials is a critical aspect in heavy metal removal and recovery, as it impacts the economic feasibility and service life of the treatment technology (Lata et al., 2015). The exhausted sorbent material is commonly exposed to thermal regeneration. This process usually causes a material loss of 10-20% due to repeated attrition. Elution of the sorbate (i.e., extracting one material from another; washing the sorbent material with a solvent to remove the captured HMIs) with regeneration by a suitable reagent is a viable alternative to thermal regeneration (Mohan and Chander, 2006). Such regenerative agents include acids (i.e., HCl, H_2SO_4, HNO_3), alkalis and salts (i.e., NaOH, NaCl), as well as chelating agents (i.e., EDTA) and deionized distilled water (Lata et al., 2015). With regards to ultimate disposal, both the regenerated zeolite and recovered metals can be reused; such that the associated waste materials are returned to the environment with minimal impacts to the environment. This is the most environmentally-friendly way to move this technology into industry. If not, the metal-contaminated zeolite will need to be disposed of at special landfill sites. The *development of an ideal eluent is required* in order to address the fate of spent, metal-laden sorbent materials and to reduce the production of associated secondary pollutants (Lata et al., 2015); *a factor in the optimization of the treatment system prototype.*

It is important to note the potential for the derivation of multi-component sorption models. The column design and modelling simulation proposed by Jarvie et al. (2005) states that the type of sorbent material, EBCT, and bed configuration/operation major process design variables; which influence the steady state mass balance relationships to establish the usage rate of a given treatment system. In order to evaluate the performance, the influence of adsorbent type, solution chemistry and solute type must be investigated. The modelling approach simulated the effluent concentration profiles leaving the fixed-bed reactor, taking (external, intra-particle) mass transfer models into consideration. The Freundlich adsorption isotherm was selected to evaluate the equilibrium between the solid- and liquid-phase solute concentrations at the sorbent surface. The ultimate objective of the model development was to represent the dependence of adsorption capacity and kinetics upon time and bed-length, to be used to estimate effective diffusivities with enough precision to make crude design calculations; stressing the need for additional field data to develop confidence of the simulation in the future.

In a study by Zolgharnein and Shahmoradi (2010), the statistical optimization in the removal of aqueous Hg^{2+} by Fraxinus tree leaves was investigated, and showed that nonlinear regression is the best way to model equilibrium data. Screening designs identify factors or key variables that influence a given response, which assist in narrowing down the parameters to save time and cost to the experimental design; a 2^3 full factorial design was used to identify significant factors and interactions. In a batch-mode bio-sorption process with a fixed contact time of 30 minutes, the pH, initial Hg^{2+} concentration, and sorbent mass were considered major factors, with a 95% confidence level. A multiple regression model was derived by using a response surface methodology (central composite design) and adequacy checked by diagnostic tests (i.e., analysis of variance (ANOVA)). In the 'presence of interaction', the factors may affect the response interactively and not in an independent way; their combined effect may be greater or less than that expected for the straight addition of the overall effects on removal. Zolgharnein and Shahmoradi (2010) state that the initial concentration had the greatest affect, such that increasing its level from low to high decreases the removal. In the analysis of the interaction between concentration and mass, increasing the level of mass has a less pronounced effect when the concentration is at a low level than when at a high level. The study by Zolgharnein and Shahmoradi (2010) determined the optimum parameter conditions under the testing conditions. *A recommendation for future analysis would be to approach this statistical experimental design of multivariate linear regression, with an emphasis on field data, and apply it to the optimization of the continuous-mode of the treatment system prototype.*

The *novelty of the treatment system prototype* presented in **Chapter 7** of this study is greatly attributed to the *unique controlled sampling technique*, with a design that enables the control of the flow distribution in the system by *various modes of operation*. The current design incorporates a unique stock flow feed in a timed 'circulate-pulse' method, with discrete three-way solenoid valves that divert 100% of the flow. The flow is controlled in the first column by the pump at the system inlet, while the flow in the second column is controlled by the 'circulate-pulse' average sampling between Mode-II and Mode-III. The three-way solenoid valves and adjustable distribution timer would enable future investigations of variable system inlet flow rates and sample configurations (i.e., collection volume, automatic timer diversion settings) in

Mode-III of operation. Future considerations to tune the nominal average flow would be to investigate modulating valves, which would divide the flow to a desired percentage, making the system a truly continuous hydraulic flow regime.

The complete removal of lead and iron is of significance to the practicality of the prototype. Under the testing conditions, this presents the opportunity to isolate a particular set(s) of HMIs for recovery, and reprocessing the effluent for use in pertinent, riveted industry. Based on the HMI removal selectivity trends reported in the current design under the study testing conditions, a third column would be ideal to refine the treatment efficiency. The particle size (d_p) and column inlet flow rate may be manipulated; coarsest and quickest for the first column to target Pb^{2+} and Fe^{3+}, finer and slower for the second column to target Cu^{2+} and Zn^{2+}, and finally the finest size and slowest rate for the third column to target Ni^{2+}; keeping in mind pump head and back pressure effects in the refinement of these parameter settings. Of the various multi-phase reactor configurations, fixed-bed reactors (FBRs) provide little axial dispersion, operating very similar to plug flow, while slurry bubble columns (SBCs) demonstrate excellent heat and mass transfer characteristics (Kantarci et al., 2005) and provide short residence time for sorption removal (Cui et al., 2006). The distributed gas in a SBC generates bubbles, which entrain the solution and causes a greater overall upflow in the column (Kantarci et al., 2005). This prompts the idea for future system design to create a FBR-SBC hybrid system. Prospective configurations may also include two columns connected in parallel to replace a single column, facilitating disconnection and replacement while maintaining the system circulation in Mode-II; all with consideration to the column aspect ratio to zeolite particle size. A significant improvement to this study would be to extend the 3-hour contact time, in order to associate the equilibrium state capacity experimentally and theoretically, as well as evaluate various operative conditions to generate further insight into associated mechanisms in the rate of uptake by natural zeolite. *With further optimization, this prototype is a major contribution to the scientific community, and is a worthwhile pursuit being a platform for future FBR design in the treatment of industrial wastewater effluents.*

This research project has explored the removal capacity of natural zeolite for heavy metals, and has provided greater insight for management and remediation. With future optimization, the innovative prototype is considered a transferrable technology in the treatment of industrial

wastewater effluents. Evidently, this proposed technology benefits both the industry and Canada, with an overall improved environmental awareness. Metal mining and industrial processing must consider the environmental sustainability and overall impact in regards to water use, reuse, and disposal. Holistic water management and site water balance are critical for existing and new industry ventures. A shift in thinking is necessary towards a more systematic and strategic approach towards a balance among risk and conservatism (Nicholson, 2015), with effective industry operation, waste management (Zinck et al., 2005), and water quality quantification (Nicholson, 2015). Hydrologic and geo-chemical characterization, mitigation measures, as well as time are all considered major modes of prediction failure (Nicholson, 2015). With this perception, the major contributions of this research will lead to a greater knowledge-base of the behaviour and mechanisms within the interaction of zeolite and heavy metallic ions, and the overall sorption removal efficiency. The critical conclusions reached by this research may evolve to enable the industry to recognize how to best employ the natural mineral zeolite in its current treatment methodology, as part of the system design protocol for industrial wastewater in the future.

APPENDIX A. Experimental Methodology Procedures

A.1.   Laboratory Health and Safety

The protocols followed and procedures conducted in the laboratory are of significance to the scientific community. This subsection is provided to establish the necessary foundation for best practice principles in the continuation and future optimization of this research project.

In accordance with Ryerson University and the Department of Environmental Health and Safety (EHS), all personnel involved underwent training with respect to handling (preservation, transportation, receiving), experimental testing and analysis. At the time of experimental design, correspondence took place with the Faculty of Engineering and Architectural Science (FEAS) EHS advisor Mr. Eric Ambroise and the Radiation-Chemical-Biosafety Officer Ms. Valerie Phelan. All chemicals (i.e., metal nitrate salts, nitric acid) were thoroughly classified (as per their respective compositions and MSDS information), to establish a detailed protocol in the laboratory; in accordance with the Ryerson University Impact Assessment procedure.

Among the heavy metals proposed, it is important to note that lead is classified as a 'designated substance' with carcinogenic risks. With a Time-Weighted Average (TWA) 0.05 mg/m^3, all manipulations must be conducted within a fume-hood to ensure that the regulated exposure limit is met. Consequently, a fume-hood inspection was established for air velocity levels and nitrate salt particulate (aerosol) movement. Ms. Phelan scheduled calibration, and verified that the rate read at 120 ft/min. A smoke test showed that all the air currents moved into the fume-hood and was consumed by the fan; its condition was confirmed as satisfactory to move forward with all experimental work. With regards to the nitrate salt particulate movement, Mr. Ambroise conducted a dust mask fit test with a 3M^{TM} (8210) N95 NIOSH certified disposable respirator. With these masks, Ms. Phelan conducted the aerosol test for specifically lead nitrate, and the meter did not detect any measurable aerosols with the demonstrated manipulations of the salt. With the solutions under containment in the fume-hood, it was determined that there was no need for masks. A baseline blood test was made for lead (Pb^{2+}) levels by the Ph.D. Candidate, and returned to their general physician following all experimental exposure, and ensured that the lead containment met health and safety requirements.

In addition to metal nitrate salt handling, concentrated nitric acid (CAS No. 7697-37-2) is a critical aspect to the proposed research. The acid was used in routine cleaning, pH control and sample preservation. Consequently, chemical-resistant, impervious material complying with approved standards was required for specific protection; including neoprene gloves to protect the hands and arms, a face shield to avoid exposure to liquid splashes, mists or dusts, as well as a body apron when handling the concentrated nitric acid. All safety gear specifications are presented in **Table A.1**.

The following points should also be highlighted in the extensive efforts made by the Ph.D. Candidate to ensure a safe research environment:

1. Proper management of all materials and equipment is executed during every experimental session, both in MON412 and the ANALEST centre, with the utmost diligence.
2. The lab bench stations are maintained in a clean and orderly manner.
3. Only clean absorbent lab paper is used for labware and experimental sequences, while soiled dry paper is kept and reused for the lab floor.
4. During the handling of the acid bath:
   a. The nitrile examination gloves are covered with the neoprene gloves.
   b. The lab coat sleeves are tucked into the neoprene gloves.
   c. The fume-hood window and face shield are used at all times.
5. All residual zeolite sorbent material and HMI sorbate solution, as well as concentrated nitric acid are routinely disposed into a jerrican and stored under the MON412 fume-hood.

It should be noted that the training provided to all personal involved are at levels which are sufficiently elaborate and commensurate with the level of their respected programs of study. The Ph.D. Candidate has administered the research project in its entirety, and delegated the undergraduate students involved primarily in labware cleaning, where deemed appropriate by the technician of the Environmental Engineering Laboratory.

A.2. Materials and Equipment – Inventory and Specifications

The record of all materials and equipment are presented **Table A.1**, followed by their specifications in **Table A.2** and **Table A.3**, respectively.

Table A.1 Inventory of Consumable Materials and Related Equipment

Item		Supplier	CAT No.	Description
Natural Zeolite		Bear River Zeolite	Z 2-gal	2 gallon bucket of -8+40 mesh BRZ
				2 gallon bucket of -14+40 mesh BRZ
				2 gallon bucket of 30x60 mesh BRZ
				5 gallon bucket of -14+40 mesh BRZ
Analytical Grade Nitrate Salts		Sigma-Aldrich	61194-500G	puriss. p.a., 99-104%
			216828-500G	98+%-ACS reagent, ≥98%
			72252 -500G	puriss. p.a., ≥98.5%
			228621-500G	99+% -ACS reagent, ≥99.0%
			228737-500G	reagent grade, 98%
ICP Standard		SCP	140-102-042	Multi-Element - Quality Ctrl.Std. 4 250 ml
			140-102-045	Multi-Element - Quality Ctrl.Std. 4 500 ml
Nitric Acid		VWR	CANX0407-2	NITRIC ACID OMNITRACE,2.5L (EM-NX0407-2)
Standard Mesh Sieves		Fisher Scientific	04881G	Fisherbrand Sieve Brass 8" 9 Mesh US #10
			04881L	Fisherbrand Sieve Brass 8" 16 Mesh US #18
		VWR	57334-104	VWR SIEVE FULL 8IN BRASS #12
			57334-106	VWR SIEVE FULL 8IN BRASS #14
			57334-108	VWR SIEVE FULL 8IN BRASS #16
			57334-112	VWR SIEVE FULL 8IN BRASS #20
			57334-114	VWR SIEVE FULL 8IN BRASS #25
			57334-116	VWR SIEVE FULL 8IN BRASS #30
			57334-118	VWR SIEVE FULL 8IN BRASS #35
			57334-120	VWR SIEVE FULL 8IN BRASS #40
Labware	**Glassware**	Fisher Scientific	10206H	Corning-Pyrex Flask Volumetric 1000mL
			10 206G	Corning-Pyrex Flask VOL 500ML CS/12
			10 206D	Corning-Pyrex Flask VOL 100ML PK/6
			08 555D	Cylinder White Line 100ML
			08 555G	Cylinder White Line 1000ML
	Sample Bottles (Polypropylene)	Fisher Scientific	02893AA	Nalgene Bottle Wide Mouth PP 1oz (30 mL) PK/12
			02 893BB	BOTTLE WM PP 2OZ 12/PK
			02893A	Nalgene Bottle Wide Mouth PP 4oz (125 mL) PK/12
ICP Sample Tubes		Fisher Scientific	05 538 59B	Corning-TB 15ML CLR PP FLT (Corning) CS/500
			05 538 60	Corning-TUBE 50ML W/RIMSEAL CAP (Corning) CS/500
Filter		VWR	CA97005-232	Syringe Filter-FILTER 30MM RC 0.45UM PK100
Syringe		Fisher Scientific	337730	SYRINGE DSP PLST LL 20ML PK100
Pipette Tips			21 377 52	FINNTIP 63 1-10ML BULK PK/100

Table A.1 Inventory of Consumable Materials and Related Equipment (continued)

Item	Supplier	CAT No.	Description
Safety Gear	Fisher Scientific	29 635 972	SILVER SHIELD APRON
		11 392 36B	GLV NEOPR 30M MEDIUM
	Acklands Grainger	MMM8210 (3KP43)	3M - RESPIRATOR N95 PARTICULATE 20/BOX (3M 8210)
	VWR	82028-026	MAT HAZ YELLOW ROLL 144FT
		CA11000-900 (A8153/40)	FACESHIELD RACHT CL8 1MM
		CA56223-087 (KHG5001)	SPARKGUARD HEADGR W/RATCHET4IN
		CA13502-275 (A8150/40)	CLEAR 8X15.5 CLEAR VISOR
Wash Tanks	Fisher Scientific	14 831 330K	TNK RECT CV LLDPE24X12X12 1CS
		14 831 330B	TNK RECT W/CV LLDPE 11GAL 18x12x12 1CS
Detergent	Fisherbrand	04-343	Versa-Clean™ Pharmaceutical Production/Multi-Purpose Cleaner
Disposal	ULINE	S-17471NAT	5GALLON NATURAL JERRICAN
Additional Consumable Materials	VWR	82026-426	VWR Powder-Free Nitrile Examination Gloves CS/100
		51138-500	Absorbent Lab Paper (Leakproof Barrier) 20" x 300' (2/CS)
	Fisher Scientific	4357Q (20560Q)	Scoopula Spatula 6/PK
		13 374 12	4 in. W x 250 ft. L (10cm x 76m) [PARAFILM 4 IN X 250FT/RL]
		087-32-113	Fisherbrand™ Polystyrene Weighing Dishes - 89x89x25mm 500/cs
		14 793 9	TT RACK FB 40 HOLE 20MM BLUE
		14 791 6C	RACK WIRE/EPOXY 50ML 36 PLACE
		14 272 4AA	125ML ERL FLASK CLAMP
Sorption System Materials	Fabco Plastics	r4-1000	PVC SCH-40 pipe
		897010	PVC SCH-80 Socket Union Fitting (viton o-ring)
		438130	PVC SCH-40 reducer bushing (nominal 1x1/2-inch) (slip x FPT)
	Cole Parmer	3386	1/4-inch I.D. Silicone tubing, 25 ft.
		RK-98553-12	PP Miniature Check Valve, 1/4" hose barb, Viton diaphragm
		RK-30625-73	Male Pipe Adapter, HDPE, NPT(M) 1/2" x ID 1/4", 100 PACK

Table A.2 Specifications of Consumable Materials

Material	CAS No.		Description		Physical Form	ρ/(g·cm³)	Solubility g/100g H$_2$O	Solubility Temp. (°C)
						Properties (Haynes, 2015)		
Analytical Grade Nitrate Salts	10031-43-3	**Cu²⁺**	Cu(NO$_3$)$_2$ · 3H$_2$O	Copper (II) Nitrate Trihydrate	blue rhomb cry	2.32	145.0	25
	7782-61-8	**Fe³⁺**	Ni(NO$_3$)$_2$ · 6H2O	Nickel(II) Nitrate Hexahydrate	viol-gray hyg cry	1.68	82.5	20
	13478-00-7	**Ni²⁺**	Fe(NO$_3$)$_3$ · 9H$_2$O	Iron (III) Nitrate Nonahydrate	grn monocl cry; hyg	2.05	99.2	25
	10099-74-8	**Pb²⁺**	Pb(NO$_3$)$_2$	Lead (II) Nitrate	col cub cry	4.53	59.7	25
	10196-18-6	**Zn²⁺**	Zn(NO$_3$)$_2$ · 6H$_2$O	Zinc Nitrate Hexahydrate	col orth cry	2.07	120.0	25
Nitric Acid	7697-37-2		**HNO$_3$**		col liq; hyg	1.51		

Natural Zeolite*	**Chemical Composition**	Mineral Component	85-95% Clinoptilolite (non-crystalline silica opaline balance)
		Cation Exchange Capacity (CEC)	180-220 meq/100 g (as ammonium,-N) (high)
		Maximum Water Retention	>55 wt% (hydrophilic)
		Overall Surface Area	24.9 m²/g (large)
		Bulk Density	approx. 55-60 lb/f³
		Hardness	Moh's No. 4 (high)
		pH	7-8.64
		Colour	Pale Green

	MSDS Composition Information	**Chemical**	**wt%**	**CAS No.**
		Clinoptilolite	90-97	12173-10-3
		Water	3-10	7732-18-5

	Analytical Rock Data		
	SiO$_2$	67.4%	
	Al$_2$O$_3$	10.6%	
	MgO	0.45%	
	K$_2$O	4.19%	
	MnO	<0.01%	
	CaO	2.23%	
	TiO$_2$	0.27%	
	Fe$_2$O$_3$	1.70%	
	Na$_2$O	0.59%	
	P$_2$O$_5$	0.10%	
	Loss-On-Ignition (LOI) 925°C	11.40%	

	Major Cation Range	
	Ca	1.60-2.0%
	K	2.93-3.47%
	Na	<0.5%

*(Bear River Zeolites, 2012; 2017)

Table A.3 Specifications of Related Equipment

Equipment	Specifications
Scanning Electron Microscopy (SEM)	6380LV (EDS, EBSD, 3D) JEOL, USA
Inductively Coupled Plasma – Atomic Emission Spectroscopy (ICP-AES)	Optima 7300 DV Part No. N0770796; Serial No. 077C8071802 Firmware Version 1.0.1.0079 Perkin Elmer Inc., Waltham, MA, USA
Mechanical Sieve	Model No. Humboldt H4330 CAT No. G118-H-4330
Orbital Shaker	MaxQ™ 4450 Benchtop Orbital Shaker CAT No. 11-675-202 ThermoFisher Scientific
pH Meter	accumet Basic AB15 pH Meter CAT No. 13 636 AB15 Fisher Scientific
Pipette	Finnpipette 0.1-1mL; 2-10mL CAT No. 21-377-821; 21-377-824 Thermo Electron Corporation
Muffle Furnace	NEY M-525 SII Serial No. AKN 9403-108 120 V; 50/60 Hz; 12.5 A; 1500 W Barkmeyer Division, USA
Oven	Isotemp® Oven Model 630G Serial No. 30300047; CAT No. 13-246-630G 115 V; 6.5 A; 60 Hz Fisher Scientific, USA
Fume-hood	CIF; Con-Test Calibration Sash Height: 18; Velocity: 175 fpm
Scale	AL204 Analytical Scale Fisher Scientific CAT No. 01910154 Mettler Toledo
DDW	Direct-Q ® Water Purification System Fisher Scientific CAT No. ZRQSVPOUS Millipore
Diaphragm Metering Pump	No. 950218125-C Plus max 45-LPD 80-psi 125-AC 50/60-Hz PULSAtron, Punta Gorda, FL, USA
Three-way Solenoid Valve	No. 00457979 0124-C, 1/8-FKM-PP, NPT-1/4 max 145-psi, 24-V, 60-Hz, 8-W, 38-mL burkert, Ingelfingen, Germany

With respect to the specifications outlined in **Table A.3**, a view of the experimental set-up for SEM analysis is provided in **Figure A.1**. The ANALEST Centre facility employed for ICP-AES analysis is captured in **Figure A.2**; providing the various components of the system as well as the software interface.

<table>
<tr><td>a.   View of Microscope System</td><td>b.   Preparation fo Conductive Layer
(Sputter Coating Station)</td></tr>
</table>

Figure A.1 Experimental Set-up for SEM Analysis
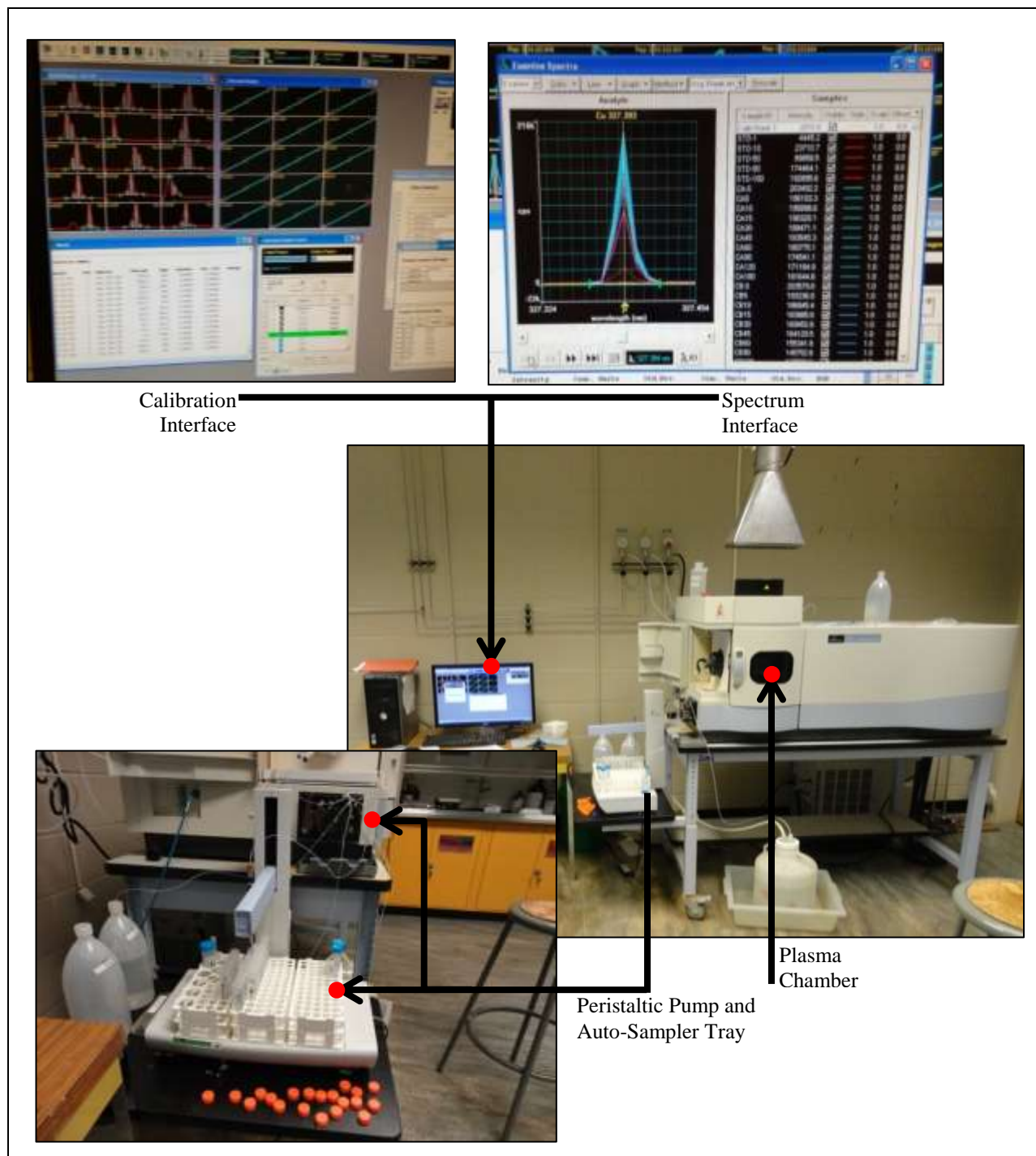
Figure A.2 Experimental Set-Up for ICP-AES Analysis

A.3. Environmental Engineering Laboratory Schedule

Table A.4 is the schedule followed in the laboratory where all experimental work was conducted (MON412). During the Fall-2015 academic term, a bi-weekly schedule was followed to accommodate the undergraduate students at the time; the nitric acid bath was transferred from the fume-hood and out of reach on the floor for the safety of all personal in the shared space. During the Winter-2016 academic term, a 'two weeks on, one week off' schedule was followed, to provide time for lab management, routine data processing, analysis, and so on.

Table A.4 Laboratory Schedule

MONDAY	AM	• Collect DDW in carboys (4 L+) (per stock preparation)
		   ○ Collect DDW-S (Blank) Sample
		• Label Labware
		   ○ Bottles (1, 2, 4 oz.)
		   ○ Glassware (2× 100 mL + 4× 1-L Volumetric Flasks, 4× 100 mL Graduated Cylinders, 4× Beakers)

	PM	• Measure Zeolite Mass to 4 oz. Bottle (4× 9 Samples)
		• Prepare HMI Influent Stock (4× 1-L Sample Sets)
		   ○ Dilute HMI Nitrate Salts; Acidify (1.5mL per 1-L)
		   ○ Refrigerator Storage
		• Set-up experimental station on lab bench for Tuesday sequence

TUESDAY	AM	• Collect DDW in carboys (per glassware clean)
		• Set Incubator to 400 rpm at 22°C (08:00AM)
		• Sample SET 1+2 (AM) (5 to 180 min)
		   ○ Zeolite and HMI Stock (100 mL to 4 oz.)
		   ○ Filter and Refrigerator Storage (1 oz.); pH Measure (4 oz.)

	PM	• Set Incubator to 400 rpm at 22°C (12:00PM)
		• Sample SET 3+4 (PM)
		• Clean Labware (4 oz. Bottles, Glassware)
		   ○ Hazardous Waste Disposal; Tap Rinse + Soap Wash + Tap Rinse
		   ○ DDW Rinse (1×) + Air Dry

WEDNESDAY	AM	• Acid Bath Labware 1 (8AM – 24 hrs+) • Collect DDW in carboys (4 L+) (per dilution preparation) • Label ICP-AES Sample Tubes

	PM	• Dilute ICP-AES Standards (1, 10, 50, 90 mg/L) (10 mL total volume)
		• Dilute Sample Sets 1-4
		   ○ 1 oz. to 2 oz. (40 mL total volume)
		   ○ By 50% levels per 0-100 mg/L Calibration Range
		   ○ Transfer to ICP-AES Sample Tubes (10 mL)
		• Clean Labware (1 + 2 oz. Bottles)

THURSDAY	AM	• Remove Acid Bath Labware 1 and DDW (3×) Rinse • Acid Bath Labware 2 (10AM – 24 hrs+)

	PM	• Transport ICP-AES Sample Tubes (Portable Refrigerator) (12PM)
		• University of Toronto ANALEST Centre
		   ○ Plasma ON (1:00PM); Calibration (1:20-1:30PM)
		   ○ Sample Analysis (1:30-2:45PM)
		   ○ Data Reprocessing and Collection (2:45-3:00PM)
		• Hazardous Waste Disposal ICP-AES Sample Tubes

FRIDAY	AM	• Remove Acid Bath Labware 2 + DDW (3×) Rinse
	PM	• Digitize Lab Notes and Compile/Analyze ICP-AES Data

A.4. Labware Cleaning Procedure

1. Create soap mixture with by filling soap bottle with 20:1 ratio; 300 mL DDW + 25 mL soap + 200 mL DDW.
2. Dispose of spent zeolite sorbent material and HMI sorbate solution from bottle(s).
3. Dispose of spent residual HMI sorbate solution from glassware.
4. Rinse labware once with warm tap water and place on clean absorbent lab paper.
5. Fill labware with soap mixture and shake well.
6. Rinse labware with warm tap water until all of the soap mixture disappears; approximately nine (9) rinse cycles.
7. Dry labware on clean absorbent lab paper.
8. Rinse labware once (1×) with DDW and dry on clean absorbent lab paper overnight.
9. Soak labware (submerge bottles and fill-parafilm cap glassware) in 1+1 acid bath overnight (24 hrs).
10. Remove labware from acid bath, shaking off any residual acid solution.
11. Rinse labware three times with DDW water.
12. Dry labware on clean absorbent lab paper.

*Note – Conventional fume-hoods significantly contribute to contamination. Consequently, all vessels are kept covered from incoming air.

A.5. HMI Influent Stock Preparation

Table A.5 provides the calculations based on a total HMI component system concentration of 0.01 N (10 meq/L) of the respective analytical grade nitrate salts (Inglezakis et al., 2002; Inglezakis et al., 2003; Inglezakis et al., 2004; Stylianou et al., 2007a). The required nitrate salt mass that corresponds to the HMI concentration (represented in mg/L) are used for the dilution preparations required for elemental analysis (discussed in **Appendix A.9**).

Table A.5 Influent Concentration Computation

HMI	Nitrate Salt CAS No.	Molecular Weight [MW] (g/mol)	
		Compound	HMI
Cu^{2+}	10031-43-3	241.602	63.546
Fe^{3+}	7782-61-8	403.997	55.845
Ni^{2+}	13478-00-7	290.794	58.693
Pb^{2+}	10099-74-8	331.200	207.200
Zn^{2+}	10196-18-6	297.510	65.380

HMI	Conversation Steps					Concentration (mg/L)	
	%HMI	Normality [N] (eq/L)	K (eq/mol)	M (mol/L) M=N/K	MW·M (g/L)	Compound	HMI
Cu^{2+}	0.263		2	0.0050	1.2080	1208.010	317.730
Fe^{3+}	0.138		3	0.0033	1.3467	1346.657	186.150
Ni^{2+}	0.202	**0.01**	2	0.0050	1.4540	1453.970	293.465
Pb^{2+}	0.626		2	0.0050	1.6560	1656.000	1036.000
Zn^{2+}	0.220		2	0.0050	1.4876	1487.550	326.900

1. Collect deionized distilled water (DDW) (18mΩ.cm @ 25°C); approximately 4-L required for influent stock preparation contained in a 20 L carboy.
2. Weigh the analytical grade nitrate salt mass (measurements from **Table A.5**) using a scoopula spatula (labelled for each HMI and zeolite), weighing dish and balance (**Figure A.3a** and **A.3b**).
3. Dispense HMI salt into a 1-L volumetric flask, and rinse weighing dish with DDW to include total mass (**Figure A.3c**).
4. Dilute influent stock to 1-L (**Figure A.3d**).
5. Cover the 1-L volumetric flask with parafilm and invert slowly three times.
6. Remove the parafilm cover.
7. Measure 1.5 mL of concentrated nitric acid (Rice et al., 2012) and dispense into HMI solution (**Figure A.3e**).
8. Cover the 1-L volumetric flask with parafilm and invert slowly three times.
9. Store HMI influent stock in refrigerator overnight (**Figure A.3f**).
10. Collect DDW sample as blank for ICP-AES analysis of that experimental week.

a. Set Aside Labware

b. Weigh Nitrate Salts

c. Dispense HMI Nitrate Salt into Flask

d. Dilute Stock to 1-L Volume

e. Acidify Stock
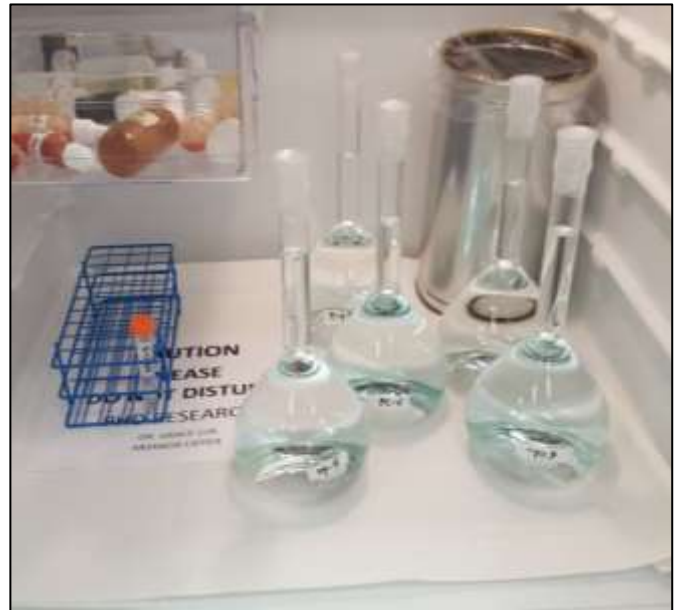
f. Store Prepared Influent Stock in Refrigerator

Figure A.3 HMI Influent Stock Preparation Procedure

A.6.   Natural Zeolite Sample Preparation

Preliminary analysis of the raw zeolite mineral supply was conducted in the geotechnical lab (KHN101), which involved a particle size range within the standard mesh fractions of -8+40, -14+40, and -30+60 from the supplier. As shown in **Table A.6**, testing of the particle size was conducted with standard mesh ranging from sieve sizes10 to 40. The results showed that the standard mesh range -14 (pass) +40 (retain) (0.420-1.41mm) provided the most material once sieved along the available gradations. The zeolite particle size supply -14+40 is the basis of the parameters discussed in **Chapter 4**, divided into the sub-fractions of A ($d_{p,A}$) (1.190-1.410mm), B ($d_{p,B}$) (0.707-0.841 mm), C ($d_{p,C}$) (0.420-0.595 mm) and D ($d_{p,D}$) (0.841-1.19 mm). The particle size range $d_{p,D}$ is selected as the controlled parameter following the analysis of the particle size operation parameter.

1. Pre-sieve zeolite mass to the specified standard sieve gradations (particle sizes A, B, C and D of supply -14+40 as outlined in **Table A.6**);.
2. Weigh approximately 300 g of raw (as-received) zeolite mass using a scoopula spatula (labelled for zeolite use), weighing dish and balance.
3. Transfer weighed zeolite to a shallow plastic container, and rinse with DDW water (approximately 1 inch of water above zeolite mass) until water solution is cleared of dust and debris; approximately nine (9) rinse cycles (**Figure A.4a**).
4. Place moist zeolite mass onto clean muffle furnace tray (**Figure A.4b**) and transfer to the oven (**Figure A.4c**).
5. Turn on oven and set to 80 ± 3°C temperature.
6. Dry zeolite mass for 24 hrs.
7. Remove tray from the oven and allow zeolite mass to reach room temperature for 24 hrs.
8. Transfer zeolite mass from tray to a plastic bag for storage and forthcoming use.

Table A.6 Particle Size Breakdown of Natural Zeolite Sorbent Supply

Zeolite Supply		-8+40		-14+40				-30+60	
Test Sample		993.40 g		992.20 g		1006.60 g		1016.90 g	
Sieve Size*		g	%	g	%	g	%	g	%
	#10 Retain	99.90	10.06	0.10	0.01				
	#10 Pass #12 Retain	217.20	21.86	0.50	0.05				
	#12 Pass #14 Retain	263.90	26.57	65.20	6.57	76.50	7.60	0.30	0.03
A	#14 Pass #16 Retain	131.40	13.23	174.70	**17.61**	199.90	**19.86**	0.40	0.04
D	#16 Pass #18 Retain	86.60	8.72	167.90	16.92	181.10	**17.99**	0.10	0.01
D	#18 Pass #20 Retain	65.50	6.59	146.00	14.71	150.90	**14.99**	0.00	0.00
B	#20 Pass #25 Retain	122.30	12.31	431.90	**43.53**	119.10	**11.83**	0.00	0.00
	#25 Pass #30 Retain					94.00	9.34	18.60	1.83
C	#30 Pass #35 Retain					68.10	**6.77**	107.50	10.57
C	#35 Pass #40 Retain					48.30	**4.80**	153.00	15.05
	#40 Pass (PAN)					57.90	5.75	729.10	71.70
	SUM	986.80	99.34	986.30	99.41	995.8	98.93	1009.0	99.22
	LOST	6.60	0.66	5.90	0.59	10.80	1.07	7.90	0.78

Sieve Conversation*

US MESH #	10	12	14	16	18	20	25	30	35	40
Standard Size (mm)	2.00	1.68	1.41	1.19	1.00	0.841	0.707	0.595	0.5	0.42

a.   Remove Residual Debris from Raw Zeolite Sample
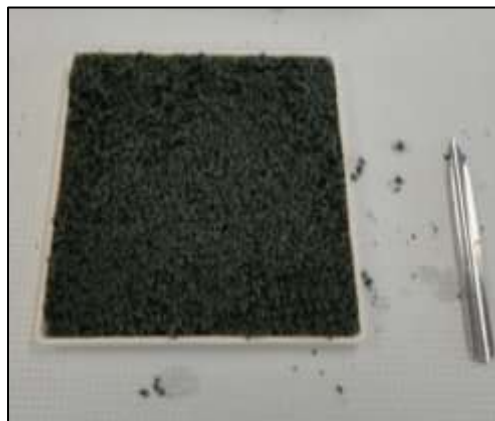
b.   Place and Span out Zeolite onto Muffle Furnace Tray

c.   Remove Residual Moisture

Figure A.4 Natural Zeolite Sample Preparation – Cleaning Cycle Procedure

A.7. Hydrothermal Pre-Treatment Preparation

1. The muffle furnace is pre-calibrated to ensure the mechanical dial system corresponds to the required heat pre-treatment level ($200^{o}C$, $400^{o}C$, $600^{o}C$) (**Figure A.5a**).

2. The cleaned natural zeolite is weighed using a scoopula spatula (labelled for zeolite use), weighing dish and balance; to the required mass of each heat level.

3. For each heat pre-treatment level, the zeolite mass is transferred to the muffle furnace tray and placed in the pre-heated muffle furnace (**Figure A.5b**).

4. Once the tray is inserted, the 1-hr treatment period starts once the desired heat level temperature is restored.

5. Remove the tray from the muffle furnace and allow zeolite mass to reach room temperature for 24 hrs.

6. Transfer zeolite mass from tray to a plastic bag for storage and forthcoming use.

a. Verify Muffle Furnace Temperature Setting

b. Place the Measured Zeolite Mass onto the Tray, then into the Muffle Furnace

Figure A.5 Hydrothermal Pre-Treatment of Zeolite Sample

A.8.   Experimental Sequence Procedure

- With reference to the lab sequence breakdown in **Appendix A.3**:

1. Remove AM SET 1+2 influent stock volumetric flasks from refrigerator (08:00).
2. Turn on orbital shaker and set to 400 rpm at 22°C set temperature (15 min prior to orbital shaker contact).
3. 'Rinse-out' (~50 mL) SET 1 and SET 2 100-mL graduated cylinders with each HMI influent stock.
4. As outlined in **Table A.7**, commence shaker-sample sequence; established to maximize space availability of shaker as specified with the order of sample bottles in (A) and out (B).
5. At each time-step, fill 4 oz. sample bottle (containing pre-weighed zeolite mass) with SET stock solution using 100-mL graduate cylinder from the 1-L volumetric flask.
6. Place in bottle clamp position and press start button to initiate orbital shaker (**Figure A.6a**).
7. Position 1 oz. sample bottle and syringe-filter at the ready on bench station.
8. Remove bottle from orbital shaker.
9. Withdraw 25-mL effluent sample with the syringe, twist-lock on the 0.45 μm filter to syringe tip, and dispense the sample into the 1 oz. sample bottle (**Figure A.6b**).
10. Cap and store the 1 oz. sample bottle containing the effluent samples in the refrigerator overnight.
11. With the residual effluent contained in the 4 oz. sample bottle, collect a pH level measurement.
12. Dispose of spent zeolite sorbent material and HMI sorbate solution from bottle(s).
13. Dispose of spent residual HMI sorbate solution from glassware.
14. Repeat steps 1 to 13 for PM SET 3+4 (12:00).

Table A.7 Orbital Shaker Sample Bottle Contact Sequence

								IN[A]	OUT[B]
AM SET	**180**	8:30	11:30					180	60
	120	8:40	10:40					120	90
		15	10:40	10:55				90	30
			45	10:55	11:40			60	120
				10	11:40	11:50		30	15
					5	11:50	11:55	15	180
	90	8:50	10:20					45	45
	60	9:00	10:00					10	10
		30	10:00	10:30				5	5
PM SET	**180**	12:30	15:30						
	120	12:40	14:40						
		15	14:40	14:55					
			45	14:55	15:40				
				10	15:40	15:50			
					5	15:50	15:55		
	90	12:50	14:20						
	60	13:00	14:00						
		30	14:00	14:30					

a. View of Sample Bottle Clamp Arrangement in Orbital Shaker

b. Separate Sorbate (HMI) and Sorbent (Zeolite) with Syringe-Filter

Figure A.6 Sorbate-Sorbent Contact and Separation

A.9. ICP-AES Sample Preparation

- With reference to the lab sequence breakdown in **Appendix A.3**:

1. Collect deionized distilled water (DDW) ($18m\Omega$.cm @ 25°C); approximately 4-L required for influent stock preparation contained in a 20 L carboy.
2. Label all ICP-AES 15-mL auto sampler tubes.
3. Prepare the ICP-AES standards by diluting the 100 mg/L Multi-Element Quality Control Standard 4 to total volumes of 10 mL at 1, 10, 50, and 90 mg/L, using the pipettes and DDW; set into the auto-sampler tubes (**Table A.8**)* (**Figure A.7a**).
4. Cap the tubes and invert slowly three (3) times.
5. Remove the 1 oz. sample bottles from the refrigerator.
6. Based on the component system concentration of each HMI of a given sequence, dilute to 20-mL** total volumes into the 2 oz. sample bottles (**Table A.9**) (**Figure A.7b**).
7. Cap the bottles and invert slowly three (3) times.
8. Once all dilutions are complete, transfer the dilutions from the sample bottles to the pre-labeled ICP-AES auto-sampler tubes.
9. Store ICP-AES auto-sampler tubes containing the diluted effluent samples in the refrigerator overnight.
10. With the residual effluent contained in the 1 oz. sample bottle, collect a pH level measurement.
11. Dispose of spent HMI effluent solution from bottles.

Table A.8 ICP-AES Calibration Standards Dilutions

Standard Concentration (C2; mg/L)	Standard Volume (V1; mL)	DDW Volume (mL)
100	10	0
90	9	1
50^{QC}	5	5
10	1	9
1	0.1	9.9
BLANK	0	10

C1 = 100 mg/L
V2 = 10 mL

Table A.9 Number of 50% Dilutions (DIL#)*** for each Component System Sample

SYSTEM	Samples		SYSTEM	Samples	
	A	B		A	B
[P]	4	3	[D-PC]	3	2
[C]	2	2	[D-PF]	3	2
[F]	1	1	[D-PN]	3	2
[N]	2	2	[D-PZ]	3	2
[Z]	2	2	[D-CF]	1	1
[T]	2	1	[D-CN]	1	1
[M]	1	0	[D-FZ]	1	1
			[D-NZ]	1	1

[A]Stock [S]; Contact Times: 5,10,15,30 min
[B]Contact Times: 45,60,90,120,180 min

|	DIL4	DIL3	DIL2	DIL1
V1 (Sample) (mL)	2.50	5.00	10.00	20.00
DDW (mL)	37.50	35.00	30.00	20.00

*Note – The calibration standards are disposed of (only one time use) and are prepared new to coincide with the sample preparations for every experimental week.

**Note – The number of 50% dilutions (DIL#) is limited to 25-mL syringe-filter capacity; where the residual 5-mL is set for pH level measurements.

***Note – The number of 50% dilutions (DIL#) for the first phase of the research project investigating the particle size range and dosage applied an additional dilution step for 45-180 min samples; due to unknown zeolite sorption capacity at the onset of the research project. The dilutions (presented in **Table A.9**) have been refined for all preceding phases of the research project.

a. ICP-AES Sample Tubes and Preparation Station
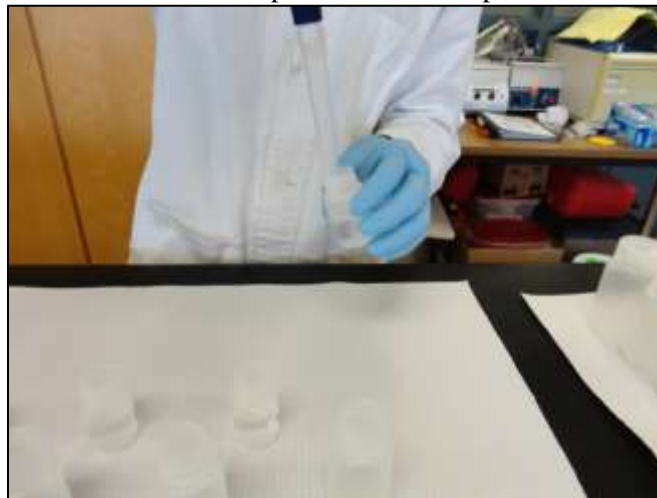
b. Dilute HMI Influent and Effluent Samples

Figure A.7 ICP-AES Elemental Analysis Preparation

A.10. Sorption System Development

Figure A.8 displays the extensive optimization to reach the final sorption system design discussed in **Chapter 7** and presented in **Figure 7.2** of the Dissertation document. What began as a simple dual-column set-up with a peristaltic pump, evolved into the innovative development of custom sampling chambers with an automated controls system mounted on a rigid support system.
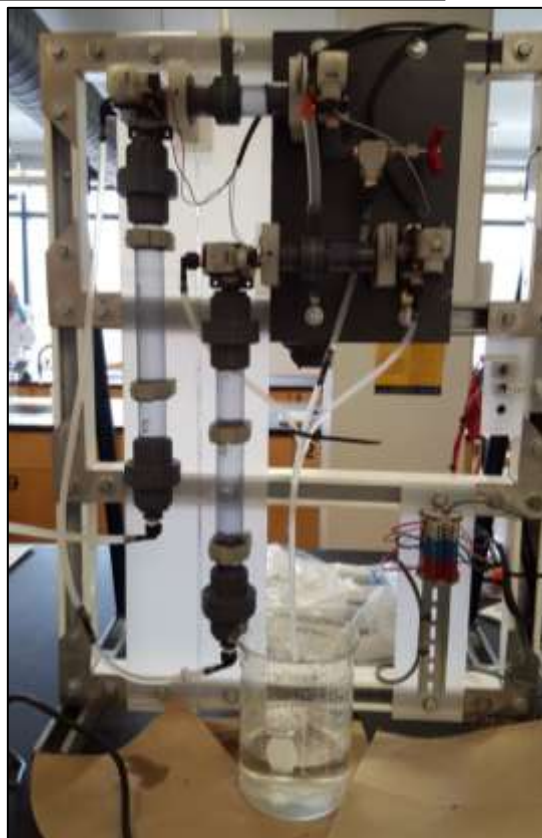
Figure A.8 Sorption System Prototype Development

APPENDIX B. ICP-AES Standard Operating Procedure

B.1.   Instrument Sequence
1. PLASMA ON 15 min before analysis
2. Method > SET + CHECK > Sample Info File (Same ID) > SAVE
   *WINLAB32 Software Check Mark×3 > PROCEED
3. Workspace Display (Spectra – Calib – Analysis)
4. Automated Analysis Control
5. Flush PLASMA> Calibration CHECK> Flush PLASMA> Rebuild List> Analyze Samples
6. Reprocess Data > EXPORT > SAVE
7. PLASMA OFF

B.2.   Gas Valves
- Air (ON)
- Argon (ON)
    - CHECK psi levels prior to analysis session
    - Direct Gas – 80/90 psi
    - Inlet Tank – 500 psi (minimum)
- Nitrogen
    - Adjust at each data run/test (1/4 turn counter-clockwise)
    - Shut down > CLOSE

B.3.   Peristaltic Pump Set-Up
- REFILL DDW
- Red/Red – Wash > Waste
    - Waste (CHECK > replace at end of week or flat/worn-out/foggy)
        - Attached to nebulizer (back-most tube)
    - Wash (DDW or 5% HNO$_3$) (analyte solution matrix); selected DDW to eliminate compounded error from unknown lab personal
- Black/Black (front-most tube)
    - Sample > Top to nebulizer
    - START – Replace with data set/lab visit
    - Pull taught and insert tubing (2-3mm)
    - LOCK on the tubing clamps (check tubing goes into the groove in the clamp)
    - MIST/SPRAY – Plasma ON (clockwise direction – movement)
    - Shut down > Release Tension

B.4.   Instrument Shut Down
- Turn off Plasma Tab
    - Wait until the gases stop flowing before you exit from the program.
    - Exit from the program. Log out of Windows. Leave the computer on.
- Release clamps from the peristaltic sample pump, and release the tubing.
- Remove standards and samples from the A/S tray.

B.5. New Method
With Reference to **Figure B.1a**
- File > New > Method (or COPY another method)
    - Default (Aqueous Mode – 3-5% TDS) > Method Editor

B.6. Instrument Start-up

Set A/S Tray
- Place Blanks + Standards + Samples into the A/S tray
    - Place into the well positions as specified in the Method and SIF

Light Plasma
With Reference to **Figure B.1c**
- Toolbar > Click "Plasma" button > Plasma Control box
- Click "Pump" button (turns on the sample pump)
    - Verify that the solutions are flowing, and flowing in the right direction
- Click on the "On" button to light the plasma (15 mins before sequence)
First, it shuts off the sample pump, then it adjusts the gas flows, it lights the plasma, and then it turns the pump back on.

B.7. Procedure Breakdown

1 Spectrometer
A Define Elements
- Multi lines per multi elements
- BEC (Background Equivalent Concentration; ppm)
    - Preferential Order (5-10ppm)
- SELECT <u>top 3 wavelengths</u> (similar BEC levels/orders-of-magnitude)
  address interferences
    - Click "Wavelength Table" button to go to the list of elements and their wavelengths
    - Control-click each line of the table that you want to import into your method, and then click on "Enter Selected Wavelengths in Method" button

B Settings
With Reference to **Figure B.1b**
- <u>Purge Gas Flow – Normal</u>
  (High at <190 nm - based on elements' wavelengths – N/A)

- <u>Read Time – 5-10 secs</u> *Method optimization*
  Literature Reference – Typical Values per Calibration

- <u>Delay Time – 45 secs</u> > ~3 mins/sample
- <u>Replicated - Triplicate Runs (3)</u>
    - one sample vial OR multi (time-dependent)
- Quantifiable Detection Limits – RSD

C Spectral Windows
- Find Emission Line (Default)

2 Sampler – Power and Plasma View
A Plasma
- Mix Mode (Same or Vary to optimize method)
  - FIRST ROW OVERRIDES ALL WAVELENGTHS*
  - Radial – 1ppm> ('high' concentration) > SELECT all radial
  - Axial – 1ppm< (5× more sensitive)
- Equilibration Delay – 15 secs
- Plasma Conditions – Wet and Instant
- 1300 watts (SET 1500 watts to increase sensitivity via Axial)

B Peristaltic
- Rate – 1 mL/min
- Flush – 30 secs

C Auto Samples
- Frequency between Samples***
  - Rate – 1.5mL/min
  - Normal Time – 45 secs
  - A/S Location WASH – Zero (0)

3 Process
A Peak Processing
- Peak Algorithm > Peak Area
- Points per Peak – 3-5

B Spectral Corrections
- 2 point
- BGC 1 & 2 – Default – Change w/ Data
- Overlap Correction – NON

*C Internal Standards – NO *click box**
- Internal Checks – Blank

4 Calibration
A Define Standards
- Calibration Blank
  - Solvent Source (analyte Stock DDW) – MON412 LAB*
- Calibration Standard – A/S (auto-sampler) Location (Reagent Blank N/A)
  - *Click on the Calibration tab on the bottom.*
  - *Give an ID and a location for each standard you will be using; ID what the element is, and its concentration*
  - *A/S Number - NOTE Line Indicator*

B Calibration Units and Concentration
- Rank Set LOW > HIGH (NO ZEROS) – per order of magnitude in concentration*
  - Double-click column to set concentration*

C Blank Usage
- Calib Blank 1 (MON412 – DDW-S)

D Equation and Sample Units
- Equations (adjust with data reprocessing)
  - **Linear Calc. Int. (set to)**
  - Through Zero

E Initial Calibration and Multiline Calibration (Default)

5 Checks
- Edit > Check Method

6 QC – Set Calibration Standard (Default)

B.8. Save Method
- Edit > CHECK Method
- File > Save Method
- Main Page > File > Save As > Method
- Enter name > OK

B.9. Sample Info File
With Reference to **Figure B.1d**
- Create a sample list
  - File > New > Sample Info File
  - Select "ppm design.sif" and click OK
- Fill in the table with the A/S location and sample ID for each sample > Batch ID - DATE
- Save your sample list
  - File > Save As > Sample Info File
  - Type in a name and click SAVE (as per saved Method)
- Close the Sample Information Editor

B.10. Automated Analysis Control
With Reference to **Figure B.1e**

- Workspace File – CLICK:
  - o Spectra TAB
  - o Calib TAB
  - o Results TAB
  - o Options > Display>AutoLayout> per wavelength (1-3)
- Toolbar > Click "Auto" button (dialog box)
  - <u>Set-Up TAB</u>
  - o Input Method
  - o Input Sample Info File
  - o CLICK > Use 'Sample Info' and <u>SAVE DATA</u>
  - o CLICK > 'Print Log During Analysis' <u>OFF</u>
  - <u>Analyze TAB</u>
  - o Click Calib BOX FIRST* (~20 min)
    - ▪ RSD < 3% target
    - ▪ Corr. Coeff = 0.999… (good correlation)
  - o Click Rebuild List BOX
    > unknown (to analyze) show
  - o *Plasma TAB > FLUSH (WASH) (15 seconds)
  - o Click Analyze Samples BOX
    - ▪ Analysis Proceeds*
    - ▪ Require ~3 min/sample (5% error)
  - o FLUSH PLASMA (~15 seconds IDLE)

B.11. Data Processing Analysis and Export

Examine
- Examine > Data > Select Data Set > Select All > Next > Select > Finish ALL OK
- <u>SELECT Primary Line</u>

Reprocess (Spectrum Alignment)
- Toggle Peak/Endpoints> Update Method Parameter > Set Peak > Update Method – CLOSE EXAMINE WINDOW
  - File > Save Method
- Toolbar> Reproc TAB> Browse Data Set > Select Raw Data (ALL ROWS)
- Select 'Rename file - …repro/2' extension (CLICK <u>SAVE</u> REPO) > Reprocess TAB
- Method > Calibration Equation> Through Zero > SAVE
  - Examine Spectra
  - Update Method
  - Save Method >> REPO (SELECT ALL)
  - CALIB EQ > TZ
  - Save Method >> REPO TZ
- NOTE
  - Reprocess curve BC1+2 and/or calibration curve relative to samples
  - Toggle curve points and center peak to line

Export
- File > Utilities > Data Manager > Select Data to import > Select Export
- Create New Design > Next (OR existing design)
- Samples and Analytes to Export (make sure all data points and desired analytes selected > *ALL BOX CHECKED)
- All Unknowns (Select Primary Line) > Next > Extension '.prn' > <u>TAB</u> delimited

Sample Parameters	**Mean-Related Parameters**	**Replicate Parameters**
• Analyte/Sample ID (name)	• Analyte Name (Date and Time)	• Number # (Date and Time)
• A/S Location	• Element Wavelength	• Intensity (corrected)
	• Intensity (corrected)	• Conc. - Calib Units
	• Conc. - Calib Units	
	• %-RSD (corr. Intensity)	
	• SD (corr. Intensity)	
	• Corr. Coeff. (corrected)	

- Save > Export Design > Save as data set (link ID/Name)
  - Open Excel > File>Open>ALL FILES > Save as '.xlx'
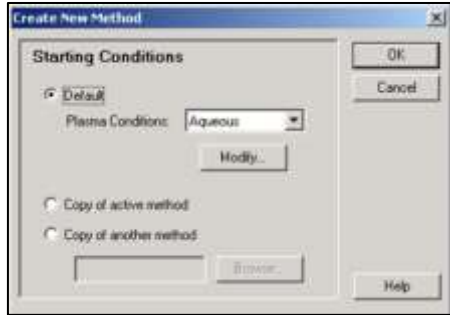
a. New Method
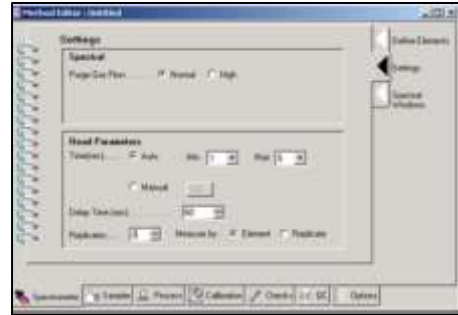
b. Spectrometer – B Settings
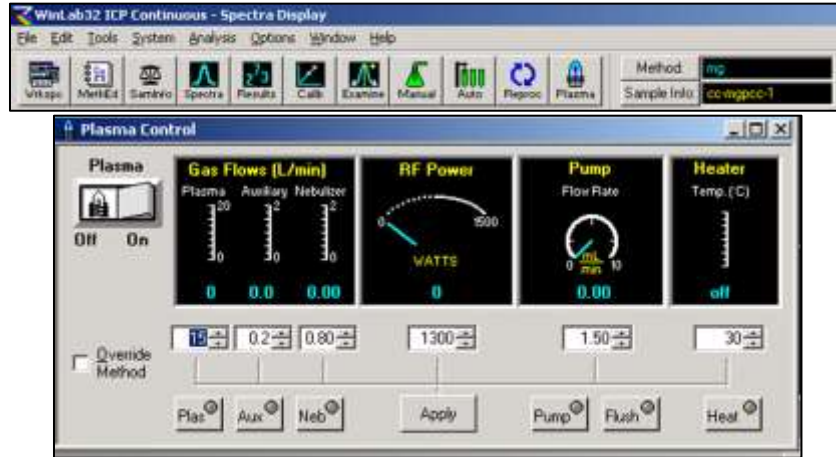
c. Instrument Start-up
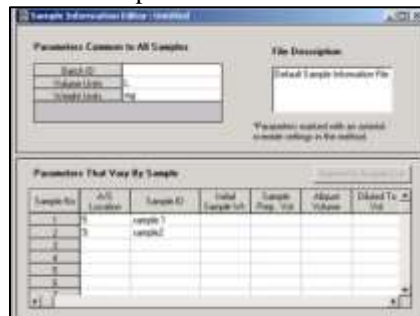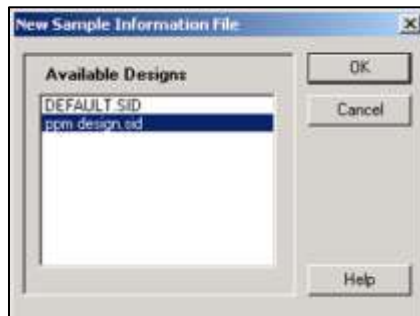
d. Sample Information File

e. Automated Analysis Control

Figure B.1 ICP-AES WinLab 32 Software Interface
(adapted from University of Michigan LSA, 2015)

176

APPENDIX C. WEAO2016 Technical Symposium

A Study on the Effects of Multiple Metallic Ions on the
Zeolite Adsorption of Lead from Mine Wastewater
Technical Session: Industrial Treatment A; Technical Session No.: 14
Paper No: 2016-03; 12 April 2016.

Abstract

This study investigates the ionic effects of Cu^{2+}, Fe^{3+}, Ni^{2+} and Zn^{2+} in multi-component systems, onto the adsorption of Pb^{2+} by natural zeolite in the form of clinoptilolite. The objective is to determine the overall adsorption of the target metal lead and the selectivity of clinoptilolite to the various heavy metallic ions (HMI) combined in the aqueous phase. Elemental analysis conclude that after just 3 hours of contact time, the target metal ion lead is removed by 77.5, 88.6, 78.3, 86.4, and 91.5% in the single-lead, dual-copper, dual-iron, triple-(lead-copper-iron), and multi-component systems, respectively. The removal efficiency order or 'selectivity series' is determined as $Pb^{2+} \gg Fe^{3+} > Cu^{2+} > Zn^{2+} > Ni^{2+}$.

APPENDIX D. WEAO2017 Technical Symposium

Effects of Heat Pre-Treatment on Metallic Ion
Adsorption and Ion-Exchange by Natural Zeolite
Technical Session: Industrial Treatment A; Technical Session No.: 4
Paper No: 2017-010; 03 April 2017.

Abstract

This study investigates the effects of heat pre-treatment on natural zeolite in its sorptive removal efficiency of the heavy metallic ions (HMIs) Cu^{2+}, Fe^{3+}, Ni^{2+}, Pb^{2+}, and Zn^{2+}. The ionic effects of these HMIs were examined in triple- [T] and multi-[M] component systems of a total 0.01N (10 meq/L) influent concentration. After 3 hours of contact time, the removal efficiency order is sustained throughout heat pre-treatment analysis to be $Pb^{2+} >> Fe^{3+} > Cu^{2+} > Zn^{2+} > Ni^{2+}$. When the Ni^{2+} and Zn^{2+} ions are introduced to the triple-[T] system, the Pb^{2+} ion and total HMI uptake is interfered in the multi-[M] system by a reduction of 37.5% and 25.3% [non-heated], 36.2% and 24.4% [200°C], 30.4% and 19.2% [400°C], and 25.9% and 25.6% [600°C], respectively. The total uptake of HMIs by zeolite is reduced by 6.1% [T] and 5.0% [M] at 200°C, 33.2% [T] and 27.8% [M] at 400°C, and 46.8% [T] and 47.0% [M] at 600°C exposure; compared to the non-heat-pre-treated form. This research has demonstrated that no major improvement of HMI sorption is achieved with progressive heat pre-treatment of zeolite.

APPENDIX E. WEAO2018 Technical Symposium

An Innovative Sorption Treatment System to Remove Heavy Metallic Ions from Mine Wastewater

Technical Session: Industrial Treatment B; Technical Session No.: 26
Paper No: 2018-072; 17 April 2018.

Abstract

This study demonstrates the performance of a sorption system prototype, consisting of fixed-bed, dual-columns packed with natural zeolite, custom sampling chambers and automated controls. The system is fed continuously with a synthetic simple solute aqueous solution of a total 10 meq/L multi-component heavy metallic ion (HMI) influent concentration; by a controlled adjustable distribution timer. The sorption process of five HMIs commonly found in industrial wastewater effluent is evaluated. The system removal efficiency is demonstrated by a selectivity order of lead(Pb^{2+}) $\gg$ iron(Fe^{3+}) > copper(Cu^{2+}) > zinc(Zn^{2+}) $\gg$ nickel(Ni^{2+}). The lead ion is removed completely throughout the 3-hour contact period in both columns. An overall higher bed capacity at breakthrough and usage rate in the second column is observed. This system prototype experimentally contributes to the advancement of industrial wastewater treatment technology.

APPENDIX F. Water Environment Research Journal Publication

Prior to the in-depth research into the removal of heavy metallic ions of this research project, the capacity of natural zeolite to address high nutrient levels was investigated by the Ph.D. Candidate in the M.A.Sc. research. The objective of the study was to target the removal of total phosphorus (TP), and to demonstrate the efficiency of an optimized clay-zeolite medium. The outcome of this study compared well to other common removal technologies, as a more simplistic and affordable system alternative. With further optimization, this system would minimize direct surface discharge of phosphorus and overall, contributes to the advancement of eutrophication control. The journal publication reference details (**Figure F.1**) are as follows.

An Innovative Design of a Clay-Zeolite Medium
for the Adsorption of Total Phosphorus from Wastewater

Amanda Lidia Ciosek[1*], Grace K. Luk[2], Michèle Warner[3], R. Anthony Warner[4]

[1*,2]Department of Civil Engineering, Faculty of Engineering and Architectural Science, Ryerson University, Toronto, Ontario, Canada.
[3,4]Virtual Engineers Inc., Markham, Ontario, Canada.

Abstract

Phosphorus significantly influences the eutrophication process, modifying the quality of waterways and habitat, especially in stagnant water bodies exposed to septic tank effluent at high nutrient levels. This research explores the development of a cost-effective, efficient, and affordable on-site wastewater treatment system targeted as total phosphorus (TP) removal technology. The research objective is to demonstrate the TP removal efficiency of an optimized clay-zeolite medium by chemical adsorption. The study observes the effects of pellet medium design and modifications, influent concentrations, and contact time. Following various stages of optimization, the preliminary testing achieves a $45 \pm 1.8\%$ removal after 45 minutes of contact time. The optimized pellets are contained within a five-layer bench-scale model, achieving equilibrium TP removal of $72 \pm 2.9\%$ after 3 hours. Theoretical extrapolation to 12 contact hours indicates an achievement of 88% removal is possible. The results show a positive correlation with the linearized Langmuir and Freundlich adsorption isotherms.

Keywords: wastewater treatment, total phosphorus, clay, zeolite, Langmuir, Freundlich, adsorption, isotherm.
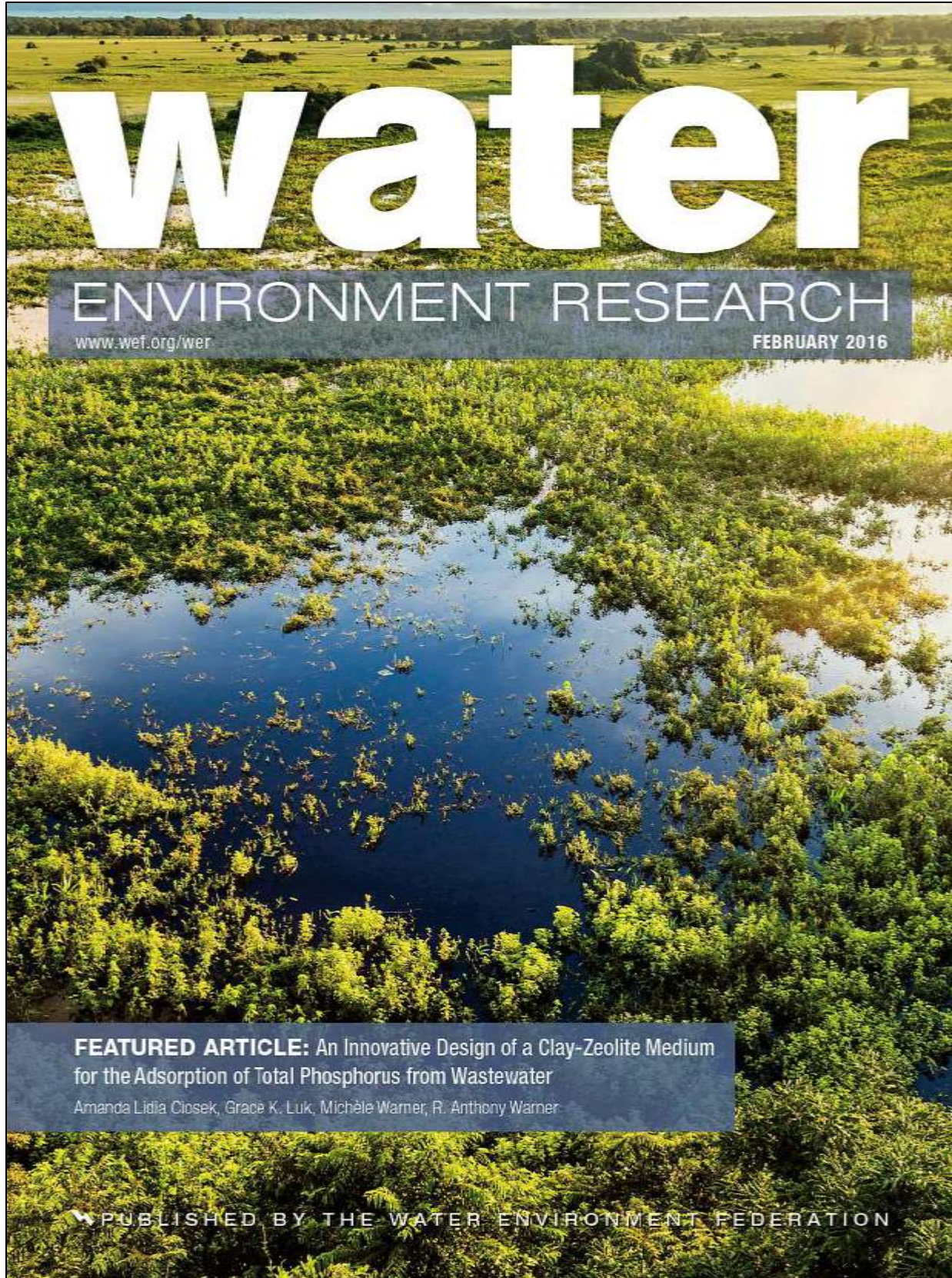
Figure F.1 Water Environment Research Journal Publication – Cover Featured Research Article

REFERENCES

1. Acheampong, M.A.; Meulepas, R.J.W.; Leans, P.N.L. Removal of heavy metals and cyanide form gold mine wastewater. *J. Chem. Technol. Biotechnol.* **2010**, *85*, 590–613, doi:10.1002/jctb.2358.

2. Acheampong, M.A. Sustainable Gold Mining Wastewater Treatment by Sorption Using Low-Cost Materials. Ph.D. Thesis, UNESCO-IHE Institute of Water Education, Delft, The Netherlands, 2013; ISBN 978-1-138-00165-7.

3. Adams, M. Cyanide recovery by tailings washing and pond stripping. *Miner. Eng.* **2008**, *21*, 501–508, doi:10.1016/j.mineng.2008.02.015.

4. Akcil, A.; Koldas, S. Acid Mine Drainage (AMD): Causes, treatment and case studies. *J. Clean. Prod.* **2006**, *14*, 1139–1145, doi:10.1016/j.jclepro.2004.09.006.

5. Akkoca, D.B.; Yilgin, M.; Ural, M.; Akcin, H.; Mergen, A. Hydrothermal and Thermal Treatment of Natural Clinoptilolite Zeolite from Bigadiç, Turkey: An Experimental Study. *Geochemistry International.* **2013**, *51(6)*, 495–504, 2013. doi:10.1134/S0016702913040022.

6. Akpor, O.B.; Ohiobor, G.O.; Olaolu, T.D. Heavy metal pollutants in wastewater effluents: Sources, effects and remediation. *Adv. Biosci. Bioeng.* **2014**, *2(4)*, 37–43, doi:10.11648/j.abb.20140204.11.

7. Alvarez-Ayuso, E.; Garcia-Sanchez, A.; Querol, X. Purification of metal electroplating waste waters using zeolites. *Water Res.* **2003**, *37*, 4855–4862, doi:10.1016/j.watres.2003.08.009.

8. Anari-Anaraki, M.; Nezamzadeh-Ejhieh, A. Modification of an Iranian clinoptilolite nano-particles by hexadecyltrimethyl ammonium cationic surfactant and dithizone for removal of Pb(II) from aqueous solution. *J. Colloid Interf. Sci.* **2015**, *440*, 272–281, doi:10.1016/j.jcis.2014.11.017.

9. Andoh, R. (2014) Filter Technology is Looking Up - Storm Water Solutions. Available online: www.estormwater.com/filter-technology-looking (accessed on 04 March 2014).

10. ASTM D2434-68. Standard Test Method for Permeability of Granular Soils (Constant Head). ASTM International, West Conshohocken, PA. 2000. Available online: www.astm.org (accessed on 01 March 2016).

11. Asubiojo, O.I.; Ajelabi, O.B. Removal of heavy metals from industrial wastewaters using natural adsorbents. *Toxicol. Environ. Chem.* **2009**, *91(5)*, 883–890, doi:10.1080/02772240802614721.

12. Babel, S., Kurniawan, T.A. Low-cost adsorbents for heavy metals uptake from contaminated water: a review. *J. Hazard. Mater.* **2003**, *97*, 219–243, doi:S0304-3894(02)00263-7.

13. Baraket, M. A. New trends in removing heavy metals from industrial wastewater. *Arab. J. Chem.* **2011**, *4(4)*, 361–377doi:10.1016/j.arabjc.2010.07.019.

14. Bear River Zeolite Co. Inc. Zeolite—Specifications and MSDS. Available online: www.bearriverzeolite.com (accessed on 01 September 2012 and 01 April 2017).

15. Behnamfard, A.; Salarirad, M. M. Equilibrium and kinetic studies on free cyanide adsorption from aqueous solution by activated carbon. *J. Hazard. Mater.* **2009**, *170*, 127–133, doi:10.1016/j.jhazmat.2009.04.124.

16. Benjamin, M.M. *Water Chemistry*, 2nd ed.; Waveland Press, Inc. 2010, Inc. ISSN 978-1-4786-2308-3.

17. Bekkum, H.V.; Flanigen, E.M.; Jansen, J.C. Ion-Exchange in Zeolites. In *Introduction to Zeolite Science and Practice—Studies in Surface Science and Catalysis*, 1st ed.; Elsevier Science: Zeist, The Netherlands, 1991; Volume 58, pp. 359–390.

18. Bektas, N.; Kara, S. Removal of lead from aqueous solutions by natural clinoptilolite: Equilibrium and kinetic studies. *Sep. Purif. Technol.* **2004**, *39*, 189–200, doi:10.1016/j.seppur.2003.12.001.

19. Borandegi, M.; Nezamzadeh-Ejhieh, A. Enhanced removal efficiency of clinoptilolite nano-particles toward Co(II) from aqueous solution by modification with glutamic acid. *Colloids Surfaces A Physicochem. Eng. Asp.* **2015**, *479*, 35–45, doi:10.1016/j.colsurfa.2015.03.040.

20. Bosso, S.T.; Enzweiler, J. Evaluation of heavy metal removal from aqueous solution onto scolecite. *Wat. Res.* **2002**, *36*, 4795–4800, doi:10.1016/S0043-135400208-7.

21. Breck, D.W. Chapters 2-4, 6-8; Zeolite Molecular Sieves: Structure, Chemistry, and Use. John Wiley & Sons, New York, 1974.

22. Cabrera, C.; Gabaldon, C.; Marzal, P. Technical Note: Sorption characteristics of heavy metal ions by natural zeolite. *J. Chem. Technol. Biotechnol.* **2005**, *80*, 477–481, doi:10.1002/jctb.1189.

23. Çakıcğlu-Ozkan, F.; Ülkü, S. Diffusion mechanism of water vapour in a zeolitic tuff rich in clinoptilolite. *J. Therm. Anal. Calorim.* **2008**, *94(3)*, 699–702, doi:10.1007/s10973-008-9357-8.

24. Canada-United States Collaboration for Great Lakes Water Quality. About the Great Lakes Water Quality Agreement. Available online: binational.net/glwqa-aqegl/ (accessed on 20 April 2018).

25. Canadian Minister of Justice—Metal Mining Effluent Regulations. Consolidation SOR/2002-222. Justice Laws—Government of Canada. Available online: laws-lois.justice.gc.ca (accessed on 01 September 2014).

26. Chemistry LibreTexts. The Rate Law. 2015. Available online: chem.libretexts.org/Core/Physical_and_Theoretical_Chemistry/Kinetics/Rate_Laws/The_Rate_Law (accessed on 01 May 2018).

27. Chmielewská, E.; Sabová, L.; Jesenák, K. Study of adsorption phenomena ongoing onto clinoptilolite with the immobilized interfaces. *J. Therm. Anal. Calorim.* **2008**, *92(2)*, 567–571, doi:10.1007/s10973-006-8315-6.

28. Cincotti, A.; Mameli, A.; Locci, A.M.; Orru, R.; Cao, G. Heavy metals uptake by Sardinian natural zeolites: Experiment and modeling. *Ind. Eng. Chem. Res.* **2006**, *45*, 1074–1084, doi:10.1021/ie050375z.

29. Ciosek, A. L.; Luk, G. K. A Study on the Effects of Multiple Metallic Ions on the Zeolite Adsorption of Lead from Mine Wastewater. Technical Session: Industrial Treatment A (14), Water Environment Association of Ontario Technical Symposium and OPCEA Exhibition – Niagara Falls, Ontario, Canada. Paper No.: 2016-03. **2016**.

30. Ciosek, A.L.; Luk, G.K. Lead Removal from Mine Tailings with Multiple Metallic Ions. *Int. J. Water Wastewater Treat.* **2017a**, *3*, 1–9, doi:10.16966/2381-5299.134.

31. Ciosek, A. L.; Luk, G. K. Effects of Heat Pre-Treatment on Metallic Ion Sorption by Natural Zeolite. Technical Session: Industrial Treatment A (4), Water Environment Association of Ontario Technical Symposium and OPCEA Exhibition – Ottawa, Ontario, Canada. Paper No.: 2017-010. **2017b**.

32. Ciosek, A. L.; Luk, G. K. Kinetic Modelling of the Removal of Multiple Heavy Metallic Ions in Mine Waste by Natural Zeolite Sorption. Special Issue: Treatment of Wastewater and Drinking Water through Advanced Technologies, In *Water.* **2017c**, *9(7)*, 482, doi:10.3390/w9070482.

33. Ciosek, A. L.; Luk, G. K. An Innovative Dual-Column System for Heavy Metallic Ion Sorption by Natural Zeolite. Special Issue: Wastewater Treatment and Reuse Technologies, In *Applied Sciences.* **2017d**, *7(8)*, 795, doi: 10.3390/app7080795.

34. Ciosek, A.L.; Luk, G.K. Effects of Operation Parameters on Heavy Metallic Ion Removal from Mine Waste by Natural Zeolite. *Int. J. Environ. Pollution and Remediation.* **2018**, *6(1)*, 10–24, doi:10.11159/ijepr.2018.002.

35. Ciosek, A. L. An Innovative Sorption Treatment System to Remove Heavy Metallic Ions from Mine Wastewater. Technical Session: Industrial Treatment B (26), Water Environment Association of Ontario Technical Symposium and OPCEA Exhibition – London, Ontario, Canada. Paper No.: 2018-072. **2018**.

36. Cui, H.; Li, L.Y.; Grace, J.R. Exploration of remediation of acid rock drainage with clinoptilolite as sorbent in a slurry bubble column for both heavy metal capture and regeneration. *Water Res.* **2006**, 3359–3366, doi:10.1016/j.watres.2006.07.028.

37. Curenature. Heavy Metal Toxicity & Effective Chelators. 2018. Available online: www.curenature.com/2013/03/heavy-metal-toxicity-effective-chelators.html (accessed on: 01 September 2014).

38. Curkovic, L.; Cerjan-Stefanovic, S.; Filipan, T. Metal ion exchange by natural and modified zeolites. *Wat. Res.* **1997**, *31*, 1379–1382, doi:10.1016/S0043-135400411-3.

39. Delgado, J.M.P.Q. A critical review of dispersion in packed beds. *Heat Mass Transfer.* **2005**, *42(4)*, 279–310, doi:10.1007/s00231-005-0019-0.

40. Dinardo, O.; Kondos, P.D.; MacKinnon, D.J.; McCready, R.G.L.; Riveros, P.A.; Skaff, M. Study on Metals Recovery/Recycling from Acid Mine Drainage Phase IA: Literature Survey. Report 3.21.1a. Mine Environment Neutral Drainage (MEND) Program. CANMET, Energy, Mines and Resources Canada and WTC, Environment Canada. 1991. Available online: mend-nedem.org/wp-content/uploads/2013/01/3.21.1a.pdf (accessed on 30 October 2014).

41. Dridi-Dhaouadi, S.; Douissa-Lazreg, N. B.; M'Henni, M. F. Removal of lead and Yellow 44 acid dye in single and binary component systems by raw Posidonia oceanica and the cellulose extracted from the raw biomass. *Environ. Technol.* **2011**, *32*(3), 325–340, doi:10.1080/09593330.2010.499545.

42. Droste, R.L. *Theory and Practice of Water and Wastewater Treatment*, 1st ed., Wiley & Sons, 1997.

43. Engels, J. Tailings Info. 2013. Available online: www.tailings.info/index.htm (accessed on 07 March 2014).

44. Erdem, E.; Karapinar, N.; Donat, R. The removal of heavy metal cations by natural zeolites. *J. Colloid Interface Sci.* **2004**, *280*, 309–314, doi:10.1016/j.jcis.2004.08.028.

45. Erdol Aydin, N.; Nasun Saygili, G. Column experiments to remove copper from wastewaters using natural zeolite. *Int. J. Environment and Waste Management.* **2009**, *3*, 319–326, doi:10.1504/IJEWM.2009.026348.

46. Ersoy, B.; Celik, M.S. Electrokinetic properties of clinoptilolite with mono- and multivalent electrolytes. *Micropor. Mesopor. Mat.* **2002**, *55*, 305–312, doi:10.1016/S1387-181100433-X.

47. Farouq, R.; Yousef, N.S. Equilibrium and Kinetics Studies of adsorption of Copper (II) Ions on Natural Biosorbent. Int. *J. Chem. Eng. Applic.* **2015**, *6(5)*, 319–324, doi:10.7763/ijcea.2015.v6.503.

48. Fierro, V.; Torne-Fernandez, V.; Montane, D.; Celzard, A. Adsorption of phenol onto activated carbons having different textural and surface properties. *Micropor. Mesopor. Mat.* **2008**, *111*, 276–284, doi:10.1016/j.micromeso.2007.08.002.

49. Fu, F.; Wang, Q. Removal of heavy metal ions from wastewaters: A review. *J. Environ. Manag.* **2011**, *92*, 407–418, doi:10.1016/j.jenvman.2010.11.011.

50. Garbarino, J. R.; Hayes, H. C.; Roth, D. A.; Antweiler, R. C.; Brinton, T. I.; Taylor, H. E. Heavy Metals in the Mississippi River. Contaminants in the Mississippi River – U.S. Geological Survey Circular 1133. 1996. Available online: http://pubs.usgs.gov/circ/circ1133/heavy-metals.html (accessed on 08 August 2014).

51. Gregory, R. Filtration Processes. IWA Water Wiki. Information Resource and Hub for the Global Water Community. 2010. Available online: http://www.iwawaterwiki.org/xwiki/bin/export/Articles/FiltrationProcesses?format=pdf&pd fcover=1&pdfcover=0&pdftoc=1&pdftoc=0&comments=0&attachments=0 (accessed on 04 March 2014).

52. Gupta, N.; Balomajumder, C.; Agarwal, V. K. Adsorption of cyanide ion on pressmud surface-A modeling approach. *Chem. Eng. J.* **2012**, *191*, 549–556, doi:10.1016/j.cej.2012.03.028.

53. Gunay, A.; Arslankaya, E.; Tosun, I. Lead removal from aqueous solution by natural and pretreated clinoptilolite: Adsorption equilibrium and kinetics. *J. Hazard. Mater.* **2007**, *146*, 362–371, doi:10.1016/j.jhazmat.2006.12.034.

54. Gunn, D.J. Axial and Radial Dispersion in Fixed Beds. *Chem. Eng. Sci.* **1987**, *42(2)*, 363–373, doi:10.1016/0009-2509(87)85066-2.

55. Han, R.; Zou, W.; Li, H.; Li, Y.; Shi, J. Copper(II) and lead(II) removal from aqueous solution in fixed-bed columns by manganese oxide coated zeolite. *J. Hazard. Mater.* **2006**, 137, 934–942, doi:10.1016/j.jhazmat.2006.03.016.

56. Haynes, W. M. CRC Handbook of Chemistry and Physics. 95th Edition 2014-2015. Available online: www.hbcpnetbase.com.ezproxy.lib.ryerson.ca/ (accessed on 13 November 2014).

57. Helfferich, F. Chapter 5, 6, 9. In *Ion Exchange*; Series in Advanced Chemistry; McGraw-Hill Book Company: New York, USA, 1962; pp. 95–322; 421-506.

58. Ho, Y.S.; McKay, G. A Comparison of Chemisorption Kinetic Models Applied to Pollutant Removal on Various Sorbents. *Process. Saf. Environ.*, **1998a**, *76(4)*, 332–340, doi:10.1205/095758298529696.

59. Ho, Y.S.; McKay, G. Kinetic Models for the Sorption of Dye from Aqueous Solution by Wood. *Process. Saf. Environ.* **1998b**, *76(2)*, 183–191, doi:10.1205/095758298529326.

60. Ho, Y.; Ofomaja, A.E. Pseudo-second-order model for lead ion sorption from aqueous solutions onto palm kernel fiber. *J. Hazard. Mater.* **2006**, *129*, 137–142, doi:10.1016/j.jhazmat.2005.08.020.

61. Huang, M.; Kalliagunie, S.; Auroux, A. Lewis basic and Lewis acidic sites in zeolites. *Stud. Surf. Sci. Catal.* **1995**, *97*, 311–318, doi:10.1016/S0167-2991(06)81903-8.

62. Imperial Metals Corporation (IMC). Mount Polley Mine – Overview. Available online: www.imperialmetals.com/s/MountPolleyMine.asp (accessed on 01 September 2014).

63. Inglezakis, V.J.; Papadeas, C.D.; Loizidou, M.D.; Grigoropoulou, H.P. Effects of Pretreatment on Physical and Ion Exchange Properties of Natural Clinoptilolite. *Environ. Technol.* **2001a**, *22*, 75–82, doi:10.1080/09593332208618308.

64. Inglezakis, V.J.; Hadjiandreou, K.J.; Loizidou, M.D.; Grigoropoulou, H.P. Pretreatment of Natural Clinoptilolite in a Laboratory-Scale Ion Exchange Packed Bed. *Water Res.* **2001b**, *35*, 2161–2166, doi:10.1016/S0043-135400500-5.

65. Inglezakis, V.J.; Loizidou, M.D.; Grigoropoulou, H.P. Equilibrium and kinetic ion exchange studies of Pb^{2+}, Cr^{3+}, Fe^{3+} and Cu^{2+} on natural clinoptilolite. *Water Res.* **2002**, *36*, 2784–2792, doi:10.1016/S0043-135400504-8.

66. Inglezakis, V.J.; Loizidou, M.D.; Grigoropoulou, H.P. Ion exchange of Pb^{2+}, Cu^{2+}, Fe^{3+}, and Cr^{3+} on natural clinoptilolite: Selectivity determination and influence of acidity on metal uptake. *J. Colloid Interface Sci.* **2003**, *261*, 49–54, doi:10.1016/S0021-979700244-8.

67. Inglezakis, V. J.; Grigoropoulou, H. Effects of operating conditions on the removal of heavy metals by zeolite in fixed bed reactors. *J. Hazard. Mater.* **2004**, *112*, 37–43, doi:10.1016/j.jhazmat.2004.02.052.

68. Inglezakis, V. J. The concept of "capacity" in zeolite ion-exchange systems. *J. Colloid Interface Sci.* **2005**, *281*, 68–79, doi:10.1016/j.jcis.2004.08.082.

69. Inglezakis, V.J.; Zorpas, A.A., Loizidou, M.D.; Grigoropoulou, H.P. The effect of competitive cations and anions on ion exchange of heavy metals. *Sep. Purif. Technol.* **2005**, *46*, 202–207, doi:10.1016/j.seppur.2005.05.008.

70. Inglezakis, V.J.; Poulopoulos, S.G. Chapter 4—Adsorption and Ion-Exchange (Kinetics). In *Adsorption*, *Ion Exchange and Catalysis—Design of Operations and Environmental Applications*, 1st ed.; Elsevier Science: Amsterdam, The Netherlands, 2006; pp. 262–266, ISBN-13: 978-0-444-52783-7.

71. Inglezakis V.J. Ion exchange and adsorption fixed bed operations for wastewater treatment – Part I: modelling fundamentals and hydraulics analysis. *J. Eng. Stud. Res.* **2010a**, *16(3)*, 29–41, doi:JESR201016V16S01A0004 [0002990].

72. Inglezakis V.J. Ion exchange and adsorption fixed bed operations for wastewater treatment – Part II: scale-up and approximate design methods. *J. Eng. Stud. Res.* **2010b**, *16(3)*, 42–50, doi:JESR201016V16S01A0005 [0002991].

73. International Joint Commission United States and Canada – Office Consolidation. Great Lakes Water Quality Agreement of 1978 - Revised. Available online: www.ijc.org/files/tinymce/uploaded/GLWQA_e.pdf (accessed on 20 April 2018).

74. Jarvie, M.E.; Hand, D.W.; Bhuvendralingam, S.; Crittenden, J.C.; Hokanson, D.R. Simulating the Performance of Fixed Bed Granular Activated Carbon Adsorbers: Removal of Synthetic Organic Chemicals in the Presence of Background Organic Matter. *Water Res.* **2005**, *39(11)*, 2407–2421, doi:10.1016/j.watres.2005.04.023.

75. Jha, B.; Sigh, D.N. Fly Ash Zeolites, Chapter 2: Basics of Zeolites. *Adv. Struct. Mat.* **2016**, *78*, 5–31, doi:10.1007/978-981-10-1404-8_2.

76. Johnson, D. B.; Hallberg, K. B. Acid mine drainage remediation options – a review. *Sci. Total Environ.* **2005**, 338, 3–14, doi:10.1016/j.scitotenv.2004.09.002.

77. Jovanovic, M.; Rajic, N.; Obradovic, B. Novel kinetic model of the removal of divalent heavy metal ions from aqueous solutions by natural clinoptilolite. *J. Hazard. Mater.* **2012**, *233*, 57–64, doi:10.1016/j.jhazmat.2012.06.052.

78. Kantarci, N.; Borak, F.; Ulgen, K.O. Bubble column reactors. *Process Biochem.* **2005**, *40*, 2263–2283, doi:10.1016/j.procbio.2004.10.004.

79. Kocaoba, S.; Orhan, Y.; Akyuz, T. Kinetics and equilibrium studies of heavy metal ions removal by use of natural zeolite. *Desalination* **2007**, *214*, 1–10, doi:10.1016/j.desal.2006.09.023.

80. Kocasoy, G.; Sahin, V. Heavy metal removal from industrial wastewater by clinoptilolite. *J. Environ. Sci. Heal. A.* **2007**, *42*, 2139–2146, doi:10.1080/10934520701629617.

81. Kostandyan, M.N.; Babayan, S.G.; Balayan, M.A. Effect of heat treatment on the structural characteristics and sorption properties of clinoptilolite. *Inorganic Materials.* **1982**, *18(10)*, 1498–1501, 0020-1685.

82. Kragovic, M.; Dakovic, A.; Markovic, M.; Krstic, J.; Gatta, G.D.; Rotiroti, N. Characterization of lead sorption by natural and Fe (III)-modified zeolite. *Appl. Surf. Sci.* **2013**, *283*, 764–774, doi:10.1016/j.apsusc.2013.07.016.

83. Kuyucak, N.; Akcil, A. Cyanide and removal options from effluents in gold mining and metallurgical processes. *Miner. Eng.* **2013**, *50/51*, 13–29, doi:10.1016/j.mineng.2013.05.027.

84. Largitte, L.; Pasquier, R. A review of the kinetics adsorption models and their application to the adsorption of lead by an activated carbon. *Chem. Eng. Res. Des.* **2016**, *109*, 495–504, doi:10.1016/j.cherd.2016.02.006.

85. Lata, S.; Singh, P.K.; Samadder, S.R. Regeneration of adsorbents and recovery of heavy metals: a review. *Int. J. Environ. Sci. Technol.* **2015**, *12*, 1461–1478, doi:10.1007/s13762-014-0714-9.

86. Langella, A.; Pansini, M.; Cerri, G.; Cappelletti, P.; De Gennaro, M. Thermal Behavior of Natural and Cation-Exchanged Clinoptilolite from Sardinia (Italy). *Clay. Clay Miner.* **2003**, *51(6)*, 625–633, doi:10.1346/CCMN.2003.0510605.

87. Margeta, K.; Zabukovec Logar, N.; Šiljeg, M.; Farkaš, A. Chapter 5: Natural Zeolites in Water Treatment—How Effective Is Their Use. InTech, Water Treatment, Dr. W. Elshorbagy, Ed., **2013**, 81–112, doi:10.5772/50738.

88. Markovic, R.; Gardic, V.; Obradovic, L.; Djordjievski, S.; Stevanovic, Z.; Stevanovic, J.; Gvozdenovic, M. The Application of a Natural Zeolite for Acid Mine Drainage Purification. *Mater. Trans., JIM*, **2015**, *56(12)*, 2053–2057, doi:10.2320/matertrans.M2015292.

89. Martin, S.; Griswold, W. Human Health Effects of Heavy Metals. Environmental Science and Technology Briefs for Citizens – Center for Hazardous Substance Research. Kansas State University. Issue 15. 2009. Available online: www.engg.ksu.edu/CHSR/ (accessed on 01 September 2014).

90. Masel, R. I. Principles of Adsorption and Reaction on Solid Surfaces. John Wiley & Sons, Inc. 1996, ISBN: 978-0-471-30392-3. pp. 235–248.

91. McMartin, P. (2014) Mount Polley Mine - Maybe if we tried putting red tape on the breach. Vancouver Sun. Available online: www.ottawacitizen.com/news/metro/Pete+McMartin+Mount+Polley+Mine+Maybe+tried+putting+tape/10109694/story.html (accessed on 10 August 2014).

92. Minceva, M.; Fajgar, R.; Markovska, L., Meshko, V. Comparative Study of Zn^{2+}, Cd^{2+}, and Pb^{2+} Removal From Water Solution Using Natural Clinoptilolitic Zeolite and Commercial Granulated Activated Carbon: Equilibrium of Adsorption. *Separ. Sci. Technol.* **2008**, 43, 2117–2143. doi:10.1080/01496390801941174.

93. Mining Association of Canada (MAC). Mining Facts. Available online: mining.ca/resources/mining-facts (accessed on 01 September 2014).

94. MOECC. Deriving Receiving Water Based Point Source Effluent Requirements for Ontario Waters. 2016. Available online: www.ontario.ca/page/b-1-5-deriving-receiving-water-based-point-source-effluent-requirements-ontario-waters (accessed 20 April 2018).

95. Mohan, D.; Chander, S. Removal and recovery of metal ions from acid mine drainage using lignite—A low cost sorbent. *J. Hazard. Mater.* **2006**, *B137*, 1545–1553, doi:10.1016/j.jhazmat.2006.04.053.

96. Motsi, T.; Rowson, N.A.; Simmons, M.J.H. Adsorption of heavy metals from acid mine drainage by natural zeolite. *Int. J. Miner. Process.* **2009**, *92*, 42–48, doi:10.1016/j.minpro.2009.02.005.

97. Motsi, T. Remediation of Acid Mine Drainage using Natural Zeolite. Ph.D. Thesis. School of Chemical Engineering, The University of Birmingham, United Kingdom. **2010**.

98. Motsi, T.; Rowson, N.A.; Simmons, M.J.H. Kinetic studies of the removal of heavy metals from acid mine drainage by natural zeolite. *Int. J. Miner. Process.* **2011**, *101*, 42–49, doi:10.1016/j.minpro.2011.07.004.

99. Mullin, J. Physical and thermal properties. In *Crystallization*. Fourth Edition. Read Educational and Professional Publishing Ltd: Woburn, MA, USA, 2001; pp. 76–77, IBSN: 0-7506-4833-3.

100. Mumpton, F.A.; Boles, J.R.; Flanigen, E.M.; Gude, A.J.; Sheppard, R.A.; Hay, R.L.; Surdam, R.C. Chapter 8; Mineralogy and Geology of Natural Zeolites. Washington, D.C.: Mineralogical Society of America. 1977; ISBN 0939950049.

101. Muttil, N.; Chau, K.W. Machine learning paradigms for selecting ecologically significant input variables. *Eng. Appl. Artif. Intel.* **2007**, *20*, 735–744, doi:10.1016/j.engappai.2006.11.016.

102. Naja, G.; Volesky, B. Multi-metal biosorption in a fixed-bed flow-through column. *Colloid. Surface.* **2006**, 281, 194–201. doi:10.1016/j.colsurfa.2006.02.040.

103. Nezamzadeh-Ejhieh, A.; Shahanshahi, M. Modification of clinoptilolite nano-particles with hexadecylpyridynium bromide surfactant as an active component of Cr(VI) selective electrode. *J. Ind. Eng. Chem.* **2013**, *19*, 2026–2033, doi:10.1016/j.jiec.2013.03.018.

104. Nezamzadeh-Ejhieh, A.; Shirzadi, A. Enhancement of the photocatalytic activity of Ferrous Oxide by doping onto the nano-clinoptilolite particles towards photodegradation of tetracycline. *Chemosphere* **2014**, *107*, 136–144, doi:10.1016/j.chemosphere.2014.02.015.

105. Nicholson, R.V. Acid Drainage and Metal Leaching Prediction: Where have we been and where do we Need to Go - An Historical Perspective. Conference Proc. CIM Symposium, Rouyn-Noranda, QC, Canada, 2015.

106. Nisbet, K.; Rasor, R. An Inventor's Guide to Technology Transfer at the Massachusetts Institute of Technology. MIT Technology Licensing Office. 2005. Available online: web.mit.edu/tlo/www/downloads/pdf/inventors_guide.pdf (accessed on 08 March 2014).

107. Nuic, M.; Trgo, J.; Peric, N.; Vukojevic Medvidovic, N. Analysis of breakthrough curves of Pb and Zn sorption from binary solutions on natural clinoptilolite. *Micropor. Mesopor. Mat.* **2013**, 167, 55–61. doi:10.1016/j.micromeso.2012.04.037.

108. Nuic, I.; Trgo, M.; Peric, J.; Vukojevic Medvidovic, N. Uptake of Pb and Zn from a binary solution onto different fixed bed depths of natural zeolite – the BDST model approach. *Clay Minerals.* **2015**, *50*, 91–101, doi:10.1180/claymin.2015.050.1.09.

109. Nuic, I.; Trgo, M.; Vukojevic Medvidovic, N. The application of the packed bed reactor theory to Pb and Zn uptake from the binary solution onto the fixed bed of natural zeolite. *Chem. Eng. J.* **2016**, *295*, 347–357, doi:10.1016/j.cej.2016.03.037.

110. Occupational Health and Safety Act (OHSA). Ontario Regulation 490/09 – Designated Substances. Consolidated Laws – Government of Ontario. Available online: www.e-laws.gov.on.ca/html/regs/english/elaws_regs_090490_e.htm (accessed on 01 September 2014).

111. Olu-Owolabi, B.I.; Diagboya, P.N.; Adebowale, K.O. Evaluation of pyrene sorption—Desorption on tropical soils. *J. Environ. Manage.* **2014**, *137*, 1–9, doi:10.1016/j.jenvman.2014.01.048.

112. Ontario Mining & Exploration Directory & Resource Guide. Ontario Mining Operations Map. 2015. Available online: www.oma.on.ca/en/resourcesGeneral/Ontario_Mining_Operations_2015.pdf (accessed on 20 April 2018).

113. Oter, O.; Akcay, H. Use of natural clinoptilolite to improve, water quality: Sorption and selectivity studies of lead(II), copper(II), zinc(II), and nickel(II). *Water Environ. Res.* **2007**, *79*, 329–335, doi:10.2175/106143006X111880.

114. Othman, M. Z.; Roddick, F. A.; Snow, R. Removal of Dissolved Organic Compounds in Fixed-Bed Columns: Evaluation of Low-Rank Coal Adsorbents. *Wat. Res*. **2001**, *35(12)*, 2943–2949, doi: S0043-1354(00)00578-9.

115. Ouki, S. K.; Kavannagh, M. Performance of natural zeolites for the treatment of mixed metal contaminated effluents. *Waste Manage. Res.* **1997**, 15 (4), 383–394, doi:10.1006/wmre.1996.0094.

116. Ouki, S.K.; Kavannagh, M. Treatment of metals-contaminated wastewaters by use of natural zeolites. *Wat. Sci. Tech.* **1999**, *39*, 115–122, doi:10.1016/S0273-122300260-7.

117. Panayotova, M.; Velikov, B. Kinetics of Heavy Metal Ions Removal by Use of Natural Zeolite. *J. Environ. Sci. Health* **2002**, *37*, 139–147, doi:10.1081/E-120002578.

118. Peric, J.; Trgo, M.; Vukojevic Medvidovic, N. Removal of zinc, copper and lead by natural zeolite – a comparison of adsorption isotherms. *Water Res.* **2004**, *38*, 1893–1899, doi:10.1016/j.watres.2003.12.035.

119. Peric, J.; Trgo, M.; Vukojevic Medvidovic, N.; Nuic, I. The Effect of Zeolite Fixed Bed Depth on Lead Removal from Aqueous Solutions. *Sep. Sci. Technol.* **2009**, *44*, 3113–3127, doi:10.1080/01496390903182230.

120. Perkin Elmer Inc. *WinLab32 for ICP—Instrument Control Software*, version 5.0; Perkin Elmer Inc.: Waltham MA, USA, 2010.

121. Perkin Elmer Inc. Atomic Spectroscopy—A Guide to Selecting the Appropriate Technique and System: World Leader in AA, ICP-OES, and ICP-MS; Perkin Elmer Inc.: Waltham MA, USA, 2011.

122. Plazinski, W., Rudzinski, W, Plazinska, A. Theoretical models of sorption kinetics including a surface reaction mechanism: A review. *Adv. Colloid. Interfac.* **2009**, *152*, 2–13, doi:10.1016/j.cis.2009.07.009.

123. Prasad, B.; Mortimer, R.J.G. Treatment of Acid Mine Drainage Using Fly Ash Zeolite. *Water, Air, Soil Pollut.* **2011**, *218*, 667–679, doi:10.1007/s11270-010-0676-6.

124. Qiu, H.; Lv, L.; Pan, B.C.; Zhang, Q.J.; Zhang, W.M.; Zhang, Q.X. Critical review in adsorption kinetic models. *J. Zhejiang Univ. Sci. A* **2009**, *18*, 716–724, doi:10.1631/jzus.A0820524.

125. Rasmussen, E.K. Recent Development – The 1978 Great Lakes Water Quality Agreement and Prospects for U.S.-Canada Pollution Control. *Boston College International and Comparative Law Review*. **1979**, *2(2,11)*, 499–520.

126. Reed, B. E.; Jamil, M.; Thomas, B. Effect of pH , empty bed contact time and hydraulic loading rate on lead removal by granular activated carbon columns. *Water Environ. Res.* **1996**, *68(5)*, 877–882, doi:10.2175/106143096X127875.

127. Rice, E.W.; Baird, R.B; Eaton, A.D.; Clesceri, L.S. Part 1000-Introduction, Part 3000-METALS. In *Standard Methods for the Examination of Water and Wastewater*, 22nd ed.; The American Public Health Association (APHA): Washington, DC, USA; The American Water Works Association (AWWA): Denver, CO, USA; The Water Environment Federation (WEF): Alexandria, VA, USA, 2012; pp. 1.1–68, 3.1–112, ISSN 978-087553-013-0.

128. Rios, C.A.; Williams, C.D.; Roberts, C.L. Removal of heavy metals from acid mine drainage (AMD) using coal fly ash, natural clinker and synthetic zeolites. *J. Hazard. Mater.* **2008**, *156*, 23–35, doi:10.1016/j.jhazmat.2007.11.123.

129. Ritcey, G. M. Tailings management in gold plants. G.M. Ritcey and Associates. *Hydrometallurgy*, **2005**, *78*, 3–20, doi:10.1016/j.hydromet.2005.01.001.

130. Riveros, P.; Wong, E.W. Metals Removal from Acid Mine Drainage by Ion Exchange. Report 3.21.1b. Mine Environment Neutral Drainage (MEND) Program. Ontario Ministry of Nerothn Development and Mines, Canada Centre for Mineral and Energy Technology (CANMET), Canada/Northern Ontario Development Agreement (NODA). 1995. Available online: mend-nedem.org/wp-content/uploads/2013/01/3.21.1b.pdf (accessed on 30 October 2014).

131. Salem, A.; Akbari Sene, R. Removal of lead from solution by combination of natural zeolite-kaolin-bentonite as a new low-cost adsorbent. *Chem. Eng. J.* **2011**, *174*, 619–628, doi: 10.1016/j.cej.2011.09.075.

132. Singer, P.C.; Stumm, W. Acidic Mine Drainage: The Rate-Limiting Step. *Science* **1970**, *167(3921)*, 1121–1123.doi:10.1126/science.167.3921.1121.

133. Skoog, D. A.; Holler, F. J.; Crouch, S. R. Principles of Instrumental Analysis. 6th Edition. Thomson – Brooks/Cole. ISBN-13: 978-0-495-01201-6. 2007.

134. Sprynskyy, M.; Buszewski, B; Terzyk, A.P.; Namiesnik, J. Study of the selection mechanism of heavy metal (Pb^{2+}, Cu^{2+}, Ni^{2+}, and Cd^{2+}) adsorption on clinoptilolite. *J. Colloid Interface Sci.* **2006**, *304*, 21–28, doi:10.1016/j.jcis.2006.07.068.

135. Stylianou, M.A.; Inglezakis, V.J.; Moustakas, K.G.; Malamis, S.P.; Loizidou, M.D. Removal of Cu(II) in fixed bed and batch reactors using natural zeolite and exfoliated vermiculite as adsorbents. *Desalination,* **2007a**, 215, 133–142. doi:10.1016/j.desal.2006.10.031.

136. Stylianou, M.A., Hadjiconstantinou, M.P.; Inglezakis, V.J.; Moustakas, K.G.; Loizidou, M.D. Use of natural clinoptilolite for the removal of lead, copper and zinc in fixed bed column. *J. Hazard. Mater.* **2007b**, 143, 575–581. doi:10.1016/j.jhazmat.2006.09.096.

137.Tchounwou, P.B.; Yedjou, C.G.; Patlolla, A.K.; Sutton, D.J. Heavy Metals Toxicity and the Environment. In: Luch A. (eds) Molecular, Clinical and Environmental Toxicology. Experientia Supplementum, **2012**, *101*, doi:10.1007/978-3-7643-8340-4_6.

138.Trgo, M.; Peric, J.; Vukojevic Medvidovic, N. A comparative study of ion exchange kinetics in zinc/lead—modified zeolite-clinoptilolite systems. *J. Hazard. Mater.* **2006**, *136*, 938–945, doi:10.1016/j.jhazmat.2006.01.032.

139.Tsitsishvili, G.V. Perspectives of Natural Zeolite Applications. Occurrence. In *Properties and Utilization of Natural Zeolites—2nd International Conference 1985*; Akademiai Kiado: Budapest, Hungary, 1988; pp. 367–393.

140.University of Liverpool. Zeolite – Clinoptilolite. Nick Greeves, ChemTube3D, 2017. Available online: www.chemtube3d.com/solidstate/SS-Z-Clinoptilolite.htm (accessed on 20 April 2018).

141.University of Michigan (LSA). ICP-OES User's Booklet. Available online: lsa.umich.edu/content/dam/chem-assets/chem-docs/ICP_OES_User_s_Booklet.doc (accessed on 06 July 6 2015).

142.US EPA Guidance on Choosing a Sampling Design for Environmental Data Collection – Use in Developing a Quality Assurance Project Plan. EPA QA/G-5S. Office of Environmental Information, Washing, DC 20460. 2002.

143.Van Reeuwijk, L.P. The Thermal Dehydration of Natural Zeolites. Department of Soil Science and Geology, Agricultural University, Mededelingen Landbouwhogeschool Wageningen 74-9, The Netherlands, **1974**.

144.Vaca-Mier, M.; Lopez-Callejas, R.; Gehr, R.; Jimenez-Cisneros, B. E; Alvarez, P. J. J. Heavy metal removal with Mexican Clinoptilolite: Multi-Component Ionic Exchange. *Wat. Res.* **2001**, *35(2)*, 373–378, doi:10.1016/S0043-1354(00)00270-0.

145.Vukojevic Medvidovic, N.; Peric, J.; Trgo, M. Column performance in lead removal from aqueous solutions by fixed bed of natural zeolite–clinoptilolite. *Sep. Purif. Technol.* **2006**, *49*, 237–244, doi:10.1016/j.seppur.2005.10.005.

146.Vukojevic Medvidovic, N.; Peric, J.; Trgo, M.; Nuic, I.; Ugrina, M. Design of Fixed Bed Column for Lead Removal on Natural Zeolite Based on Batch Studies. *Chem. Biochem. Eng. Q.* **2013**, *27*, 21–28, doi:http://hrcak.srce.hr/99433.

147.Wang, C.; Li, J.; Sun, X.; Wang, L.; Sun, X. Evaluation of zeolites synthesized from fly ash as potential adsorbents for wastewater containing heavy metals. *J. Environ. Sci.* **2009**, *21*, 127–136, doi:10.1016/S1001-074260022-X.

148.Wang, S.; Peng, Y. Natural zeolites as effective adsorbents in water and wastewater treatment. *Chem. Eng. J.* **2010**, *156*, 11–24, doi:10.1016/j.cej.2009.10.029.

149.Wang, W.C.; Xu, D.M.; Chau, K.W.; Lei, G.J. Assessment of river water quality based on theory of variable fuzzy sets and fuzzy binary comparison method. *Water Resour. Manag.* **2014**, *28*, 4183–4200, doi:10.1007/s11269-014-0738-4.

150. Wilson, L.J. Canada-Wide Survey of Acid Mine Drainage Characteristics. Project Report 3.22.1—Job No. 50788. Mineral Sciences Laboratories Division Report MSL 94–32 (CR). Ontario Ministry of Northern Development and Mines. Mine Environment Neutral Drainage (MEND) Program: Canada, 1994. Available online: http://mend-nedem.org/wp-content/uploads/2013/01/3.22.1.pdf (accessed on 30 October 2014).

151. Wingenfelder, U.; Hansen, C.; Furrer, G.; Schulin, R. Removal of Heavy Metals from Mine Waters from Natural Zeolites. *Environ. Sci. Technol.* **2005**, *39*, 4606–4613, doi:10.1021/es048482s.

152. Wu, F.C.; Tseng, R.L.; Juang, R.S. Characteristics of Elovich equation used for the analysis of adsorption kinetics in dye-chitosan systems. *Chem. Eng. J.* **2009**, *150*, 366–373, doi:10.1016/j.cej.2009.01.014.

153. Xu, W.; Li, L.Y.; Grace, J.R. Zinc removal from acid rock drainage by clinoptilolite in a slurry bubble column. *Appl. Clay Sci.* **2010**, doi:10.1016/j.clay.2010.07.005.

154. Xu, W.; Li, L.Y.; Grace, J.R. Regeneration of natural Bear River clinoptilolite sorbents used to remove Zn from acid mine drainage in a slurry bubble column. *Appl. Clay Sci.* **2012**, *55*, 83-87, doi:10.1016/j.clay.2011.10.009.

155. Xu, W.; Li, L.Y.; Grace, J.R., Hebrard, G. Acid rock drainage treatment by clinoptilolite with slurry bubble column: Sustainable zinc removal with regeneration of clinoptilolite. *Appl. Clay Sci.* **2013**, *80–81*, 31-37, doi:10.1016/j.clay.2013.05.009.

156. Xu, W.; Li, L.Y.; Grace, J.R. Dealumination of clinoptilolite and its effect on zinc removal from acid rock drainage. *Chemosphere* **2014**, *111*, 427–433, doi:10.1016/j.chemosphere.2014.03.125.

157. Yabe, M.J.S.; de Oliveira, E. Heavy metals removal in industrial effluents by sequential adsorbent treatment. *Adv. Environ. Res.* **2003**, *7*, 263–272, doi:S1093-0191(01)00128-9.

158. Yörükoğulları, E.; Yılmaz, G.; Dikmen, S. Thermal treatment of zeolitic tuff. *J. Therm. Anal. Calorim.* **2010**, *100(3)*, 925–928, doi:10.1007/s10973-009-0503-8.

159. Zhao, M.Y.; Cheng, C.T.; Chau, K.W.; Li, G. Multiple criteria data envelopment analysis for full ranking units associated to environment impact assessment. *Int. J. Environ. Pollut.* **2006**, *28*, 448–464, doi:10.1504/IJEP.2006.011222.

160. Zinck, J. Review of Disposal, Reprocessing and Reuse Options for Acidic Drainage Treatment Sludge. Report 3.42.3. Mine Environment Neutral Drainage (MEND) Program. Mining Association of Canada. CANMET Mining and Mineral Sciences Laboratories. Canada, 2005. Available online: mend-nedem.org/wp-content/uploads/2013/01/3.42.3.pdf (accessed on 30 October 2014).

161. Zolgharnein, J.; Shahmoradi, A. Characterization of Sorption Isotherms, Kinetic Models, and Multivariate Approach for Optimization of Hg(II) Adsorption onto Fraxinus Tree Leaves. *J. Chem. Eng. Data* **2010**, *55*, 5040–5049, doi:10.1021/je1006218.